Cure behavior of epoxy polymers used in microelectronics.

Citation

Taweeplengsangsuke, Jantrawan - Lehigh University. *Cure Behavior of Epoxy Polymers Used in Microelectronics*. 2000, https://preserve.lehigh.edu/lehigh-scholarship/graduate-publications-theses-dissertations/theses-dissertations/cure-behavior.

INFORMATION TO USERS

This manuscript has been reproduced from the microfilm master. UMI films the text directly from the original or copy submitted. Thus, some thesis and dissertation copies are in typewriter face, while others may be from any type of computer printer.

The quality of this reproduction is dependent upon the quality of the copy submitted. Broken or indistinct print, colored or poor quality illustrations and photographs, print bleedthrough, substandard margins, and improper alignment can adversely affect reproduction.

In the unlikely event that the author did not send UMI a complete manuscript and there are missing pages, these will be noted. Also, if unauthorized copyright material had to be removed, a note will indicate the deletion.

Oversize materials (e.g., maps, drawings, charts) are reproduced by sectioning the original, beginning at the upper left-hand corner and continuing from left to right in equal sections with small overlaps.

Photographs included in the original manuscript have been reproduced xerographically in this copy. Higher quality 6" x 9" black and white photographic prints are available for any photographs or illustrations appearing in this copy for an additional charge. Contact UMI directly to order.

Bell & Howell Information and Learning
300 North Zeeb Road, Ann Arbor, MI 48106-1346 USA
800-521-0600

UMI®

Reproduced with permission of the copyright owner. Further reproduction prohibited without permission.

CURE BEHAVIOR OF EPOXY POLYMERS USED IN MICROELECTRONICS

by

Jantrawan Taweeplengsangsuke

A Dissertation
Presented to the Graduate Committee
of Lehigh University
In Partial Fulfillment of the Requirements of the Degree of
Doctor of Philosophy
in
Polymer Science and Engineering

August, 2000

UMI Number: 9995567

UMI®

UMI Microform 9995567

Bell & Howell Information and Learning Company
300 North Zeeb Road
P.O. Box 1346
Ann Arbor, MI 48106-1346

Certificate of Approval

Approved and recommended for acceptance as a dissertation in partial fulfillment of the requirements for the degree of Doctor of Philosophy

Aug 7, 2000
Date

Raymond A. Pearson
R. A. Pearson
(Professor in charge)

Accepted:

Aug. 7, 2000
Date

Special Committee
Directing the doctoral work of
Jantrawan Taweeplengsangsuke

Raymond A. Pearson
Chairman: R. A. Pearson

John P. Coulter
J. P. Coulter

Thomas B. Lloyd
T. B. Lloyd

L. H. Sperling

M. S. Vratsanos

Dedication

To my dear family, teachers, and friends

Acknowledgments

Several years in Lehigh have been my great experience in education and living. I would not be able to get through these years without the assistance from several people. First of all I would like to express my appreciation and respect to my advisor, Dr. Raymond A. Pearson, who has been so kind, patient, understandable, encourage and helpful to me. His laughing made the research more enjoyable than it should be. He will be an example of being a good advisor in my future career.

I would also like to thank the members of my doctoral committee: Dr. John P. Coulter, Dr. Tom B. Lloyd, Dr. Leslie H. Sperling, and Dr. Menas S. Vratsanos for their advices and useful discussion on my research.

This work could not be achieved without the help from my friends at Lehigh: Dr. J. C. Hsiung, Dr. Michael DiBerardino, and Jinwen Fan, who helped me to start the research and Dr. Jongwoo Park and Dr. Jason Goodelle, who helped me to finish the experiment at last. The kind help from staff and technicians of Material Science and Engineering Department; Gene Kozma, Arlan Benscoter Michael Rex, and Virginia Newhard, is appreciated.

I would like to express a special gratefulness to Dr. Robert Molloy, who always sends all kinds of support through e-mail.

Unquestionably, without a moral support from my family, friends and Anusorn Pumchusak, it would have been much more difficult for me to endure the long period to complete the dissertation. I am indebted to their loves and supports.

Finally, I acknowledge the financial support from Semiconductor Research Cooperation (SRC) and Thai Government.

Table of Contents

List of Tables

List of Figures

Abstract

Underfill resins are used to reduce solder fatigue in flip-chip assemblies. Both underfilling and curing processes are critical to achieve reliable finished products. This study included two main themes; the development of processing diagrams for commercial underfill resins and the fundamental understanding of cure kinetics and evolution of cure stresses in model epoxies. A variety of techniques have been used to characterize the fundamental phenomena involved in the processing of underfill resins. The flow behavior, cure kinetics, cure stresses, outgassing phenomena and void formation of underfill resins were studied. Processing diagrams for underfill resins were developed by mapping fundamental phenomena involved to provide a guideline for underfilling and curing steps. With these processing diagrams one should be able to design his underfilling and curing process with scientific approach.

Two commercial underfill resins, which were evaluated as part of a SEMATECH program, where shown to possess significantly different processing characteristics. However, the appropriate explanation could not be made without knowing the proprietary chemistry of the systems. Therefore, model epoxies were formulated. Three different systems were investigated; amine, imidazole, and anhydride curing agent systems. With the known chemistry, the reaction kinetics and developed cure stress can be explained more clearly. Vitrification, which severely retards the rate of reaction, was found in amine (N-aminoethylpiperazine) and anhydride (Hexahydro-4-methylphthalic anhydride) cured systems when the cure temperatures were lower than the glass transition

temperature (T_g) of fully cured samples; however, imidazole(2-ethyl-4-methyl-imidazole) did not show vitrification when it was cured at 20 degrees below the T_g of fully cured sample due to the large exotherms. Interestingly for imidazole system, the higher cure temperature exhibited a lower T_g. This could possibly be explained by the occurrence of etherification at high cure temperature.

Evolution of cure stress depends not only on the crosslink density (which impact the volume shrinkage) and modulus of resin, but the correlation between the time scales that display the heat of reaction and the gelation also affect the magnitude of cure stress.

CHAPTER 1

Introduction

A "microelectronic package" is a structure that serves to protect a microelectronic circuit (silicon die) from its environment and allows both mechanical and electrical connections. The performance of the microelectronic circuits is affected by package design. Packaging serves several distinct functions in microelectronics as listed below:

(a) protection of the device from mechanical and chemical hazards,

(b) signal and power distribution,

(c) signal timing, and

(d) heat dissipation

Consequently, packaging of electronic components, in particular integrated circuits (IC), has become an issue that challenges the microelectronics industry today [1]. Essentially, the point has been reached where advancement in IC performance now drives packaging technology. As the trend of the microelectronics industry has gone towards higher circuit densities and operating speeds, several effects have become important for packaging technology. One of those problems in high density IC packages (e.g., flip-chip assembly) is the delamination between epoxy adhesives and polyimide passivation layer [2] because the adhesive strength at the interface is reported as very weak [3]. An IC package is made of a variety of materials ranging in nature from ductile, as in the metallization of the leadframe, to brittle, as in the silicon based devices, the plastic of a molded package, or the ceramic of a ceramic package. The materials that make up the electronic package are crucial to its ability to function properly and reliably. In addition, the difference in their properties, such as thermal expansion and elastic moduli, lead to the generation of stresses when the package is subjected to thermal excursions.

Several different types of package have been developed. Some of them will be listed as the following [1,4-5].

(a) Single-In-Line Package (SIP)

The single-in-line package has a single row of leads extending from one edge of a package (see Fig. 1.1 (a)). SIPs are usually through-holes packages where the leads are inserted into metallized vias in the printed circuit board. When the leads come out from a single edge of the body but are formed into a zigzag pattern, the design is called a zigzag-in-line package (ZIP). This kind of design can increase the lead density. The advantage of SIPs is the use of minimal circuit board area.

(b) Dual-In-Line Packages (DIPs)

Rectangular dual-in-line package is one of the earliest packaging designs. It is also the most popular package design. DIP has I/O (input/output) leads, which extend from two opposite sides of the package and are bent downward (Fig. 1.1 (b)). Most DIPs are designed for through-hole interconnection. The leads of DIPs are inserted through holes in the PWB and soldered to the back of the board. Lead counts for DIPs range from 8 to 68 [1]. Above 68 leads, molding and leadframe problems limit the production of larger DIPs because of excessive cost, and as the number of the leads is increased, the DIPs take too much space on printed circuit board. The advantages of Plastic DIPs (PDIPs) are low cost and a predictable uniform factor. However, PDIPs have not been recommended for use in high-temperature/moisture environments.

In ceramic DIPs (CDIPs), the integrated circuit die is sandwiched between the two ceramic plates. The bottom half of the sandwich holds the integrated circuit die, while the top of the sandwich protects the integrated circuit die from mechanical stress during sealing operations. The leads of CDIPs are the same as that of PDIPs; however, leadframes can be brazed to the top or side of the package, which makes them superior to PDIPs in lead strength. CDIPs are expensive; nevertheless, they are preferred for high-quality electronic system because of their high reliability.

(c) Chip Carrier

When the number of leads is high, DIP becomes impractical and wasteful of circuit board area. Therefore, packages with leads on all four sides (chip carrier or quads, see Fig. 1.1 (c) for its structure) are preferred in high-pin-count packages. There are three main types of chip carriers: ceramic and plastic leaded chip carriers (PLCC) and leadless ceramic chip carrier (CLCC, or LCC).

(d) Pin Grid Array (PGA)

A pin grid array is a type of chip carrier package where the leads are not restricted to the edge of the package, but are instead distributed in an array over the entire area of the package (see Fig. 1.1 (d)). This kind of package is typically used with VLSI (very large scale integration) chips with lead counts greater than 100.

(e) Quad Flat Pack (QFP) and Plastic Quad Flat Pack (PQFP)

QFP is the fine-pitch, thin body version of the LCC, with leads on all four sides of a square or rectangular package. The body of the package can be either plastic or ceramic. The flat pack is similar to the DIP with the exception that the leads are bent outward to form a flat surface (Fig. 1.1 (e)) and are mounted on pads rather than inserted into holes in the board. A rectangular geometry can accommodate a greater interconnection density on a circuit board with a pin count over 256.

(f) Ball Grid Array (BGA)

BGA package has evolved from the flip-chip technology, also refer to as controlled collapse chip connect (C4) for ICs. There are solder bumps on the substrate. The solder bumps can be rearranged in a uniform full matrix array, a staggered full array, or around the perimeter in a multiple number of rows (Fig. 1.1 (f)). BGA package provides more I/O than quad flatpacks. Thus, BGA package is considered the package of choice for high-density and high I/O ICs.

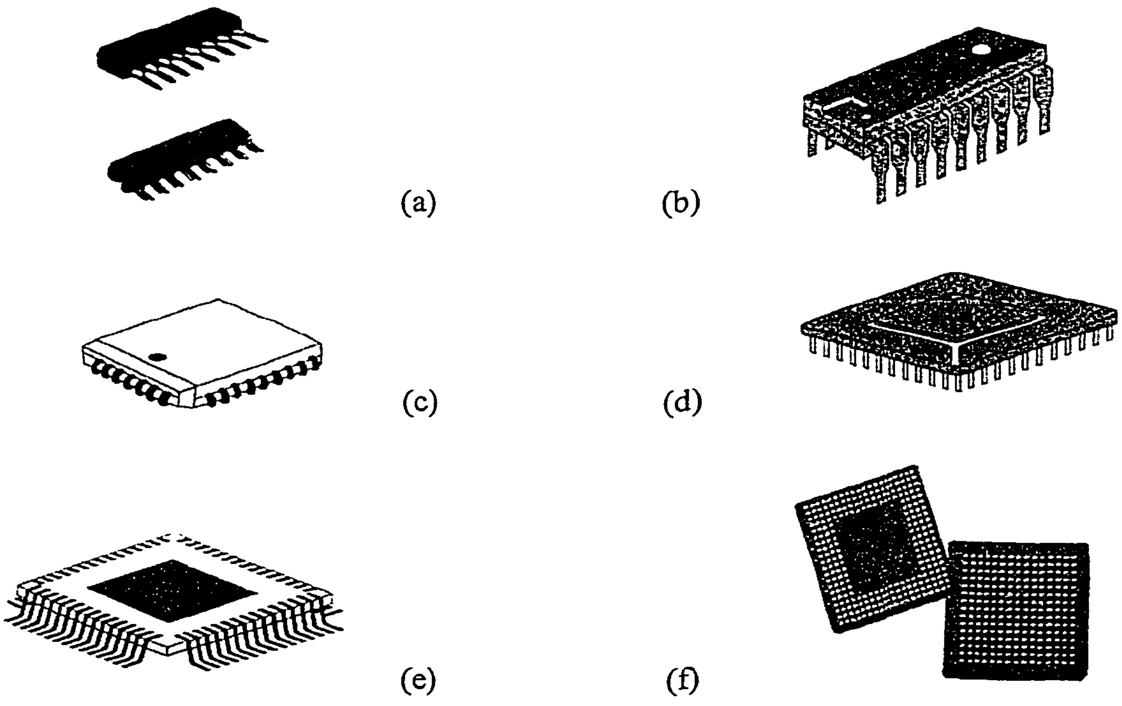

Fig. 1.1: Commercially important package types [6].

Plastic packages are less expensive than other package options, yet they provide performance and reliability that is acceptable for most products except those with the strictest reliability criteria, notably military hardware [3]. However, continued improvements in the passivation and protection layers on the device and further improvements in the packages themselves will continue to promote the use of plastic packages.

In plastic packaging, the most widely used materials are epoxy-based resins because epoxies react with a variety of curing agents, and resin systems can be formulated with a wide range of properties such as high mechanical strength, low cure shrinkage yielding low residual stress, good wetting and adherence, fast curing, low moisture permeability, sufficient dimension stability, reasonable end use temperatures, effective dielectric properties, and a wide range of viscosities [6]. However, new epoxy resins will need to be formulated as the reliability performance of advanced packages increase.

In this study, only epoxy polymers, which are used as the adhesives in electronic packaging, will be discussed. Both commercial epoxy adhesives and model epoxies were studied. For commercial adhesives, they were focused on constructing the processing diagrams for underfill resins. This study also intended to understand the developed stress during the curing of epoxy. The created cure stresses of a commercial die attach adhesive (see Appendix) and underfill resins were investigated. However, the complete compositions for commercial materials are proprietary and generally not known, which makes it difficult to understand their characteristics during the curing. Therefore, model epoxies had been used to get a better understanding of their kinetics and of stress development. Throughout this study, it had been attempted to develop a model to explain stress generation during curing.

CHAPTER 2

Background

2.1 Processing Diagram

The construction of a cure diagram for thermoset resins has been developed in the 1980s in the form of the isothermal time-temperature-transformation (TTT) cure diagram (Fig.2.1) [7], thus providing an intellectual framework for understanding the curing processes. The TTT isothermal curing diagram records the phenomenological changes that occur during the cure reaction of the thermoset, such as gelation and vitrification. The diagram also contains a carbonization or thermal degradation curve and iso-T_g curves.

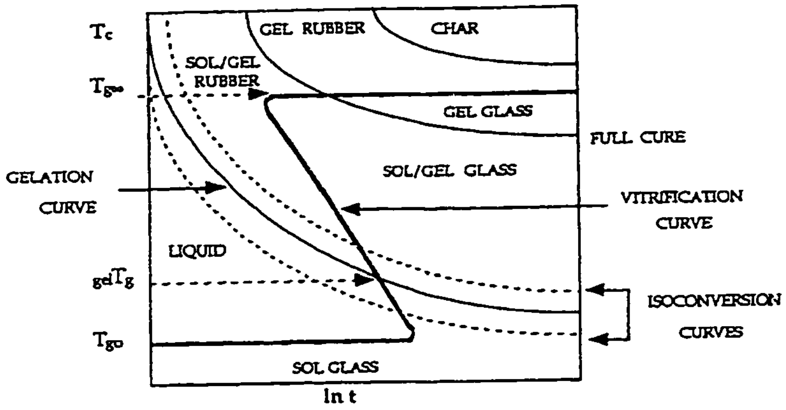

Fig. 2.1: Generalized TTT isothermal cure diagram.

On the diagram three temperatures play an important role. T_{go} is the temperature below which no significant reaction of the system occurs, usually the glass transition temperature of the uncured reactants. It can be considered as the storage temperature of uncured resin mixture. $T_{g,\,gel}$ is the temperature at which gelation and vitrification can occur simultaneously. This may be found in the ideal system. $T_{g\infty}$ is the cure temperature at which the degree of conversion reaches its maximum value. Theoretically $p = 1$ at a fully cured stage; however, from the experimental standpoint it is impossible to reach this value. If the cure temperature lies between T_{go} and $T_{g,\,gel}$ the liquid resin will react until its glass transition reaches the cure temperature, then vitrification will start. Thus, in this cure temperature range no gelation is taken place. Between $T_{g,\,gel}$ and $T_{g\infty}$, gelation occurs before vitrification. Above $T_{g\infty}$, which is the glass transition of the fully cured resin, the material cannot vitrify at the cure temperature. The TTT cure diagram can be used as a guide for scheduling the cure temperature for ones system. Depending on the value of $T_{g\infty}$-T_{cure}, a resin may vitrify before reaching the completed cross-linking, leaving the system in a nearly-stable undercured state. The resin then has a glass transition temperature less than $T_{g\infty}$. Many mechanical properties including various moduli, hardness, and tensile and shear bond strengths of undercured resin are similar to those of the fully cured state. J. W. Sinclair [8] studied the effects of incomplete resin cure on the dynamic moduli and tensile strength of amine-cured epoxy adhesives. It has been revealed that storage modulus (G') dropped significantly at a temperature higher than T_g. This is because at that temperature the undercured resin is in an incompletely cross-linked elastomeric state with low modulus. The degree of undercuring is a considerable factor in adhesive strength. Therefore, to schedule the temperature for curing, T_g of resin must be considered.

Although a TTT isothermal cure diagram can be a guide for a production engineer in choosing a cure temperature to avoid the vitrification, it cannot provide the optimum cure schedule for adhesive curing in electronic packaging technology. This is because in the adhesive field, bond strength is the most important factor. To achieve a reliable device, the appropriate processing diagram should be developed for the particular type of thermosetting resin.

A remarkable bondability diagram was developed for die attach adhesives [9, 10] as in Fig.2.2. Such diagram was built on a fundamental understanding of the phenomena occurring during the cure process to provide a processing window. The diagram summarizes the phenomena that have an impact on adhesion and reliability at the adhesive/substrate interface such as effects of gelation, extent of reaction, degradation, surface tension, melt viscosity, and cure stress. In this diagram, the upper limit of the processing window is defined by the temperature at which degradation reactions, outgassing, resin bleed, and surface oxidation will occur. The lower limit is the onset cure temperature. Polymerization below this temperature leads to low performance products due to the formation of voids. This work also studied the effect of extent of reaction on the adhesive shear strength and found that shear strength is strongly related to the extent of reaction (Fig. 2.3). The extent of reaction lines establish the short and long time limit at isothermal cure temperature. The minimum time to provide high enough extent of reaction (> 90%) to give a high strength cured adhesive, while the maximum time indicates no improvement in properties with additional cure. Such a bondability diagram is a guideline for processing optimization for die attach adhesives. In case of underfill resins, their processing is different from that of die attach adhesives. Therefore, the processing diagram for this particular system should be constructed. In this work it has been intended to construct processing diagrams for underfill resins.

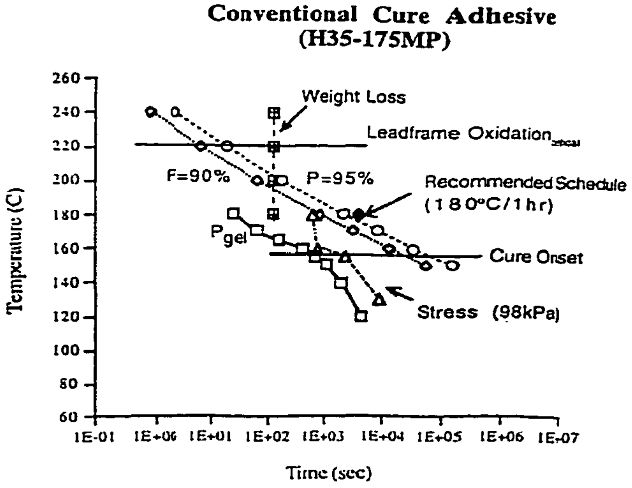

Fig. 2.2: Bondability diagram for H35-175MP die attach adhesive.

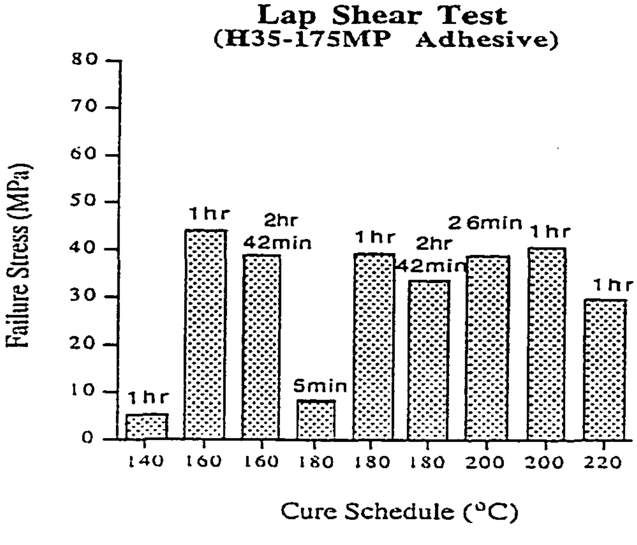

Fig.2.3: Lab shear strength of H35-175MP at different cure schedules.

2.2 Underfill Resins and Their Requirements

Flip-chip technology is where a solder-bumped silicon die is inverted and attached directly to a chip carrier [6]. The necessity of using an underfill encapsulant for improving flip-chip device reliability is well documented [11, 12]. The major advantages of flip-chip packages are higher input/output (I/O) connections, higher speed, lower emission, smaller sizes, and better heat transfer characteristics. In recent years, flip-chip technology has migrated to systems using larger and much more powerful chips. Due to high I/O density, flip-chips have become larger, bump pitches have become finer [11], and their locations have become quite complex and unpredictable; therefore, underfill resins have been required to optimize the penetration speed and resistance to void formation. To ensure desirable reliability performance, underfill must be resistant to filler segregation during penetration, which is done at elevated temperatures. In addition, underfill resins should have wetting capability and good adhesion with both the substrate (with and without solder mask) and the outermost passivation layer of the chip. One of the issues that must be considered in flip-chip assembly is the difference in the coefficient of thermal expansion (CTE) between the chip and substrate (organic material or ceramic). As temperature increases, the substrate and chip start to expand at different rates, but the solder bumps attempt to keep the die and substrate together. Therefore large stresses are developed in the bumps, which often results in solder joint fatigue. The use of underfill resins, which surround the solder bumps and fill the space between the chip and substrate, has typically resulted in a 5-10 times improvement in package reliability, but solder fatigue remains the major failure mechanism [13]. The CTE of epoxy resin is lowered by adding 65-75 % of filler (silica is the most commonly used) in order to get the value to close to that of solder (20-40 ppm/°C). However, filler affects the flow of underfill between the chip and substrate; therefore it is crucial to study optimization of filler characteristics and flow behavior of underfill resins. Finally, in order to maintain flip chip device reliability during operation, the underfill resin should have low ionic content, low alpha particle content, and low moisture absorption.

2.3 Fundamentals of Manufacturability

The underfilling process is conceptually simple and fast. The most important variables are dispensing volume and adhesive viscosity. Viscosity changes rapidly with time and temperature, making temperature control critical throughout the system. Advanced IC packaging is being driven toward smaller sizes with higher I/O requirements, especially for microprocessors, telecommunications, consumer devices, and automotive electronics [14]. The elimination of the need of wire bonding from chip to leadframe is the most compact and efficient of flip-chip packaging. The wire bonds are replaced by small metallic (Pb/Sn or Pb/In alloy) bumps (generally 100-250 μm in diameter and 50-200 μm high) on the circuit side of the chip (Fig. 2.4). The connection from the chip to the substrate is made by placing the chip circuit side down onto pads and reflowing the bumps to make a connection. This circuit-side-down placement of the chip gave rise to the name “flip-chip”. The process was patented by IBM and called “C4” (Controlled Collapsed Chip Connection). The interconnections of this design are made on the inside of the chip, providing shorter transmission paths and higher speed. Moreover, the package also allows efficient heat transfer because a heat sink can be directly attached to the chip, rather than working through an encapsulant cover or leadframe. The assembly is quite simple as is described at the following [14]. After the pads or bumps are fluxed, the chip is placed onto them. Then the bumps are reflowed onto the I/O pads. After that the parts may go into a preheated station where they are heated 70-100 °C, then moved to the underfill dispensing station. The underfill dispenser delivers a volume of adhesive in a straight line along the chip's perimeter (one or two sides). Proper underfilling requires a heated substrate to heat the dispensed epoxy to lower its viscosity. The capillary force draws the epoxy under the chip. After that, the parts are moved to a post-heat station to complete the filling. Then another dispenser dispenses a bead of encapsulant around the entire chip in order to eliminate any induced stress caused by unsymmetrical fillets on the chip. Finally the parts are sent to a curing oven to cure the adhesive fully. In order to process successfully, various characteristics of underfill resins were studied.

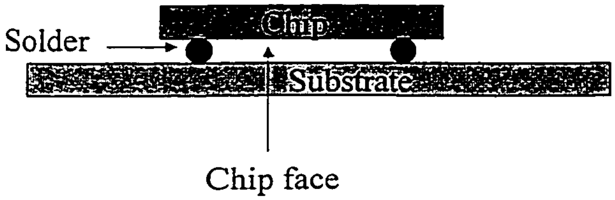

Fig.2.4: Schematic diagram for flip-chip assembly.

2.4 Characterization of Underfill Resins

In flip-chip assembly, the most desirable underfill resins are those with fast processing (cost-efficient) and with no voids (reliable). In order to obtain these goals, several techniques must be applied to understand the behavior and characteristics of underfill resins. From the assembly procedure as mentioned previously, two steps of processing are needed: underfilling and curing of the adhesives. The factors that influence underfilling are viscosity, surface tension energy, contact angle of adhesives on substrates, and the gelation time. To design a curing process, void formation, extent of reaction, cure stress, and adhesive strength had been investigated. Determining these characteristics leads to proper processing, and a reliable product can then be obtained.

2.4.1 Flow Behavior

As the standoff height in flip chip assembly continues to decrease, the number of challenges in the study of an underfill resin as a liquid/particle suspension increases. Many factors can play a role in the rate of flow of the underfill in the gap [15]. These factors include the filler particles factors (e.g., loading, size, size distribution, surface morphology, shape, material, density, and dispersion), underfill material factors (e.g., temperature, rheology, density, and surface tension), gap surface factors (e.g., temperature, surface energy, and roughness), and obstructions (e.g., solder bump pattern, particle size to gap height ratio, and contamination). The flow rate of an epoxy material under the chip is not linear. Initially the flow rate is very high, then the material flows at a slower rate as shown in Fig.2.5 [16]. The flow of underfill resin in the standoff region between the chip and substrate is explained by the capillary flow process. As mentioned earlier, an underfill resin with the desired CTE is commonly obtained by adding high volume fraction of solid particle filler to an epoxy resin. Nevertheless, the effects of such fillers on the capillary flow process are not well understood [17].

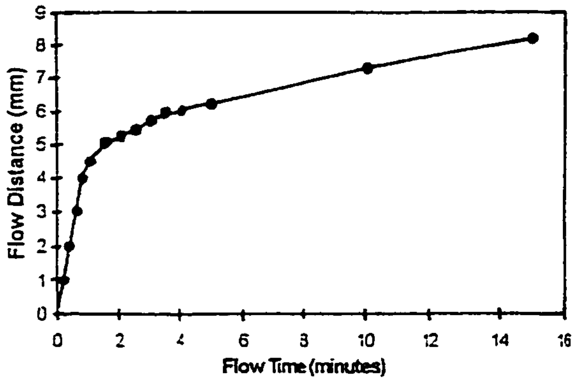

Fig. 2.5: Flow rate of an epoxy based flip chip materials with 65% silica filled by weight. Capillary flow was on glass; with a 3 mil gap; the substrate was heated to 70 °C [16].

A simple flow model was presented by Lehmann et al. [18] as in Fig. 2.6. The suspension displaces an air body. The position of the liquid-air interface (x_f) is measured as a function of time, t. In this model solid particles are suspended in a carrier liquid as a single phase, and the air and suspension are taken as Newtonian fluids. In both regions the local flow conditions correspond to laminar, Poiseuille flow. It has been found that the overall features of the flow correlate with the Washburn model [19]:

$$\frac{d}{dt}(x_f)^2 = \frac{\gamma}{6}(\cos\theta_o + \cos\theta_s)\frac{s}{\eta_o} = b \qquad (2.1)$$

where γ is the liquid surface tension, θ_o and θ_s are the contact angles at the lower and upper channel surfaces, s is the channel spacing, η_o is the resin viscosity, and b is the flow parameter, which is independent of time. Driscoll et al. [20] stated that Equation (2.1) is valid for suspensions of relatively small particles (s/d size>>1) or neutrally buoyant particles. However, for negatively buoyant particles (ρ_s/ρ_o>1) and the particles whose sizes approach the channel spacing, the flow parameter varies with time, which is believed to be caused by particle settling.

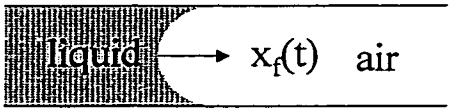

Fig. 2.6: Sketch of a capillary flow through a planar channel.

The first generation of underfill resins enhance penetration speed by lowering a viscosity with a carboxylic acid anhydride curing agent [21, 22]. However, carboxylic acid anhydride curing agent readily absorbs moisture to generate carboxylic acids. Free carboxylic acids react with epoxides to rapidly increase the viscosity of the resins and to degrade its penetration capability. Moisture also causes a volumetric expansion to lift solder bumps and increase contact resistance. Anhydride cured underfill resins absorb high moisture because of their polarity, and at high temperature they consume more moisture due to the hydrolysis of ester linkages. Sumita et al. [23] claimed that amine catalyzed ring opening polymerization of epoxides is a better underfill. It exhibits low stress performance along with excellent penetration capability. It is also resistant to hydrolysis and has an improved storage/floor stability. Furthermore, the reduction in viscosity could be accomplished by adding large percentages of low molecular weight epoxy resins to the system [16]. The low molecular weight species causes extensive cross-linking with lower molecular weight between cross-links (M_c). This formulation thus leads to high shrinkage upon cure, high internal stress, and high modulus of elasticity.

2.4.2 Viscosity and Gelation

Viscosity of an underfill resin should be in the range of 1,000 to 3,000 Pa.s in order to facilitate penetration [16]. Before dispensing the underfill resin into the standoff between the chip and substrate, the assembly is preheated in order to lower the viscosity of the underfill resin. However, the cross-linking reaction also occurs during this step, which causes an increase in viscosity. Therefore, it is important to study resin viscosity as a function of temperature and time. Rheology is a powerful tool for observing the gelation process. The evolution of molecular structure has a very pronounced effect on molecular mobility, which is easily monitored by the change in viscosity and elasticity. To understand how viscosity is changing while cross-links are formed, the total volume of a polymer is considered in detail. Hesecamp et al. [24] described the total volume of a polymer as a sum of the intrinsic volume of the molecules (V_m) and the free volume (V_f). The intrinsic volume includes the volume occupied by the molecular chains and the volume covered by the oscillations of the molecular chains. Note that the volume of oscillations of molecular chains is occupied and cannot be replaced by other molecules. A cross-linking leads to a decrease of the intrinsic volume because the mobility, and therefore the oscillation capability of the molecular chains, is reduced by the cross-links points as in Fig. 2.7. The free volume is the volume of holes between the molecular chains. A conformation rearrangement of a molecular chain can occur only if V_f is large enough. Cross-links caused densification, diminishing the hole volume. Therefore, the conformational rearrangement is impeded, which leads to the increase in viscosity. Eloundou et al. [25] studied the temperature dependence of dynamic rheology in the epoxy-amine system. The dependence of initial real part of the complex viscosity, η'$_0$ (measured at time zero) on temperature between 80 and 160 °C is shown in Fig. 2.8. The viscosity of the initial monomer mixture decreases as a function of temperature. This η'$_0$ data obeys an Arrhenius law (Equation 2.2) in the temperature range considered.

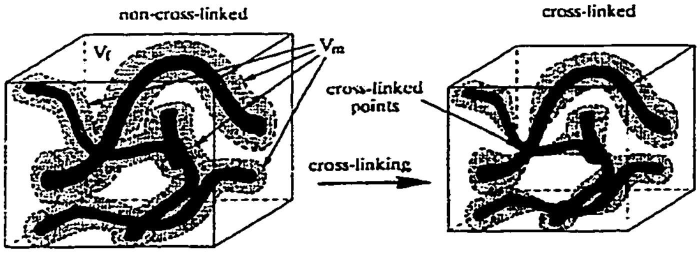

Fig. 2.7: Influence of cross-linking on the volume of a chemically cured adhesive.

$$\eta = Ke^{E_a/RT} \tag{2.2}$$

where η is viscosity, K is a constant, E_a is the activation energy, R is gas constant, and T is temperature. They also investigated the real part of the complex viscosity as a function of cure time at different temperatures before the gel point, the result is shown in Fig.2.9.

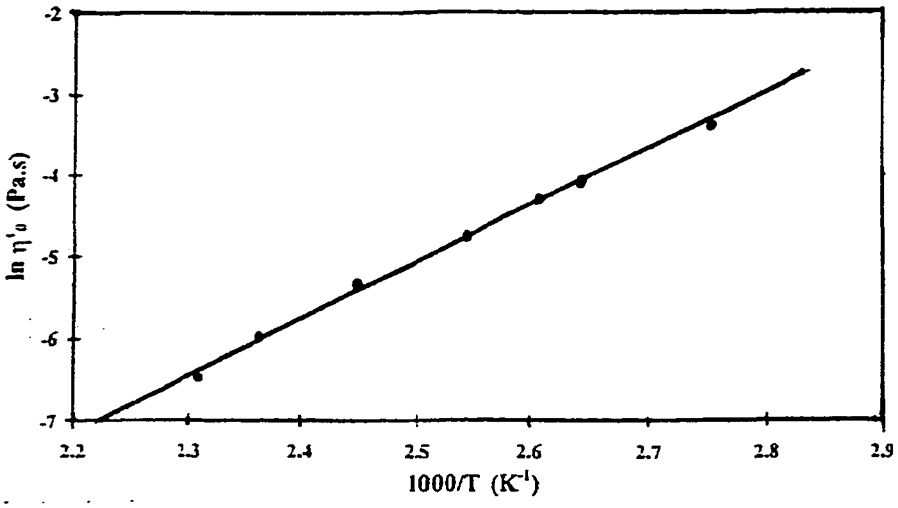

Fig. 2.8: Arrhenius plot of the real part of dynamic viscosity at the initial time, η'_0 of DGEBA and 4,4'-methylenebis[3-chloro-2,6-diethylaniline.

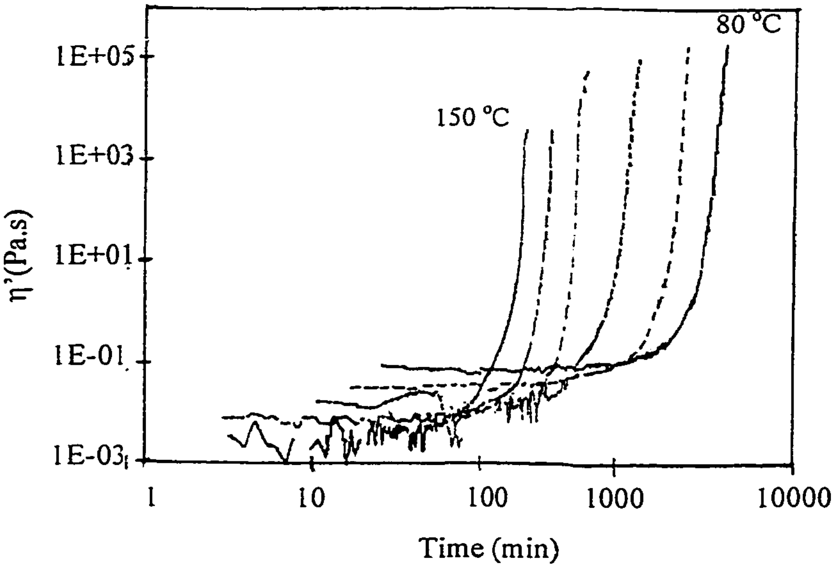

Fig. 2.9: Dependence of the real part of dynamic viscosity, η', with time of reaction obtained from experimental results at 80, 90, 105, 120, 135, and 150 °C of DGEBA and 4,4'-methylenebis[3-chloro-2,6-diethylaniline].

The underfilling process has to be completed before the resin has gelled since, after this point, the flow is not possible. Therefore, one of the most important factors influencing the processing of thermosetting resins is gelation. When gelation initiates, resin viscosity rises exponentially and thus has a marked effect on processing. Consider the forming of a molecule during curing; the cure of epoxy resins involves the formation of a rigid three-dimensional network by reacting with hardeners that have more than two reactive functional groups ($f>2$). The cure of epoxy resins is complicated, and it is useful to visualize the process in several stages as illustrated in Fig. 2.10 [26]. Initially there is a reaction between epoxy and hardener reactive groups, thus slightly larger molecules are formed, which are called oligomers. As cure progresses, molecules become larger and larger; however, the average molecular size is still small, even when half of the reactive groups have reacted. Eventually, the molecular size increases to that of very highly branched molecules. Then more and more highly branched structures are developed. During these stages, the system is considered a liquid polymer, which is called a "sol" since it is soluble in good solvents [27]. When the branched structures extend throughout the whole sample, the system reaches the gelation point. After this critical point, the system is called "gel". It becomes solid and is not soluble even in a good solvent; however, low molecular weight molecules (the sol fraction) are still extractable from the gel. Consequently, the curing sample contains sol as well as gel fractions. The gel initially formed is weak and can be easily disrupted. To produce a structural material or a good adhesive, cure has to continue until all or most of the sample is connected into the three-dimensional network.

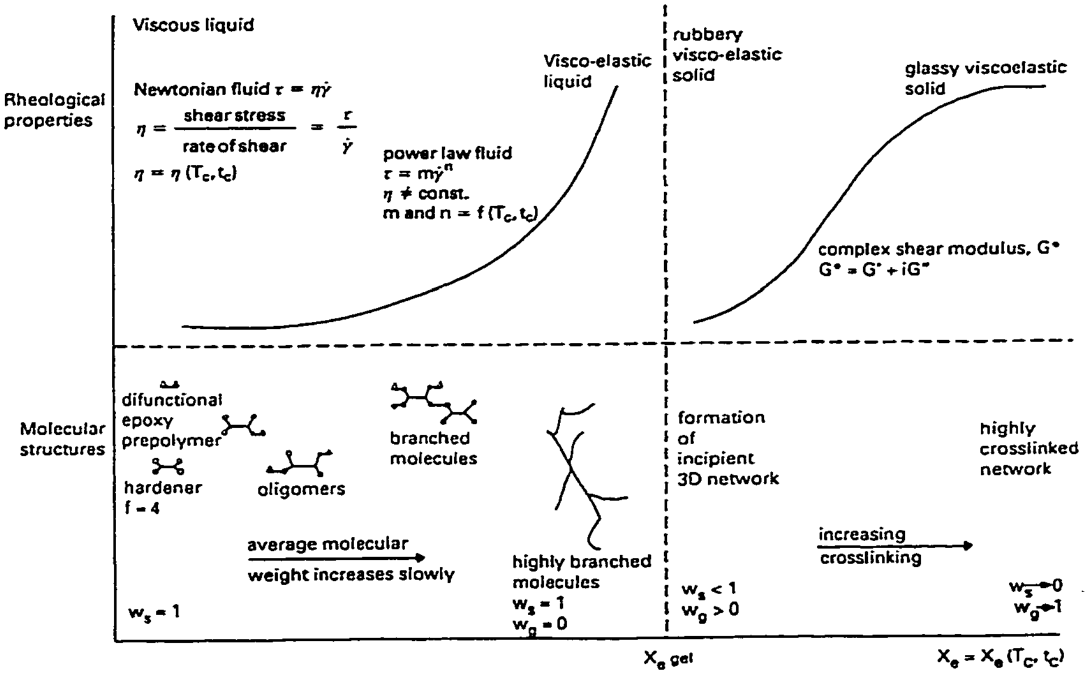

Fig.2.10: The cure of epoxy resin [26]. Note that $X_e = p$, the extent of reaction.

2.4.3 Filler Settling

Filler settling takes place when the viscosity and the curing rate of the epoxy resin are not well balanced. For rapid penetration, viscosity of resin is often set too low, therefore the filler segregation can happen. An optimized cure schedule, and a proper type and amount of catalyst can minimize such filler segregation. The density difference between silica particles (2.4 g/cm^3) and epoxy in liquid state (1.15 g/cm^3) creates a negative buoyancy which can give rise to settling effects. Due to the higher density of filler, it tends to settle when stored or during a curing process. The schematic diagram in Fig.2.11[28] shows an example of the curing process of a typical thermosetting epoxy casting resin, as represented by density changes. From point A to point B, the density decreases due to the thermal expansion of the liquid epoxy; B-D is a shrinkable process due to the reaction; D-F is a thermal shrinkable process of a fully cured resin. Point C and point E are the gelation point and T_g respectively. The settling can occur in the path of A-B-C. The rate of sedimentation can be represented by Stokes Equation [29] if a particle is uniform and a suspension is homogeneous. The equation is given as the following:

$$H = \frac{g(d_p - d_s)D_p^2 t}{18\eta_s} \tag{2.3}$$

where H is the settling distance of the filler particle, g is the acceleration due to gravity, d_p is the density of the filler, d_s is the density of the suspension, D_p is the diameter of the filler, t is the settling time (~ gelation time of the suspension), and η_s is the viscosity of the suspension. Since η_s varies as the cure proceed, therefore Equation (2.3) can be put in the form of Equation (2.4). In this case η_s in a short time Δt_k is considered to be constant.

$$H = \frac{g(d_p - d_s)D_p^2}{18\eta_s} \sum_{k=1}^{n} \frac{\Delta t_k}{\eta_s(\alpha_k)} \tag{2.4}$$

where $\Delta t_k = t_k - t_{k-1}$ ($t_o = 0$, and $t_k =$ t), α_k is the middle point in Δt_k, and $\eta_s(\alpha_k)$ is the viscosity at α_k.

However, as the concentration of particle increases, the settling velocity decreases. This is because the density of the suspension becomes larger than that of fluid, which raises the buoyancy of a particle.

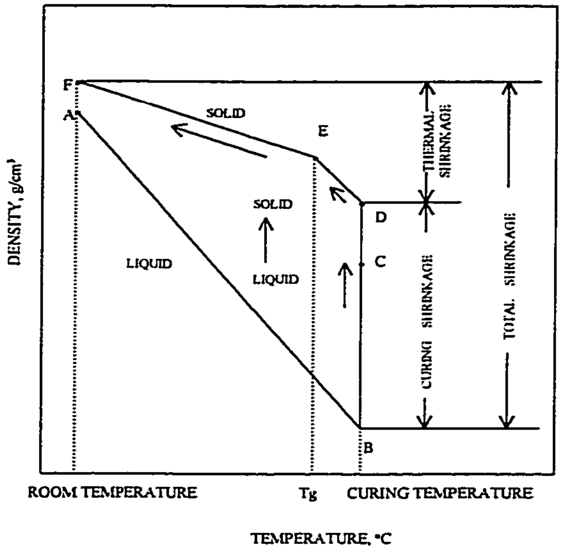

Fig. 2.11: Schematic diagram of density changes of a typical epoxy casting resin during the curing process.

2.4.4 Adhesion

Reliability of the packaging technology substantially relies on the adhesion between the substrate and adhesive. Adhesive strength depends upon the rheology of an adhesive as well as its interaction with substrate. There are many factors affecting the adhesion [30], including acid-base interaction, cleaning adhering surface, surface modification, environmental condition, extent of reaction, type of adhesive promotion. Therefore, to successfully understand adhesion one requires a combination knowledge of physical chemistry of surfaces and polymer, rheology of polymer, and fracture mechanics [31]. It is now generally recognized that the principal forces contributing to the work of adhesion between two phases, W_A, are the Lifshitz-van der Waals forces and acid-base interactions. Dupré [32] has defined the work of adhesion as the energy required to pull apart two adhering materials and create new surfaces of materails 1 and 2. Therefore, it is assumed that the adhesion strength is at least proportional to the work of adhesion [33]. Maugis [34] has developed a theoretical basis for W_A. W_A is the Helmholtz free energy change per unit area. It can be expressed in terms of surface free energy by following the first law of thermodynamics, and is called Dupré Equation:

$$W_A = \gamma_1 + \gamma_2 - \gamma_{12} \qquad (2.5)$$

where γ_1, γ_2, and γ_{12} are surface free energies (or surface tension) of material 1 and 2 (assuming they will contact with air) and the interfacial free energy of material 1 and 2 interface respectively. Nevertheless, the surface free energy of a solid and at the interface is not generally accessible. The unavailable terms can be replaced by using the Young's equation:

$$\cos\theta = \frac{(\gamma_2 - \pi_e) - \gamma_{12}}{\gamma_1} \qquad (2.6)$$

Combining equation (5) and (6), one obtains the Young-Dupré equation:

$$W_A = \gamma_1(1 + \cos\theta) + \pi_e \qquad (2.7)$$

where θ is the contact angle of material 1 against material 2, and π_e is the equilibrium spreading pressure of the liquid's vapor upon solid (if material 1 is liquid, and material 2 is solid). π_e is effectively zero for many low-energy solids [35]. Therefore, Young-Dupré equation can be simplified to:

$$W_A = \gamma_1(1 + \cos\theta) \qquad (2.8)$$

One of the properties, which are important to adhesion, is the wetting between two surfaces. The key to understand the wettability is the recognition that it is determined by the balance between adhesive forces (between the liquid and solid) and cohesive forces in the liquid. Adhesive forces cause a liquid drop to spread. Cohesive forces cause the drop to ball up. The contact angle is determined by competition between these two forces [36]. The contact angle is readily measured by optical goniometer as done by Lloyd [37].

Wetting may be thought of as the process of achieving molecular contact [38]. The extent of wetting may be defined as the number of molecular contacts between the two phases comprising the system relative to that exhibited when wetting is complete. Equilibrium contact angles are functions of the surface free energies of the solid substrate and the liquid and of the free energy of the interface between two phases as show in Equation (2.8) above. Huntsberger [38] claimed that equilibrium contact angle represents the extent to which a liquid spreads over the substrate and not the extent of wetting at the interface. Fig. 2.12 shows the spreading of fluid adhesive over a nonplanar substrate. The system is depicted in a state in which the solid is not completely wetted (upper) and the wetted state (lower). Johnson et al. [39] found that both stable and metastable equilibria can be encountered in systems exhibiting incomplete wetting. Hunsterberger [38] proposed the new form of Young-Dupré equation by considering the change in surface free energy associated with the change from any given nonwetted state to the wetted state for a single asperity. The change in free energy is expressed by Equation (2.9).

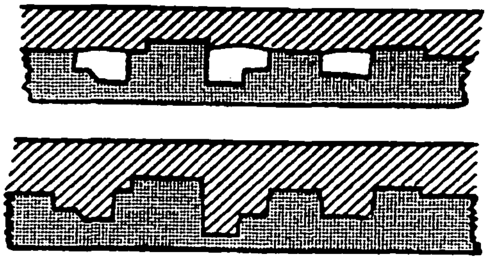

Fig. 2.12: Wetting of solid substrate by fluid adhesive. Substrate incompletely wetted (upper); substrate completely wetted (lower).

$$\Delta\gamma = \Omega^{SV}\gamma_{SL} - \left[\Omega^{SV}\gamma_{SV} + A^{LV}\gamma_{LV}\right] \qquad (2.9)$$

where Ω^{SV} and A^{LV} are integrated or actual area of the solid-vapor interface and the area of the liquid-vapor interface, respectively, in the nonwetted state. γ_{SV} and γ_{LV} are the surface free energy of the solid and liquid phases, respectively in equilibrium with the saturated vapor phase. F_{SL} is the free energy of the solid-liquid interface. Therefore, the Young-Dupré equation then can be written in terms of surface free energy as:

$$\gamma_{SV} - \gamma_{SL} = \gamma_{LV}\cos\theta \qquad (2.10)$$

substituting the value $\gamma_{SV}-\gamma_{SL}$ in Equation (2.9) gives:

$$\Delta\gamma = -\gamma_{LV}\left[1 + \left(\Omega^{SV}/A^{LV}\right)\cos\theta\right] \qquad (2.11)$$

From Equation (2.11) the equilibrium complete wetting is expected unless $(\Omega^{SV}/A^{LV})\cos\theta < -1$. For most practical adhesive systems, the adhesive will exhibit equilibrium contact angles with the substrate of less than 90°. $\cos\theta$ will be positive, and thermodynamic equilibrium will correspond to a completely wetted state. The wetting and non-wetting conditions related to the contact angle of liquid on solid substrate as,

$\theta = 0^{\circ}$	*spontaneously spreading*
$0^{\circ} < \theta < 90^{\circ}$	*partially spreading*
$90^{\circ} < \theta < 180^{\circ}$	*non-wetting*

In flip chip assembly, different passivation on the chip, different solder mask materials on the substrate, and different types of solder and flux are used. Therefore, their surface properties have to be considered in order to understand their behaviors. They will all have some effect on the flow, contact angle, and wettability. Due to the fact that if the underfill resin cannot wet the surfaces of the gap it cannot flow through the gap. Thus, the rate of flow of an underfill resin in a gap of a given height is proportional to a rate of wetting.

There are a number of researchers trying to increase the adhesive strength between adhesives and various kinds of substrate [40-42]. The cleanness of substrate surface is critical to the adhesion. Wong et al. [40] studied several methods of cleaning the substrate surfaces. SiO_2, SiN, and SiON, the inorganic substance which are normally used as the coating materials in IC devices, were investigated and found that UV-O_3 and O_2-plasma cleaning alone can clean off the organic substances on the surface, but not the inorganic part. They proposed that by using the series of cleaning of EC-7 (d-limonene), surfactant, isopropanol, DI-water rinse plus UV-O_3 or O_2-plasma, the cleanest surface was observed. Polyimides have been widely used as protective overcoats and dielectric layers for semiconductor devices because of their low dielectric constant, excellent thermal and mechanical properties, and good planarizability [43]. Since polyimides lie in between the substrates (e.g., metals, and ceramics) and the adhesive polymers, the adhesion between polyimides and adhesives is important for the performance of semiconductor devices. Delamination is often seen at this interface. Yun et al. [44] improved the adhesion between polyimide and epoxy by treating the polyimide surface with amines. The adhesive strength is stronger by the reaction of primary amine of diamines and imide of polyimide. This reaction leads to the poly (amic amide), and then the other primary amine of poly (amic amide) reacted with the imide groups of adjacent polyimide chains to form a cross-linked structure.

There are numerous different tests, which are used for measuring the bond strength between an adhesive and a substrate. Fracture mechanics is applied to investigate both the cohesive and adhesive strengths [45]. In addition, the mechanism of failure is revealed by this approach. The fracture behavior of adhesive joints is extremely complex compared to bulk material. Fracture occurs at the interface of two materials. The required strength to pull the two materials apart relates to the work of adhesion. When the mechanically applied energy (fracture energy, G_c^{inter}) per unit extension of crack area is equal to or greater than the thermodynamic work of adhesion (W_A), the fracture can take place. The fracture energy of a real system is generally a rate dependent quantity, which can be several orders of magnitude higher than the thermodynamic work of adhesion. In these cases the excess energy (G_c^{inter}-W_A) is dissipated by a viscoelastic mechanism operating at or near the crack tip region [46]. Maugis [34] has proposed the interfacial strain energy release rate, G_c^{inter}, and the thermodynamic work of adhesion as:

$$G_c^{inter} = W_A(1+\phi) \qquad (2.12)$$

where ϕ is a term related to viscoelastic/plastic losses at the crack tip. For viscoelastic polymers, the maximum value of ϕ can be as large as the ratio of glassy modulus of polymer to its relaxed modulus [47-50]. On that account, considerable amplification of fracture energy is possible in viscoelastic systems. Gent et al. [51] proposed that strength of adhesion and cohesion consist of two factors as in the following equation.

$$G_c^{\text{inter}} = G_o\left[1 + f(R,T)\right] \tag{2.13}$$

where G_o is a threshold value, below which no failure occurs, the second term is a function of rate R of separation and temperature T, reflecting energy expended in irreversible processes [52-53].

2.4.5 Void Formation

Voids often develop during the processing of epoxy resins. These isolated pores are usually regarded as inhomogeneities and act as stress concentrators and consequently initiate plasticity or failure in materials. Thus the presence of such voids can reduce reliability. In composites, it is well documented that interlaminar strength is sensitive to voids [54-56]. Wisnom et al. [56] found that with a high fraction of voids the interlaminar strength was reduced; however, the ultimate failure occurred at much higher displacement compared to the discrete void. Shukla et al. [57] stated that voids increase the probability of vertical cracking. Edwards et al. [58] reported that voids can produce non-uniformity in stress across a die surface after temperature cycling. In addition voids may interfere in the performance of the device by causing a non-uniform temperature distribution and enhancing the susceptibility to delamination of the chip from the substrate. It also provides sites for moisture to accumulate in the chip assembly. There are two sources of void formation in a cured epoxy; phase separation of the volatile components in an underfill resins, and the trapped air bubbles which could be formed by non-uniform flow of an underfill during penetration. The size of filler is also important in developing a successful underfill material. The maximum filler particle size, including agglomeration of filler during the processing, cannot be larger than the 1/3 of the gap width. Void formation due to non-uniform flow was suppressed by optimization of the filler size distribution in reference to the gap between a chip and a substrate. It was found that the penetration time can be shortened and trapped air bubbles were reduced by using filler whose average particle diameter was below 1/10 – 1/20 of the gap size and maximum particle diameter was below 1/2 -1/4 of the gap [23]. When the average and maximum diameters of the filler used were above these ranges, the filler particles tend to aggregate at the tip of the gap, disturbing the flow and generating voids.

2.4.6 Stress During Cure

The impact of cure stress on the reliability of microelectronic packaging is different in case of die attach adhesive and underfill resin due to the fundamental difference in the assemblies. Die attach adhesive is used in wire bonding (Fig. 2.13) or tape automated bonding (TAB) assembly. In these kinds of assembly the back of chips are mounted to the leadframe by conductive die attach adhesive (the most common are silver filled adhesives) in order to allow electrical contacts. In this kind of assembly stress in the encapsulant is developed only in a horizontal direction. On the other hand, stress is developed in both horizontal and vertical directions (due to the CTE mismatch between chips and substrates) at the underfill resins under the chip in flip-chip assembly (Fig. 2.4). Therefore, the effect of stress in flip-chip assembly is more significant than in chip-on-board assembly.

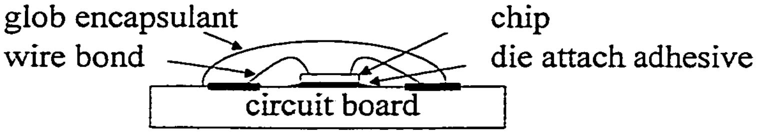

Fig. 2.13: Chip-on-board-attachment.

The magnitude of the residual stress developed in an epoxy resin depends on a number of factors, such as physical and mechanical properties (Tg, CTE, elastic moduli) of resins. In addition to the cure schedule, the degree of constraint also affects the magnitude of the residual stress. During the curing of epoxy resin, the mechanical properties change significantly from a liquid to a rubber- like solid, and subsequently to a glassy material upon the cool down process to below the glass transition temperature.

The build-up of residual internal stresses is related to the development of shrinkage strain and mechanical stiffness during the cure process. Although the cure stress is small and frequently neglected, it can cause delamination or fracture in the finished product, since the partially cured resin is not as tough as the fully cured resin. Such failures have been observed in polymer resins used to encapsulate a variety of electrical assemblies. One way to prevent such failures during cure and to improve the quality of encapsulated components is to optimize the curing process to reduce the cure stress.

When epoxy resin is cured, chemical reactions form a cross-linked, three dimensional molecular network. As the reaction progresses, the molar volume decreases while the viscosity increases. In the early stages of curing, epoxy resin is in the liquid form. At these stages, the liquid epoxy can flow to relax stresses. Eventually, the system reaches the gelation point where molecular weight becomes infinite. After this point, the moduli of cured resin increase as the reaction goes to the completion and stress is generated. There have been a number of investigators attempting to predict the stress during cure. Vratsanos [59] and Plepys et al. [60-61] used an incremental approach to linear elasticity and assumed that the material is isotropic and no viscoelastic behavior is presented. The stress increment is calculated from strain increments encountered over a period that the material properties are assumed to be constant. In this study, the equation was generated based on the fact that the total strain in the resin during the curing comes from three sources, which are the mechanical strain, the linear shrinkage due to chemical reaction, and the thermal expansion due to temperature changes.

The general equation of thermoelastic material is as the following equation:

$$E(T,p)\{d\varepsilon_{ij} - \delta_{ij}[\alpha_T(T,p)dT - \alpha_p(T,p)dt]\} = [1+\upsilon(T,p)]d\sigma_{ij} - \delta_{ij}\upsilon(T,p)d\sigma_{kk} \qquad (2.14)$$

where, $d\sigma_{ij}$ is incremental stress, $d\varepsilon_{ij}$ is incremental strain, *E(T,p)* is modulus as a function of temperature and extent of reaction, $\alpha_T(T,p)$ is thermal expansion coefficient as a function of temperature and extent of reaction, *dT* is temperature increment, *dt* is time increment, p is extent of reaction, $\alpha_p(T,p)$ is linear rate of shrinkage due to reaction as a function of temperature and extent of reaction, $\upsilon(T,p)$ is Poisson's ratio as a function of temperature and extent of reaction, and δ_{ij} is the Kronecker delta.

If we consider a one-dimension constraint, Equation (2.14) is simplified to the following equation.

$$d\sigma_{11} = -E(T,p)\left[\alpha_T(T,p)dT - \alpha_p(T,p)dt\right] \tag{2.15}$$

Vratsanos [59] measured the stress and equilibrium tensile modulus (E_{eq}) during the isothermal curing of Epon 828/NMA (nadic methyl anhydride)/BDMA (benzyldimethylamine) system in a uniaxial dimension by Dynastat mechanical spectrometer (Fig.2.14).

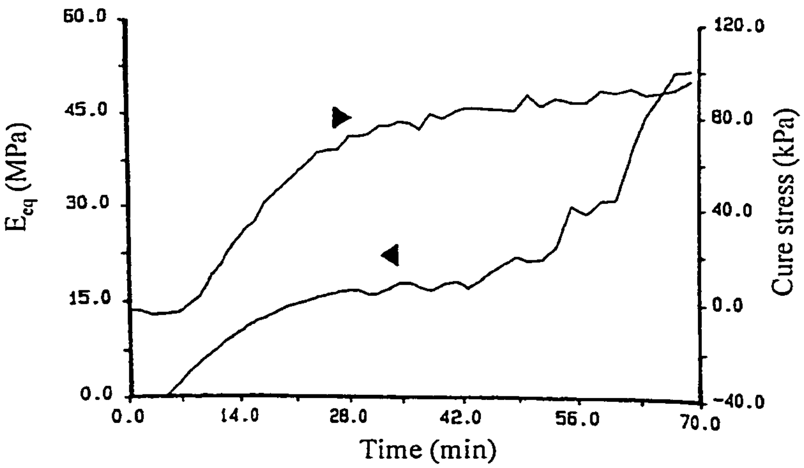

Fig. 2.14: Equilibrium tensile modulus and cure stress obtained during the isothermal polymerization of sample EPON/NMA/BDMA [59].

This work stated that the time at which E_{eq} becomes nonzero is the gelation time. Cure stress is generated at the point that E_{eq} becomes finite as dictated by Equation (2.15). Note that the magnitude of the cure stress is relatively small (85 kPa).

Chambers et al.[62] stated that rubber model (simplified to the linear elasticity equation) gives a matched predicted normalized hoop strain to the measured values when applied to the epoxy system which are cured at temperature higher than its T_g. However, this model is not valid if the resin is cured at lower than its T_g, thus a viscoelastic model is needed.

Adolf et al. [63-65] developed a formalism to predict the evolution of stresses during the curing of cross-linking polymers wherein the T_g exceeds the cure temperature, and found that the calculated values agreed well with the experimental values. They related the thermophysical properties to the extent of reaction, and calculated the stress based on the idea that the total stress is the sum of the shear contribution and the bulk contribution as Equation (2.16).

$$\sigma = 2\int_{-\infty}^{t} ds\left[G_d\left(\int_{s}^{t}\frac{du}{\tau(u)}\right) + < G_\infty(t,s) >\right]\left[\frac{d}{dt}\left(\gamma - \left\{\frac{1}{3}tr\gamma\right\}I\right)\right] + \int_{-\infty}^{t} dsK\left(\int_{s}^{t}\frac{du}{\tau(u)}\right)\left[\frac{d}{dt}(tr\gamma)I\right]$$

$$-\Psi(T - T_o)I - \Phi(p - p_{gel})I \qquad (2.16)$$

where, $G(t) = G_d(t) + G_\infty$ is the shear modulus, $K(t)$ is the bulk modulus, γ is the strain tensor, p and T are the extent of reaction and temperature, T_o is the temperature at the gel point p_{gel}, and I is the identity tensor. ψ is a constant equal to the product of the glassy bulk modulus, K_g, and the glassy volumetric coefficient of thermal expansion, α_g. Φ is a constant equal to the product of the rubbery modulus, K_∞, and the total volumetric strain due to cure. It can be seen that this equation includes four sources that cause the build-up the stress: imposed shear strain, imposed bulk strains, thermal expansion or contraction strain, and cure shrinkage strains. As we can see from the equation, bulk modulus is not sensitive to the extent of reaction. This is because the bulk modulus does not depend on the long-range network topology. So this group of researchers claimed that it is accurate to assume that the glassy and rubbery bulk moduli are independent of reaction. However, the shortest bulk relaxation time increases with the reaction, as revealed by the increasing glass transition temperature. From the last term on the above equation it can be noted that the total volume change upon cure is used instead of the incremental volume change as a function of the extent of cure as it should. Then they assumed a linear dependence of the volume on extent of reaction. To verify their equation, the equilibrium shear modulus as a function of extent of reaction and the stress during the isothermal curing of the EPON 828/DEA system were measured on RDA II (Figs. 2.15 And 2.16, respectively). These figures show a good agreement between the formalism and the measurements.

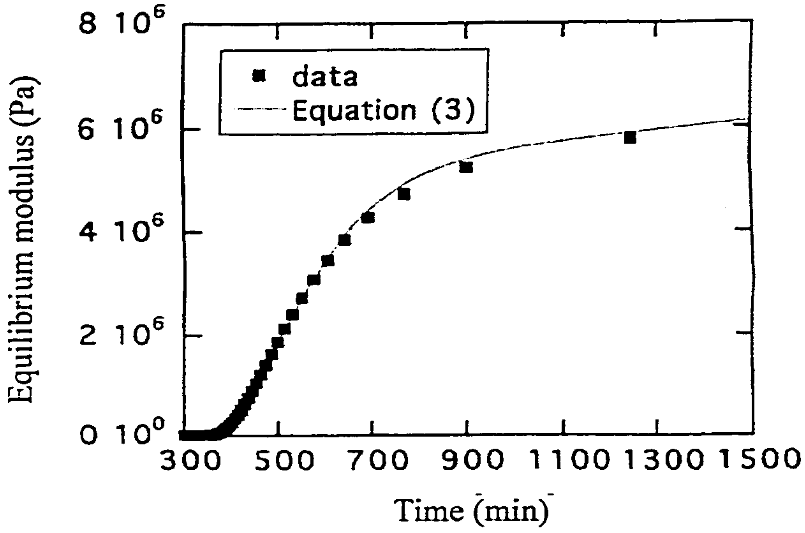

Fig. 2.15: The measured and predicted increase in equilibrium modulus with time as EPON 828/DEA isothermally cures at 65 °C.

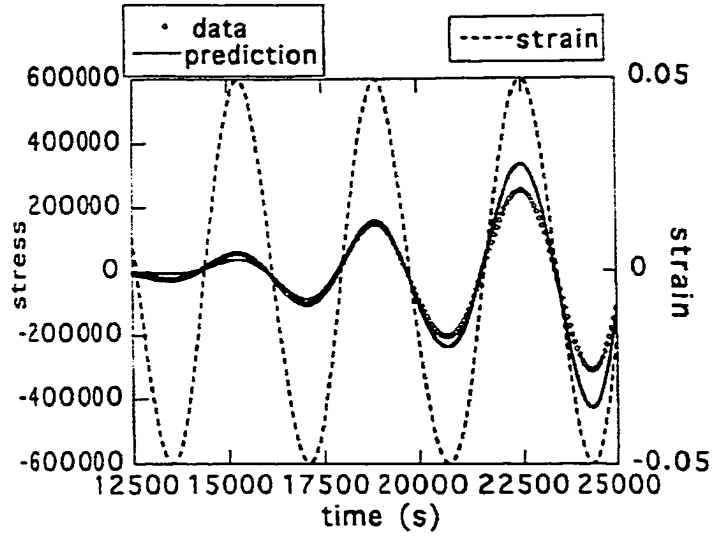

Fig. 2.16: The stress in response to a slow sinusoidal strain as EPON 828/DEA cured at 90 °C as measured experimentally and predicted by theory. The gel time is 12450 s.

Adolf and Martin [66] also presented the stress calculation for three cases:

(a) a large coefficient of thermal expansion and no cure shrinkage (α = 300 x 10^{-6} /°C, $\gamma_{vol} = 0$)

The result is shown in Fig. 2.17. In this case thermal expansion dominates, so a large negative stress starts to occur when the epoxy vitrifies at about 90 °C. At about 100 minutes, the stress starts to decay as the sample enters the post-cure at 175 °C giving the compressive stress. During the cool down process, the stress vanishes at 155 °C, which is 20 °C below the final cure temperature. This reveals that the common use of $\sigma = E_o\alpha(T-T_o)$ is not valid, and it is necessary to be consider cure stress (E_o is the glassy modulus).

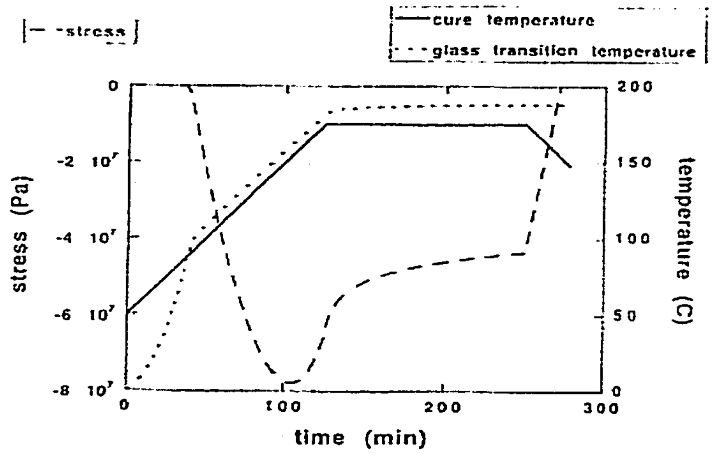

Fig. 2.17: Evolution of stress in an epoxy for case (a).

(b) Low coefficient of thermal expansion and high-cure shrinkage (α= 100 x 10^{-6} /°C, $3\gamma_{vol} = 0.06$)

The result is shown in Fig. 2.18. Since cure shrinkage dominates, a tensile stress occurs after vitrification. Once the system vitrifies, compressive stress is developed during cure. These stresses relax slightly during the post-cure at 175 °C. The stress is zero out at 235 °C which is higher than the final cure temperature.

(c) coefficient of thermal expansion and cure shrinkage typical for commercial epoxies (α = 180 x 10^{-6}/°C, $3\gamma_{vol} = 0.03$)

At the first period of cure, tensile stress is generated due to the cure shrinkage, but then opposed by thermal expansion until the large compressive stress occurs. During the post cure at 175 °C, stress is relaxed and almost offset at the end of an annealing. The stress-free temperature is equal to the final-cure temperature.

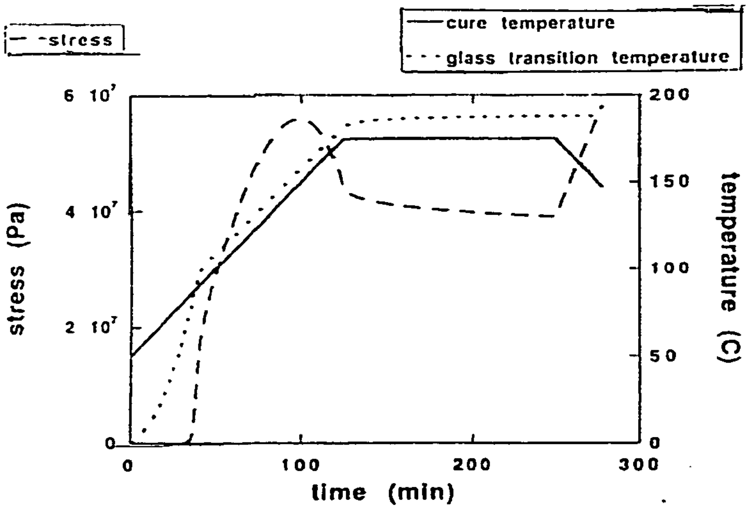

Fig. 2.18: Evolution of stress in an epoxy for case (b).

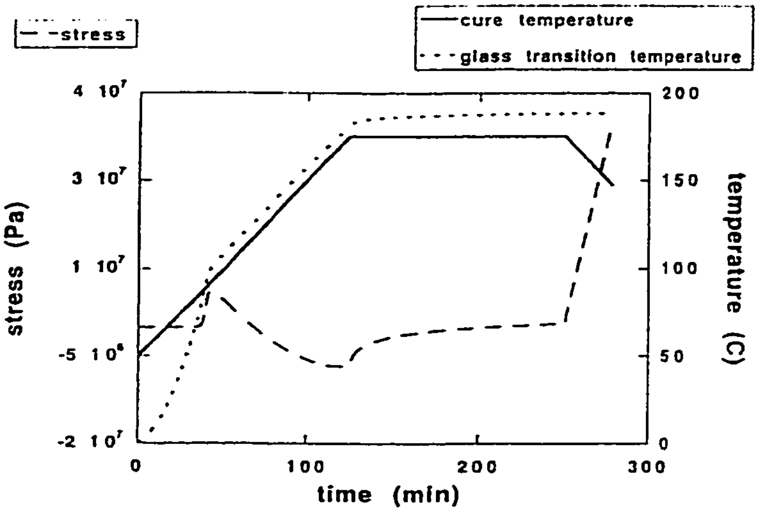

Fig. 2.19: Evolution of stress in an epoxy for case (c).

Therefore, to minimize the cool down stress the stress-free temperature should be reduced. Choosing cure cycle is also critical for residual stress magnitudes. To minimize the stress at final temperature, the final temperature should exceed the T_g of the fully cured polymer since in this case the rubbery modulus will determine the final stress level.

2.4.7 Curing Kinetics

It is known that the curing kinetics and the maximum extent of reaction to be attained in an isothermal curing process have to be considered because they are the basic requirements that determine a cure cycle. There are many techniques that can be used to study cure reaction kinetics such as Fourier transform infrared spectrometry (FTIR), high performance liquid chromatography (HPLC), torsional braid analysis (TBA), and DSC. DSC is a fast and simple method to characterize the curing reaction kinetics. In this thesis conventional and modulated DSC (DSC and MDSC, respectively) techniques will be mentioned and applied to obtain the reaction kinetics of the epoxies. During the isothermal curing of an epoxy resin the system changes from viscous liquid to highly cross-linked network. Since the reaction occurs in a condensed phase, the rate of the cure reaction is controlled by the functional group activity and their mobility. At the first stages of reaction, when the rate of displacement of the groups is much faster than the rate of collisions, the reaction is controlled by the groups' reactivity (kinetically controlled). As the reaction progresses, chain branching and viscosity increase until the system reaches the gelation point. Beyond this point, polymerization causes an increase in the density of cross-linking and may enter the vitrification, the mobility of the reactive groups is restricted. During the last stages the reaction is controlled by the rate of diffusion (diffusion controlled) [7]. This is the factor that limits the degree of conversion at curing temperature, T_c, below the maximum T_g of the fully cured epoxy. As the reaction progresses, T_g of the epoxy increases and approaches T_c. At this point the system reaches the glassy state, i.e. vitrifies. The enthalpy and the volume of the system are expected to decrease continuously until the system vitrifies. It is also anticipated that the heat capacity would decrease on vitrification as what has been observed by Cassettari et al. [67]. They used a specially designed differential microcalorimeter, where the heat flow was perturbed periodically by a heat pulse. Recently several works [68-71] have studied the vitrification of both isothermal and non-isothermal curing of epoxy systems by MDSC. Monserrat and his coworker [72] utilized MDSC to study the curing of a diepoxide-triamine system. The modulus of the complex heat capacity follows a three step variation as shown in Fig. 2.20 for the epoxy cured at 50 °C and 80 °C. At the first stage, $|C_p^*|$ increases until a maximum at the degree of conversion between 0.42 and 0.56. Then $|C_p^*|$ decreases slightly, while the degree of conversion increases until it reaches the final value at each cure temperature.

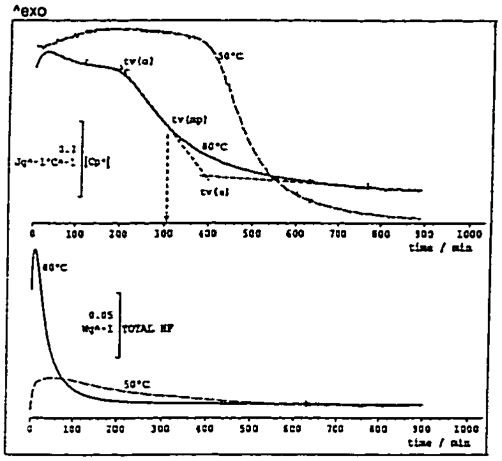

Fig. 2.20: Total heat flow and modulus of the complex specific heat capacity for the qausi isothermal curing of the epoxy-triamine system at 50 °C and 80 °C, with 0.5 K and 1 min modulation. $|C^*_p|$ curve at 80 °C indicates the determination of the extrapolated onset $t_{v(o)}$, midpoint $t_{v(m)}$, and extrapolated endset $t_{v(e)}$ vitrification times.

The stage of curing can be monitored by the DSC peak appearances. W. H. Park et al. [73] studied the cure behavior of a catalyzed epoxy/anhydride system for an epoxy-rich formulation using DSC (Fig. 2.21). They observed two exothermic peaks at a low temperature from an esterification reaction and at a high temperature from etherification, which would not be able to be observed in the stoichiometric ratio system except at the later stages of cure. It was noticed that both peaks are shifted to lower temperatures as the cure proceeds. As the reaction advances further, the esterification peak disappeared.

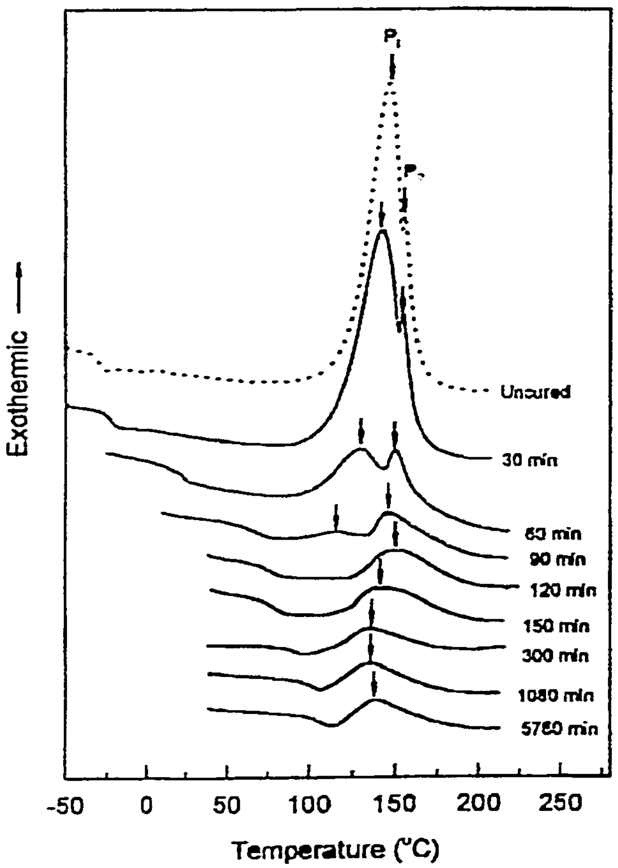

Fig. 2.21: DSC thermograms of epoxy/anhydride system isothermally cured at 85 °C for various cure times.

At the final period of the curing, the etherification peak begins to increase to higher temperature with cure time. The decrease of the peak temperature at the fist stage, which is the kinetically controlled stage, of curing may be explained by the relative increase of concentration of accelerator with curing. As the cure proceeds further, it becomes a diffusion-controlled reaction and then results in the increasing of peak temperature at the final period. The etherification reaction, which has known to be slower than esterification

[74], is responsible for optimum cured properties. Therefore, one of the factors influencing the properties of the cured epoxies is epoxy/anhydride composition. The optimum mixing ratios generally are less than the stoichiometric equivalents [75-76].

Several kinetic models have been proposed [77-80]. The epoxy cure reaction has been found to be an autocatalytic. Therefore, a simple n-th order kinetic model cannot describe the entire curing process. However, a recently published paper [81] has used the simple n-th order kinetic model to describe the cure behavior of the commercial encapsulant. Among the various equations used to model reaction kinetics, two equations are mentioned most often, which are the single rate constant model (Equation 2.17) and the model that has separated the noncatalytic reaction and the autocatalytic reaction from each other (Equation 2.18).

$$\frac{d\alpha}{dt} = K\alpha^m (1-\alpha)^n \qquad (2.17)$$

where $d\alpha/dt$ is the cure rate, K is the reaction rate constant, α is fractional conversion, and m and n are adjustable parameters (order of reaction).

$$\frac{d\alpha}{dt} = (K_a + K_b\alpha^m)(1-\alpha)^n \qquad (2.18)$$

where K_a is the rate constant for noncatalytic reaction and K_b is the rate constant for an autocatalytic path. However, Lee et al. [79] studied the system of tetraglycidyl-4,4'-diaminodiphenyl methane (TGDDM) cured with diaminodiphenylsulphone (DDS) and found that Equation (2.17) fitted the experimental values only within a certain temperature range as in Fig. 2.22. In addition, the physical meanings of kinetic parameters (m and n) were not clear. By using Equation (2.18), they found that there is a large deviation from the DSC data in the values of maximum rate. So they claimed that the kinetic parameters established in Equation (2.18) are not accurate. This group of researchers has developed the equation based on the reaction mechanisms to describe the epoxide/amine system as the following.

$$\frac{d\alpha}{dt} = K_a(1-\alpha)^l + K_b\alpha^m(1-\alpha)^n \tag{2.19}$$

Equation (2.19) fits the experimental data better than Equation (2.17 and 2.18). This is because in Equation (2.17) the non-autocatalytic reaction part was left out. Equation (2.18) assumes the non-autocatalytic reaction order, n, equal to 2, which is true only at the beginning of the reaction. For the epoxide/amine system, the reaction is assumed to be a pseudo second order, so $l = 2$ and $m+n = 2$.

In addition to the kinetic models as mentioned above, a simulation method was used to describe the relation among the molecular weight of polymers and the conversion or reaction time during cure. Cheng et al. [82-84] had developed two generalized kinetic methods: the generating function method and the Monte Carlo simulation procedure. The generating method was applied over the pregelation stage, while the Monte Carlo was applied over the whole stage. These two methods have been successfully used to simulate the complicated systems under isothermal conditions. Recently Cheng et al. [80] also applied these two kinetics methods with the non-isothermal epoxy curing. By using their own generating function (Equation 2.20) incorporation with the diffusion controlling effect, which was derived by Chern and Polhlein [85] (Equation 2.21), they succeeded in matching the generalized methods to the experimental data.

$$K_1^{''} = k_1^{''}[EP]_0^2 = K_{10}^{''} \exp\left[-E_a / RT(t)\right] \tag{2.20}$$

where $K_{10}^{''}$ is the frequency factor, *[EP]_o* is an initial epoxy concentration, E_a is the activation energy, R is the gas constant, and *T(t)* is the absolute temperature, which will be changed with time under non-isothermal conditions.

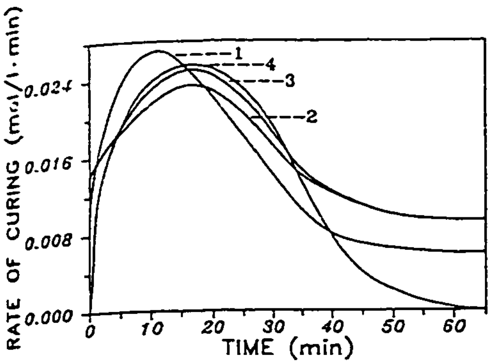

Fig. 2.22: Comparison of experimental (curve 4) and predicted (curves 1-3) cure curves for TGDDM/DDS (1/1) resin at 160 °C. (Curves 1-3 based on Equations 2.19-2.21, respectively).

$$K''_{10} = K^{\bullet}_{10} \exp\left[-D_f\left(\alpha(EP) - \alpha_C(EP)\right)\right], when\, \alpha(EP) \geq \alpha_c(EP) \qquad (2.21)$$

where D_f is the parameter of diffusion control which depends on the curing temperature, $K^{\bullet}_{10}$ is the value of K''_{10} before the gel point, $\alpha(EP)$ is the epoxy conversion, and $\alpha_c(EP)$ is the critical epoxy conversion upon which gelation occurred.

Along with the stress evolution investigation, the reaction kinetics of the model epoxies has been focused in this study. The reaction kinetics may clarify how the stress is developed during the curing since the kinetics reveals how network is formed. With the different in chemical structures of the known epoxy systems, which the reactions can be postulated, we anticipate relating the stage of cure to the stress evolution.

2.5 Objectives

The purpose this work is to twofold. First we will apply a combination of techniques to characterize the commercial underfill resins to provide a fundamental understanding of their curing behavior in order to improve the manufacturability and reliability of the electronics packaging process. Thermal analysis method (e.g., DMA (dynamic mechanical analysis), DSC (differential scanning calorimetry), TGA (thermogravimetric analysis), and TMA (thermomechanical analysis)), DuNouy ring method, and goniometer are utilized to obtain the properties of resins as a function of temperature. We intend to study the viscosity, gelation time, surface tension, and contact angle of resin on a polyimide substrate as a function of temperature. Moreover, the cure kinetics, which is the important issue for obtaining a reliable bond, is investigated. It is known that delamination is one of the problems in flip-chip assembly, and cure stress is suspected to cause this problem. Therefore, the evolution of cure stress during the curing is monitored by Force Oscillatometer experiment (Rheovibron), which can provide the stress directly. In this study multistep cure processes are performed to reduce or offset the residual stress within the cured epoxy. From this we anticipate the more reliable epoxy adhesives. Processing diagrams of underfill resins were constructed to provide the two processing windows; underfilling and curing windows, which will be a guide for manufacturers to set their cure schedule to obtain an optimized product in a scientific approach rather than the trial and error method.

However, to improve our understanding on how resin properties have changed during the curing, their chemistry should be known. Therefore, model epoxies have been formulated to use for this purpose. As it is known that the origins of the cure stress of constrained sample involve modulus and increase shrinkage of resin. Thus, the shear modulus and volume shrinkage during the curing are monitored. A simple equation is used to calculate the cure stress of model epoxies. For the kinetics study, it has been well documented that the polymerization of epoxy system is an autocatalytic reaction; therefore, an autocatalytic kinetic model is employed to fit the experimental result.

CHAPTER 3

Experimental Approach

3.1 Epoxy Resins

There are many factors governing the physicomechanical properties of a final epoxy resin. For example, it has long been recognized that the chemical nature of the curing agent can have significant influence on the gelation time and the physical properties of epoxies, largely because it determines both the morphology and cross-link density of the growing network. The strength and toughness of the epoxy, for instance, can be markedly affected by small changes in the curing agent.

Both commercial epoxies and model epoxies were employed in this study. For the commercial epoxies, a die attach adhesive (see Appendix I) and two underfill resins were explored. The study focused on the characterization of underfill resins, while a die attached adhesive was used as a preliminary study on the relation between the cure schedule and adhesive strength. Model epoxy formulations were made based on the commercial underfill proposed matrix chemistry. However, only epoxy and hardener (and catalyst if needed) were included in the mixture in order to simplify the system.

3.1.1 Commercial Underfill Resins

Two underfill resins were investigated: FP4511 from Dexter and X6-82-5 from Zymet. They were delivered in 10 ml syringes and stored at –45 °C. Both of resins were filled with silica (particles) in order to bring their CTE down to close to that of the eutectic Pb-Sn solder. The recommended cure schedule from the manufacturers for FP4511 and X6-82-5 are at 150 °C for 2 hours and 15 minutes respectively. While the T_g of FP4511 and X6-82-5 are 165°C and 120-140 °C, respectively. Therefore, their resin chemistries are significantly different. All the formulations are proprietary. The FP4511 resin contains a mixture of epoxy resins cured with an anhydride and X6-82-5 is said to be bisphenol F based cured with an imidazole derivative.

3.1.2 Model Epoxies

In order to get a better understanding of underfill epoxy systems, three formulas of epoxy model were prepared.

A) AEP-cured diglycidyl ether of bisphenol A epoxy

This model epoxy system was studied by previous students in our research group. Therefore, some information was available, and this system was easy for us to start with. AEP is the very first aliphatic polyamine with a (hetero-)cyclic backbone bridging the active amino hydrogen sites to gain commercial prominence in epoxy applications. AEP contains primary, secondary, and tertiary amine groups. However, only primary and secondary active hydrogens participate in the reaction with epoxy resin [26]. It is probable that the tertiary nitrogen, which possibly promotes catalytic cure, is greatly hindered in the resin system. Therefore, for practical purposes it can be disregarded as a catalytic site unless the system has been left for a long time [86].

The diglycidyl ether of bisphenol A, DGEBA, (DER 332) epoxy resin was provided by the Dow Chemical Company. The epoxy equivalent molecular weight of DER 332 is 172-176 g/eq. The hardener was N-aminoethylpiperazine (AEP, ≥ 96% purity) from Air Products. The epoxy resin and hardener were hand mixed in the stoichiometric ratio of 100:24.7 (by weight). After mixing, the mixture was degassed for about 15 minutes, and then stored at –45 °C for later used. The recommended cure schedule is 1 hour at room temperature and 2 hours at 100 °C [87]. The chemical structure of DGEBA and AEP are shown below.

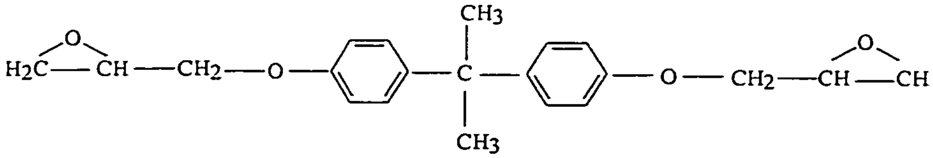

Diglycidyl Ether of Bisphenol A (DGEBA)

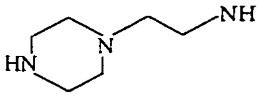

N-Aminoethylpiperazine (AEP)

B) Imidazole-cured diglycidyl ether of bisphenol F epoxy

The base compositions of this model epoxy system are similar to that of the X6-82-5 underfill resin from Zymet.

Some imidazoles are highly effective, fast curing agents and are added to commercial epoxy systems to catalyze the homopolymerization of epoxide groups to yield a thermoset network. However, unmodified imidazoles have low stability when mixed with epoxies, making them unsuitable for use in one-pot compositions, and therefore, much work has been carried out into stabilizing imidazoles for use as latent epoxy curing agents [86]. Substituted imidazoles have been reported as curing agents for the epoxy resins; these provide a long pot life with DGEBA from about 2 to 20 days, depending on the type of substitution on the imidazole. J. Vogt [88] used microcalorimetry to study the curing of several kinds of imidazoles with DGEBA, and found that each molecule of imidazole induces more than 20 epoxy groups to undergo polyaddition. Therefore, optimum glass transition temperature-ranges can be obtained with 0.025 to 0.05 mol of catalyst/ equivalent of epoxy. There is a report stating that among imidazoles curing agents, 2-ethyl-4-methyl-imidazole is particularly effective and gives excellent physical properties, such as resistance to chemicals and oxidation, high heat distortion temperature, and superior electrical characteristics [89].

In this model, epoxy resin was diglycidyl ether of bisphenol F provided by Shell (EPON 862). The epoxy equivalent weight of this resin is 166-177 g/eq. The hardener is 2-ethyl-4-methyl-imidazole (EMI-24, ≥ 87 % purity) from Air Products. The epoxy resin and hardener were hand mixed for 10 minutes in the ratio of 100:4 (by weight). Then the mixture was degassed for about 15 minutes. The mixture was stored at –45 °C if it was not in use. The recommended cure schedule for this epoxy system is 4 hours at 60 °C and 2 hours at 150 °C. The chemical structures of diglycidyl ether of bisphenol F and EMI-24 are shown below.

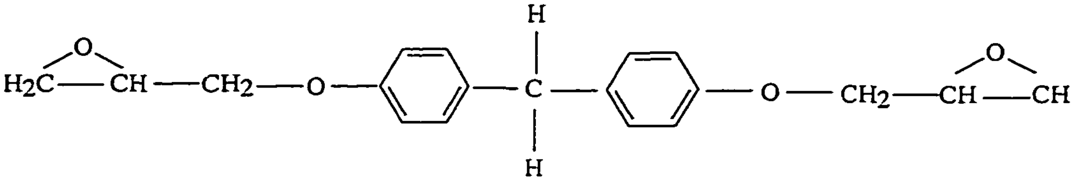

Diglycidyl Ether of Bisphenol F

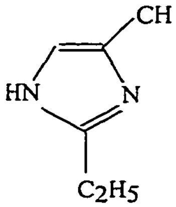

2-Ethyl-4-Methyl Imidazole (EMI-24)

C) Anhydride-cured cycloaliphatic epoxy

This epoxy system is similar to FP4511 commercial underfill resin from Dexter. Anhydrides generally are selected to provide low viscosity and long pot life [86]. Anhydride-cured epoxy exhibits improved high temperature stability over amines and better physical and electrical properties. Anhydride will not react directly to the epoxy group; therefore, accelerator is needed. The use of low molecular weight alcohol reduces the cure time 60 % when used in 5 phr with DGEBA [90].

In this epoxy model, the epoxy was 3,4-epoxycyclohexylmethyl -3,4 epoxycyclohexane carboxylate from Ciba-Geigy (CY-179). The epoxy equivalent weight of this epoxy is 131-143 g/eq. Hexahydro 4 methylphthalic anhydride was used as a hardener, N,N-dimethylbenzyl amine and ethylene glycol were used as accelerators. These three chemicals were bought from Aldrich. All chemicals were used as received. The model epoxy system was mixed in the following ratio:

3,4-epoxycyclohexylmethyl-3,4 epoxycyclohexane carboxylate: hexahydro-4-methylphthalic anhydride: N,N-dimethylbenzyl amine : Ethylene glycol =100:100:5:5

This mixture composition was recommended by Kramer [91]. Recommended cure schedule is 4 hours at room temperature, then ramp the temperature up to 90 °C with the rate of 4 °C/min and dwell for 1 hour. After that the temperature was raised at 4 °C/min to 150 °C and dwell for 3 hours. The epoxy system was first prepared by hand mixing and mechanical mixing at room temperature. However, voids were observed in the cured sample in silicone tubing. This may be caused by the phase separation of anhydride from the epoxy due to the poor solubility of anhydride in epoxy liquid. To improve the solubility, the epoxy system was mechanically mixed with anhydride at 400 rpm for 10 minutes at 80 °C before adding the accelerators. The chemical structures of all ingredients are shown below.

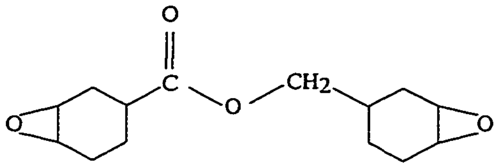

Cycloaliphatic Epoxy

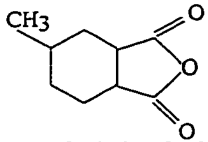

Hexahydro-4-Methylphathalic Anhydride

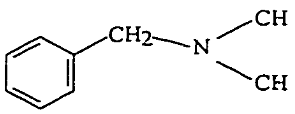

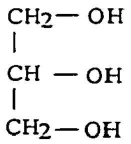

$$\begin{array}{l} CH_2-OH \\ | \\ CH-OH \\ | \\ CH_2-OH \end{array}$$

N, N Dimethylbenzyl Amine

Ethylene Glycol

3.2 Characterization Techniques

A variety of experiments were carried out to investigate the characteristics of epoxies and to follow the cure reactions. These experiments employed various kinds of equipment including Dynamic Mechanical Analyzer (DMA) in shear and tensile modes, Differential Scanning Calorimeter (DSC), Thermogravimetric Analyzer (TGA), Optical Microscope (OM), Contact Angle Goniometer, Du-Nouy ring-pull apparatus for surface tension measurement, double cantilever beam method, and Thermodynamic Analyzer (TMA).

3.2.1 Dynamic Mechanical Analysis (DMA)

DMA measures complex modulus, compliance, and viscosity in several different modes of oscillatory deformation: flexure, tensile, shear, bending, and compression [92]. In our study only shear and tensile modes were employed. In a dynamic mechanical measurement, the sample is subjected to a sinusoidal strain (ε). The resulting stress (σ) is also sinusoidal with the same frequency, but with a lag in the phase. This phase lag is expressed as an angle, δ (Fig. 3.1). The applied sinusoidal strain of frequency ω can be represented as [93-94]

$$\sigma(t) = \sigma_o \sin(\omega t + \delta) \qquad (3.1)$$

where σ_o is the maximum stress amplitude and the stress proceeds the strain by a phase angle δ. The strain is given by

$$\varepsilon(t) = \varepsilon_o \sin(\omega t) \qquad (3.2)$$

where ε_o is the maximum strain amplitude. These quantities are related by

$$\sigma(t) = E^{*}(\omega)\varepsilon(t) \qquad (3.3)$$

where $E^{*}(\omega)$ is the dynamic complex modulus and

$$E^{*}(\omega) = E'(\omega) + iE''(\omega) \qquad (3.4)$$

$E'(\omega)$ and $E''(\omega)$ are the dynamic storage modulus (a real part) and dynamic loss modulus (imaginary part), respectively. For viscoelastic polymer E′ characterizes the ability of the polymer to store energy (elastic behavior or solid-like nature), while E″ reveals the tendency of the material to dissipate energy (viscous behavior or liquid-like nature). The phase angle is calculated from

$$\tan\delta = \frac{E''}{E'} \qquad (3.5)$$

It is noted that E′ and E″ are substituted with G′ and G″ respectively in case of the shear mode testing.

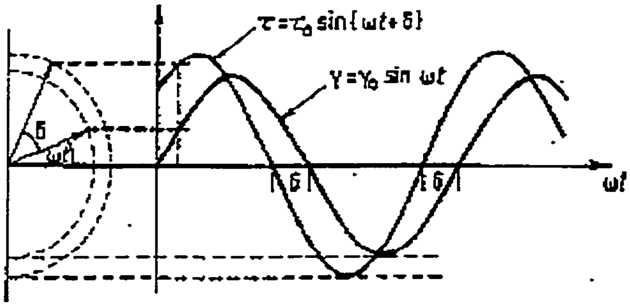

Fig. 3.1: Vector representation of an alternating stress leading an alternating strain by phase lag δ.

Polymers are viscoelastic, so both the viscous and elastic properties of these materials must be measured to understand their rheology and application behavior. DMA can measure both properties simultaneously. This is the fundamental feature of dynamic mechanical analysis that distinguishes it from other mechanical testing techniques. This technique has been widely used to monitor the cure behavior of thermosetting resins [95-96] such as the gelation time, generated stress during cure, and shear modulus as a function of temperature.

3.2.1.1 Dynamic Mechanical Analysis- Shear Mode

In our study Rheometrics dynamic analyzer II (RDA II) was utilized. This system is capable of investigating samples in the form of solid, melt or liquid [92]. This instrument is classified as a mechanical spectrometer. The instrument applies a precise oscillatory, steady or step shearing, to the test sample and precisely measures the sample response. Microprocessor analysis of the applied strain and resulting response yields the sample's elastic shear modulus (G′), viscous shear modulus (G″), and damping (tanδ) along with other derived factors such as complex modulus (G*), complex viscosity (η*) in- and out-of-phase viscosity (η′, η″), shear storage compliance (J′), and shear loss compliance (J″).

A fixture is mounted between the instrument actuator that applies the test strain, and the transducer that senses the sample's response. The test sample is loaded into a test fixture appropriate for the sample and the test as in Fig. 3.2 Testing is controlled by the test control/analysis station.

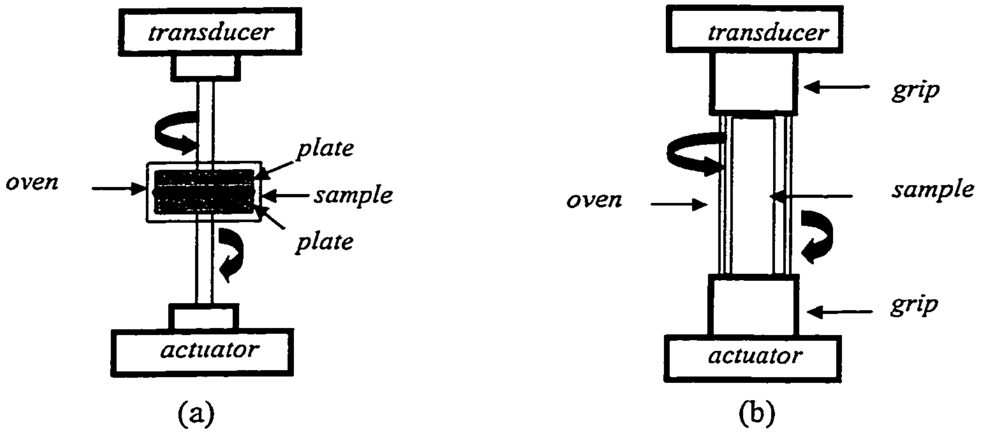

Fig. 3.2: (a) parallel plates geometry, (b) rectangular torsion geometry.

In our study DMA was used to determine the gelation point of epoxy samples at different temperatures. Parallel plate geometry (Fig. 3.2(a)) was utilized (25 mm in diameter of 6061T6 aluminum alloy plates) with 0.5 mm sample thickness. The samples were oscillated in a sinusoidal fashion at 1.6 Hz. This frequency corresponds most closely to the shear rate used in the standard gel test [97]. G′ and G″ were recorded as a function of time at specific temperature. Gelation point is the cross over between G′ and G″ as in Fig. 3.3. The shear moduli of the fully cured samples were measured by preparing the sample as a bar in the size of 12 x 50 x 3 mm (Fig. 3.2 (b)). Samples were oscillated in a sinusoidal function at 1 Hz in a temperature scan from -100 °C to 50 degree above the T_g of sample.

RDA II was also employed to monitor the post gel shear modulus of model epoxies at isothermal cure temperature. The sample was gelled and then quenched to stop the reaction before subject to the isothermal curing on RDA II until the plateau modulus was reached.

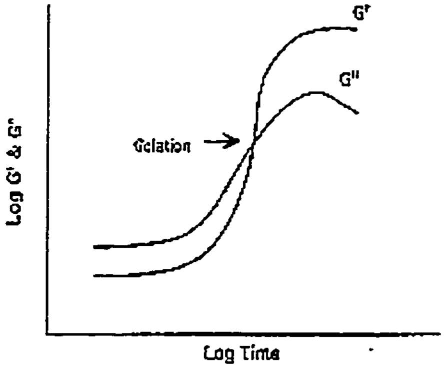

Fig. 3.3: Determination of gelation by G' and G" cross over.

3.2.1.2 Dynamic Mechanical Analysis - Tensile Mode

Rheovibron DDV II-B and Rheovibron DDV III-C were used to monitor the generated stress and the volume contraction during the cure respectively. Rheovibron is a forced vibration unit capable of operating at several constant frequencies for the determination of the dynamic mechanical response of the system [98-99].

The basic construction of Rheovibron DDV II-B is shown in Fig. 3.4. This unit was modified at Lehigh University [100]. It consists of:

a) an electromagnetic driver, which generates a signal

b) strain gage (displacement ≤ 300 μm), and stress gage (550 gf)

c) furnace (practical temperature ≤ 200 °C) with OMEGA (CN-2002) programmable temperature controller

d) HP data acquisition/control unit

e) HP computer set with the suitable software for each task and printer

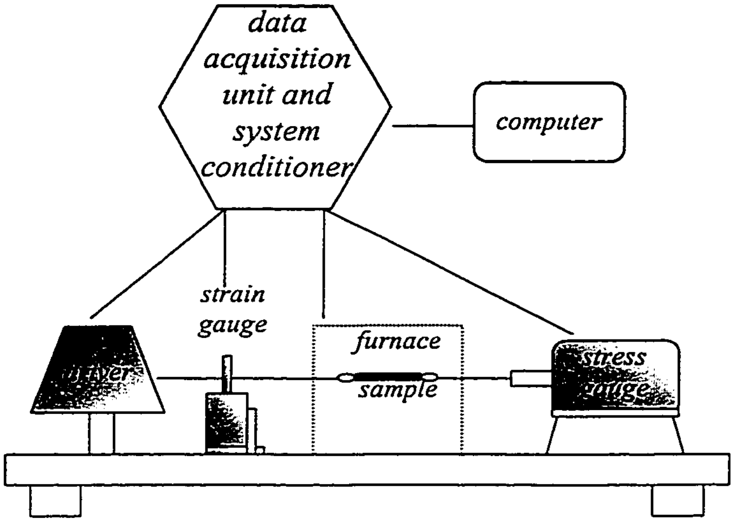

Fig. 3.4: The schematic diagram of Rheovibron DDV II-B.

Basically, the sinusoidal tensile strain is applied on one end of the sample, the sinusoidal stress is generated at the other end of the sample. Then the complex modulus can be obtained by the ratio of the maximum stress amplitude to the maximum strain amplitude. The phase lag, δ, between stress and strain is measured. Then E′ and E″ can be calculated by the following equations.

$$E' = E^{*} \cos\delta \qquad (3.6)$$

$$E'' = E^{*} \sin\delta \qquad (3.7)$$

In our experiment epoxy sample was placed in a soft and low modulus silicone tubing support, having stainless studs at both ends. The diameter of the silicone tubing was 1. 59 mm and 2.38 mm for the curing with and without the cooling down process respectively.

The length of the silicone tubing was 40-45 mm. The sample was oscillated under displacement control with the amplitude at 27 μm and the frequency at 100 Hz. The stresses during curing were monitored as a function of time. The cure experiments were isothermal curing (followed by a cooling down process in case of X6-82-5) and multi-step curing (Table 3.1).

Table 3.1: Isothermal and multi-step cure schedules for underfill resins.

Sample	Cure schedule
FP4511	a) Isothermal: 120, 150, and 165 (°C)
	b) Multi-step:
	b.1) 2-step: 30 min @ 85 °C and 120°C
	60 min @ 85 °C and 120°C
	b.2) 3-step: 30 min @ 85 °C / 30 min @ 120 °C, and 150 °C
X6-82-5	a) Isothermal: 130, 150 and 170 °C, then cool down to 130 °C
	b) Multi-step:
	b.1) 2-step: 5 min @130 °C and 150 °C
	b.2) 3-step: 10 min @ 85 °C, 5 min @ 130 °C, and 150 °C

3.2.2 Differential Scanning Calorimetry (DSC)

DSC is well suited to record heat released from chemical and physical processes in order to follow the kinetic of systems. Epoxy curing is an exothermic reaction, therefore, DSC is widely used to monitor the curing reaction. The structure of the DSC instrument is shown in Fig. 3.5. The base of the sample holder assembly is placed in a reservoir of coolant. The sample and reference holders are individually equipped with a resistance sensor, which measures the temperature of the base of the holder, and a resistance heater. If a temperature difference is detected between the sample and reference, energy is supplied until the temperature difference is less than a threshold value, typically less than 0.01 °C [101]. The energy input is recorded as a function of temperature or time.

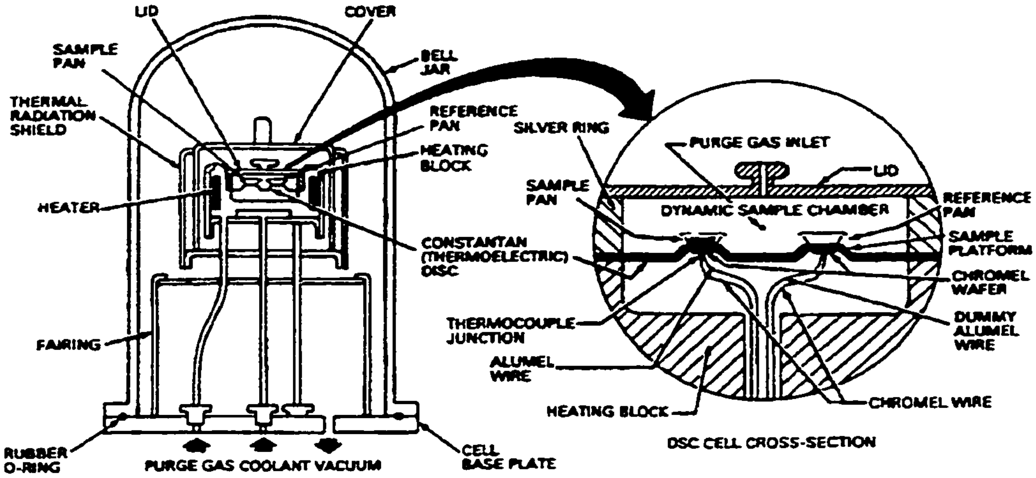

Fig. 3.5: DSC (TA 2920) cell construction.

Recently, a variation on the standard temperature programs has been applied to the DSC instrument, and is called temperature modulated DSC (TMDSC) [93, 102]. In TMDSC a sinusoidal temperature modulation is superposed on the linear (constant) heating profile to yield a temperature program in which the average sample temperature varies continuously in a sinusoidal manner:

$$T(t) = T_o + \beta t + A_T \sin \omega t \qquad (3.8)$$

where T_o is the initial temperature, β is the underlying heating rate, $A_T(\pm K)$ is the amplitude of the temperature modulation, $\omega(s^{-1})$ is the modulation frequency and $\omega = 2\pi/p$, where $p(s)$ is the modulation period. Fig 3.6 illustrates a modulated temperature profile for the TMDSC heating experiment.

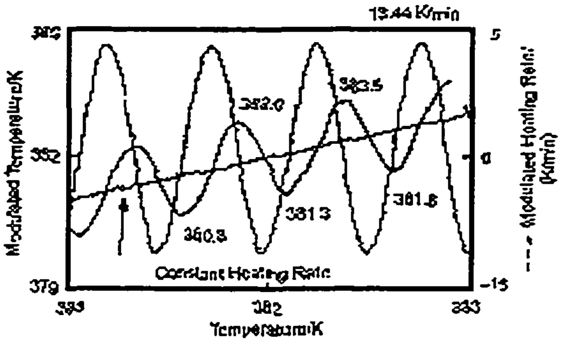

Fig. 3.6: Typical TMDSC heating profile with the following experimental parameter: β = 1 K/min, p = 30 s, and At = ±1 K (courtesy of TA Instruments Inc.).

Conventional DSC only measures the total heat flow. In TMDSC, the constant heating profile provides total heat flow, while the sinusoidal heating profile provides the heat capacity information corresponding to the rate of temperature change. As mentioned earlier in Chapter 2 that the heat capacity would decrease on vitrification as what has been observed by Cassettari et al. [67], therefore, in our study TMDSC was utilized to determine the vitrification of model epoxy systems at different curing temperatures.

A TA instrument DSC 2920 was used to determine the T_g and extent of reaction. Samples were taken out from the –45 °C freezer and allowed to warm up to room temperature for about 20 minutes. Approximately 10-15 mg of sample were sealed in the aluminum pan before placing in the sample holder. Several isothermal temperatures were applied to each epoxy sample. The selected temperatures lay between the onset temperature and $T_{g\infty}$ of each sample. Furthermore, the dynamic temperature scan was applied to the fresh sample and the cured sample from isothermal curing (in DSC) in order to determine the T_g and the amount of unreacted part of sample. The temperature was scanned from –60 °C to 300 °C for the fresh sample, and from 25 °C to 300 °C for the partially cured and fully cured sample. The total heat of reaction of the fresh sample ($\Delta H_{uncured}$) represents a 100% extent of reaction. The heat of reaction from the partially cured sample is defined as ΔH_{cured}. Therefore the extent of reaction of sample (p) is:

$$p = \frac{\Delta H_{uncured} - \Delta H_{cured}}{\Delta H_{uncured}} \qquad (3.9)$$

For the isothermal experiment, the autocatalytic kinetic model (Equation 3.12) was employed to explain the kinetics of reaction for the various epoxy resins [103]. The analysis program determined the heat flow (dH/dt) and the partial heats (ΔH_t) as a function of time at various isothermal temperatures. These data values are then converted to a fractional conversion (p), by using a reference or theoretical heat of reaction (ΔH_o). The fractional conversions are calculated as a function of time using the following relations:

$$p = \frac{\Delta H_t}{\Delta H_o} \tag{3.10}$$

$$\frac{dp}{dt} = \frac{dH}{dt}\frac{1}{\Delta H_o} \tag{3.11}$$

$$\frac{dp}{dt} = kp^m (1-p)^n \tag{3.12}$$

3.2.3 Thermogravimetric Analysis (TGA)

TGA examines the mass change of a sample as a function of temperature in the scanning mode or as a function of time in the isothermal mode. There are some thermal events, which have a change in mass of the sample. These include desorption, absorption, sublimation, vaporization, oxidation, reduction, and decomposition [93]. The mass change characteristics of a material are strongly dependent on the experimental conditions employed. The factors that influence the characteristics of the recorded TGA curve are sample mass, volume and physical form, the shape and nature of the sample holder, the nature and pressure of the atmosphere in the sample chamber, and the scanning rate. TGA curve for a one-stage reaction process is shown in Fig. 3.7. The principal elements of a thermobalance are an electronic microbalance, a furnace, a temperature programmer and a recorder. The reaction is characterized by two temperatures, T_i and T_f. T_i represents the lowest temperature at which the onset of a mass change can be detected, while T_f represents the lowest temperature at which the process responsible for the mass change has been completed.

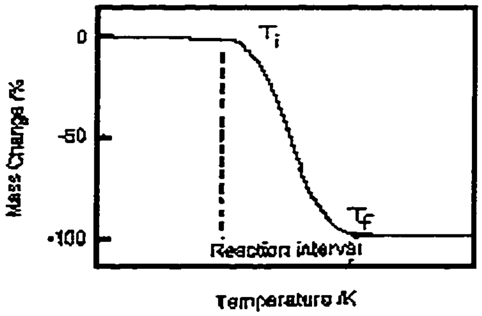

Fig. 3.7: Schematic single-stage TG curve.

A TA instruments TGA 2950 was employed to determine the outgassing phenomena and degradation of epoxy samples. This TGA model operates on a null balance principle [104]. The balance of the balance arm is indicated by the equal amount of light to each of the photodiodes (the light is supplied by a constant current infrared LED). As sample weight is lost or gained, the beam becomes unbalanced, causing an unequal amount of light to strike the photodiodes. The unbalanced signal causes the increasing or decreasing in the current to the meter movement to bring it back to the original position (null position). The change in current required to accomplish this task is directly proportional to the change in mass of the sample. Then the current is converted to the weight signal.

The samples were taken out from the – 45 °C freezer and allowed to warm up to room temperature for about 20 minutes. Approximately 20 mg of samples was weighed in the aluminum pan before placing in the ceramic (or platinum) sample holder. Note that using an aluminum pan avoids the damage that may occur to the expensive ceramic (or platinum) sample holder. The temperature scanning is from 25 °C to 600 °C at the rate of 10 °C/min.

3.2.4 Optical Microscopy

A Zeiss Optical Microscope under transmitted light was used to detect the presence of voids as a function of cure schedule. The sample consisted of a 50 μm film sandwiched between a glass slide and a cover slip. A cover slip was preheated at 90 °C for 30 minutes before placing down onto the dispensed underfill epoxy on glass slide. The underfill resin was allowed to flow under the gap for a few minutes. Then the samples were cured in an air circulating oven as the isothermal and two steps curing as shown in Table 3.2. The number of voids in a certain area was counted under the microscope.

Table 3.2: Cure schedules for underfill resins in which used to investigate the void formation.

Sample	Cure schedule
FP 4511	1) Isothermal: 120, 150, and 165 (°C) 2) Two steps: 90/120, 90/150, and 90/165 (°C)
X6-82-5	1) Isothermal: 130, 150, and 170 (°C) 2) Two steps: 90/130, 90/150, and 90/170 (°C)

Note: Specimen was subjected to 90 °C for 10 minutes before going to the second step.

3.2.5 Surface Tension Measurement

The molecules at the surface of a liquid are subject to the strong attractive forces of the interior molecules. A resultant force, whose direction is in a plane tangent to the surface at a particular point, acts to make the liquid surface as small as possible. Surface tension is a property of the interface. Generally, it is measured by balancing it along a certain boundary line against an equal force that can be measured [105].

There are a few methods for determining the surface tension (i.e., capillary-rise method, drop weight method, and ring method). The Ring method was applied in our work. The DuNouy ring-pull apparatus for measuring surface tension is shown in Fig. 3.8. There is a platinum-iridium ring supported by the stirrup attached to the beam of a torsion balance. The ring is pulled upward from the liquid by turning the torsion wire, thus applying a force that is known by the calibration of the instrument. The force calibration was done by using small wires as weights. The shape of the liquid held up influences the force necessary to break the liquid film [106]. The shape is a function of R^3/V and R/r where V is the volume of the liquid held up and r is the radius of the wire. Therefore, a correction factor is needed. The surface tension is given by the equation

$$\gamma = \frac{f}{4\pi R} F_r \tag{3.13}$$

where γ is the surface tension, f is a maximum force registered on torsion balance scale, F_r is a correction factor due to shape of liquid held up and ring dimensions, R is the mean radius of the ring. In this study, the effect of temperature on surface tension was investigated. A heated stage is used for elevated temperatures, and the studied temperature range was from room temperature to 120 °C.

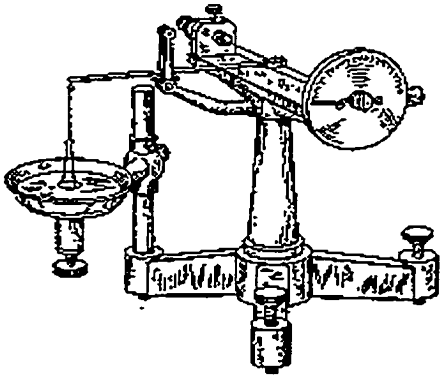

Fig. 3.8: DuNouy ring-pull apparatus for measuring surface tension.

3.2.6 Contact Angle Measurement (Goniometer)

The difference in contact angle values depends on the difference in metastable states, which exist in the system having three-phase (solid/liquid/vapor) boundaries [36]. The maximum stable angle is called the advancing (or advanced) angle, while the minimum stable angle is referred to as the receding (or receded) angle. The sessile drop method is widely used to measure the contact angle because it is fast and convenient. In the sessile drop method, a drop is placed on a horizontal surface and observed in cross section through a telescope. A goniometer in the eyepiece is utilized to measure the angle. The angle vision is just slightly off horizontal so the edge of the drop and it's reflected images are both visible. Therefore, the tangent can be determined accurately at the contacted point between the drop and the surface.

A computer-driven goniometer manufactured by Connelly Applied Research located in Nazareth, PA was employed in this study (Fig. 3.9). Contact angle of epoxy samples was determined at different temperature from room temperature to 120 °C. A heated stage is used for elevated temperatures. The substrate for the underfill resins was the Polyimide (PI 2525 from DuPont) coated on a glass slide. 1:1 by weight mixture (mixed with magnetic stirrer in plastic bottle for 6 hours) of PI 2525 in T-9039 thinner (from DuPont) was used to obtain the thin film with 15 ± 5 μm thickness. First glass slides were cleaned for five minutes by an ultrasonic cleaner in an ethanol bath. Then they were cleaned by OV-ozone for 5 minutes. After that they were rinsed by DI water. After drying by air, they were ready for the following spin coating procedure:

DI water for 100 seconds at 2000 rpm,

silane adhesion promoter solution (90 ml methanol, 10 ml DI water, and 1 drop of VM-651 from DuPont) for 30 seconds at 1000 rpm,

and PI2525/T-9039 mixture for 30 seconds at 1000 rpm

Finally, the coated slide was cured by the following cure schedule:

30 min @ 100 °C, 30 min @ 150 °C, 1 hour @ 200 °C, 1 hour @ 300 °C, and 10 min @ 400 °C (the temperature ramping rate was 5 °C/min)

Only the advancing contact angle measurements were performed. The liquid epoxy was dropped on the substrate surface from the micro-syringe with a long needle. The drop size is usually as small as 0.5 mm in diameter. The angle was advanced by adding liquid sample slowly; this is controlled by the small power pump. After the addition, the needle is left in the drop. Deformation of the drop by contact with the needle will not change the contact angle. After each advance, the drop was allowed to equilibrate for a minute before taking an image. Then the tangent between the edge of the drop and the surface was determined on both sides. About ten measurements were made on each sample at each temperature, then the average was taken as the advanced contact angle.

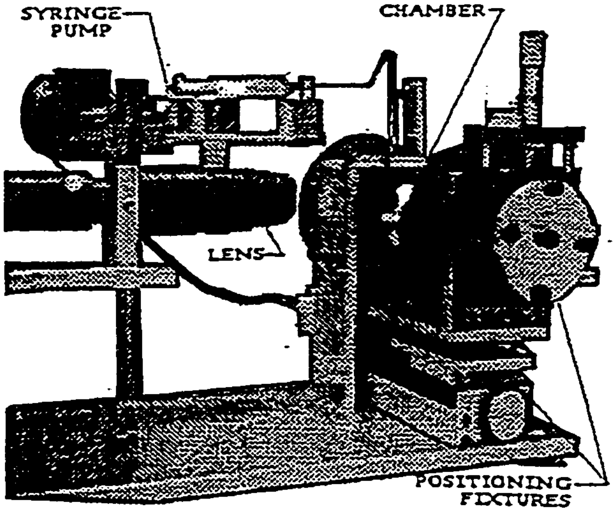

Fig. 3.9: The schematic of goniometer for measuring contact angle.

3.2.7 Double Cantilever Beam Method (DCB)

Delamination at interfaces between the polyimide and adhesive is common in flip chip assembly. Therefore, characterization of this process is crucial to study. DCB tests have been widely used to measure the strength of stiff structural adhesives because the experiments are simple to perform and analyze [45, 107-109]. The specimen consists of two simple rectangular bars, with a layer of adhesives sandwiched between them. This method can be used to determine the pure mode I (tensile) interfacial fracture toughness.

Linear elastic fracture mechanics may be used to compute the fracture toughness. Mostovoy et al. [108-109] developed the following equation to calculate the adhesive fracture toughness, G_{IC}.

$$G_{IC} = \frac{12P^2a^2}{B^2h^3E_s} \tag{3.14}$$

where, P is the applied load, a is the crack length, B is the specimen width, h is the thickness of adherend, and E_s is the modulus of the substrate (69 GPa for aluminum).

The specimen employed for the DCB testing was aluminum alloy bar (6061 T6) which was machined into cantilever beams 3 in. long, 0.5 in. thick and 0.5 in. high (Fig. 3.10). To control the surface roughness, one of the aluminum substrates was polished to a 1 μm finish using standard metallographic techniques and the mating surface was ground to a 400 grit finish. Both substrates were cleaned by the same process that mentioned in section 3.2.6. The polished bar was coated by PI 2525 (same procedure as the coating on glass slides for contact angle measurement). Silane coupling agent was used to improve the adhesive strength. The DCB specimens were fabricated using the following general method. One bar (the PI coated bar was chosen here) was sprayed with a dry lubricant release agent to make a one inch pre-crack. Both bars were then preheated at 90 °C for about 30 minutes. After that the sample was dispensed onto the polished substrate. Next the rough surface bar was laid on top of the sample to make a sandwich specimen. The sample thickness was controlled by 250 μm Teflon spacers. Excess adhesive on the beam side was removed and the adhesive was then placed in a circulating air oven with cure schedules in Table 3.3. Notably, the study from DSC showed that 15 minutes is enough for the reaction to reach the maximum extent of reaction at the studied temperature range. DCB tests were conducted on a screw-driven Instron 1011 testing machine with a crosshead speed of 2 mm/min.

Note that only X6-82-5 was selected to study the fracture toughness in order to investigate the effect of the cure schedule.

Table 3.3: Isothermal and multistep cure schedule for X6-82-5 on DCB specimen.

Isothermal and multistep	Cure schedule
a) isothermal 130 °C	130 °C for 15 minutes
b) isothermal 150 °C	150 °C for 15 minutes
c) isothermal 170 °C	170 °C for 15 minutes
d) 2 step	130 °C for 5 minutes and 150 °C for 15 minutes
e) 3 step	80 °C for 10 minutes, 130 °C for 5 minutes and 15 °C for 15 minutes

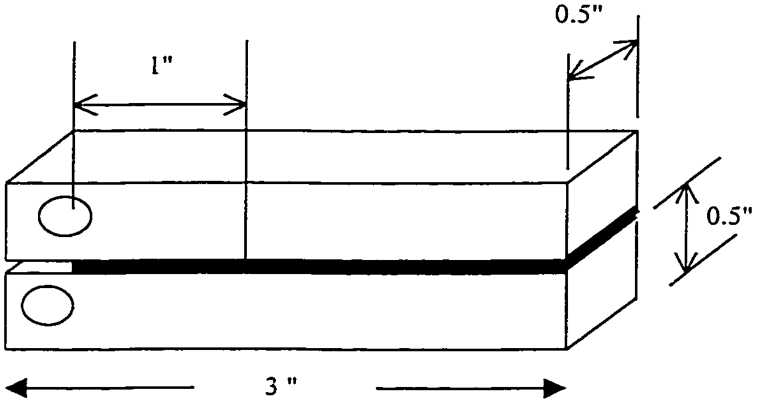

Fig. 3.10: DCB specimen with 250 μm adhesive thickness and 1 inch thickness.

3.2.8 Thermomechanical Analysis (TMA)

TMA can be used to measure the deformation characteristics of solid polymers, films, thin films, coatings, viscous fluids and gels. The optimization of the experiment depends on the appropriate load, deformation mode, and also the attached part of the equipment. TMA40 module of Mettler Toledo in a compression/expansion mode was employed to determine to linear thermal expansion coefficient (CTE, α) of cured epoxy sample in this research. The construction of TMA40 module is shown in Fig. 3.11. The sample should be homogeneous, and where possible the upper and lower surfaces should be parallel and smooth. The sample is placed on the sample support made of quartz glass. The selected probe was the quartz-flat probe with 3 mm diameter. Any dimensional changes are monitored by the displacement sensor, LVDT. The ferromagnetic core of the LVDT moves up and down with the probe that is in contact with the sample surface. The probe force is controlled by the magnetic force compensation device and ranges from 0 to 0.5 N. The samples were subjected to the temperature scan from 25 °C to the 50 degree above their T_g with the heating rate 5 °C/min. The CTE (α) is defined as

$$\alpha = \frac{dL}{dT}\frac{1}{L_o} \qquad (3.15)$$

where L_o is the original length of the sample and dL/dT is the slope of the TMA curve. The α is temperature dependent. T_g is also obtained by this testing. For thermal expansion measurement T_g is the temperature at which the sample exhibits a significant change in its thermal expansion as in Fig. 3.12.

TMA was also employed to monitor the post gel volume change of model epoxies. The sample was gelled in the oven and then quenched to stop the reaction. Gelled sample was subjected to TMA under the isothermal condition (100 °C for AEP-cured diglycidyl ether of bisphenol A, 130 °C for EMI-24-cured diglycidyl ether of bisphenol F, and 150 °C for anhydride-cured cycloaliphatic epoxy).

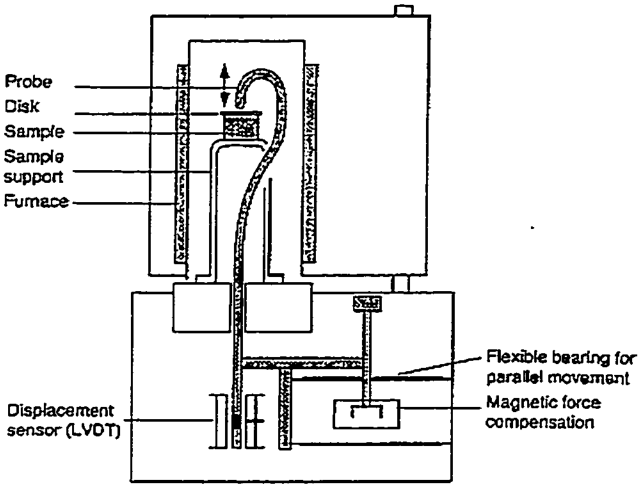

Fig. 3.11: Construction of the TMA40 module.

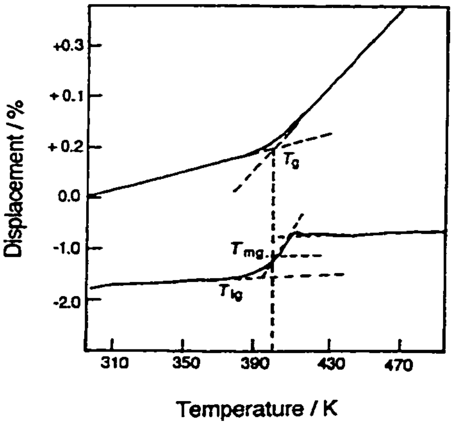

Fig. 3.12: Determination of the T_g from a TMA curve and the corresponding derivative TMA curve.

CHAPTER 4

Results and Discussion

Both commercial materials and model epoxies were characterized. For the commercial underfill resins, the focus was on understanding flow behavior and cure characteristics. Processing diagrams were constructed to provide a guideline for processing. Model epoxies were investigated to obtain a better understanding of cure kinetics, gelation, and generated cure stresses. This chapter presents the characterization results and discussion of commercial underfill resin and model epoxies separately.

4.1 Commercial Underfill Resins

In order to obtain economical and reliable products, it is important to study the processing behavior of underfill resins. The processing of underfill resins can be divided into two distinct steps: the underfilling step, which is the step at which underfill resins flow under the gap between a chip and substrate to complete the filling, and the cure step, which is the step at which the cure of underfill resin is completed to achieve good adhesion and mechanical strength. To design the underfilling step, several properties of underfill resins are required (e.g., viscosity, gelation time, contact angle of sample on a substrate, and surface tension). For the cure step, extent of reaction and cure stress are the important factors investigated. Void formation and outgassing phenomena are also examined but not as the same detail as cure stress and extent of reaction. The correlation between the cure stress and adhesive strength was studied as well.

4.1.1 Shear Viscosity and Gelation

The shear viscosity and gelation times were measured as a function of cure temperature. The shear viscosities at different temperatures as a function of time for FP4511 and X6-82-5 are shown in Figs. 4.1 and 4.2, respectively. Viscosity depends on both temperature and extent of reaction. Shear viscosity decreased at the beginning while the sample adjusted its temperature to the chamber temperature. As expected, the higher temperature, the lower the viscosity at the beginning. Once the cross-linking reaction started, viscosity began to increase until it was near the gelation point. Viscosity changed rapidly and went to infinity at the gelation point. Because of the higher rate of cross-linking at the higher temperature, the initial viscosities of the samples at the higher cure temperature were not always lower than that of the lower cure temperature.

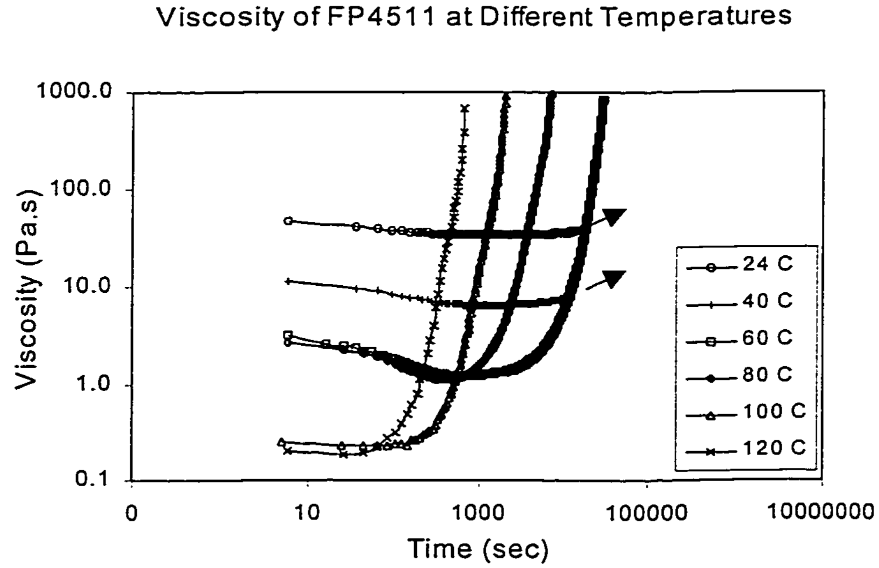

Fig. 4.1: Shear viscosity as a function of temperature of FP4511. The viscosity decreases with increasing temperature before approaching the gelation point.

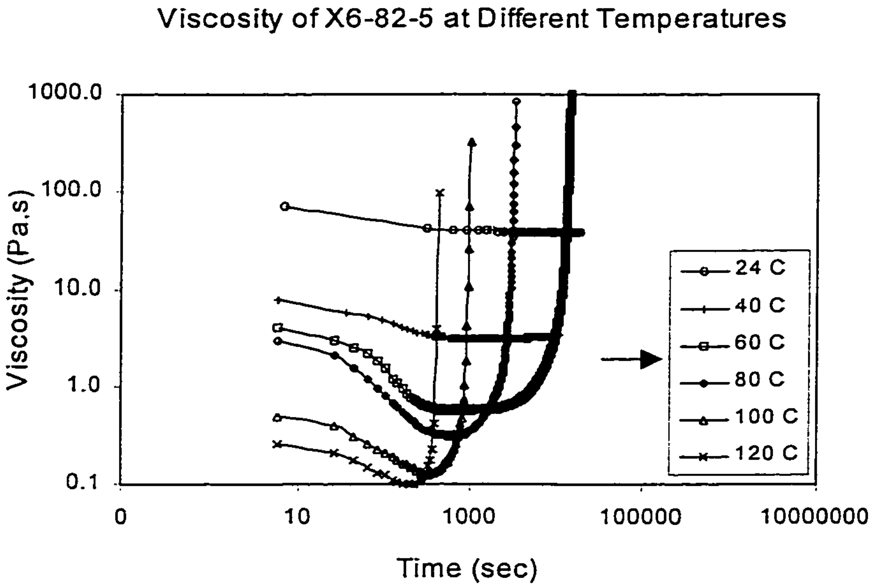

Fig. 4.2: Shear viscosity as a function of temperature of X6-82-5. The viscosity decreases with increasing temperature before approaching the gelation point.

The dynamic mechanical properties (G' and G") of the 130 °C isothermal cure of X6-82-5 underfill resin are shown in Fig. 4.3. As the system approaches the gelation point, storage shear modulus (G') and loss shear modulus (G") increase sharply and crosses each other at tan δ equals to 1. The crossover of G' and G" was used to indicate the apparent gelation time. However, G' and G" of FP4511 at 130 °C did not crossover each other (see Fig 4.4). The G' and G" came closed to each other and finally the values dropped down due to the plates separated from each other. The point where G' and G" came closest to each other was selected to indicate the apparent gelation time. This study intended to determine the apparent gelation time of the samples at different temperatures. Therefore, the testing conditions were not carried in a way to adjust the sensitivity of the instrument in order to detect the small value of shear moduli of the liquid far below the gelation. The limit of the selected transducer did not allow us to get the shear moduli of the solid after gelation either.

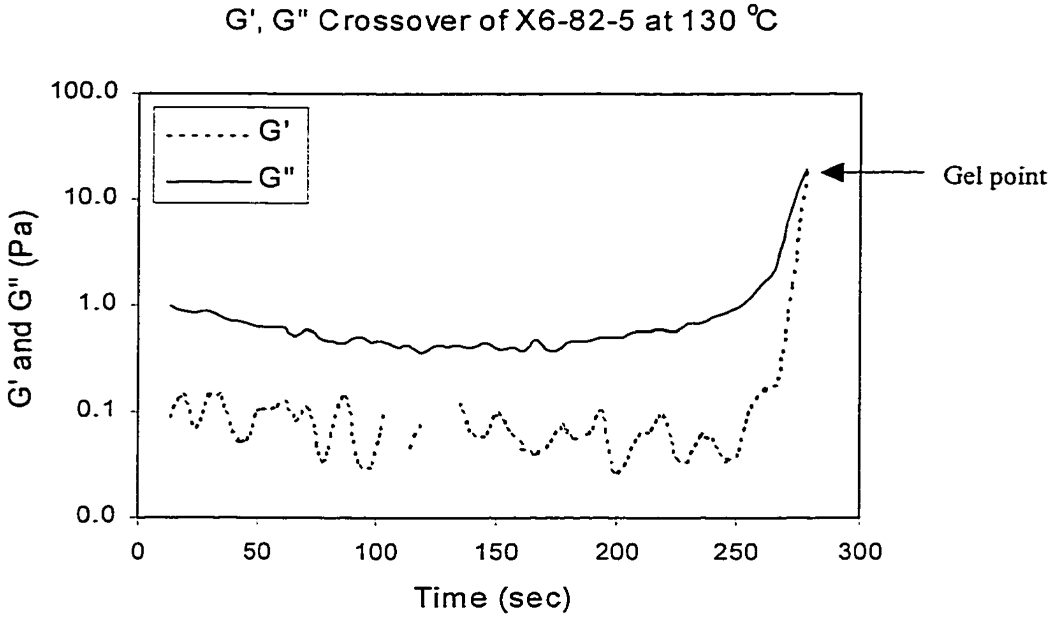

Fig. 4.3: G' and G" crossover indicates the gelation point of X6-82-5 at 130 °C isothermal.

Fig. 4.5 shows the gelation time as a function of temperature. The higher temperature, the lower gelation time. Because gelation represents a specific extent of reaction, the temperature dependence of the time to gel should be described by the Arrhenius equation:

$$\ln t = \text{constant} + \frac{E_a}{RT} \tag{4.1}$$

The plot of the natural log of gelation times versus the reciprocal of temperatures gives the activation energy as in Fig. 4.6 and 4.7 for FP4511 and X6-82-5, respectively. The apparent activation energy for gelation of X6-82-5 system (44.85 kJ/mol) is a little bit lower than that of FP4511 system (47.53 kJ/mol). However, there were some deviations from the straight line. This may caused by the influence of vitrification that occurred at cure temperature lower than $T_{g\infty}$ of the samples.

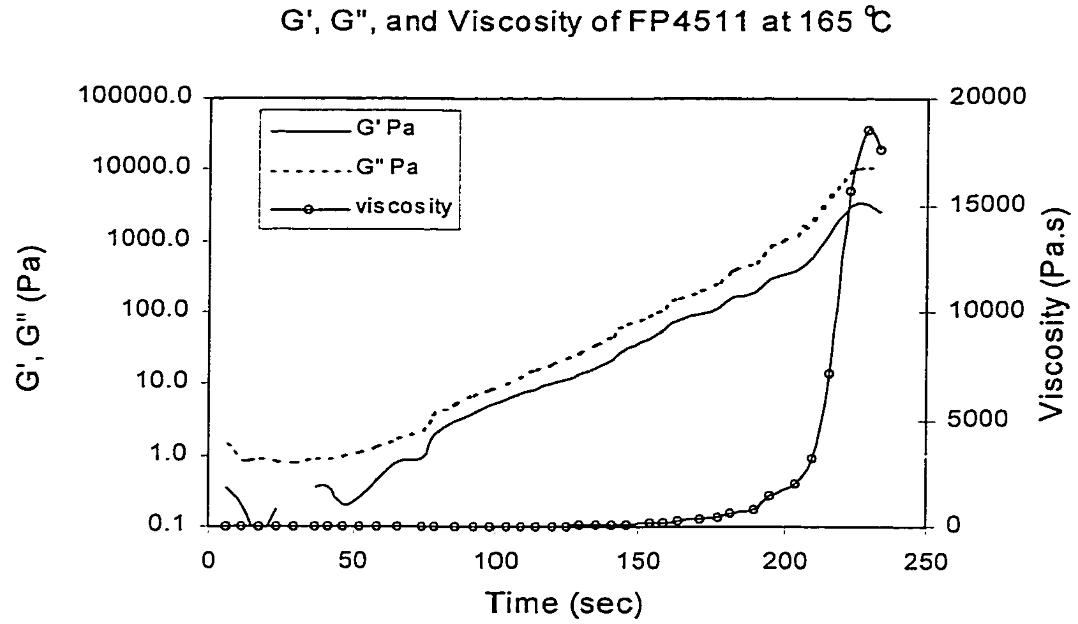

Fig. 4.4: G' and G" do not crossover. The sharp increasing of viscosity indicates the gelation point in case of FP4511at 165 °C isothermal.

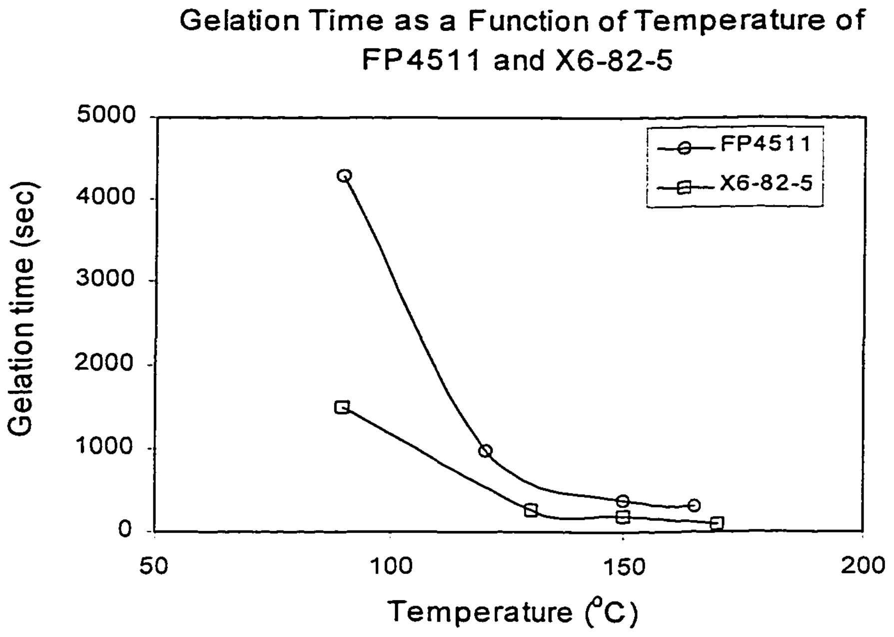

Fig. 4.5: The higher cure temperature, the shorter gelation time.

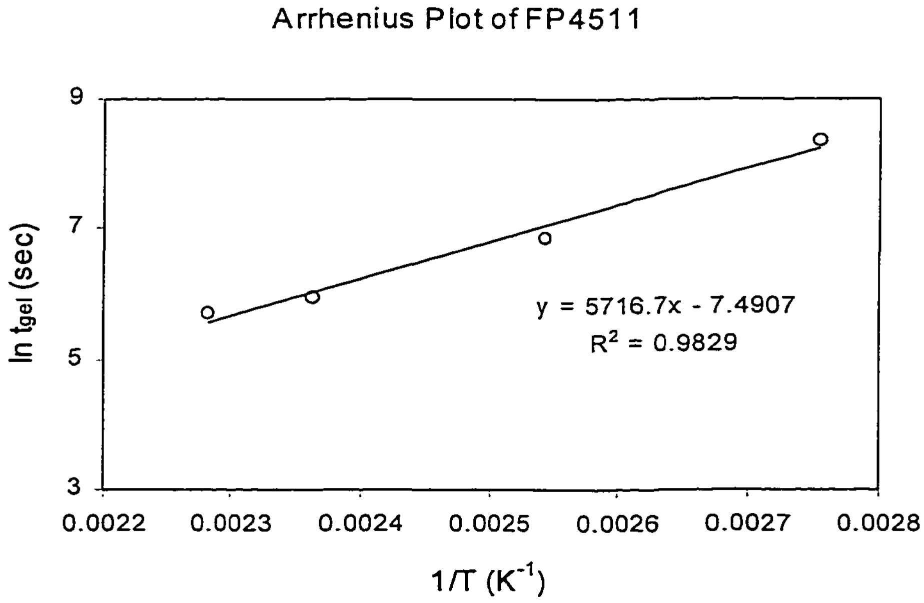

Fig. 4.6: Arrhenius plot of FP4511 gave apparent activation energy of 47.53 kJ/mol.

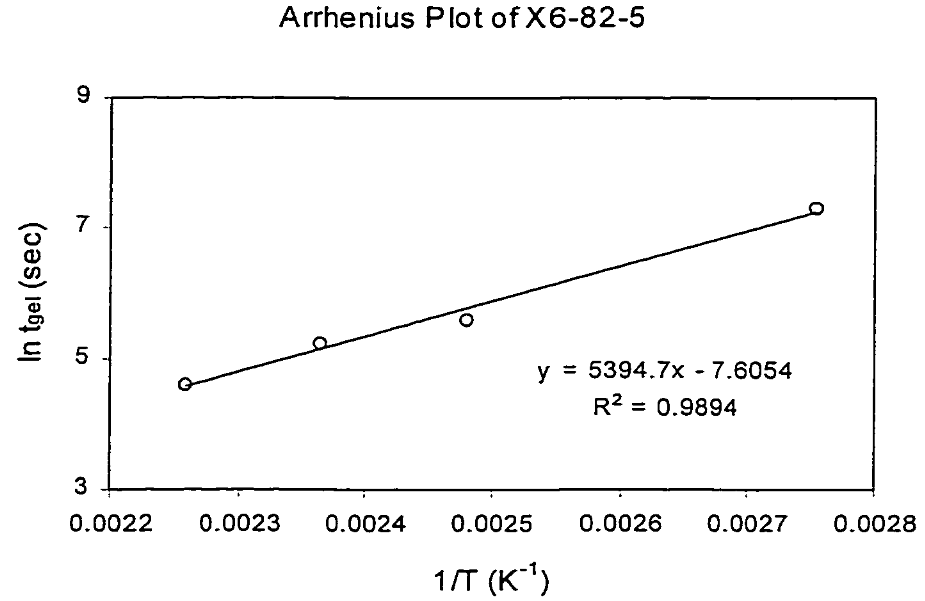

Fig. 4.7: Arrhenius plot of X6-82-5 gave apparent activation energy of 44.85 kJ/mol.

4.1.2 Surface Tension as a Function of Temperature

The effect of temperature on surface tension is shown in Fig. 4.8. It can be seen that the surface tension decreases with increasing temperature as in contact angle measurement. However, the values of surface tension at room temperature and elevated temperatures were not much different as in case of the contact angle. X6-82-5 has a higher surface tension than FP4511.

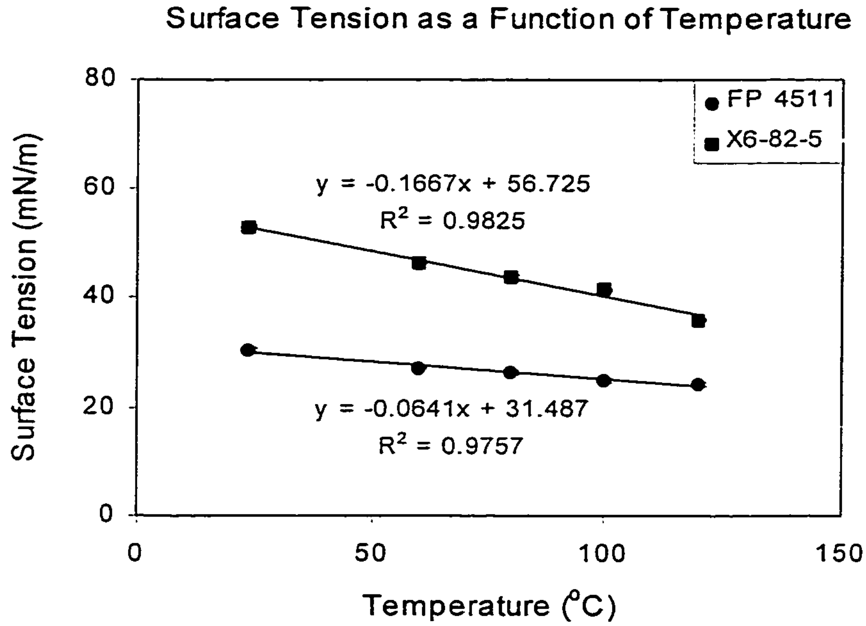

Fig. 4.8: Surface tension decreases with increasing temperature.

Zisman [110] found that the contact angle of hydrocarbons on a low energy surface (low-energy fluorocarbons) was a function only of the surface tension of the liquid. This meant that the interfacial tension was a function of only solid and liquid surface tensions. However, for the studied resins, it can be clearly seen that surface tension is not the only factor for contact angle. The higher surface tensions of X6-82-5 than those of FP4511 at elevated temperatures did not give the higher degree of contact angle. An acid-base interaction between a polyimide surface and the samples should influence the contact angle value as well. This concept was developed by Fowkes [33]. He recognized that the critical factors controlling wettability were interactions between the phases across the interfaces.

From the data of surface tension as a function of temperature, surface entropy can be calculated from the slope of the curves as the following relationship [111].

$$\Delta S^{s} = -\frac{d\gamma}{dT} \qquad (4.2)$$

where ΔS^{s} is the surface entropy. The surface energy indicates the organization of chain at the interface or the surface. X6-82-5 exhibited a higher surface energy than FP4511 (0.167 compared to 0.064 mN/m-°C). The surface entropy of common polymers is in the range of 0.04 – 0.07 mN/m-°C. Poly (butadiene) with carboxyl acid end group has a higher surface energy as 0.14 mN/m-°C [112]. However, literature values of the surface entropy of epoxy polymers have not been reported.

4.1.3 Contact Angle as a Function of Temperature

The effect of temperature on the contact angle of the underfill resins on polyimide was investigated, and the results were shown in Fig. 4.9. As expected, the contact angle decreases with increasing temperature. The contact angles of X6-82-5 are much lower than those of FP4511; however, there was an exception at room temperature. Therefore, to understand the wettability of the samples on a surface, one should consider the contact angle at elevated temperature, which is the actual working temperature. In addition, the contact angle at elevated temperature is necessary for the flow behavior study. Only the contact angle measurements at room temperature can be misreading. The contact angle measurement shows that X6-82-5 wets polyimide surface better than FP4511.

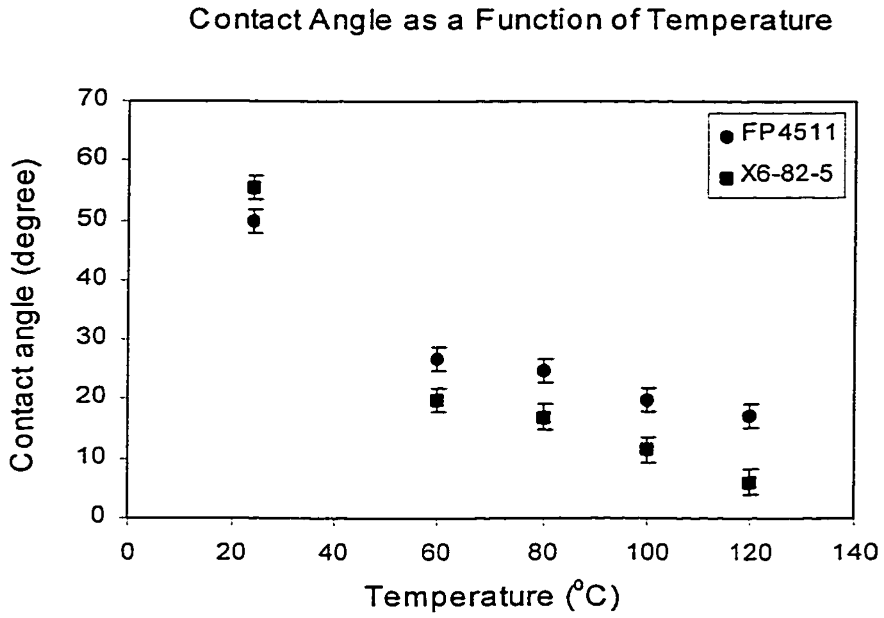

Fig. 4.9: The contact angles decrease with increasing temperature.

4.1.4 Cure Kinetics and Extent of Reaction

DSC was used to monitor the cure kinetics of samples as a function of temperature and time. Fig. 4.10 shows the DSC thermograms of FP4511 and X6-82-5 when subjected to the dynamic temperature scan from 25 °C to 300 °C. The onset temperature, which is the temperature at which the rate of curing becomes significant, of each underfill resin was at the same range of temperature (120 – 130 °C). However, the temperature at the peak of X6-82-5 was about 25 degrees higher than that of FP4511. The exothermic reaction peak indicates the maximum curing rate of a system. Generally, the recommended cure temperature would be at, or above, this peak temperature. Nevertheless, the recommended cure temperature of both of these underfill resins is at

150 °C. At this point, there are no questions about how the manufacturer designed the cure temperature on X6-82-5, but FP4511. $T_{g\infty}$ (see Fig. 4.12) of X6-82-5 was about 120 –140 °C, while that of FP4511 was about 165 °C. To explain this difference, one has to deal with the chemistry and reaction mechanism of the system, which will be presented later in this thesis on model epoxies. Furthermore, the exothermal heat of reaction of X6-82-5 was much higher than that of FP4511. The appearances of the exothermic peaks of the underfill resins were different; X6-82-5 has a sharp and narrow peak, which refers to the fast rate of reaction, while FP4511 has a broad peak. This was caused by the difference in reaction mechanisms and cure chemistry of the systems.

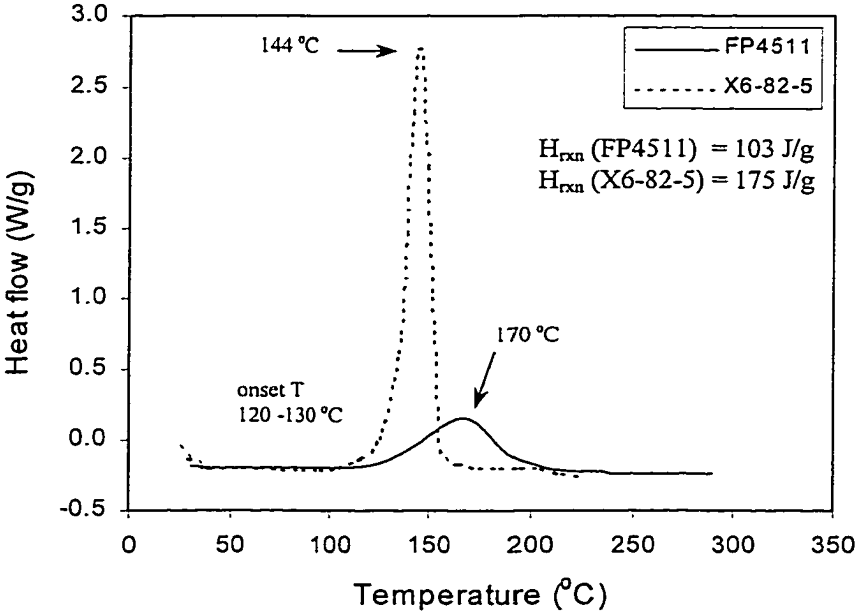

Fig. 4.10: Temperature dynamic DSC thermograms for fresh samples of FP4511 and X6-82-5 show the faster rate of reaction of X6-82-5.

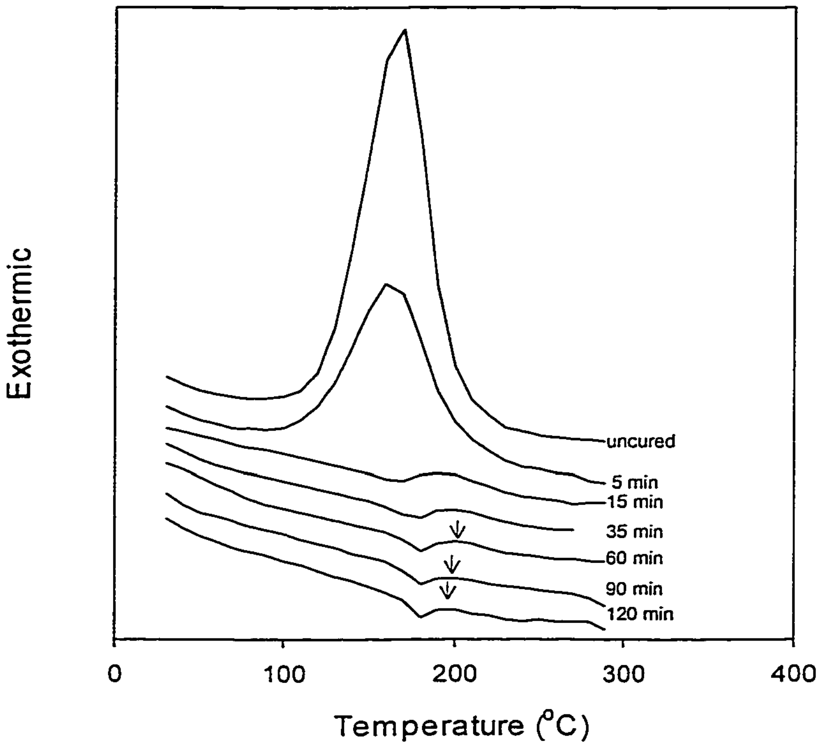

Fig. 4.11: DSC thermogram of the residual heat of reaction of FP4511 after partially cured at 165 °C.

Figs. 4.11 and 4.12 contain DSC thermograms of the residual heat of reaction of FP4511 after partially cured at 165 °C and of X6-82-5 partially cured at 130 °C for different periods of time, respectively. The thermograms show the variation of the exotherm and the glass transition. In these figures, the exotherm changes greatly in terms of the peak temperature and the area as cure proceeds. Noticeably, FP4511 thermograms have a bump after the T_g transition, even at the higher temperature and longer period of time than what the manufacturer recommended. This could be the unreacted sample. Park et al. [65] studied an isothermal cure of epoxy-rich/anhydride system, and reported that the bump peak represented the etherification reaction, which occurs at a high temperature. Interestingly, this peak shifted to a lower temperature scale with curing. The shift of the peaks may be attributed to the change from kinetically controlled to diffusion-controlled reactions.

The extent of reaction is an important factor for the adhesive strength; therefore the extent of reaction as a function of cure time at different temperatures was monitored. The results are shown in Fig. 4.13 and 4.14 for FP4511 and X6-82-5, respectively. As expected, the higher cure temperature, the higher rate of curing. X6-82-5 has a much faster cure rate than FP4511. At the cure temperature much lower than $T_{g\infty}$ of the samples ($T_{g\infty}$ for FP4511 and X6-82-5 are 165 and 120-140 °C, respectively), such as at isothermal 120 °C curing for FP 4511, the reaction could not go to completion due to the vitrification (the maximum extent of reaction was about 88 %).

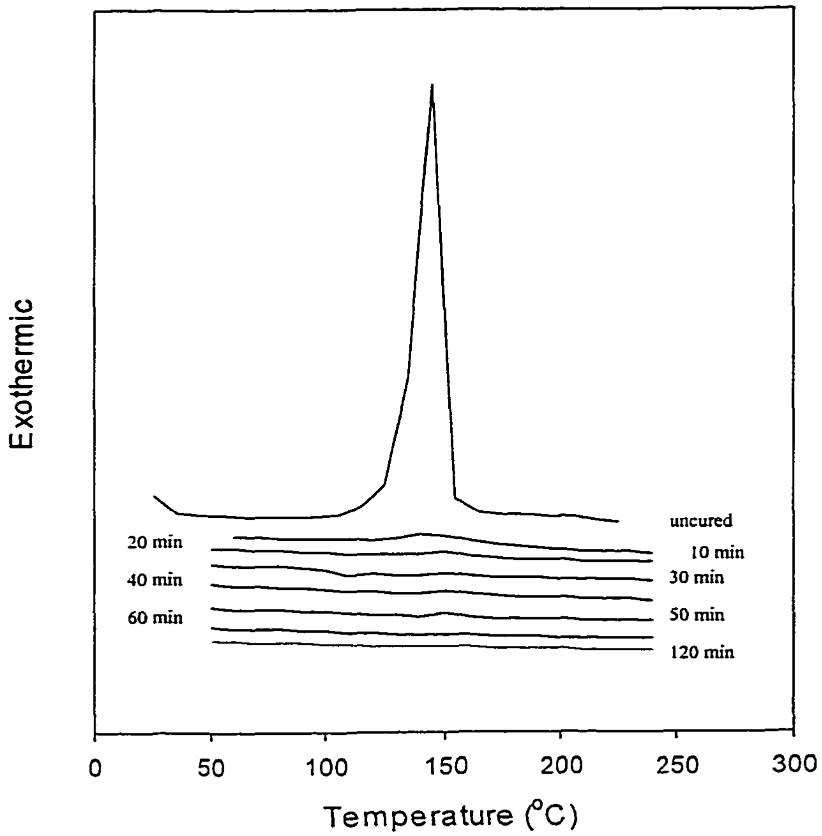

Fig. 4.12: DSC thermogram of the residual heat of reaction of X6-82-5 after partially cured at 130 °C.

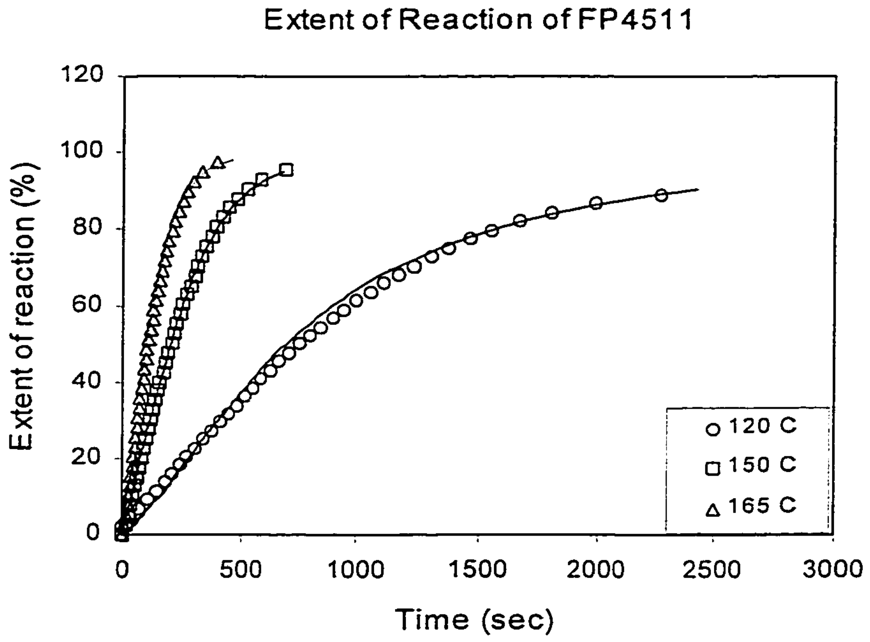

Fig. 4.13: Extent of reaction of FP4511 as a function of time at different temperatures; the higher cure temperature, the faster cure rate.

By numerically fitting the data to the autocatalytic kinetic model (Equation 3.12 p. 62), the orders of reaction were obtained (the fitting curves are the solid lines in Figs. 4.13 and 4.14). The orders of reaction for FP4511 and X6-82-5 are shown in Table 4.1. Malhotra et al. [81] studied the kinetics of cure of FP4511 by using the n-th order model, and found that the order of reaction for FP4511 is equal to 1.

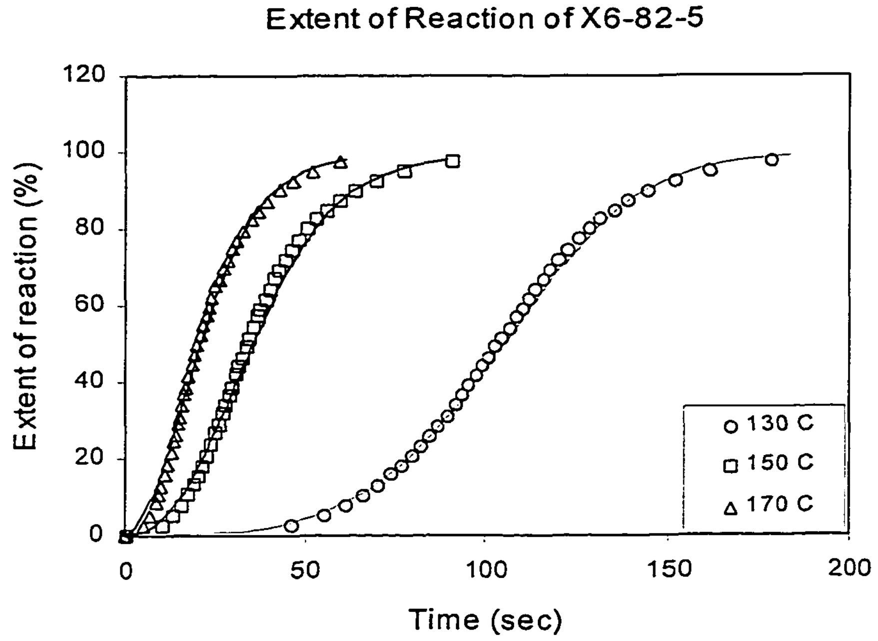

Fig. 4.14: Extent of reaction of X6-82-5 as a function of time at different temperatures; the higher cure temperature, the faster cure rate.

Table 4.1: Kinetic parameters for FP4511 and X6-82-5 resins.

Sample	Isothermal temperature	k	n	m
FP4511	120	0.072	0.50	0.24
	150	0.20	0.29	0.10
	165	0.40	0.29	0.10
X6-82-5	130	0.50	0.092	0.72
	150	1.40	0.19	0.55
	170	2.20	0.21	0.43

4.1.5 Outgassing

TGA was used to monitor the weight loss during dynamic temperature scanning. The weight loss prior to 100 °C is often associated with solvent evaporation such as in die attach adhesives [113]. The loss of any volatile products from the sample during the curing could be one of the factors that causes the void formation or porosity, which is undesirable. Outgassing is a critical problem in the case of die attach adhesives [57] since they contain solvents and other additives. In underfill resins, typically solvents are not included; however, other compositions, such as defoaming agents, surface tension modifiers, hardener, and catalyst can evaporate at elevated temperatures (higher than their boiling points). In addition, this technique was utilized to investigate the thermal degradation of the samples at high temperatures. Thermal stability is one of the requirements for epoxy resins to be used as the adhesives. Fig.4.15 displays the weight loss behavior at a heating rate of 10 °C/min for FP4511 and X6-82-5. There was about 3% weight loss at about 80–150 °C in case of FP4511, which was most likely caused by the anhydride volatilization, and the major weight loss at 240 °C was caused by resin degradation. For X6-82-5, there was no significant weight loss at low temperatures. The degradation began at about 350 °C. Note that X6-82-5 has better thermal stability than FP4511.

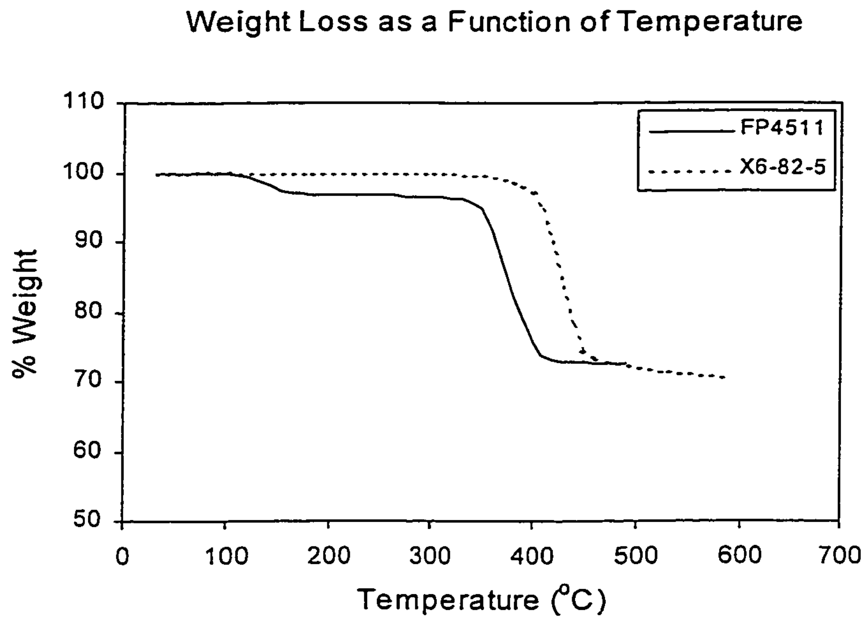

Fig. 4.15: FP4511 exhibits weight loss at 150 °C due to anhydride volatilization, and degrades at 340 °C, while X6-82-5 does not show any weight loss until it degrades at 380 °C.

4.1.6 Void Formation

The ultimate aim of adhesive processing is to produce void-free joints to optimize the reliability. This depends on a complex interaction involving heat transfer, resin flow and chemical reaction. Once the material properties and processing inter-relationships have been identified it is possible to obtain an optimum condition for accomplishing the most reliable products. In epoxy adhesives, entrapped air and the release of volatile materials during cure are the main causes of voids in the cured epoxy. Viscosity is also important because it correlates to the resistance of the medium to molecular motion, which controls both self-diffusion and diffusion of any dissolved species.

Entrapped air is considered as pre-existing bubbles in the system. There are a number of studies trying to get rid of these bubbles. In the colloidal field of study, it has been stated that one needs to apply a sufficiently great pressure to collapse all bubbles in the system [114]. The magnitude of the pressure required will of course depend on the size of the bubble to be removed. However, generally very great pressure is needed. In addition, microbubbles can be nucleated when the applied pressure is released. Therefore, this method may not be suitable for removing the entrapped air in epoxy resins.

Bubbles present within the resin will either grow or collapse, according to the concentration of the mobile species, the temperature, and the hydrostatic pressure in the resin during the cure cycle. Changes in temperature and pressure have an effect on bubble behavior and the solubility of mobile species in the resin. An increase in temperature or a decrease in pressure will cause the gas within the bubble to expand, resulting in the bubble growth. An increase in temperature also causes an increase in the diffusion coefficient and mass transfer of mobile species, resulting in more bubble growth or collapse, depending on the direction of the diffusion gradient relative to the host bubble [115]. Models based on a mass-diffusion theory [115] successfully represent the growth and collapse of gas bubbles in an epoxy resin. Wood et al. [114-116] have tried to evaluate the input parameters for a diffusion model using a solubility parameter approach [115] and a free-volume approach [117].

The viscosity of a resin system is extremely temperature dependent, initially decreasing sharply as the temperature is raised and then rapidly increasing as cross-linking reactions lead to gelation of the resin (see Fig. 4.1 and 4.2). This increase in viscosity decreases the flow and diffusion; therefore, if the entrapped air and volatile product cannot escape from the sample before it gels, then voids will be left inside the cured resin.

In this study, different isothermal temperatures and 2 step cure schedules were used to see how they affected void formation. Optical microscopy revealed that X6-82-5 contained many more voids (diameter 20-50 μm) than did FP4511, as shown in Table 4.2. A contributing factor to the high amount of voids contained in cured X6-82-5 is most likely due to the short gelation times. The higher cure temperatures, the higher number of voids observed. At higher temperatures the gelation time is shorter, so there is not enough time for entrapped air or volatile products to escape from the resin.

Furthermore, the surface tension of a sample, which is related to the cohesive energy density of the resin as forces between molecules, which leads to a drawing together of liquid molecules [118], also plays a significant role in bubble behavior. X6-82-5 has a higher surface tension than FP4511; therefore, entrapped air and volatile need a greater driving force to diffuse out from the sample (e.g., at 24 °C, surface tension of FP4511 and X6-82-5 were 30.3 and 52.7 mN/m, respectively). There was a slight decrease in surface tension with the increase of temperature (see Fig. 4.9); however, cross-linking reaction is fast and shields out the effect of the decreasing of surface tension on void formation. In addition, non-uniform flow during penetration can cause trapped air bubbles in an underfill. The 2 step void formation experiment revealed that 2 step curing could either reduce the number of voids or decrease the size of voids. At 90 °C, there was enough time for some amount of volatile or entrapped air to diffuse out from the sample before the sample reached the gel point (see Fig.4.16).

Table: 4.2: Amount of voids observed for different isothermal curing condition as well as for 2 step curing of FP4511 and X6-82-5.

Temp. (°C)	FP4511	X6-82-5
120	Negligible	-
150		
165		
130	-	0.55 % area
150		0.95 % area
170		1.33 % area
90/120	None	-
90/150		
90/165		
90/130	-	Reduced amount/size
90/150		Reduced in size
90/170		Reduced in size

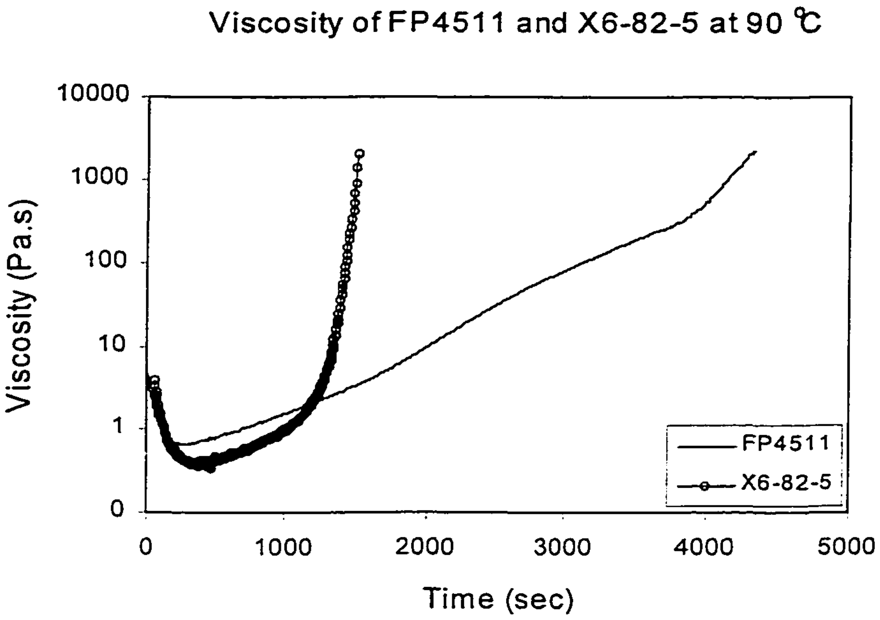

Fig. 4.16: Gelation time of FP4511 at 90 °C is long enough for anhydride to diffuse out rather than causing void formation.

4.1.7 Cure and Cooling Stress

Stress is generated in the cured thermosets under constraint due to the volume shrinkage and modulus of the thermosetting resin during cure. Residual stress in thermosets affects the reliability of the adhesive bond as mentioned previously in the background section. Therefore, in the research that attempts to improve the reliability of the adhesive bond, it is important to know if the curing conditions influence the cure stress and the stress after cooling from the cure temperature. The curing process of thermosets involves not only chemical reactions, but also their physical phenomena, such as chemical and thermal shrinkage and volatile desorption. Volumetric chemical shrinkage of the curing for a typical epoxy resin is 5% [86]. The shrinkage stresses due to the chemical reaction are usually significantly less than the stresses due to the temperature change (e.g., during the cool down process). Nonetheless, the influence of isothermal cure stresses on the thermosetting resins is often misjudged. However, for electronic packaging, this small magnitude of stress could tremendously affect the adhesive bond. It can facilitate the fracture failure and delamination between adhesives and substrates. Korotkov et al. [119] and Chekanov et al. [120-121] found that the cure shrinkage stress during isothermal curing of epoxy resins in a constraining vessel causes the formation of defect at the vessel surface. They also stated that the mechanisms of shrinkage damage and type of defects are defined initially by gelation and vitrification processes.

In a cure schedule it is usual to specify a cure time (t_c) and a cure temperature (T_c). In this study, stress was measured during the isothermal cure process of the underfill resins; FP4511 and X6-82-5. Furthermore, for X6-82-5, after the isothermal was completed, the system was cooled down to about the $T_{g\infty}$ of the sample.

4.1.7.1 Isothermal Cure Stresses

The cure stress measurements at different isothermal temperatures as a function of time are shown in Figs. 4.17 and 4.18 for FP4511 and X6-82-5, respectively. Since the sample was cured isothermally, there were no thermal stresses and the shrinkage stress is exactly the one-dimensional of the cure stress. However, it is assumed that no exothermic heat is generated and that the thermal conductivity of the sample is high enough to bring the sample temperature to the chamber temperature during the experimental period. It is also reasonable to assume that there is no cure stress developed until the sample gels. It was found that at a higher cure temperature the stress developed faster than at a lower temperature, but once they reached a plateau, the magnitude of cure stresses was similar at most cure temperatures. At the cured temperature far below the $T_{g\infty}$ of the material (85 °C isothermal curing of FP4511), a lower cure stress was obtained. This is most likely due to the material vitrifying right after the gelation. Surprisingly, X6-82-5 exhibits a small cure stress. In contrast, FP4511 displays a cure stress of 450 kPa.

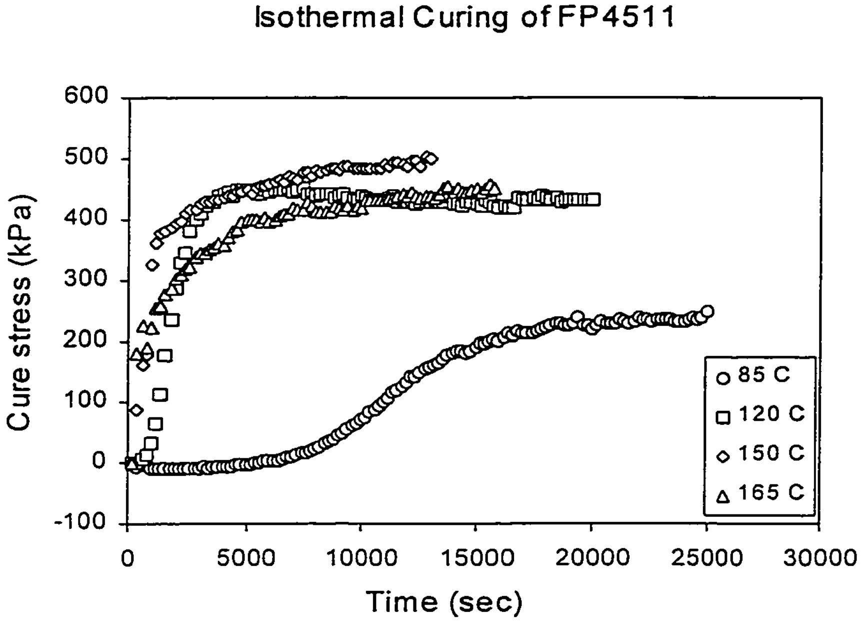

Fig. 4.17: Isothermal curing of FP4511 gave about 450 kPa of cure stress except at 85 °C, when the lower cure stress was obtained due to vitrification.

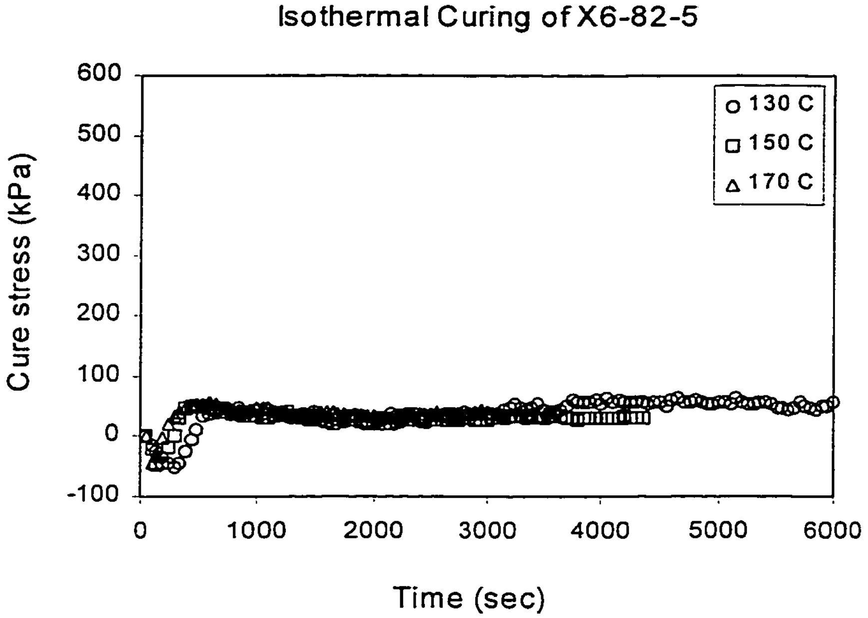

Fig. 4.18: Isothermal curing of X6-82-5 gave about 50 kPa cure stress.

4.1.7.2 Multistep Cure Stresses

Since the thermal expansion during the temperature changes causes a build-up of compression stress, multi-step curing can reduce or offset the cure stress as suggested by Plepys et al. [60]. Therefore, 2 and 3-step curing were studied for both FP4511 and X6-82-5, and the results are shown in Figs. 4.19 and 4.20. It was found that multi-step curing could reduce the cure stress. Furthermore, in the case of X6-82-5, a build-up of compressive stress was observed. Raising the temperature during cure in a controlled fashion (e.g., raise the temperature when tensile stress starts to develop) can reduce the cure stress; therefore, the flow temperature may influence the tendency for delamination.

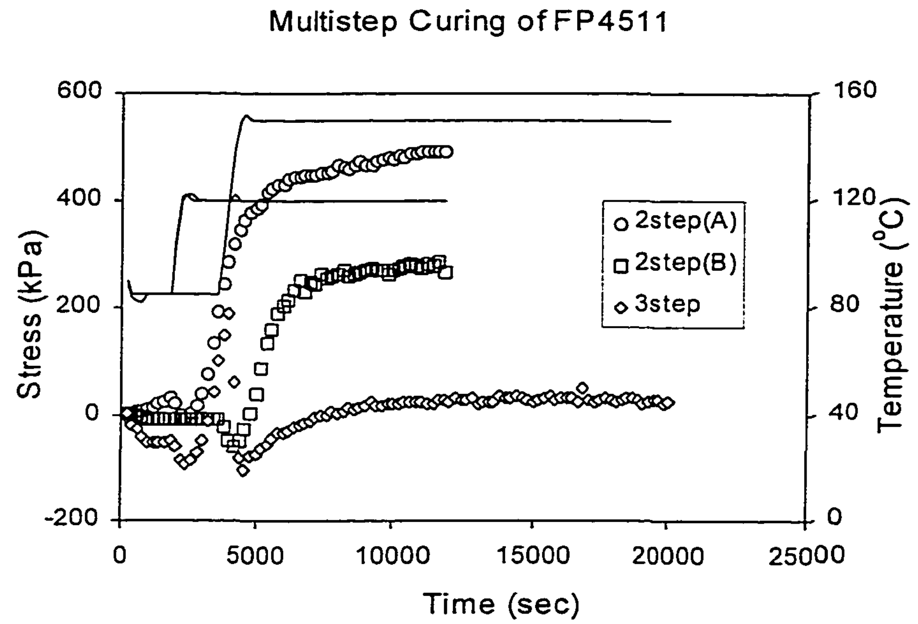

Fig. 4.19: Multistep curing of FP4511 provided lower cure stresses.

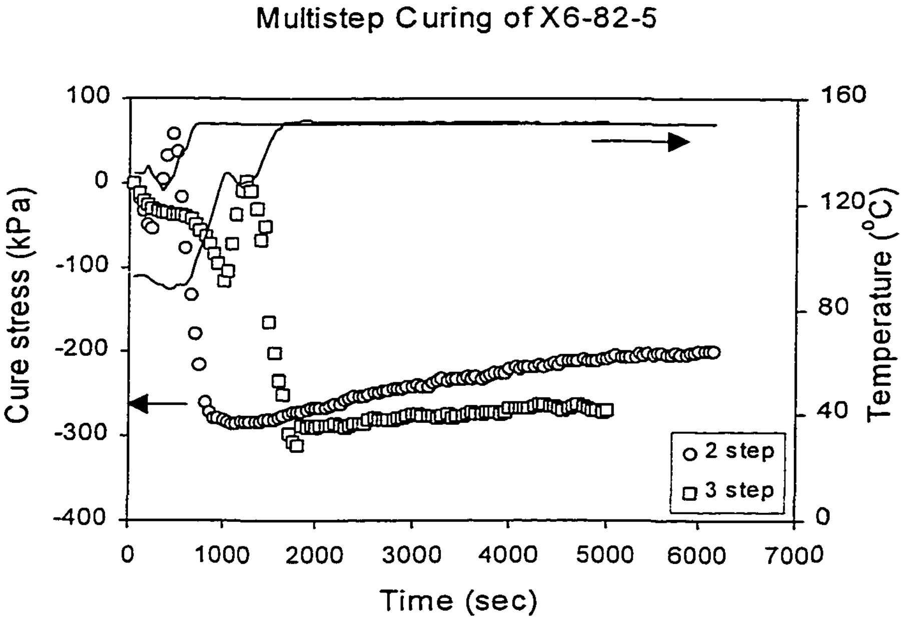

Fig.4.20: Multistep curing of X6-82-5 provided compressive stresses.

4.1.7.3 Cooling Stresses

When a cured sample is cooled down, it turns from a rubbery state to the solid (glassy) state at below its T_g. Once the sample becomes solid, its modulus increases about 100-fold from what it is at above T_g [61]. Therefore, upon cooling below T_g, the thermal stresses are largely due to the increase in modulus of the epoxy resin. The sample also contracts when it is cooled down, which makes an increase in stress as well. In conclusion, both the extents of shrinkage and modulus of sample affect the magnitude of stress. The cooling down process was applied to X6-82-5 after the polymerization was completed with isothermal curing as in Fig. 4.21. Although the cure stresses of different isothermal temperatures were similar, the stresses of systems after cooling down to the same temperature were different. The larger temperature excursion, the higher stress.

The rate of cooling influences the stress as well; however, this study did not cover this factor and we shall examine the literature. Biernath [122] explored the impact of cooling rate by a bending beam technique. He found that an epoxy exhibited a higher T_g when the cooling rate was faster. This is because faster cooling rates, because they are much faster than the response times of the molecules, create more thermal stress in the amorphous matrix below the T_g. This stress, in turn, leads to long-range forces, which decrease long-range molecular mobility resulting in an increase in T_g [102]. A higher T_g material initiates stress-induction by thermal expansion at higher temperatures, thereby giving rise to a higher stress at room temperature. However, in the range of cooling rates that he studied (5 and 15 °C/min), no effect of cooling rate on the stress-behavior was observed.

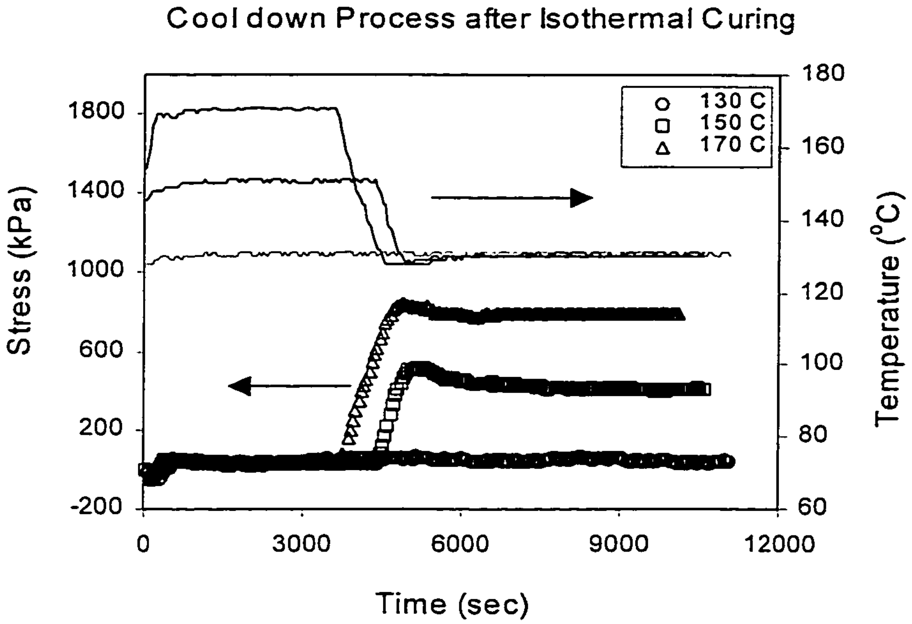

Fig. 4.21: Stresses of X6-82-5 during isothermal curing with cooling down process.

The magnitude of the stress due to the cooling down process can be calculated from the modulus and the CTE (α) of resin by Equation (4.3). The shear modulus and CTE as a function of temperature of X6-82-5 are shown in Figs. 4.22 and 4.23. The cooling down process was performed from the cure temperatures to 130 °C, which is higher than T_g of X6-82-5 when it was cured at high temperatures (150 and 170 °C). Therefore, the rubbery modulus and CTE were used to estimate the cool down stress.

$$\sigma_{cool} = E\alpha\Delta T \qquad (4.3)$$

where E is Young's modulus, which is equal to 2(1+υ)G, ΔT is the difference in degree of temperature from the cure temperature to the final stage. Possion's ratio (υ) of rubbery materials is 0.49. The calculation shows that the developed stress from the cooling from

150 and 170 to 130 °C are 0.44 and 0.88 MPa, respectively. This is comparable to the experimental result of 0.41 and 0.80 MPa (see Fig. 4.21).

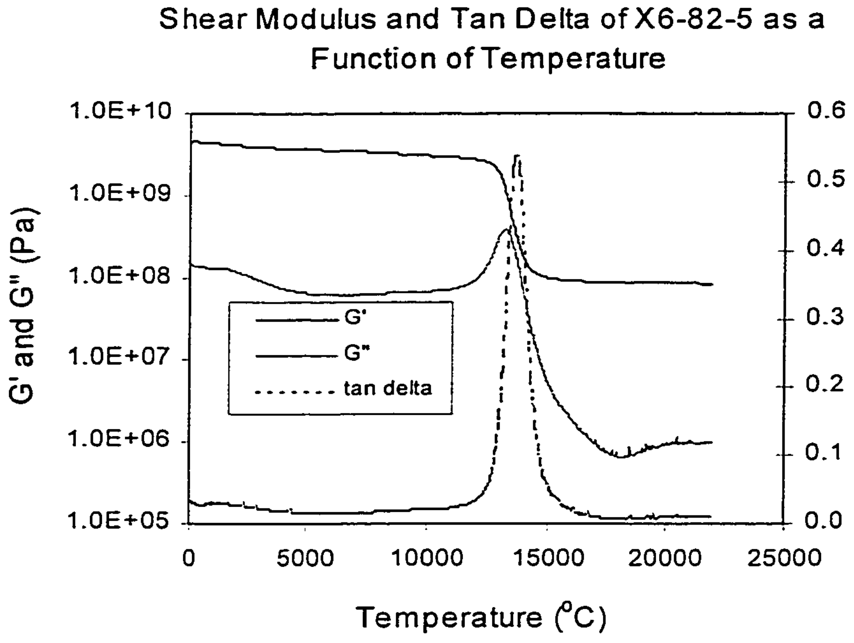

Fig. 4.22: Shear modulus and tan delta of fully cured X6-82-5.

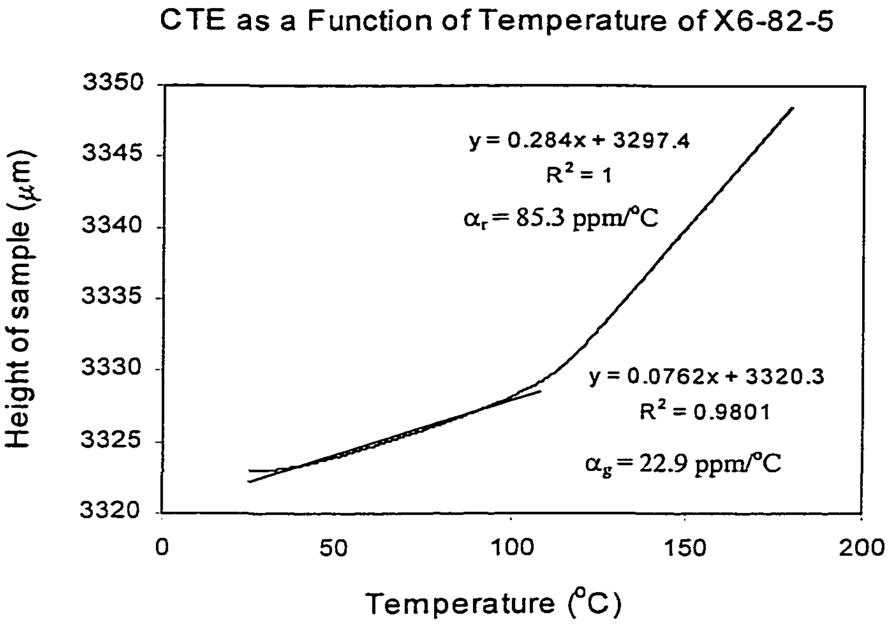

Fig. 4.23: Coefficient of thermal expansion (CTE) of X6-82-5 as a function of temperature.

4.1.8 Adhesive Strength

To examine the effect of residual stress on the adhesive strength, the interfacial fracture energy (G_{IC}) of X6-82-5 sample was measured using a DCB method. The sample was cured at the same cure schedules as performed on cure stress measurement (Table 3.1). The result is shown in Table 4.3. The failure mode of all specimens, which was simply determined by inspection, was cohesive failure. Obviously, the magnitude of residual stress did not greatly affect the adhesive strength. The DSC study revealed that this sample gave a high enough (97%) extent of reaction even when it was cured at 130 °C (20 degrees lower than the recommended cure temperature). However, the higher cure temperature can bring the cure reaction closer to completion, and may yield higher adhesive strength. Because of the difference in sample sizes that were used on DSC and DCB testing, it is meaningful to note that the extent of reaction under the same cure temperature and time on the two techniques may not be the same. Furthermore, the adhesive strength is also a function of the wettability between two surfaces. The higher temperature provided lower viscosity at the beginning of the curing, and also the lower surface tension and contact angle. These liquid properties enhanced the wetting of the sample onto the polyimide and the aluminum bar surfaces, then gave a better adhesive strength.

The adhesive strength of FP4511 was studied by one of the students in "Lehigh Electronic Packaging" research group [123]. She found that the interfacial fracture energy of this sample, which was cured at 150 °C for 2 hours, was about 19 ± 2 J/m^2. The mode of failure was in the adhesive mode. A comparison between the two underfill resins showed that X6-82-5 posed a better adhesive strength to polyimide.

Table 4.3: Interfacial fracture energy of X6-82-5 to polyimide PI 2525 at different cure schedules.

Cure Schedule	G_{IC} (J/m^2)	Extent of rxn. (%)
Isothermal 130 °C	41.6 ± 7	97
Isothermal 150 °C	89.9 ± 19	98
Isothermal 170 °C	92.0 ± 28	98
2 Step	75.3 ± 13	98
3 Step	86.9 ± 24	98

4.2 Processing Diagrams for Underfill Resins

Generally, the underfill process includes the filling and cure processes. After the dispensing of an underfill resin into the standoff gap between the printed circuit board and the chip, underfill resin needs to flow to complete the filling. After the filling is completed, the component is sent to the second step to complete the curing reaction of the resin in order to achieve a reliable adhesive bond. The requirement of the 2 step process leads to the longer cycle time in assembly process. In order to reduce the total cost of packaging, this process must be shortened as much as possible. Furthermore, the reliability of the adhesive bond is very important in electronic packaging assembly. However, the material that has a faster cure kinetics may cause poorer reliability [124], due to poor flowability from gelation during cure. Therefore, the optimum processing condition is substantial to acquire.

4.2.1 Underfilling Step

The underfilling step must occur quickly and without void formation. In addition, the segregation of filler must be avoided. Fillers in underfill resins have strong effects on the flow of the encapsulant, particularly in assemblies with gap height less than 100 μm. In our study, the effect of fillers was not included. However, it is important to mention here that fast filling requires a low viscosity resin, which can be obtained by raising the filling temperature to a certain temperature. This low viscosity promotes the segregation of filler. Therefore, the optimization of the filling step is essential to study. Two underfill resins, which were used in this study, contain silica particles in similar amounts at about 60-70 weight %. In order to provide guidelines for underfill process, the flow-processing window of underfill resin was drawn by the cooperation of a few simple properties and their corresponding theories. These properties include viscosity, contact angle, surface tension, and gelation time as a function of temperature.

4.2.1.1 The Minimum Time Limit of the Underfilling Step

The minimum time limit of the underfilling step is the time that is needed to complete the filling of the sample through the stand gap of a specific dimension. Due to the fact that the onset temperatures for both underfill resins were at 120-130 °C (see Fig. 4.11), the properties that influence the flow of underfill resins were studied in the range of 24 – 120 °C. The filling time was calculated for a 100 μm gap at the flow length of 10 mm.

The filling time was calculated by using the Washburn model (Equation 4.4) for capillary flow. This equation describes the relation between the flow length and the flow time through the properties of a liquid between two surfaces.

$$\frac{d}{dt}(x_f)^2 = \frac{\gamma}{6}(\cos\theta_o + \cos\theta_s)\frac{s}{\mu_o} = b \qquad (4.4)$$

where γ is the liquid surface tension, θ_o and θ_s are the contact angles at the lower and upper channel surfaces, s is the channel spacing, μ_o is the effective viscosity, and b is the flow parameter, which is independent of time.

Although an epoxy resin reacts with a hardener during the filling process, its properties (e.g., surface tension, contact angle at the lower and upper surfaces, and viscosity) were assumed to be constant with time. The processing diagram was constructed in a function of time versus temperature; therefore, the filling time line was drawn in a corresponding relation to temperature. The sample properties as a function of time were put in mathematical equations from the trend that concluded with the series of measurements. Surface tension as a function of temperature was measured in the range of 24 – 120 °C. A linear relation between surface tension and temperature was obtained in both FP4511 and X6-82-5 as in Fig. 4.24.

Contact angle as a function of temperature was measured in the range of 24 – 120 °C as the results in Fig. 4.25. The contact angle in the range of 60 – 120 °C was in a linear relationship with the temperature, but not at 24 °C. Therefore, the data points at 24 °C of both underfill resins were excluded.

From the results of viscosity as a function of time at different temperatures in Figs.4.1 and 4.2 for FP4511 and X6-82-5 respectively, which were shown previously, the viscosity at the point that the sample equilibrated to the chamber temperature was taken as the viscosity of that temperature. Typically, this was the constant value of viscosity or the lowest value of viscosity before it increased due to polymerization. An Arrhenius relationship (Equation 4.5) is often used to describe the temperature dependence of the viscosity. The viscosity data obeyed an Arrhenius equation in the studied temperature range. However, there was some deviation from the linear line in the case of X6-82-5. The cause of this deviation is most likely due to the reaction kinetics, i.e. the average molecular weight increases significantly before the equilibrium temperature is reached.

$$\eta = Ke^{E_a/RT} \qquad (4.5)$$

where η is viscosity, K is a constant, E_a is the activation energy, R is gas constant, and T is temperature. Viscosity was plotted as a function of 1/T, and the exponential trended equation was attained as in Fig. 4.26 and 4.27 for FP4511 and X6-82-5 respectively.

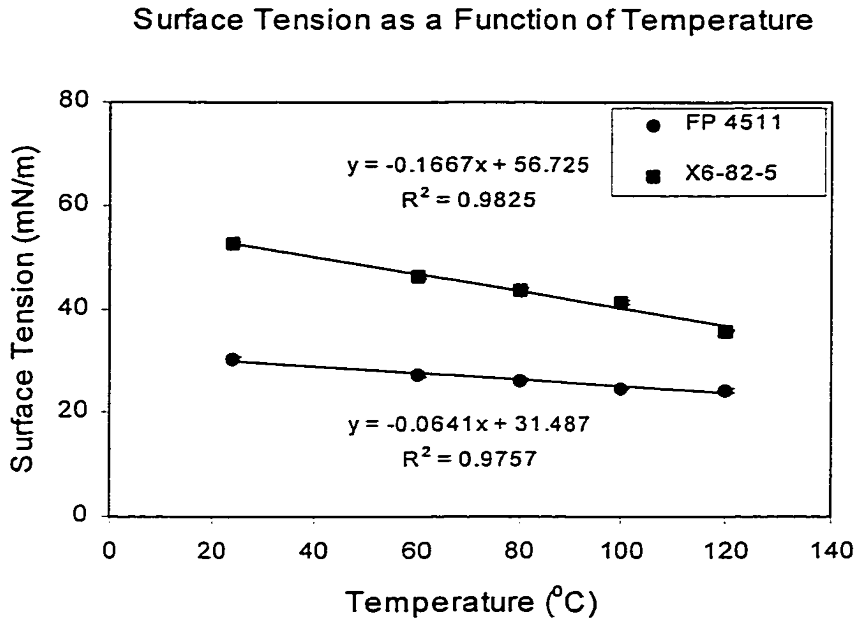

Fig. 4.24: Surface tension as a function of temperature for FP4511 and X6-82-5. Their mathematical relations are labeled near the data lines where x is temperature and y is surface tension.

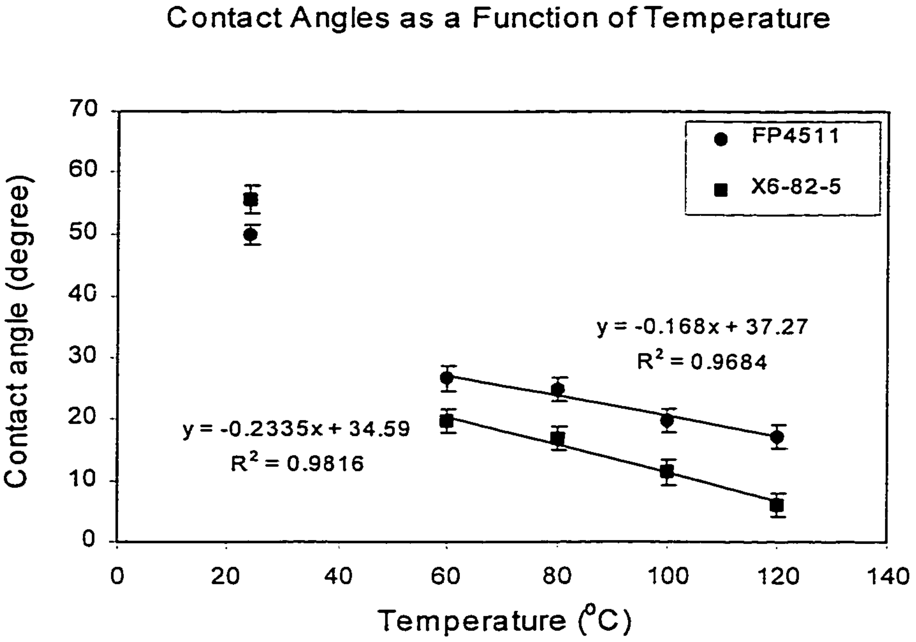

Fig. 4.25: Contact angle as a function of temperature for FP4511 and X6-82-5. Their mathematical relations are placed beside their data lines where x is temperature and y is contact angle.

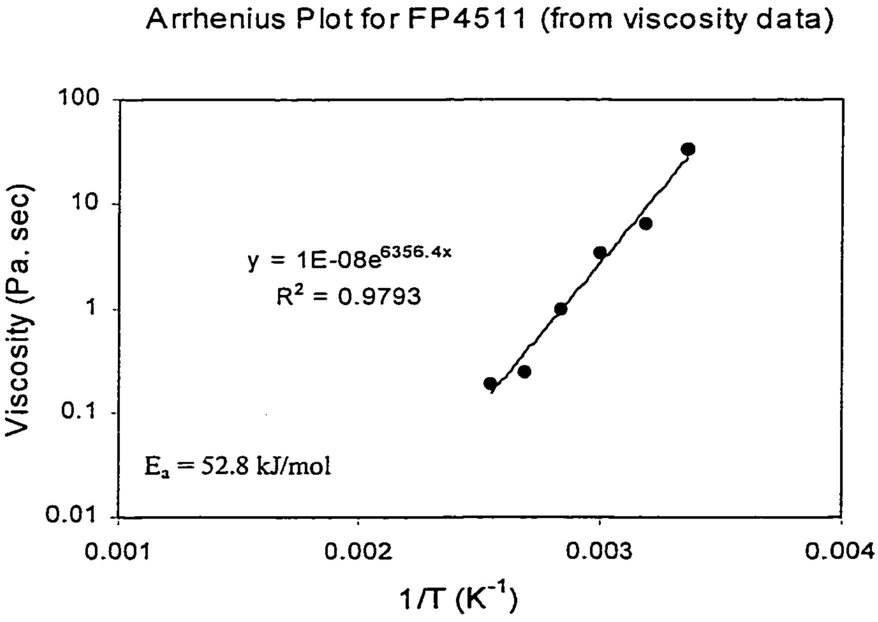

Fig. 4.26: Arrhenius plot of viscosity of FP4511.

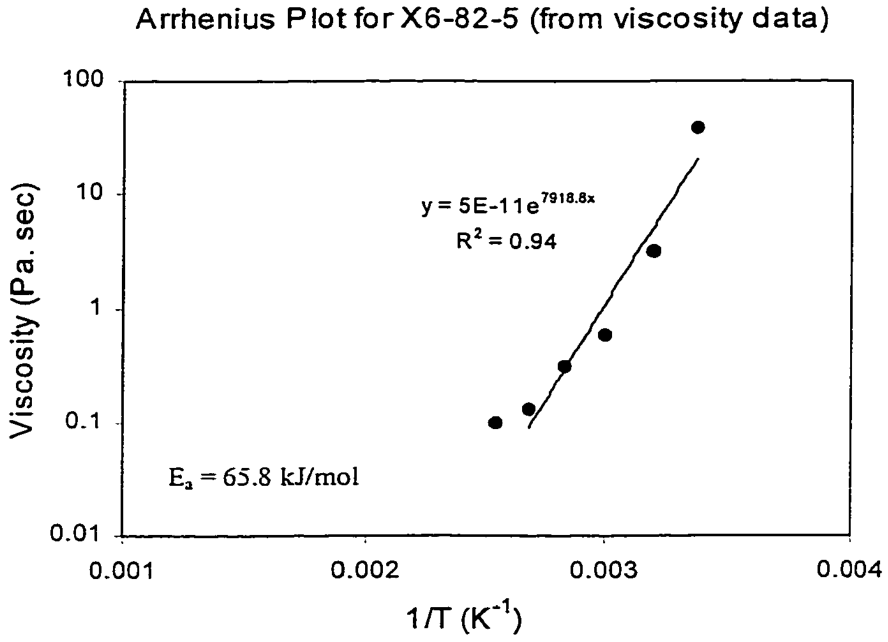

Fig. 4.27: Arrhenius plot of viscosity of X6-82-5.

The filling process is typically operated in the range of 80 – 90 °C; however, the filling time line was drawn in a wider range of temperature (60 – 120 °C) to provide more alternative operating temperatures.

The Washburn equation (Equation 2.1) was integrated under the initial condition (x(t) = 0 at t = 0). The integration solution is:

$$x_f^2 = \left[\frac{\gamma}{6}(\cos\ \theta_o + \cos\ \theta_s)\frac{s}{\mu_o}\right]t \qquad (4.6)$$

The flow length (x_f) and stand gap (s) were fixed at 10 mm and 100μm respectively. Surface tension, contact angle (the lower and upper contact angles were assumed to be equal), and viscosity in the range of 60 –120 °C (1 degree interval) were calculated using

Excel® spreadsheet. Then the filling at the same range of temperature was calculated by Equation 4.6. The calculated filling time as a function of temperature is shown in Fig. 4.28 for FP4511 and X6-82-5. It is clearly seen that X6-82-5 has a shorter filling time at the same temperature.

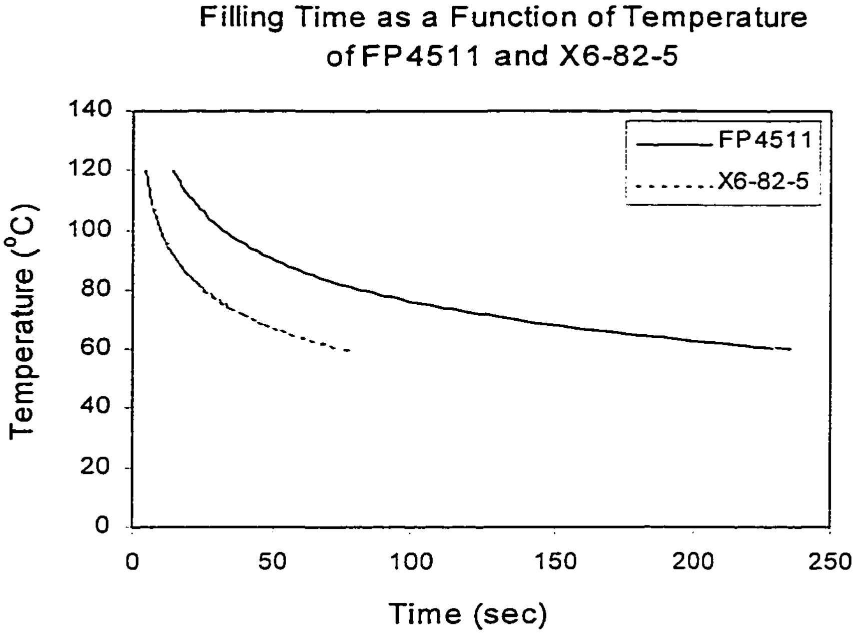

Fig. 4.28: Filling time as a function of temperature of FP4511 and X6-82-5.

To verify the pragmatism of this filling step, the flow behavior under this same range of temperature through the 100 μm gap and 10 mm flow length was performed experimentally for FP4511 and X6-82-5. It was found that the experimental-filling time is greater than the predicted filling time by Washburn model by a factor of 1.6-2.5 in case of FP4511 and 0.6–1.9 in case of X6-82-5 (Fig. 4.29). Note that at 120 °C, FP4511 could not complete the filling. The main factor that influenced the difference was the temperature. The difference in temperature caused the difference in all parameters (e.g., viscosity, surface tension, and contact angle), which were used to predict the filling time by the Washburn model. The epoxy sample reacts during the raising of its temperature to the equilibrium temperature; therefore, it is impossible to measure each parameter at equilibrium temperature. The way the experiments were performed also caused the difference. The sample viscosity determination was done between the preheated stainless steel plates in a closed oven. Contact angle measurements were done on a preheated glass slide on a hot stage and in a closed chamber as well. Surface tension measurement was done on a hot stage, but in open air, while the filling experiment was done between the preheated glass slides on the hot plate (opened to air).

The deviation from the Washburn model was found to be in a factor of more than two by Driscoll et al. [20] when the model was applied to the encapsulant. They attributed the discrepancy to particle setting effects.

Schwiebert et al. [125] proposed a 2-D underfill flow model. They modeled the flow of the underfill resins under the chip as quasisteady. The laminar flow between parallel plates is driven by surface tension (capillary action) as in the Washburn model. The flow length is given as:

$$L = \sqrt{\Phi h t} \qquad (4.7)$$

where Φ is the coefficient of planar penetrance, h is a separation distance, and t is filling time. The term Φ is defined as

$$\Phi \equiv (\gamma \cos\theta)/3\mu \qquad (4.8)$$

where γ is the surface tension of the liquid-vapour interface, θ is the contact (wetting) angle, and μ is the viscosity of the liquid. The coefficient of penetrance defined by Washburn [19] is:

$$\Phi \equiv (\gamma \cos\theta)/2\mu \tag{4.9}$$

By assuming the perfect wetting between underfill resins and the parallel plate surfaces (θ = 0), they found that their model in Equation (4.7) correlated well with the experimental result as in Fig. 4.30. Note that Equation (4.6) (while Φ in Equation 4.8 was employed) and Equation (4.6) are similar.

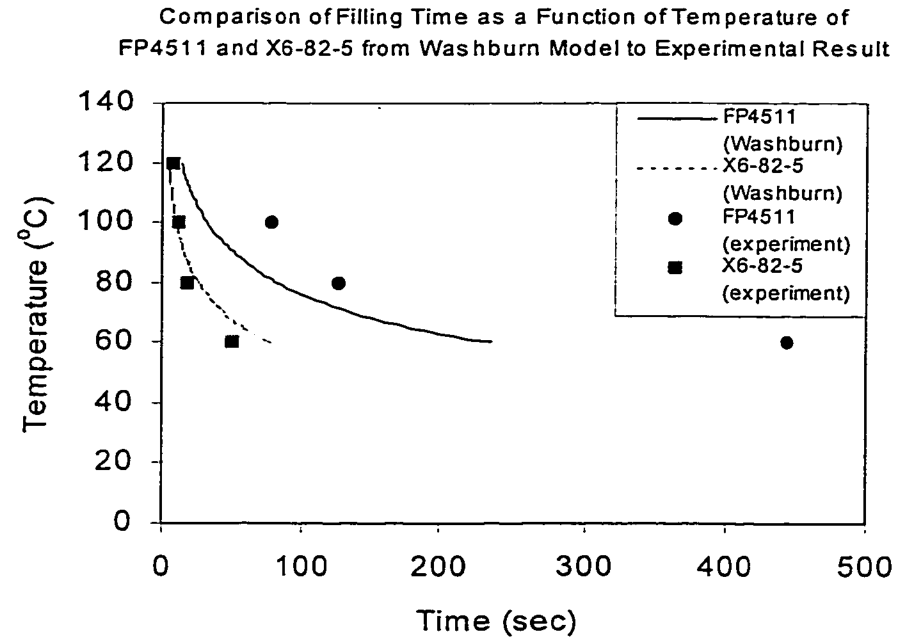

Fig. 4.29: The Washburn model's predicted filling time and experimental filling time of is off by a factor of about 1.6-2.5 in case of FP4511 and 0.6-1.9 in case of X6-82-5.

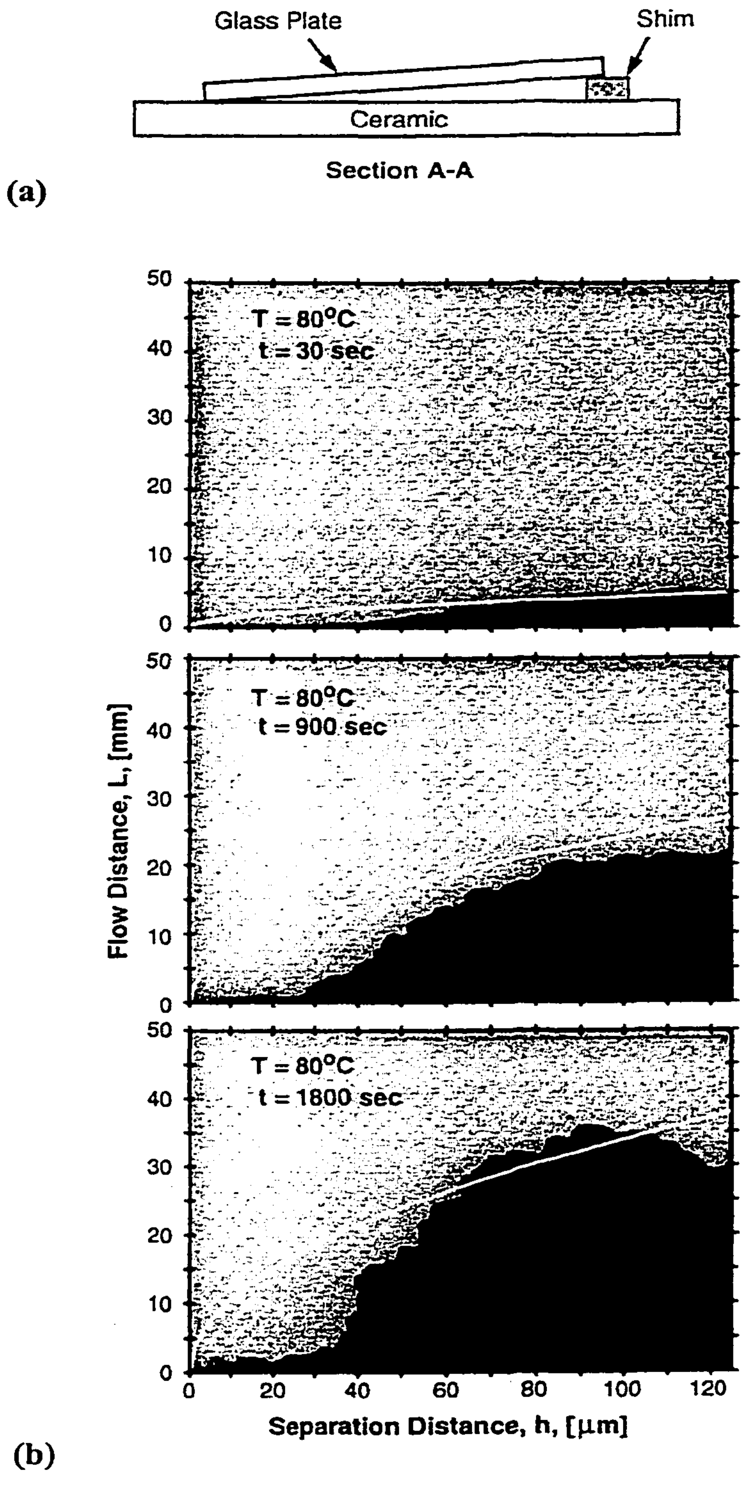

Fig. 4.30: (a) Flow test setup. (b) Experimental results versus model.

4.2.1.2 The Maximum Time Limit of the Underfilling Step

The maximum time limit of the flow step is the point where the sample cannot move further, i.e. the no flow time. The gelation time could be employed to be the long time limit of the underfilling step in a processing diagram, since it is the point where the viscosity is infinity and the sample cannot flow anymore. However, gelation time is a too long time limit in practice. At high viscosity of resin (when the system approaches the gelation), the resin can hardly move under the gap. Therefore, 10 Pa.s viscosity was chosen to be the "no flow" line in the diagram. 10 Pa.s viscosity line can be obtained from the data of viscosity as a function of time at different temperatures (Figs. 4.1 and 4.2 as shown previously). Figs. 4.31 and 4.32 show the underfilling step for FP4511 and X6-82-5, respectively. The underfilling step of X6-82-5 is wider than that of FP4511.

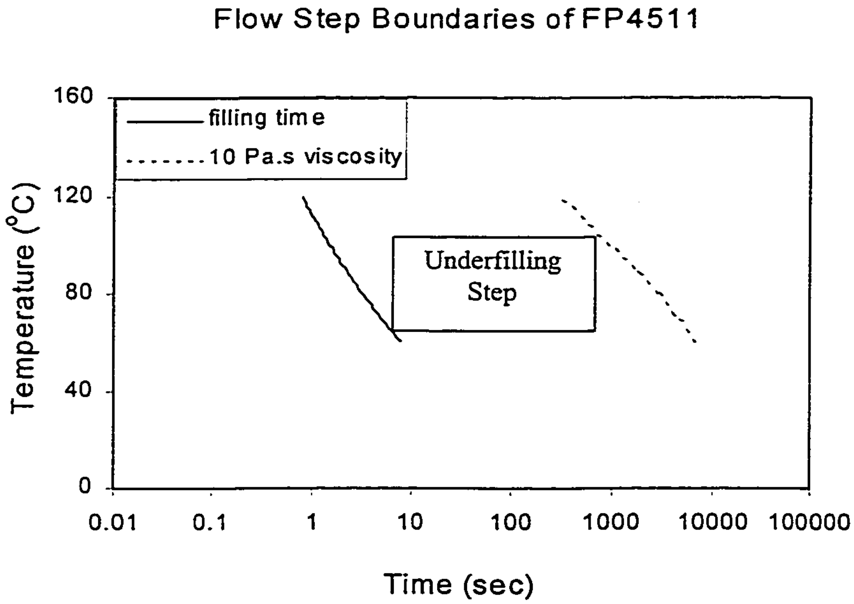

Fig. 4.31: Underfilling step of FP4511 is indicated by the filling time and the gelation time line.

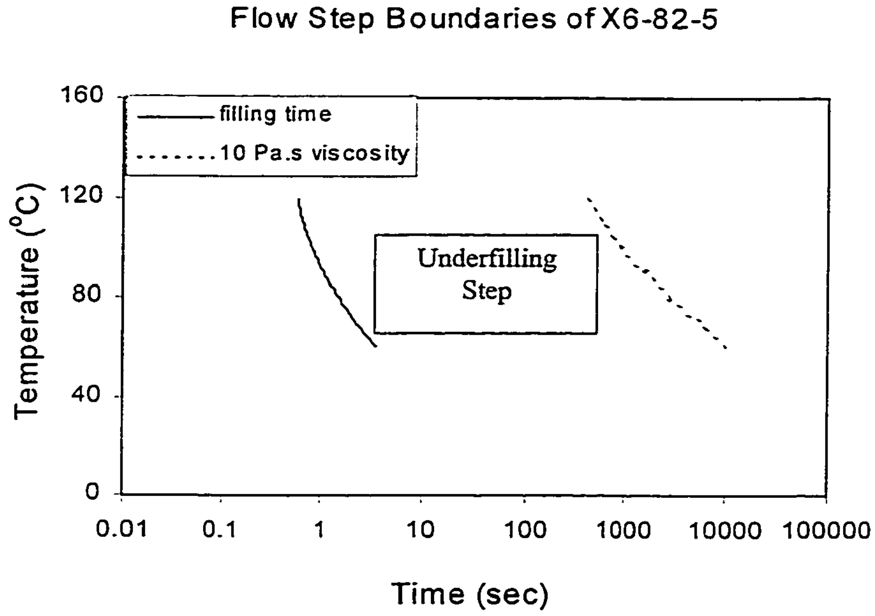

Fig. 4.32: Underfilling step of X6-82-5 is indicated by the filling time and gelation time line.

4.2.2 The Cure Step

The cure step is the step where adhesive is cured with a suitable cure schedule in order to provide a reliable adhesive bond. The boundaries of this step are indicated by the onset temperature, glass transition of the fully cured sample, the temperature and time that give 90% extent of reaction, and the solder melting temperature. The starting boundary of the cure step can be indicated by both the gelation time line and the 100 Pa.s viscosity, which is the viscosity that can hold the assembly together while transferring to the cure step.

4.2.2.1 Gelation

From the gelation time measurement, apparent gelation times and the reciprocal of temperatures were plotted. The straight line of the exponential function of gelation time and temperature was obtained as in Figs. 4.33 and 4.34 for FP4511 and X6-82-5, respectively. This phenomenon obeyed the Arrhenius equation (Equation 4.10).

$$\ln t = \text{constant} + \frac{E_a}{RT} \qquad (4.10)$$

where t is gelation time, E_a is the activation energy, R is the gas constant, and T is the absolute temperature.

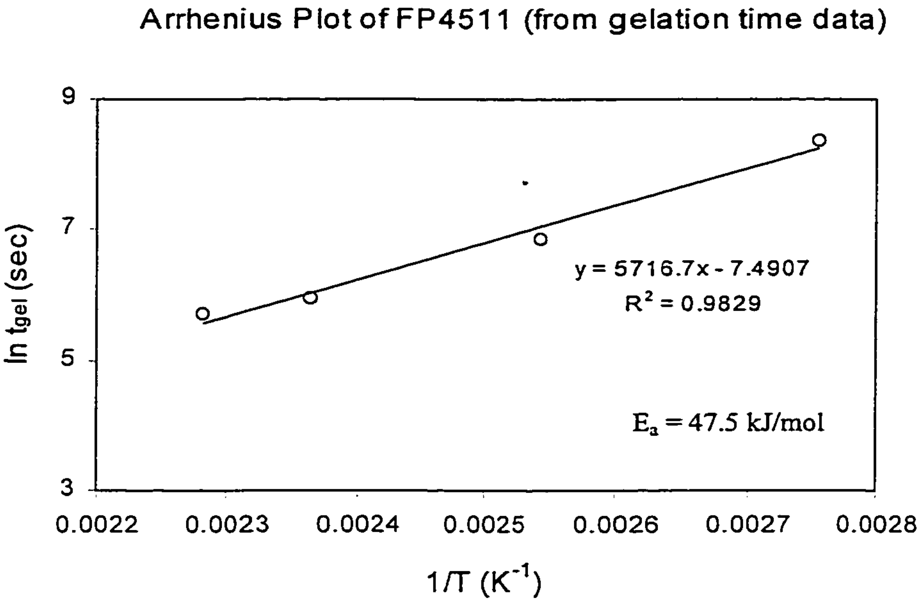

Fig. 4.33: Arrhenius plot of gelation time versus 1/T for FP4511 gives an apparent activation energy of 47.5 kJ/mol.

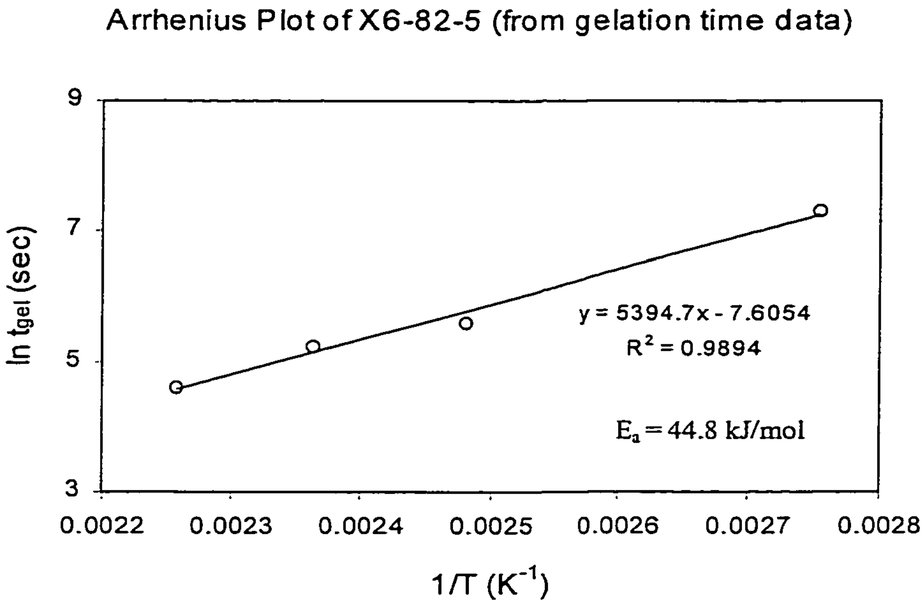

Fig. 4.34: Arrhenius plot of gelation time versus 1/T for X6-82-5 gives an apparent activation energy of 44.8 kJ/mol.

From the equations, which were obtained from the Arrhenius plots above, the series of gelation time as a function of temperature could be calculated. The gelation times in the range of 120 – 183 °C (1 degree interval) were calculated. Then the relation of gelation times and temperatures was plotted to set the starting boundary for cure step. Figs. 4.35 are the calculated gelation time as a function of time for FP4511 and X6-82-5.

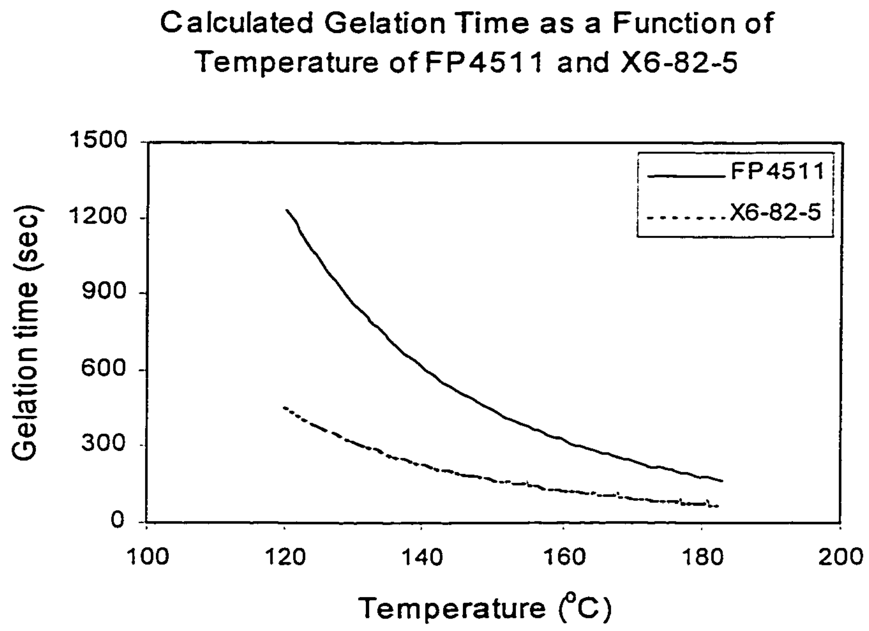

Fig.4.35: Calculated gelation time as a function of temperature of FP4511 and X6-82-5.

4.2.2.2 Onset Temperature and $T_{g\infty}$

The temperature dependence of the rate of reaction or the rate constant is commonly expressed by Arrhenius equation [126] (Equation 4.12), the higher cure temperature, and the faster rate of reaction. The onset cure temperature indicates the starting point of a significant rate of reaction. Below this point, the rate of reaction is too slow for the general processing in industry, and the reaction may not be able to go to completion. Then the mechanical properties of the adhesive would not be good enough to provide a reliable product. In order to avoid the vitrification, cure temperature should be higher than the $T_{g\infty}$ of the sample. Thus, in this diagram the onset temperature or $T_{g\infty}$ was suggested the lower limit of cure temperature. The selecting between these two temperatures depends on the properties of the sample and the purpose of each task. Void formation may be the other issue to consider when designing the cure temperature. Although the higher cure temperatures provide the faster reaction rate and the higher extent of reaction, they give more possibilities in void formation, which diminishes the reliability of the cured resin.

4.2.2.3 Solder Melting Point

Soft solders [6, 57] have been used in direct chip assembly because of their high degree of plastic strain capability. This allows for a reduction of the thermally induced stresses on the chip. However, viscoelasticity makes solder prone to fatigue and creep rupture failures at the device operating temperature [127-128]. They also have a low melting point (≈ 183 °C). The cure temperatures cannot be higher than their melting point; therefore the solder melting point was used to be the upper limit of the cure step.

4.2.2.4 Extent of Reaction

The most important factor in this step is the extent of reaction, which was reported as a minimum of 90% in order to obtain optimal adhesive properties [129-130]. Therefore, the lower limit of curing step was indicated by the 90 % extent of reaction at a series of curing temperatures. The autocatalytic equation (Equation 4.11) was used to characterize the cure kinetic behavior of underfill resins.

$$\frac{dp}{dt} = kp^m (1-p)^n \tag{4.11}$$

where p is an extent of reaction, k is a rate constant, m and n are orders of reaction. Based on the dependence of the reaction constant on the temperature, which follows Arrhenius law (Equation 4.12), rate constant, and the reciprocal of corresponding temperature were plotted in order to obtain their relationship. In addition, the activation energy can be obtained from the slope of the curve.

$$k = k_o \exp\left(\frac{-E_a}{RT}\right) \tag{4.12}$$

where k is the temperature dependence rate constant, k_o is a frequency factor, E_a is activation energy, R is gas constant and T is an absolute temperature. The plots of rate constant versus reciprocal of temperatures of FP4511 and X6-82-5 are shown in Fig. 4.36 and 4.37, respectively.

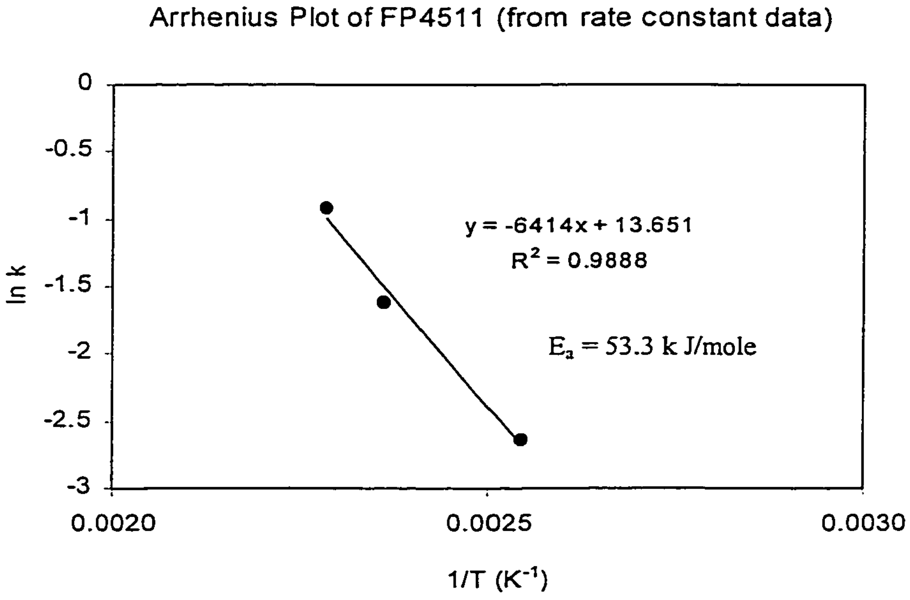

Fig.4.36: Arrhenius plot of rate constant of FP4511.

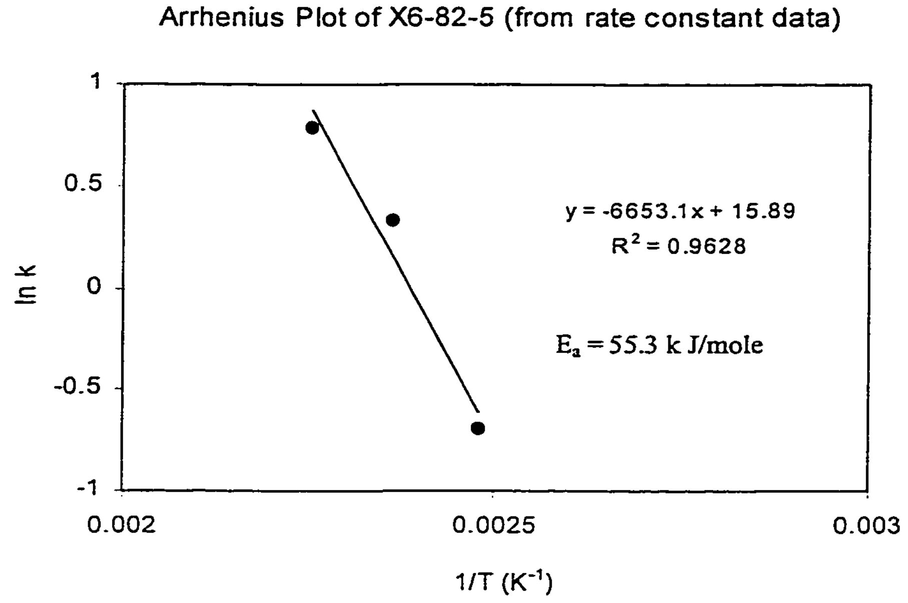

Fig. 4.37: Arrhenius plot of rate constant of X6-82-5.

From the Arrhenius plots of rate constant above, rate constant can be calculated at different curing temperatures. The cure temperature in the range of 120- 165 °C was utilized to calculate the rate constant. Integration was applied to Equation (4.11) to get the solution in Equation (4.13).

$$p = kp^m(1-p)^n t \qquad (4.13)$$

By substituting the values of m, n, and k as a function of temperature, the time needed to achieve the specific extent of reaction was obtained. The plots of cure temperatures and needed cure times were at 90 % and 95 % extent of reaction as in Fig. 4.38 and 4.39 for FP4511 and X6-82-6, respectively. However, the selected range of cure temperatures was assumed to reach the 90% and 95% extent of reaction.

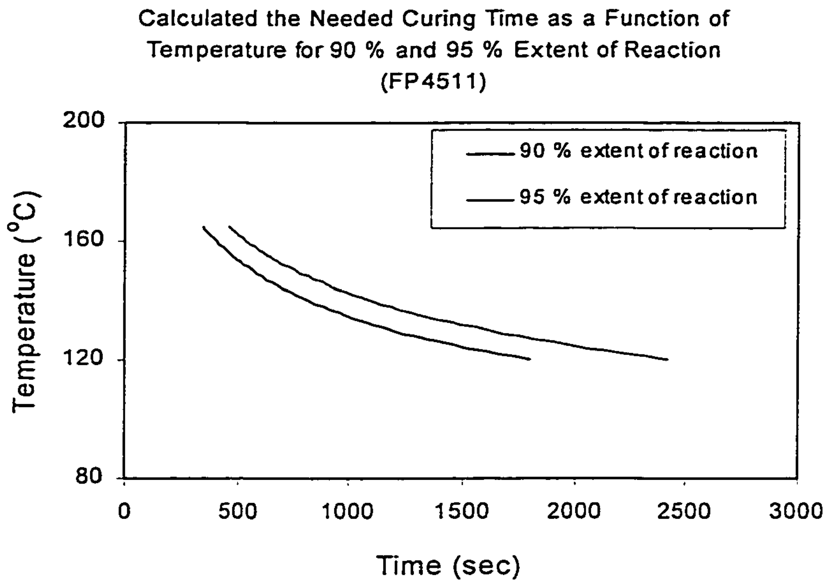

Fig. 4.38: Cure temperature and cure time relationship to achieve 90% and 95% extent of reaction of FP4511.

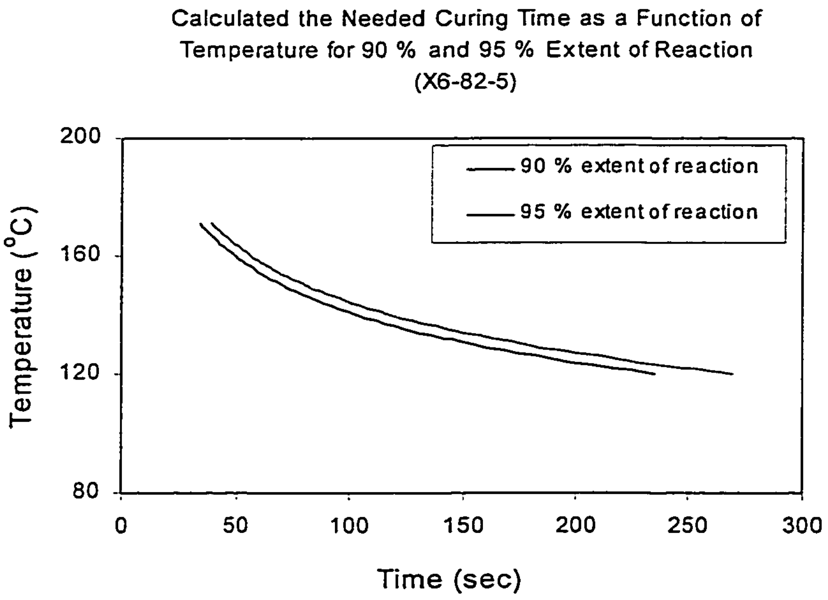

Fig. 4.39: Cure temperature and cure time relationship to achieve 90% and 95% extent of reaction of X6-82-5.

4.2.3 Construction of Processing Diagram

Filling and cure steps are consecutive steps; therefore placing both steps on the same time-temperature plot would provide a useful processing diagram. The processing diagram of FP4511 and X6-82-5 are shown in Figs. 4.40 and 4.41, respectively.

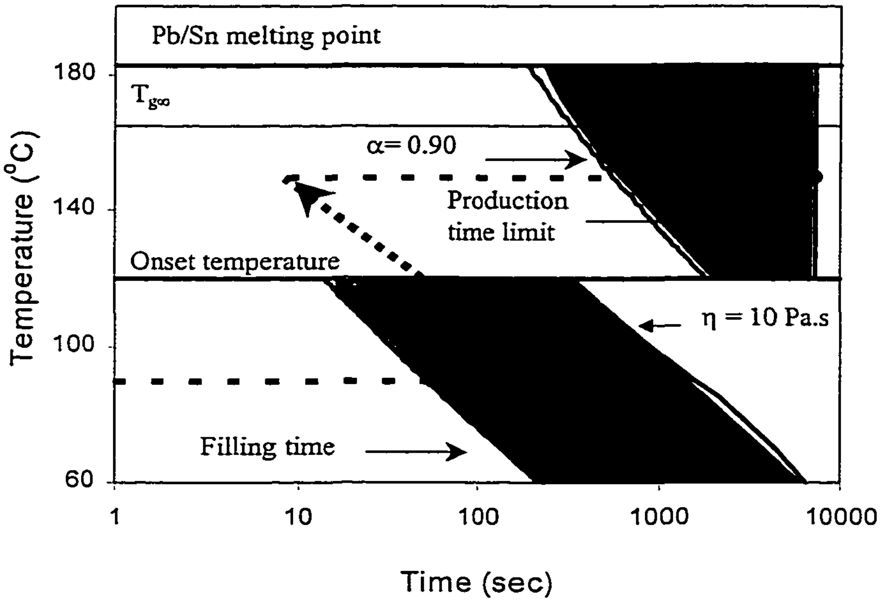

Fig. 4.40: Processing diagram for FP4511(● recommended cure schedule).

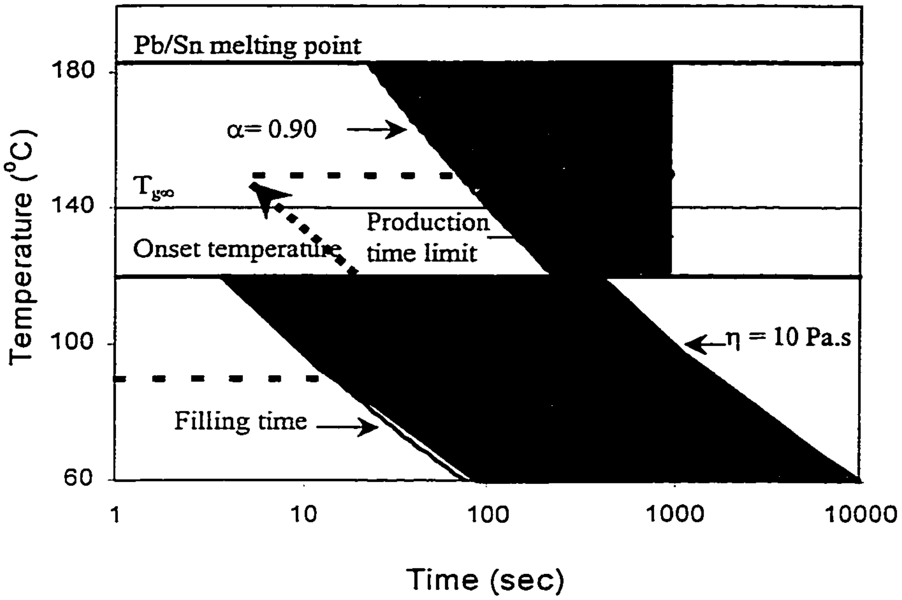

Fig. 4.41: Processing diagram for X6-82-5 (● recommended cure schedule)

The filling time in these diagrams was calculated for the gap between the two smooth surfaces. However, in the realistic situation, numbers of solder bumps are placed in the stand gap in various kinds of arrangements. In that case, the filling time would be longer because of the obstructions. Then the filling time line would be shifted to the right of this diagram, making the filling window narrower. The minimum limit of cure step is the time-temperature relationship line, which gives 90 % extent of reaction. This extent of reaction was reported to be the minimum value that can provide a reliable adhesive bond [9]. The maximum time limit is indicated by the production time limit. There is no improvement in adhesive strength at longer than this time limit.

The processing diagrams may not contain all the parameters that influenced the reliability of the finished product; however, they contain many of the essential factors that play an important role in an underfill adhesive processing. These processing diagrams should be able to help the process engineers in designing the proper cure schedules for underfill resins.

The dotted lines show the example of the processing path, performing the underfilling and cure processes at 90 and 150 °C, respectively. For FP4511, the sample is dispensed at 90 °C and left to flow at this temperature for 500 seconds. At 90 °C for 500 seconds, autocatalytic kinetic model (Equation 4.13) and kinetic parameters of this sample gives the extent of reaction at 0.10. From the DSC data (or the calculation by using an autocatalytic kinetic model), to reach the extent of reaction of 0.10 at 150 °C, 9 seconds of cure time is needed. Therefore, when the sample is transferred to the cure step at 150 °C, the cure time begins at the second 9th. The same explanation can be applied to X6-82-5.

4.3 Model Epoxies

The analysis of different adhesive characteristics by utilizing model systems provides the opportunity for obtaining a fundamental understanding of material's processing-structure-property interrelationships, which are essential for design and manufacturing purposes.

The mechanical properties of crosslinked, amorphous polymers are expected to depend on the chemical structure and molecular architecture, free volume, crosslink density, and their distribution on the other. Chang et al. [131] have stated that to get an explicit understanding of the effect of crosslink density on mechanical properties, it is preferable to vary the cure time rather than stoichiometry. However, the highest crosslink density is generally obtained in the stoichiometric composition. The structures of the various compositions are different as they contain different amounts of the resin and curing agent. There are various conflicting observations on the mechanical properties changes due to the stoichiometry. While some authors have reported that the elastic modulus is independent of stoichiometry [132-133], others have observed a minimum elastic modulus at the stoichiometric composition [134-135]. For model epoxies, the intention was not to invent new epoxy systems, but to imitate commercial underfill resins in order to explain the behavior of the systems based on their chemistry. From the study of commercial underfill resins, there were some points that needed clarification such as the difference in the magnitude of cure stress and in the rate of reaction. To understand the cure behavior of epoxy resins, their chemistry, mechanical and physical properties, and cure kinetics should be known.

4.3.1 Chemistry of Model Epoxies

In epoxy systems, the conversion to a crosslinked network is accomplished by the addition of a chemically active compound known as a curing agent, known to polymer scientists as a crosslinker. Some curing agents promote cure by catalytic action; others participate directly in the reaction and are chemically bound into the resin chain [86]. Depending on the particular curing agent, curing may be achieved at room temperature with heat produced by an exothermic reaction or may require application of external heat. The reactivity of the epoxy ring (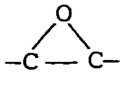), known to organic chemistry as an oxirane ring, depends on its location in the structure (e.g., terminal, internal, or in the ring). The environment of the epoxide group also has a great influence on the curing process. Steric factors can play a major part [135-137] in determining the ease with which polymerization can take place. In addition, the electronic influences exerted on the epoxide group are extremely important. Groups adjacent to the epoxide ring, which withdraw electrons, often enhance the reactivity of the epoxide to attacking nucleophilic reagents, and also reducing its reactivity towards electrophilic reagents [136, 138]. Basically the cured structure may be a homopolymer (epoxy molecules linked together through their own reactive sites) or a heteropolymer (epoxy molecules linked together through the active sites of curing agents).

The epoxy group may react in an anionically or a cationically way. The simplified mechanisms for the formation of epoxy anion and cations are shown as the following schemes. In the anionic mechanism, the epoxy group may be opened in various fashions to produce anion, which is capable for further reaction:

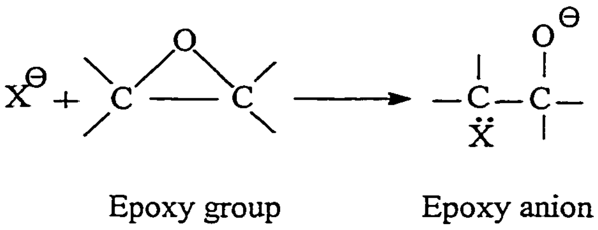

Fig. 4.42: Epoxide ring opening mechanism to form epoxy anion.

In the cationic mechanism, the epoxy group may be opened by active hydrogen to produce a new chemical bond and a hydroxyl group. The cationic mechanism may proceed in several ways, such as the following:

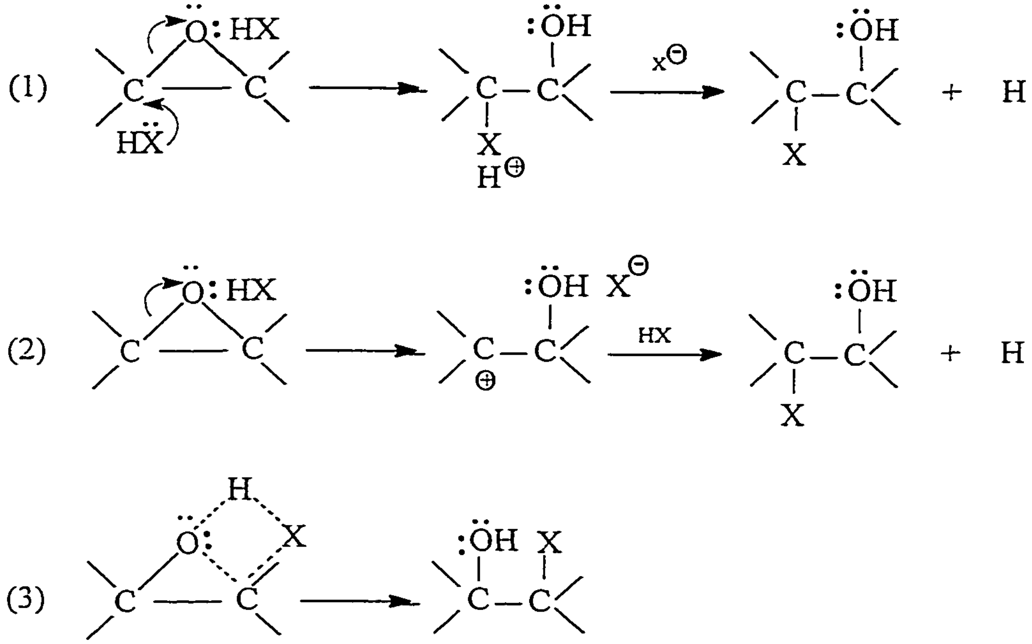

Fig. 4.43: Epoxide ring opening mechanism to form epoxy cation.

4.3.1.1 AEP-Cured Diglycidyl Ether of Bisphenol A (DGEBA) Epoxy

Among curing agents, amines retain a prominent position due to their enhanced environmental (hydrolytic) stability [139]. At a stoichiometric ratio of the epoxy and amines, the reaction between the epoxy ring and primary amines produce chain growth. Later reactions with secondary amines build chain branches. Eventually the system will gel to form a network and vitrify. The secondary amine can be much less reactive towards epoxy functionality.

N-aminoethylpiperazine (AEP) was used as the curing agent to form the network in the system of DGEBA with the stoichiometric ratio in this study. The reaction of an epoxy resin with AEP curing agent would be expected to follow the reaction sequences shown in Fig. 4.44. The reaction with a primary amine leads to the formation of a secondary hydroxyl group and a secondary amine. This secondary amine can then undergo reaction with another epoxide group to form a further secondary hydroxyl group and a tertiary amine. The secondary amine at position 4 also reacts with the epoxide group in the same manner as the previous description. In addition, secondary hydroxyl groups could then act as a catalyst for epoxide homopolymerization. However, in stoichiometric epoxide-amine systems and the system with the excess of amine group, the reactions do not undergo any further reaction, at least below 180 °C. Tanaka et al. [140] concluded that with based-catalyzed systems etherification did not occur between 70 – 140 °C. If epoxide groups are in excess, etherification (reaction (b) in Fig. 4.44) by the ring opening reaction induced by the OH groups of the formed amino alcohol can interfere [141-142] with the amine addition reaction.

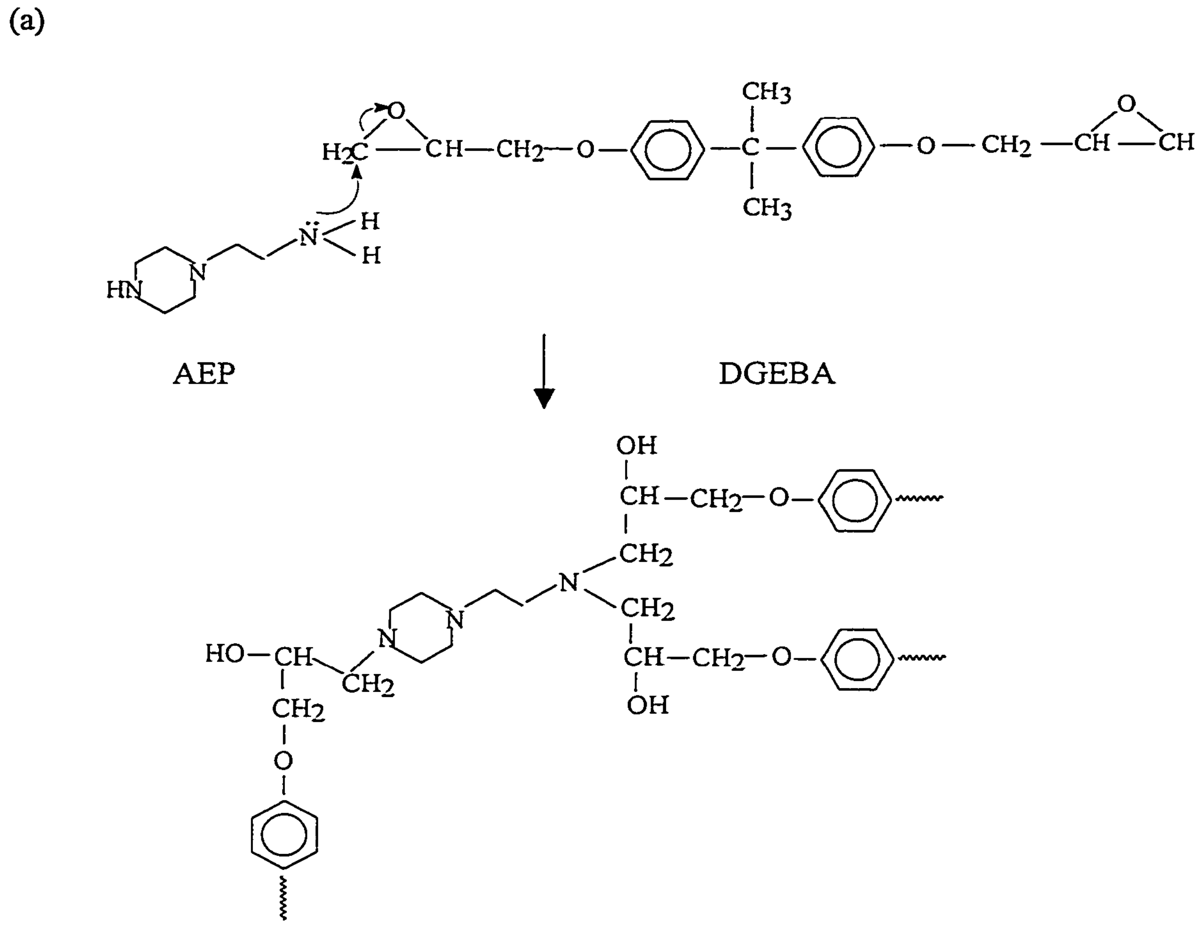

Network Resin

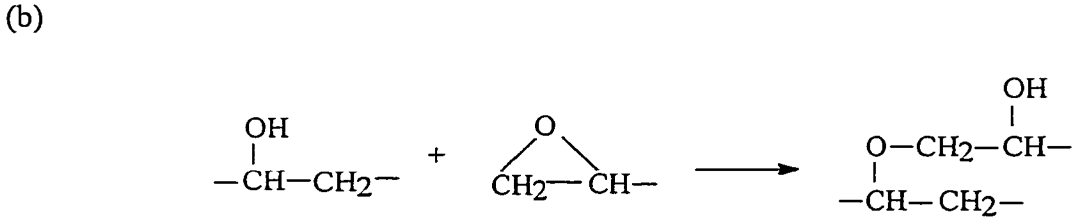

Epoxide Homopolymerization

Fig. 4 44: The reaction mechanism sequence of AEP-cured diglycidyl ether of bisphenol A system.

4.3.1.2 Imidazole-Cured Diglycidyl Ether of Bisphenol F Epoxy

2-ethyl-4-methyl-imidazole (EMI-24) is a substituted imidazole that has been used as a curing agent for epoxy to obtain a long pot live. The reaction between an imidazole and an epoxide group includes a catalytic mechanism in which only small amount of imidazole is needed to complete the crosslinking reaction. Generally 0.025 to 0.05 mol of imidazole/equivalent of epoxy is used. Farkas and Strohm [143] have investigated the mechanism of cure of EMI-24/ epoxy system and found that the imidazole becomes permanently attached to the polymer chain. The imidazole is an effective curing agent, operating through both the secondary amino hydrogen and the tertiary amine, in a catalytic mechanism. The sequence of reaction has been suggested as in Fig. 4.45. An active hydrogen in the imidazole molecule could react with an epoxide group and thereby become incorporated into the resin. An NMR study [143] revealed that the second molecule of epoxy resin added to the second nitrogen and not to the hydroxyl group. Furthermore, an alkoxide ion can initiate further reaction with the epoxide group to create the new alkoxide ion. At the appropriate condition, etherification can occur as in the case of amine curing (see reaction (b) in Fig. 4.44)

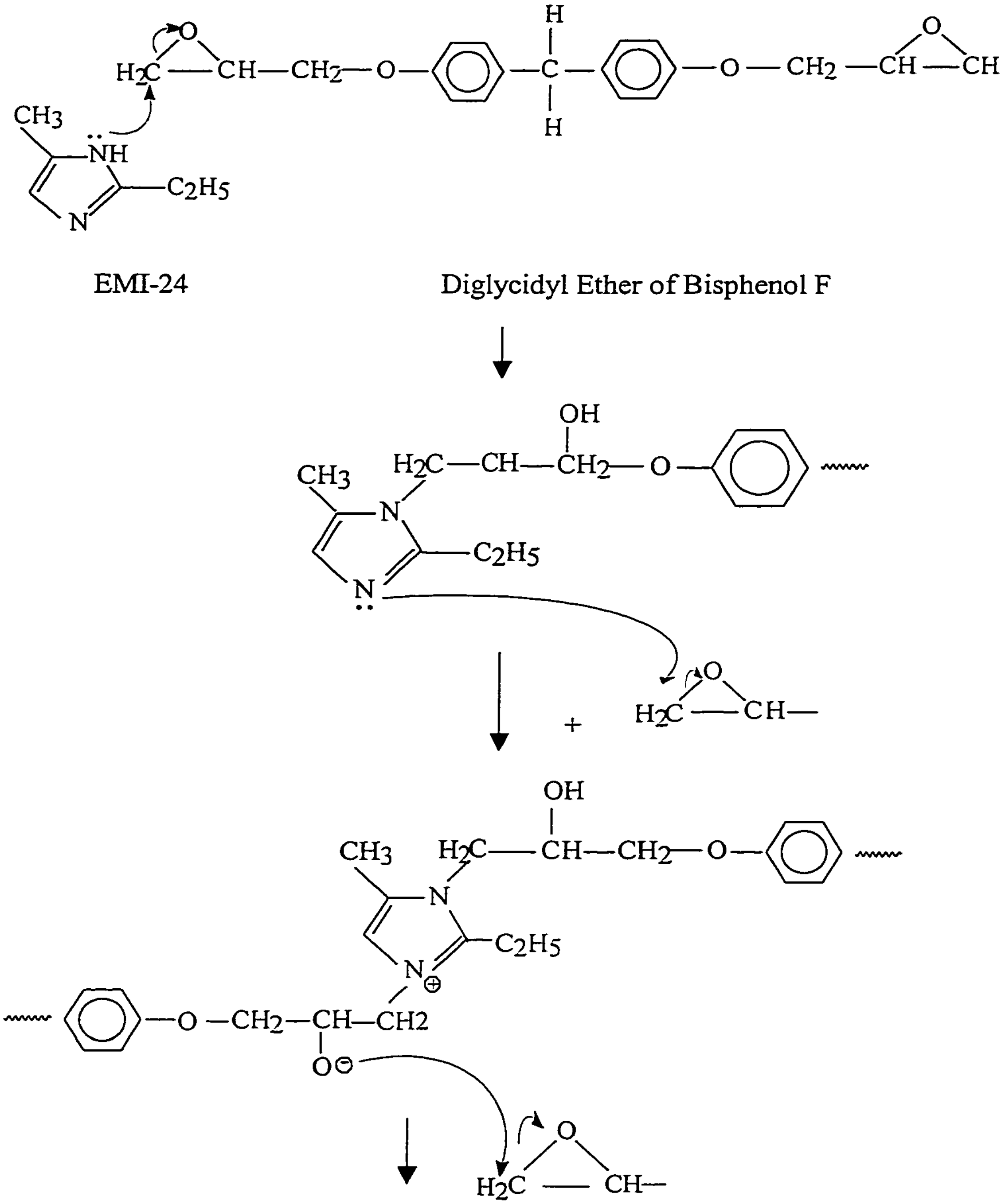
EMI-24
Diglycidyl Ether of Bisphenol F
CH3
NH
C2H5
N
H2C
CH
CH2
O
H
C
OH
N⊕
O⊖
+

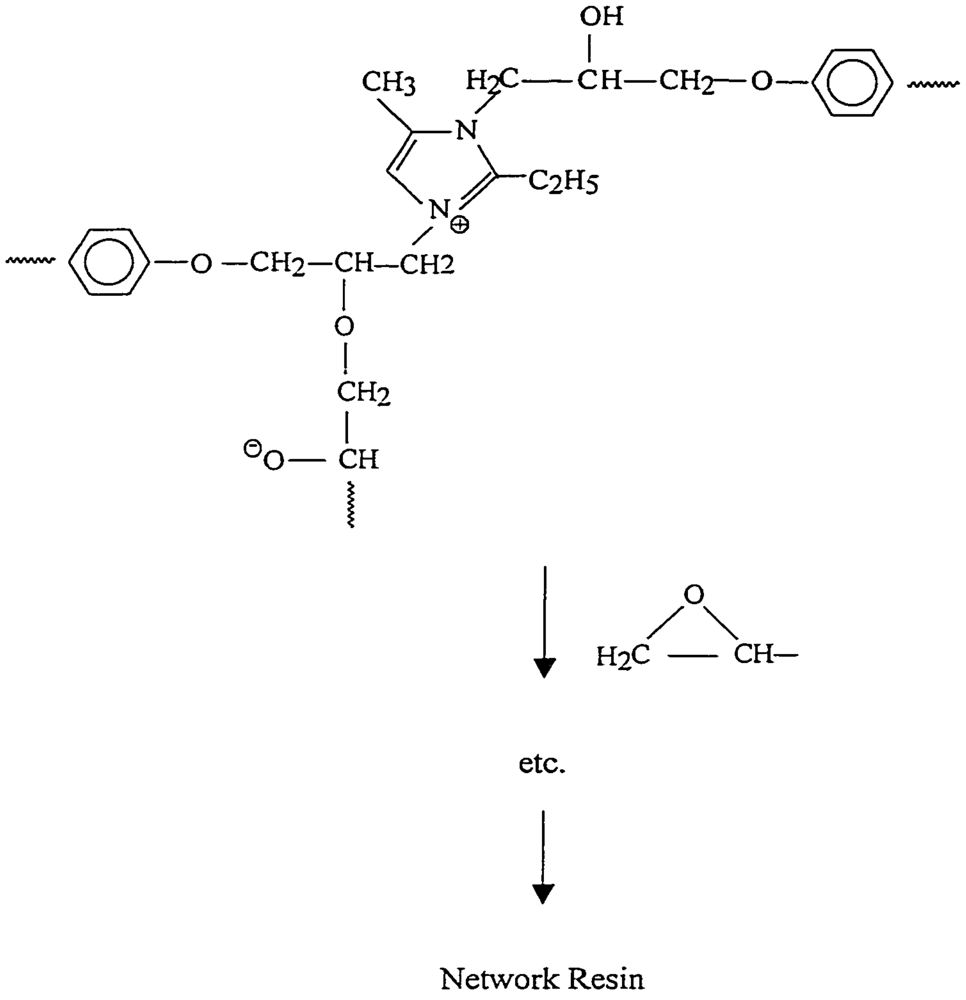

Fig. 4.45: The reaction mechanism sequence of EMI-24-cured diglycidyl ether of bisphenol F.

4.3.1.3 Anhydride-Cured Cycloaliphatic Epoxy

In epoxy chemistry, only cyclic anhydrides are used. These anhydride groups will not react directly with epoxy groups. In order for the reaction to occur, it is first necessary that the anhydride ring be opened. The ring may be opened either by active hydrogens present as water, or hydroxyls, or by Lewis bases. In anhydride-cured cycloaliphatic system, N,N-dimethylbenzyl amine, and ethylene glycol were used as accelerators. Ethylene glycol opened the epoxide rings to produce a carboxyl group as in the scheme (a) in Fig. 4.46. Then N,N dimethylbenzyl amine reacted with a carboxyl group from scheme (a) led to an alkoxide ion (scheme (b)), which can react with epoxide group to give ester linkage (scheme (c)). It can also react with anhydride (scheme (d)) or be re-protonated.

(a) Ring opening by glycerol:

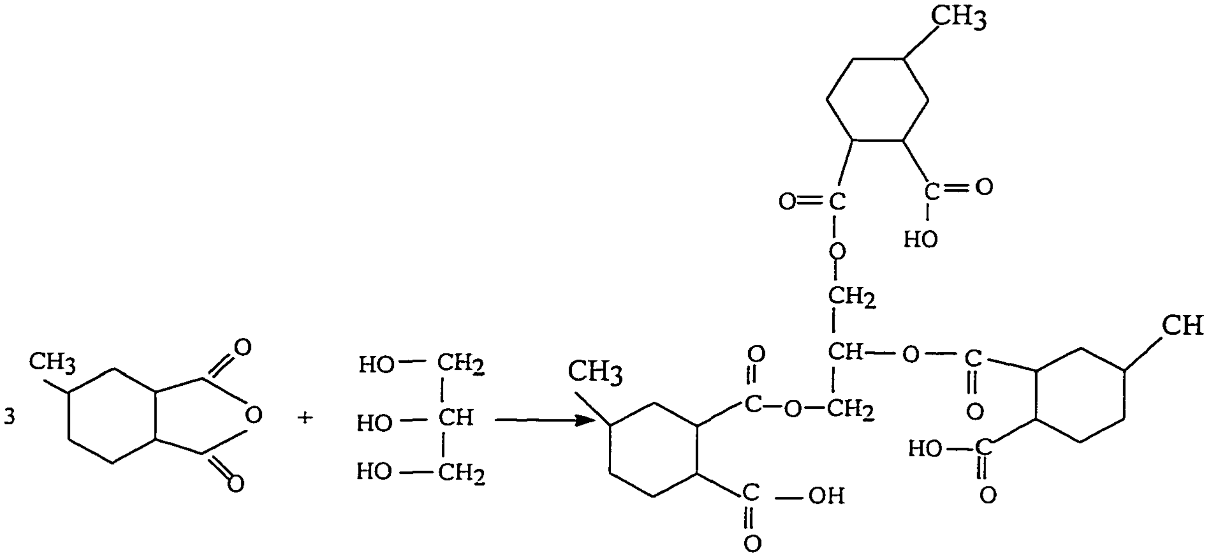

Anhydride Glycerol Carboxylic Acid

(b) Alkoxide formation:

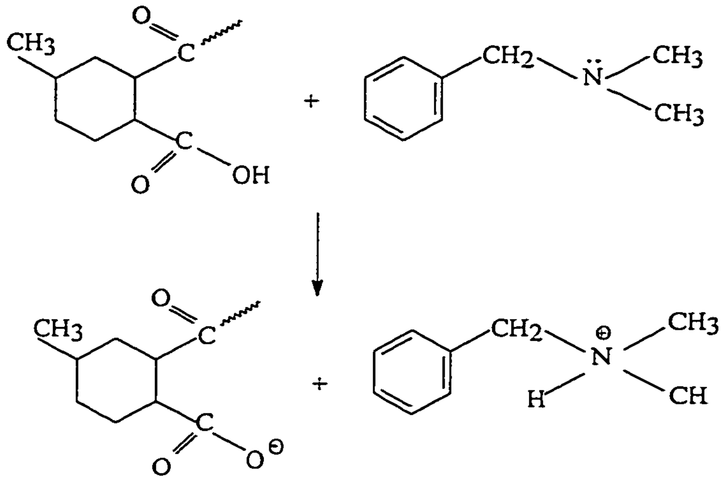

Alkoxide Ion

(c) Reaction between alkoxide ion and epoxide groups:

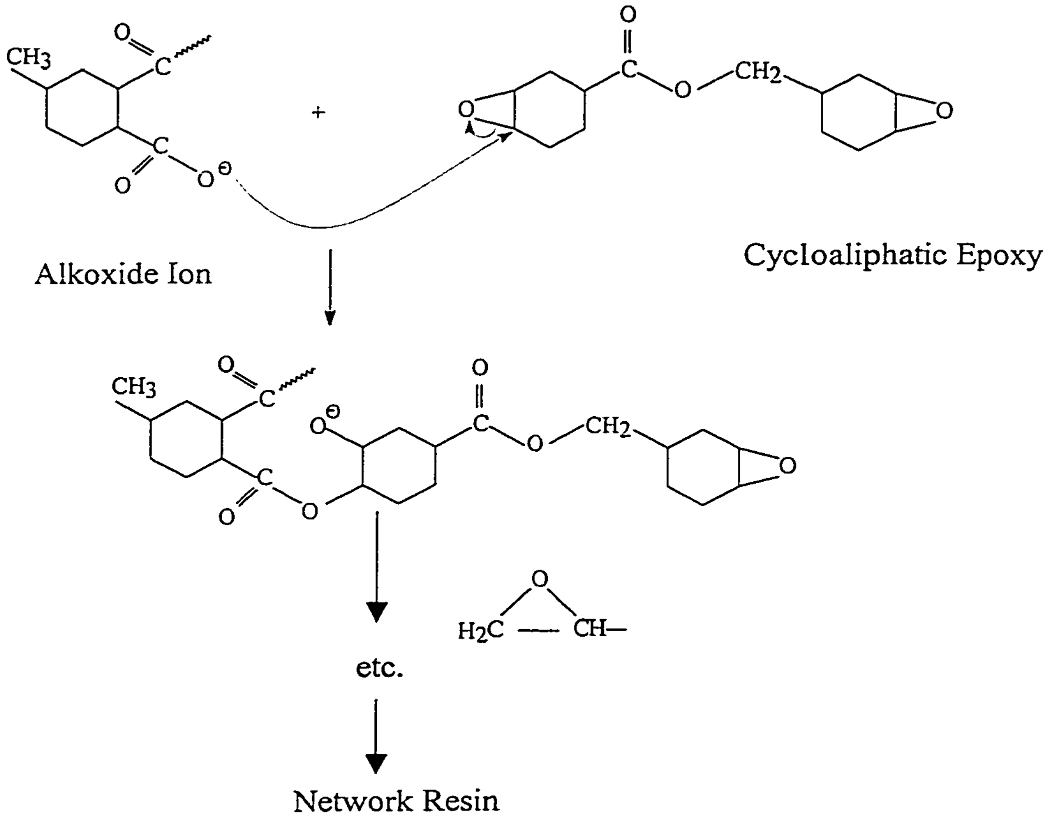

(d) Reaction between alkoxide ion and anhydride

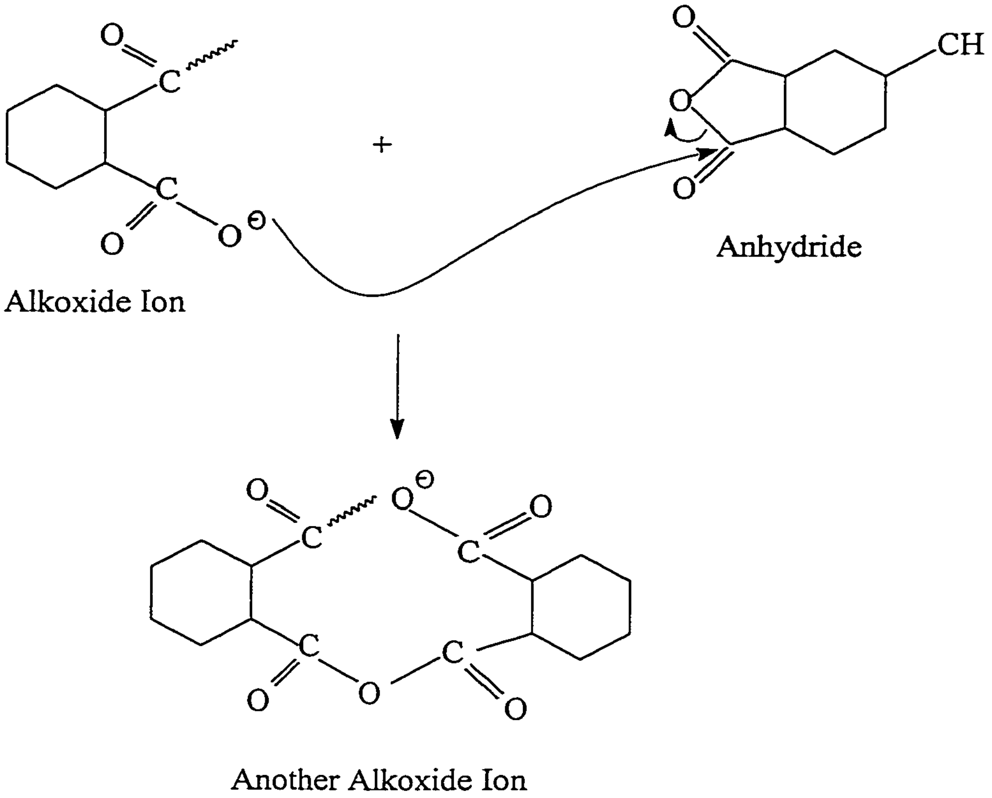

Fig. 4.46: The reaction mechanism sequence of anhydride-cured cycloaliphatic epoxy system.

4.3.2 Shear Viscosity and Gelation

Both shear viscosity and gelation time are important for the processing of thermosetting polymers. The shear viscosity and apparent gelation time were measured as a function of temperature. Shear Viscosity of AEP-cured diglycidyl ether of bisphenol A system, EMI 24-cured diglycidyl ether of bisphenol F system, and anhydride-cured cycloaliphatic epoxy system are shown in Fig. 4.47- 4.49, respectively. As expected, the viscosity decreased with the increasing of temperature. However, AEP-cured diglycidyl ether of bisphenol A at 100 °C gave the higher viscosity than that at lower temperatures. This is most likely due to the reaction kinetics of this system at 100 °C, which causes enough cross-linking to increase the viscosity in a short period of time and before the instrument can measure the first data point. The EMI-24-cured diglycidyl ether of bisphenol F had a higher viscosity at room temperature than that of the other two epoxy resins and at elevated temperature it exhibited the drop of viscosity while the sample was adjusting its temperature to the chamber temperature.

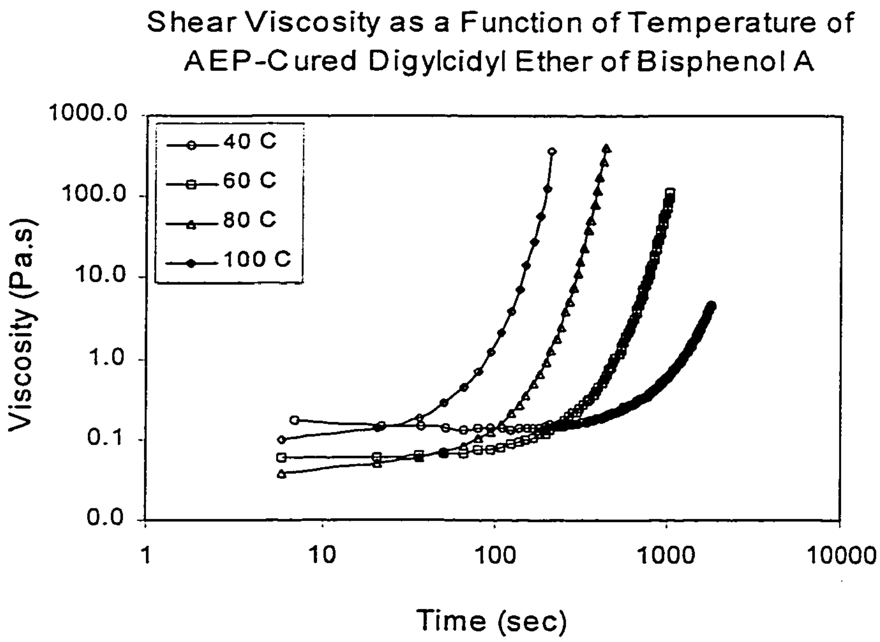

Fig. 4.47: Shear viscosity as a function of temperature of AEP-cured diglycidyl ether of bisphenol A. The viscosity decreases with increasing temperature before approaching the gelation point except in the case of 100 °C, where reaction was fast.

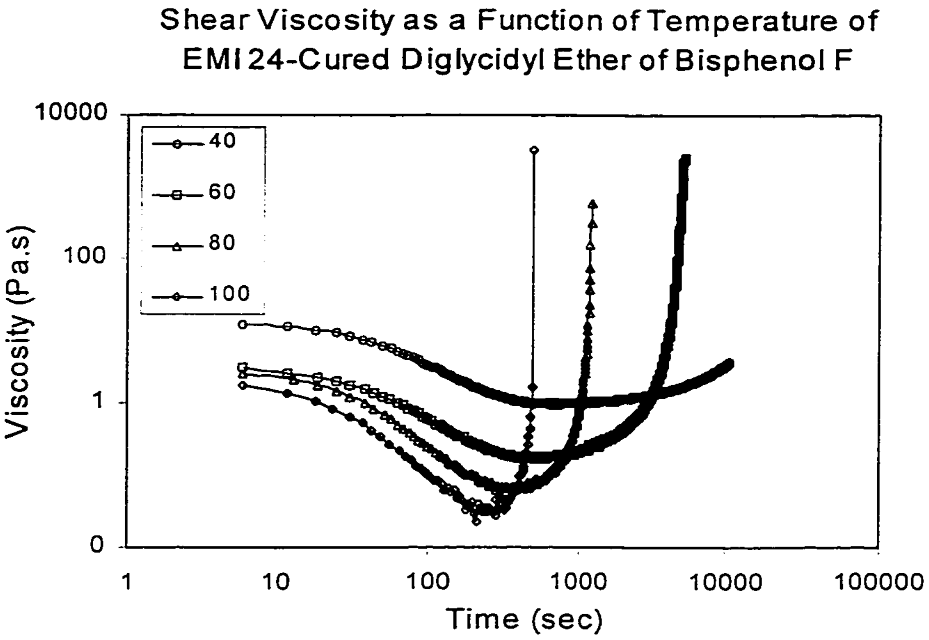

Fig. 4.48: Shear viscosity of EMI 24-cured diglycidyl ether of bisphenol F decreases with increasing temperature before approaching the gelation point.

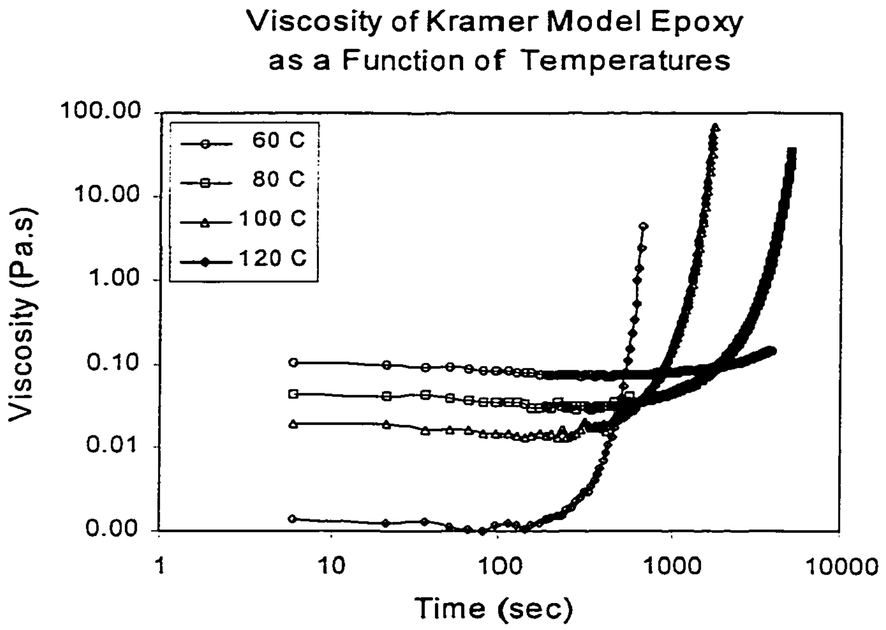

Fig. 4.49: Shear viscosity of anhydride-cured cycloaliphatic epoxy decreases with increasing temperature before approaching the gelation point.

Viscosity as a function of temperature follows the Arrhenius Equation; therefore, from the plot of viscosity and the reciprocal of temperature, one can obtain the activation energy for viscous flow. Figs. 4.50 – 4.52 show the Arrhenius plot from the viscosity values at different temperatures of the three model epoxies. The anhydride-cured cycloaliphatic epoxy system has a very low viscosity, especially at high temperature; therefore, the sensitivity of the instrument may not be enough to detect an accurate value of viscosity. The viscosity data at 120 °C of this system deviated from the straight line.

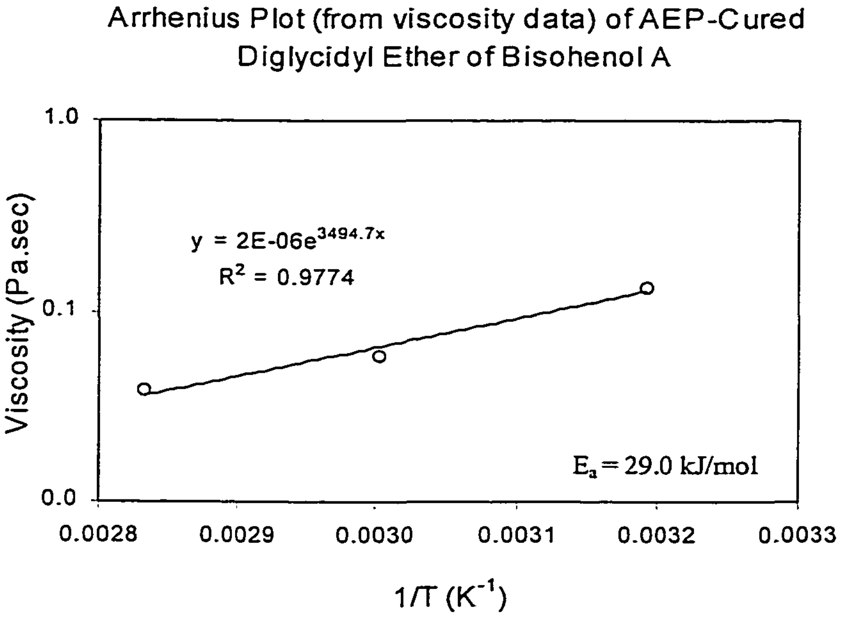

Fig. 4.50: Arrhenius plot from the viscosity at different temperature of AEP-cured diglycidyl ether of bisphenol A gave an activation energy of 29.0 kJ/mol.

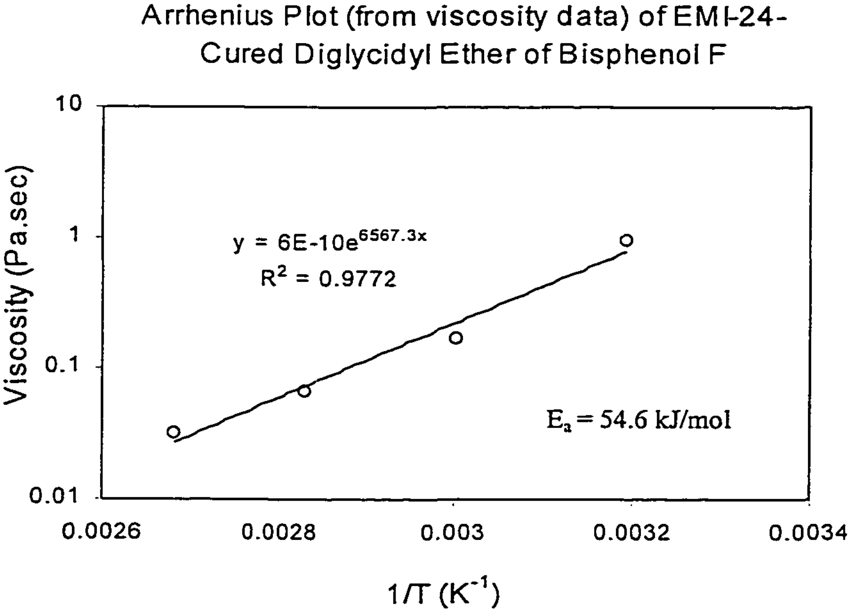

Fig. 4.51: Arrhenius plot from the viscosity at different temperature of EMI-24-cured diglycidyl ether of bisphenol F gave an activation energy of 54.6 kJ/mol.

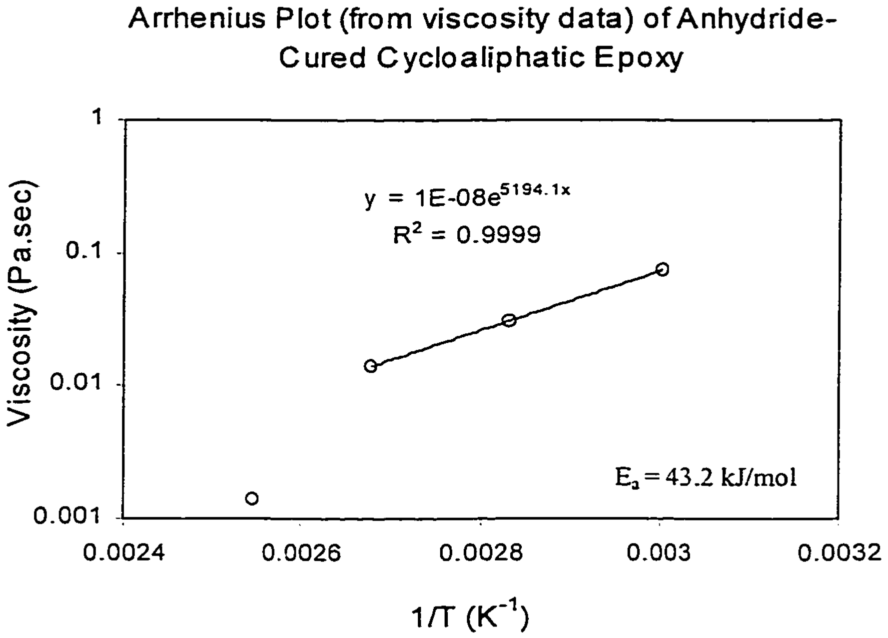

Fig. 4.52: Arrhenius plot from the viscosity at different temperature of anhydride-cured cycloaliphatic epoxy gave an activation energy of 43.2 kJ/mol.

Gelation corresponds to the incipient formation of a network with an infinite weight-average molecular weight. Gelation time of the chemistry known epoxy system can be told by the extent of reaction. Carothers [144] derived a relationship between the extent of reaction at the gel point and the average functionality; f_{avg}, of the polymerization system for the case where the two functional groups are present in equivalent amounts. The average functionality of a mixture of monomers is the average number of functional groups per monomer molecule for all types of monomer molecules. It is defined by:

$$f_{avg} = \frac{\sum N_i f_i}{\sum N_i} \tag{4.14}$$

where N_i is the number of molecules of monomer i with functionality f_i. The critical extent of reaction; p_c, at the gel point is given by:

$$p_c = \frac{2}{f_{avg}} \tag{4.15}$$

Equation (4.10) can be used to calculate the extent of reaction required to reach the onset of gelation in a mixture of reacting monomers from its average functionality. However, Equation (4.9) can be applied only to a stoichiometric system. For nonstoichiometric systems, Equation (4.9) gives a too high calculated average functionality value. Due to the fact that the extent of reaction depends on the deficient reactant, this point should be included in the calculation. Pinner [145] proposed that the average functionality of nonstoichiometric mixtures should be calculated by double the total number of functional groups that are not in excess. In a similar manner, the average functionality of nonstoichiometric mixture containing more than two monomers has been obtained. The equation for calculating the average functionality of a nonstoichiometric ternary mixture is as the following:

$$f_{avg} = \frac{2(N_A f_A + N_C f_C)}{N_A + N_C + N_B} \tag{4.16}$$

where N_A, N_B, and N_C are the number of molecule A, B, and C, respectively, and f_A, f_B, and f_C are the functionality of A, B, and C, respectively. In this system A and C contain the same functional groups, and the total number of functional groups is less than the number of B group.

Flory [146] and Stockmayer [147] used a statistical approach to derive an expression for predicting the extent of reaction at the gel point by calculating when $\overline{X}w$ approaches infinity. In this approach the critical extent of reaction is given by:

$$p_c = \frac{1}{[1+(f-2)]^{1/2}} \tag{4.17}$$

where f is the functionality of the branch unit. Nevertheless, Equation (4.17) does not apply for reaction systems containing monofunctional reactants, and/or both reactants are branch units. In the more general case, thermosetting systems have reactants ranging from monofunctional to ith functional for both A and B functional groups. The extent of reaction at the gel point is given by [148-151]:

$$p_c = \frac{1}{\{r(f_{w,A}-1)(f_{w,B}-1)\}^{1/2}} \tag{4.18}$$

where $f_{w,A}$, and $f_{w,B}$ are weight average functionalities of A and B functional groups, respectively. r is the stoichiometric imbalance; $r = \frac{N_A}{N_B}$ (less than unity).

The functionalities $f_{w,A}$ and $f_{w,B}$ are defined by:

$$f_{w,A} = \frac{\sum f_{A_i}^2 N_{A_i}}{\sum f_{A_i} N_{A_i}} \tag{4.19}$$

$$f_{w,B} = \frac{\sum f_{B_i}^2 N_{B_i}}{\sum f_{B_i} N_{B_i}} \tag{4.20}$$

The Carothers Equation always predicts a higher value of p_c than the experimental value, while statistical approaches give a lower value of p_c than the experimental value. However, the calculation can be applied only to a system that contains monomers that do not react with themselves or do not create the intermediate which can initiate the reactions. Among the three model epoxies, only AEP-cured diglycidyl ether of bisphenol A had a possibility that can be applied by the theoretical equations to calculate the extent of reaction at the gel point if the homopolymerization is ignored (see the reaction mechanism in Fig. 4.44).

AEP-cured diglycidyl ether of bisphenol A was used in a stoichiometric ratio. From the formula of chemicals, it can be seen that AEP has 3 functional groups per molecule, while Bisphenol A has 2 functional groups per molecule. By the Carothers Equation, the average functionality is 12/5 or 2.4, and the critical extent of reaction at the gel point is 2/2.40 or 0.833. For the same system, but using the statistical approach the calculated extent of reaction at gel point is 0.707.

In this study, gelation can be deduced from the beginning point of the cure stress development as well. The comparison of the gelation time from experiments and theories is shown in Table 4.4. The calculated extent of reaction values were used in cooperation with the extent of reaction as a function of time from isothermal DSC to state the predicted gelation time. From the table, the gelation from theories gave a greater gelation time than the experimental value. There was a possibility that the reaction of this system were not only the reaction between the amine group and epoxide group. In addition if etherification occurs in this system at the studied condition it will speed up the reaction as well. However, the etherification should not take place at the studied temperatures as stated by some authors as mentioned previously. It is worthy to note that the sample sizes of different techniques were different. The different sample sizes resulted differences in temperature gradient and the amount of heat given off, which may be one of the reasons for the deviation.

Table 4.4: Comparison of the gelation time from experiments and theories.

Sample/ Temperature (°C)	t_{gel} (DMA) (sec)	(Calculated from theory) (sec)		t_{gel} (Stress development) (sec)
AEP system		Carothers' $t_{p=0.83}$	Statistical $t_{p=0.71}$	
25	10708	-	-	
40	4410	-	-	
60	1656	-	4474	1400
80	566	1134	843	400
100	223	1029	659	200
EMI system				
60	5150	N/A		
80	1200			900
100	490			400
130	80			-
150	15			-
Anhydride system				N/A
80	6360			
120	1035			
150	200			
165	171			

From the gelation time data, activation energy could be obtained from an Arrhenius plot as in Figs. 4.53 – 4.55 for three model epoxies. Activation energy of gelation of AEP-cured diglycidyl ether of bisphenol A was 47.6 kJ/mol, which corresponds to the value of the activation energy of an aliphatic amine curing system from the literature (46-54 kJ/mol) [152-155]. EMI-cured diglycidyl ether of bisphenol F gave a higher activation energy; 73.1 kJ/mol, than that of amine curing system. This activation value agreed with the study of imdazole-catalyzed curing by Vogt [88], which found that EMI-24-cured diglycidyl ether of bisphenol A (0.05 mol. cat/equi. epoxy) gave 71.0 kJ/mol. The anhydride-cured cycloaliphatic epoxy system gave activation energy of gelation as 57.3 kJ/mol. Tanaka and Kakiuchi [140] obtained activation energy for diglycidyl ether of bisphenol A – hexahydrophthalic anhydride with triethanolamine (catalytic system) as 59-60 kJ/mol, while Shimazaki [155] studied the similar system but without the catalyst, and found a higher activation energy (67.9 kJ/mol).

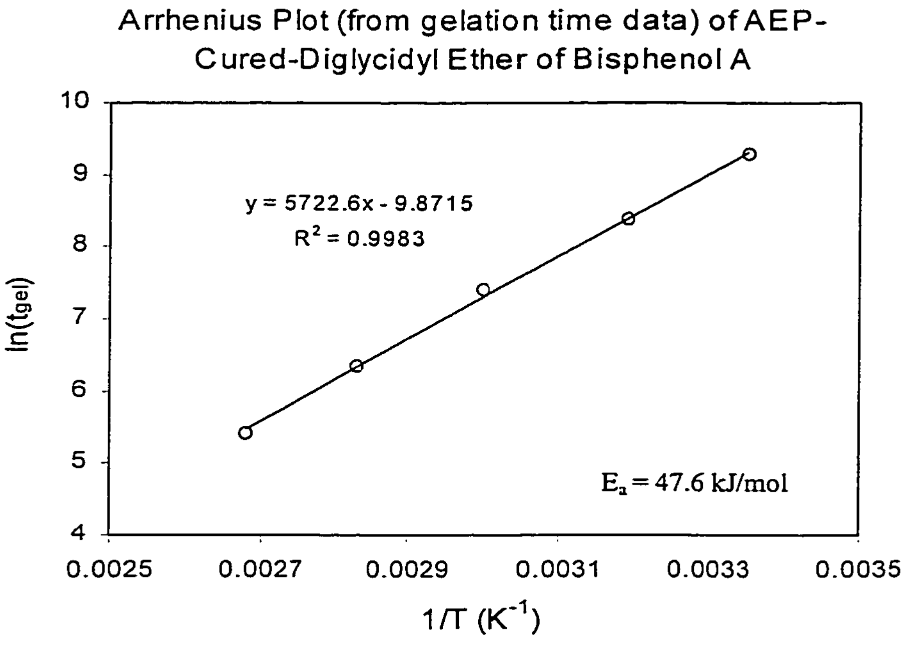

Fig. 4.53: Arrhenius plot of AEP-cured diglycidyl ether of bisphenol A gave an activation energy of gelation of 47.6 kJ/mol.

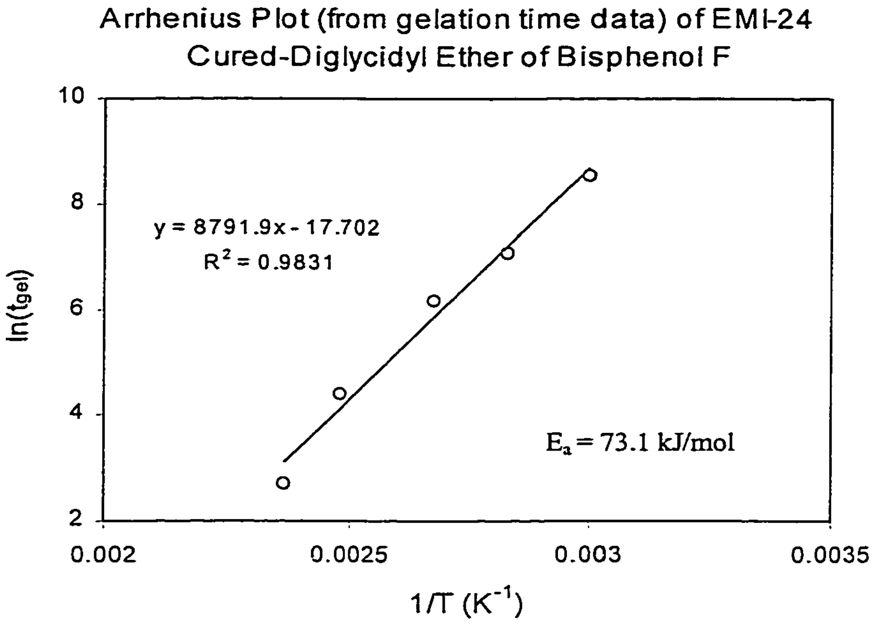

Fig.4.54: Arrhenius plot of EMI-24-cured diglycidyl ether of bisphenol F gave an activation energy of gelation of 73.1 kJ/mol.

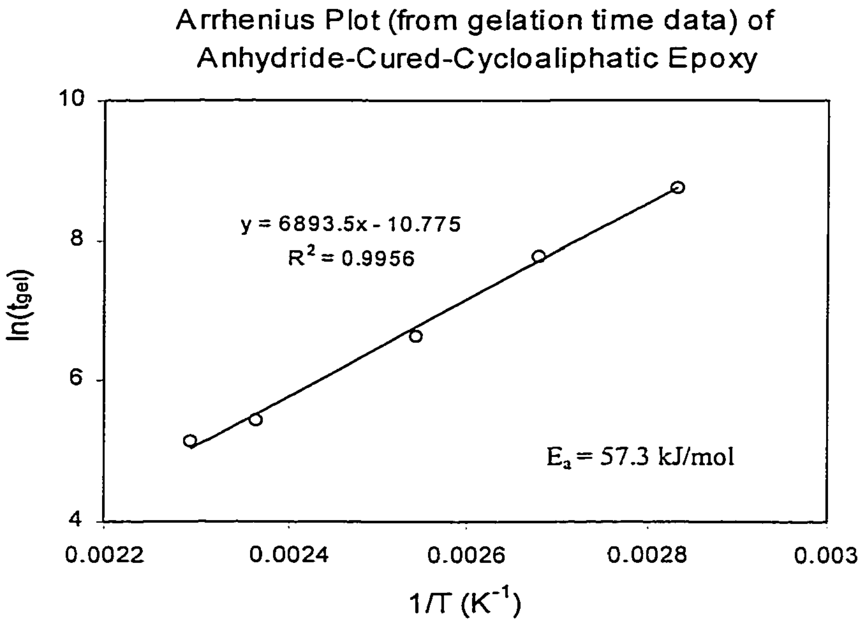

Fig. 4.55: Arrhenius plot of anhydride-cured cycloaliphatic epoxy gave an activation energy of gelation of 57.3 kJ/mol.

4.3.3 Cure Kinetics

The history of network formation can be revealed by its kinetics. The study of the cure kinetics contributes both to a better knowledge of the process development and to improving the quality of the final product.

4.3.3.1 Thermal Characteristics of Fresh Sample

Fresh model epoxies were subjected to a dynamic temperature scan on DSC to obtain the glass transition of the fresh sample (T_{go}), onset temperature, peak temperature, and the amount of exothermic heat of reaction of each sample. The thermograms and their analysis of the three model epoxies are shown in Fig. 4.56 and Table 4.5, respectively.

Table 4.5: The analysis of the thermograms from temperature dynamic DSC scan of model epoxies.

Sample	Onset T_{go} (°C)	Onset rxn. temperature (°C)	Peak Temperature (°C)	Heat of reaction (J/g)
AEP/Bisphenol A	-49	60	105	540
EMI-24/Bisphenol F	-28	107	124	544
Anhydride/Cycloaliphatic	-54	122	150	321

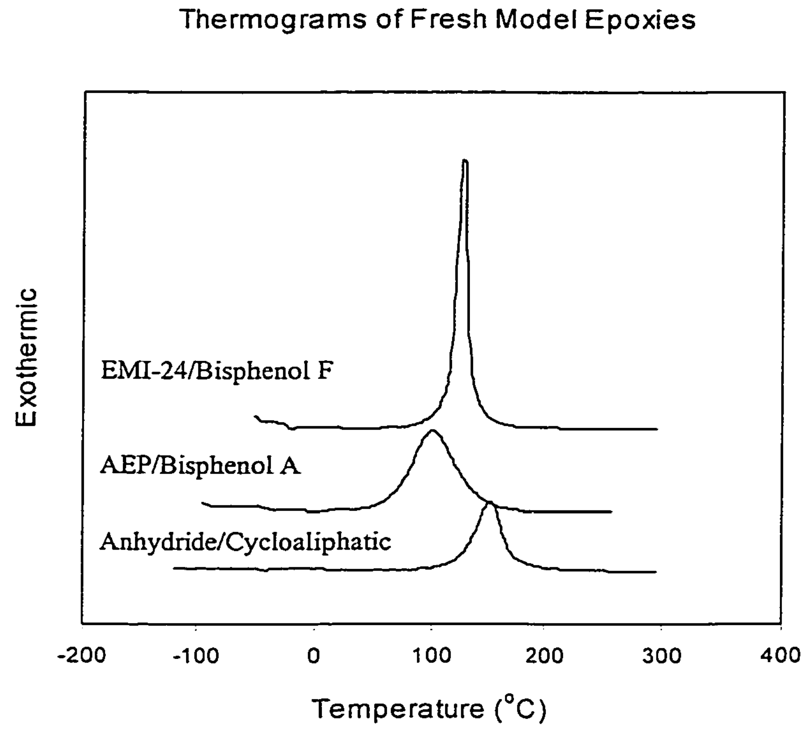

Fig. 4.56: DSC temperature dynamic scan thermograms of model epoxies.

4.3.3.2 Vitrification

Vitrification involves a transformation from a liquid or rubbery state to a glassy state. In the study of kinetics, MDSC was utilized in order to observe vitrification behavior of the model epoxies. Vitrification could be indicated by the reduction of the heat capacity as the reaction proceeded to a certain point at a certain condition. Generally vitrification will be observed if the cure temperature is less than the $T_{g\infty}$ of the sample. However, there are always the influences of the exothermic heat of reaction. AEP-cured diglycidyl ether of bisphenol A showed vitrification when the sample was cured at 60, 80 and 100 °C (see Fig. 4.57), but not at 120 and 140 °C (see Fig. 4.58). The

$T_{g\infty}$ of this sample is about 120 °C (the onset T_g). It has been known that after vitrification the reaction rate comes to be controlled by diffusion of the reacting species. In this regime, the rate of reaction is affected by both chemical and physical aging. The rate of reaction after vitrification is very slow if it does not completely stop. Vitrification can be indicated by the leveling off of the heat flow thermograms after vitrification.

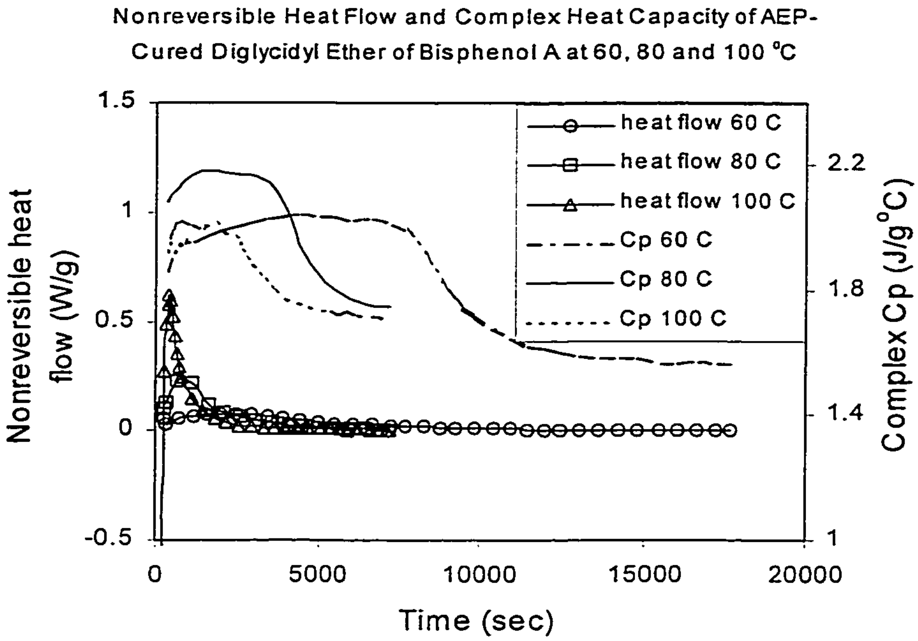

Fig. 4.57: Vitrification occurs in AEP-cured diglycidyl ether of bisphenol A system when it was cured at the temperatures lower than $T_{g\infty}$.

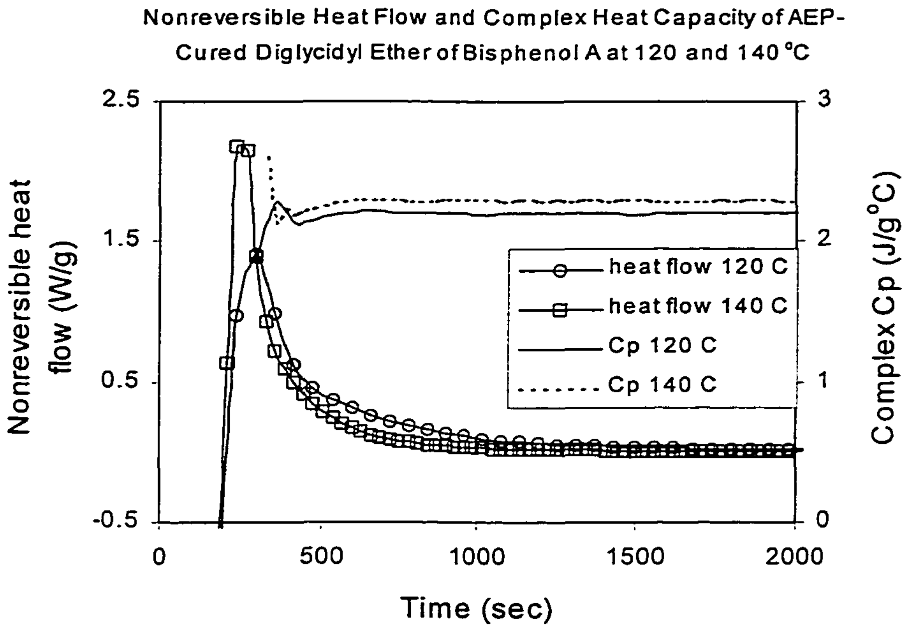

Fig. 4.58: No vitrification was observed for AEP-cured diglycidyl ether of bisphenol A system when it was cured at temperature at close to or higher than $T_{g\infty}$.

MDSC thermograms of EMI-24 cured diglycidyl ether of bisphenol F showed the vitrification when the sample was cured at 80 °C (see Fig. 4.59). However, at 100 °C, which is still lower than $T_{g\infty}$ (onset $T_{g\infty}$ is 127 °C), vitrification did not take place. This may be caused by the influence of high exothermic heat of reaction, which raised the system temperature. Fig. 4.60 shows the thermograms from MDSC of sample when it was cured at 100 and 130 °C. The peak of complex heat capacity that occurred due to the reaction peak could cause the misreading on the occurrence of vitrification. The drop of the complex heat capacity could be either due to the drop of the reaction heat or vitrification.

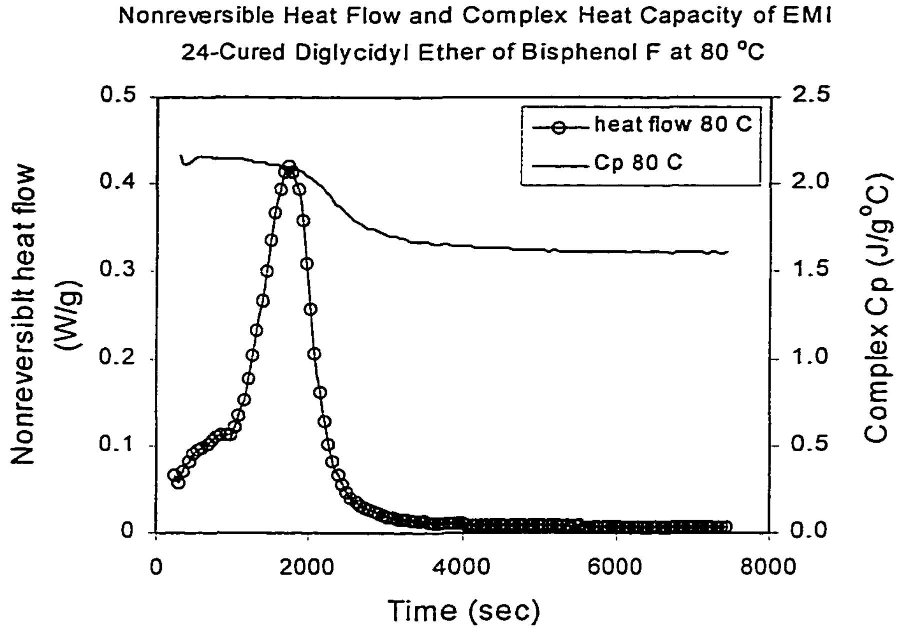

Fig. 4.59: Vitrification was observed in EMI-24-cured diglycidyl ether of bisphenol F system when the sample was cured at 80 °C.

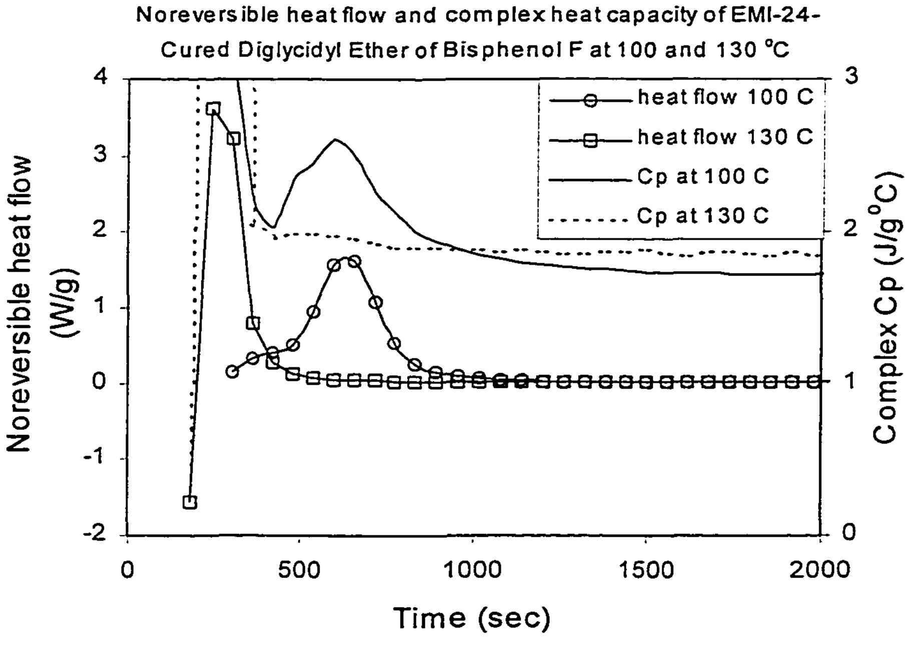

Fig. 4.60: No vitrification in EMI-24-cured diglycidyl ether of bisphenol F system when the sample was cured at 100 and 130 °C.

The onset of $T_{g\infty}$ of anhydride-cured cycloaliphatic epoxy was about 124 °C. Vitrification took place at 120 °C as well as at 100 °C curing (see Fig. 4.61). The reaction could go to completion when the sample was cured at 150 and 165 °C (see Fig. 4.62). This system gave a lower heat of reaction less than that of the other two systems; therefore, at 120 °C, which is close to $T_{g\infty}$ of the sample, vitrification was observed.

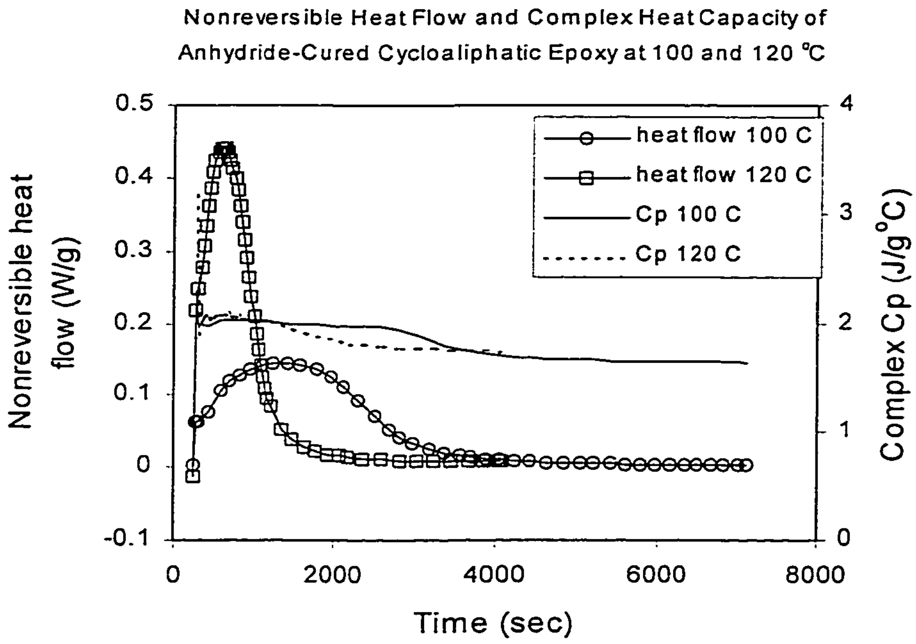

Fig. 4.61: Vitrification was observed in anyhydride-cured cycloaliphatic epoxy system when the sample was cured at 100 and 120 °C.

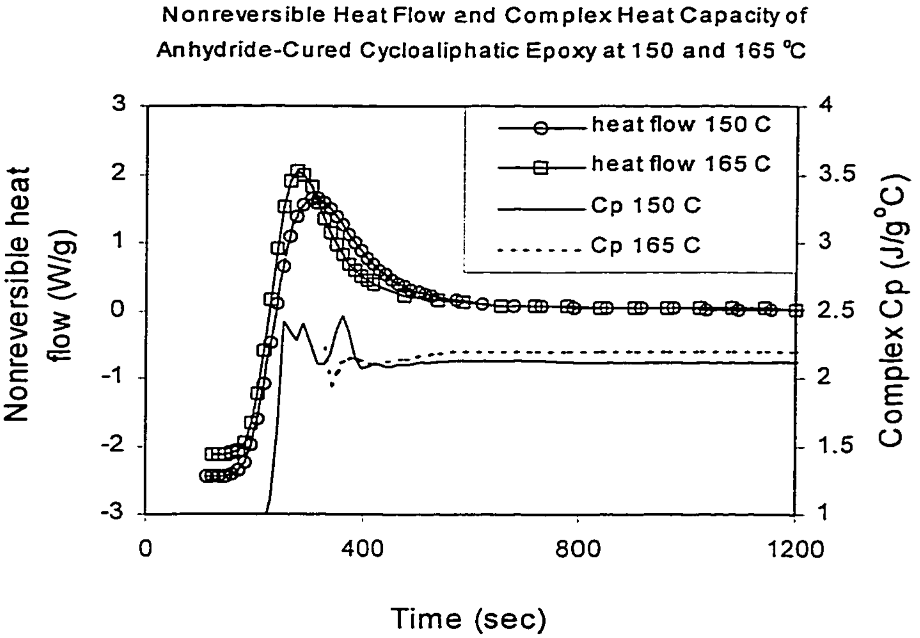

Fig. 4.62: No vitrification was observed in anhydride-cured cycloaliphatic epoxy system when the sample was cured at 150 and 165 °C.

4.3.3.3 Reaction Rate

A series of isothermal reaction rate (dp/dt) curves for epoxy resins with different hardeners as a function of time are shown in Figs. 4.63 – 4.65 for the three model epoxies. The shape of these curves revealed an autocatalytic kinetic mechanism as suggested by a number of studies [156-158]. The overall characteristics of the reaction rate curve as a function of time of all three model epoxies are similar. The peak value of the reaction rate was increased and shifted to shorter time with increasing temperature. The reaction rate of AEP-cured diglycidyl ether of bisphenol A and EMI-24-cured diglycidyl ether of bisphenol F were much faster than that of anhydride-cured cycloaliphatic epoxy. Interestingly, for EMI-24-cured diglycidyl ether of bisphenol F system at low cure temperature (80 and 100 °C), the rate of reaction at the beginning is slow and has a small peak before accelerating to a the high rate.

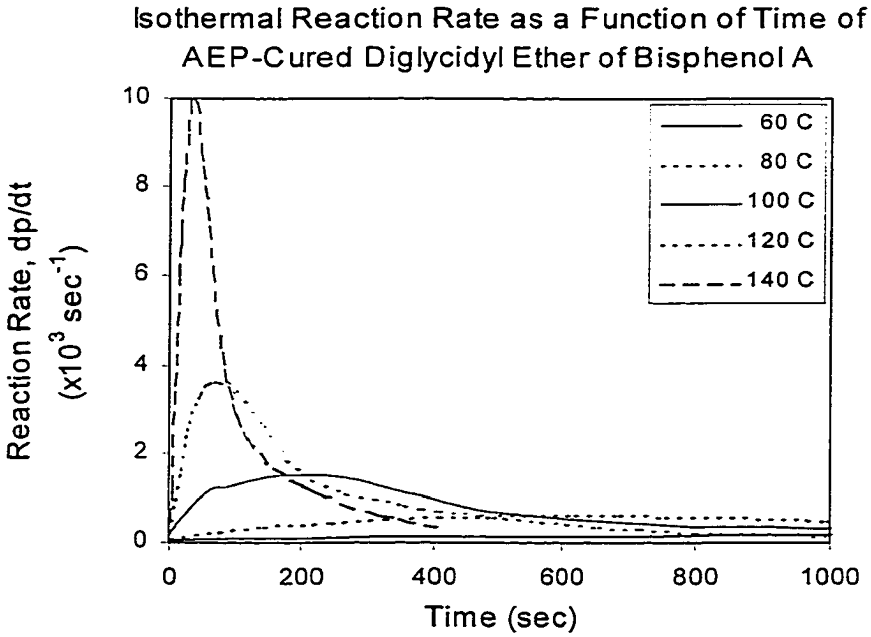

Fig. 4.63: Reaction rate as a function of time at different temperatures of AEP-cured diglycidyl ether of bisphenol A.

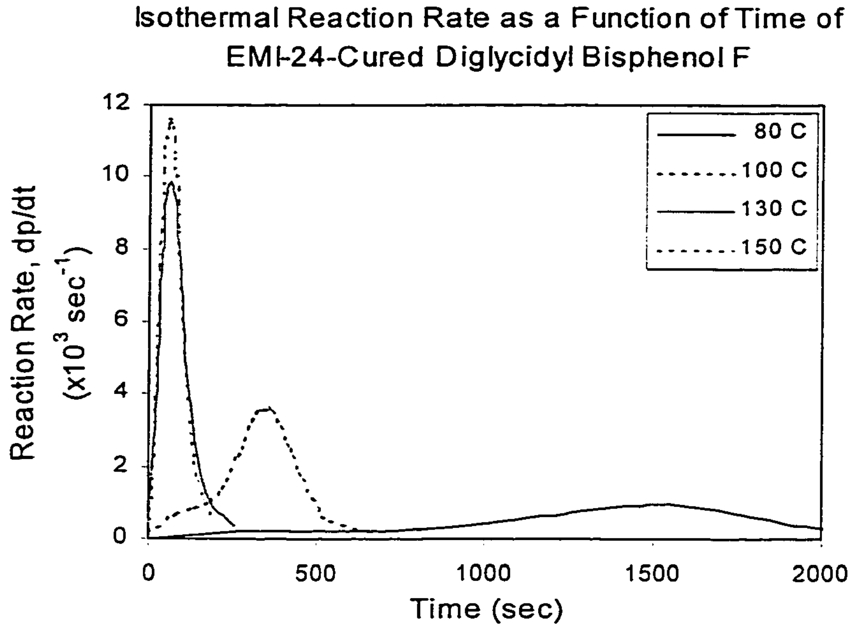

Fig. 4.64: Reaction rate as a function of time at different temperatures of EMI-24-cured diglycidyl ether of bisphenol F.

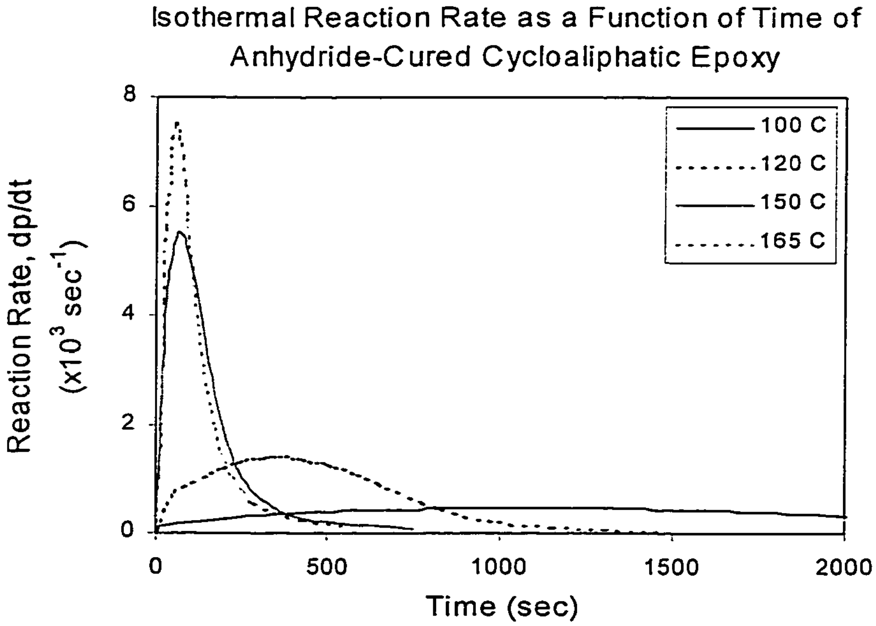

Fig. 4.65: Reaction rate as a function of time at different temperatures of anhydride-cured cycloaliphatic epoxy.

4.3.3.4 Extent of Reaction and Kinetic Parameters

The basic assumption of the DSC kinetic method is that the rate of heat evolution from a reaction is proportional to the rate of the chemical reaction and hence, the total heat evolved up to any point during the reaction is proportional to the amount of reactants consumed [159]. Extent of reaction during isothermal curing was obtained from an integration of the area under the heat of reaction peak as a function of cure time. The rate constant (*k*), and order of reaction (*n* and *m*) were numerically fitted the data to autocatalytic kinetic model. The kinetic parameters of the three model epoxies at various isothermal cure temperatures are shown in Table 4.6. The order of reaction *n* and *m* had changed with the cure temperature, but there was not a trend. The effect of temperature on the order of reaction is not been clearly understood.

Rate constant as a function of temperature of a sample should follow the Arrhenius equation. The plot of ln k versus a reciprocal of absolute temperature of the three model epoxies are shown in Figs. 4.66-4.68. Activation energy could be acquired from the plot. The activation energy of AEP-cured diglycidyl ether of bisphenol A and EMI-24-cured diglycidyl ether of bisphenol F at low and high cure temperatures were different. The rate constant of the AEP-cured diglycidyl ether of bisphenol A system was more sensitive to temperature at high cure temperature than at low cure temperature. On the other hand, EMI-cured diglycidyl ether of bisphenol F exhibited a more sensitive of a rate constant at low temperature. The anhydride-cured cycloaliphatic epoxy showed a linear relationship between ln k and 1/T.

Table 4.6: Kinetic parameters for model epoxies at various isothermal cure temperatures.

Sample/Temperature	n	m	k
AEP-cured diglycidyl ether of bisphenol A			
60 °C	1.02	0.69	0.03
80 °C	0.35	0.54	0.05
100 °C	0.44	0.04	0.10
120 °C	0.42	0.01	0.20
140 °C	0.32	0.35	1.0
EMI-24-cured diglycidyl ether of bisphenol F			
80 °C	0.20	0.70	0.04
100 °C	0.22	0.70	0.17
130 °C	0.52	0.70	1.0
150 °C	0.50	0.86	1.4
170 °C	0.28	0.45	1.9
Anyhydride-cured cycloaliphatic epoxy			
100 °C	0.35	0.40	0.04
120 °C	0.28	0.48	0.12
150 °C	0.62	0.60	0.70
165 °C	0.67	0.66	0.96

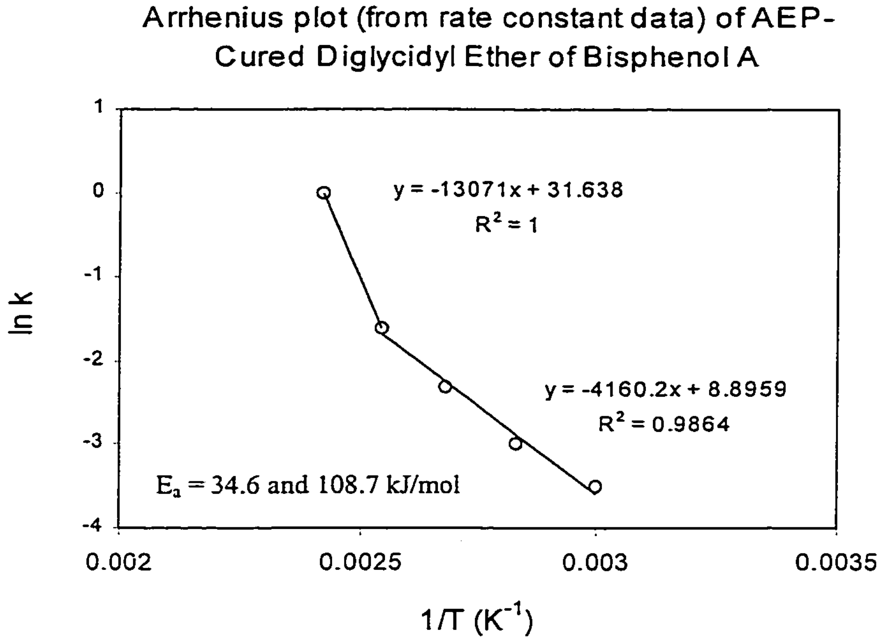

Fig.4.66: The rate constants of AEP-cured diglycidyl ether of bisphenol A display an Arrhenius temperature dependence with an activation energy of 34.6 and 108.7 kJ/mol at low and high cure temperature, respectively.

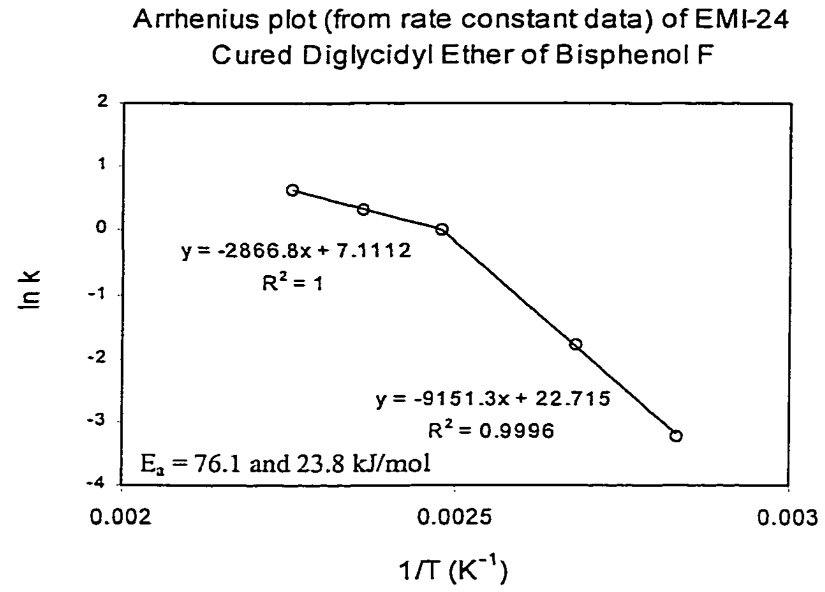

Fig.4.67: The rate constants of EMI-24-cured diglycidyl ether of bisphenol F display an Arrhenius temperature dependence with an activation energy of 76.1 and 23.8 kJ/mol and low and high cure temperature, respectively.

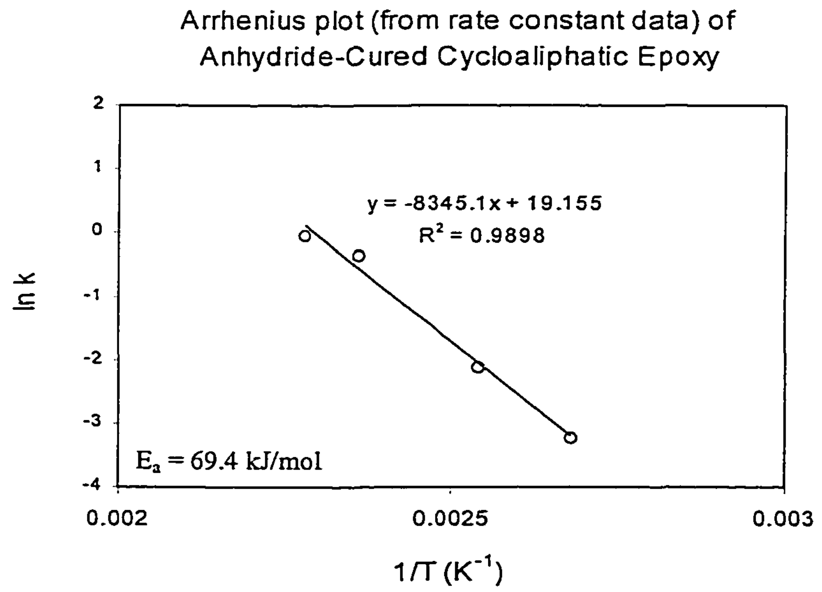

Fig.4.68: The rate constants of anhydride-cured cycloaliphatic epoxy display an Arrhenius temperature dependence with an activation energy of 69.4 kJ/mol.

Table 4.7 displays the Arrhenius activation energy from different sets of data. The viscous flow activation energy is lower than the gelation activation energy and reaction activation energy. The activation energy from the rate constant of the anhydride-cured cycloaliphatic epoxy is higher than the gelation activation energy. However, the reaction activation energy of the AEP-cured diglycidyl ether of bisphenol A and the EMI-cured diglycidyl ether of bisphenol F depended on the cure temperature as mentioned previously.

Table 4.7: Activation energy of model epoxies from different sets of data.

Sample	Activation energy (kJ/mol)
AEP-cured diglycidyl ether of bisphenol A	
Viscous flow	29.0
Gelation	47.6
Reaction	34.6 and 108.7
EMI-cured diglycidyl ether of bisphenol F	
Viscous flow	54.6
Gelation	73.1
Reaction	23.8 and 76.1
Anhydride-cured cycloaliphatic epoxy	
Viscous flow	43.2
Gelation	57.3
Reaction	69.4

Figs.4.69 - 4.71 show the series of the extent of reaction curves for each model epoxy as a function of time. The reaction curves of every system had a slightly sigmoidal

shape. As expected the higher cure temperature, the faster reaction rate. AEP-cured diglycidyl ether of bisphenol A exhibited the undercured products at 60 and 80 °C (the maximum extents of reaction were 80 and 87 %, respectively). Although vitrification was observed by MDSC in this system when the sample was cured at 100 °C, extent of reaction could get to 93 %. Extent of reaction of EMI-24-cured diglycidyl ether of bisphenol F system could go to 87 % when the sample was cured at 80 °C, and more than 95 % for the higher cure temperatures (≥ 100 °C). Even though vitrification was found when anhydride-cured cycloaliphatic epoxy was cured at 100 and 120 °C, extent of reaction could reach 93 and 98 %, respectively.

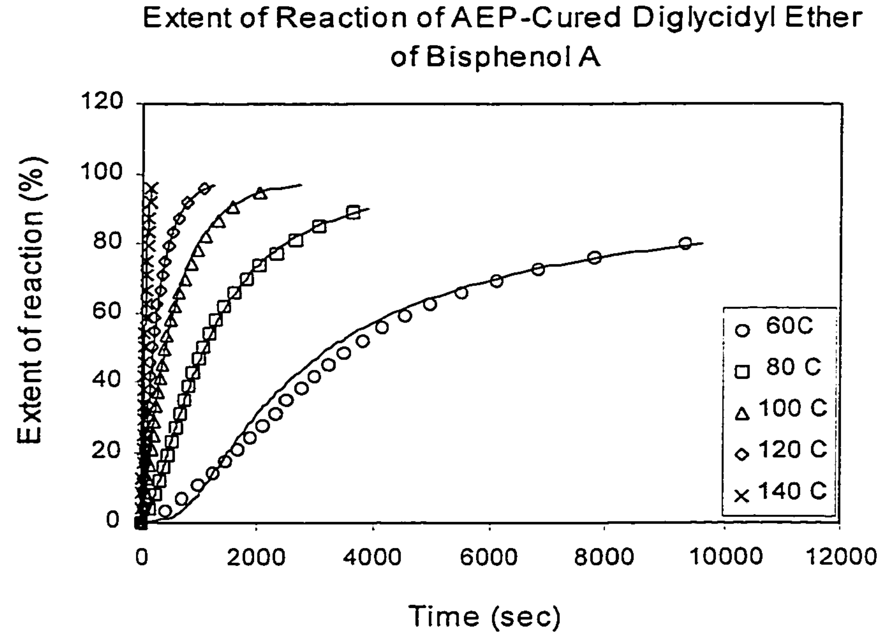

Fig. 4.69: Extent of reaction of AEP-cured diglycidyl ether of bisphenol A at different isothermal cure temperatures.

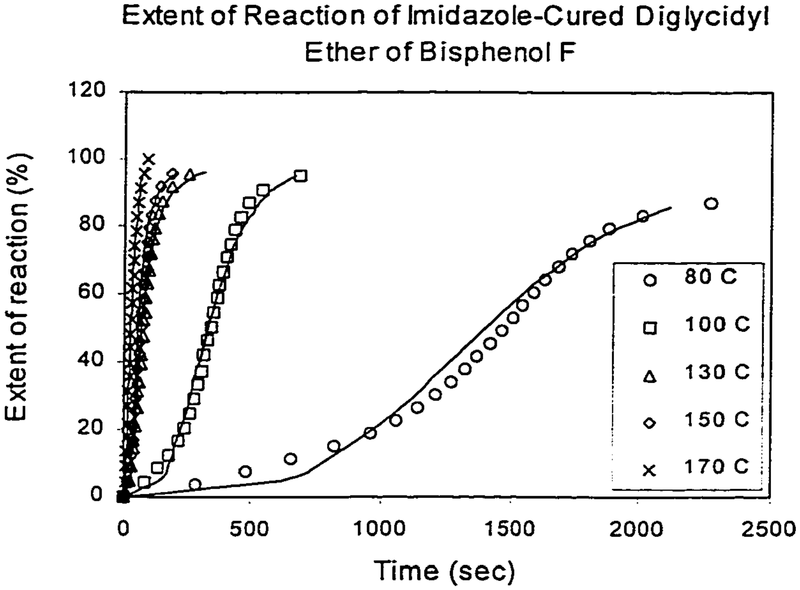

Fig. 4.70: Extent of reaction of EMI-24-cured diglycidyl ether of bisphenol F at different isothermal cure temperatures.

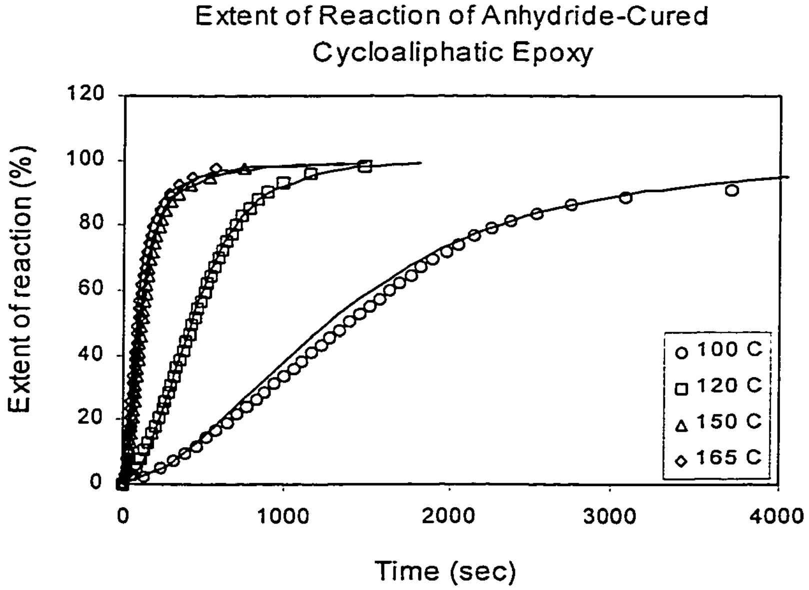

Fig. 4.71: Extent of reaction of anhydride-cured cycloaliphatic epoxy at different isothermal cure temperatures.

4.3.4 Glass Transition – Conversion Relationship

The fundamental property that determines the state of a thermoset is its chemical conversion or extent of reaction. Several researchers have shown that there is a unique relationship between extent of reaction and its T_g, independent of cure temperature and thermal history [7, 160-165]. This behavior holds for most thermosetting systems, but not for all. The uniqueness of the relationship has been found to hold for epoxy-amine systems whose structure does change with cure temperature [160-162]. However, a temperature-independent T_g-conversion relationship did not hold for a dicyandiamide system [166], for bisphenol A-based cyanate ester systems cured with greater than 100 ppm zinc catalyst and greater than 4 ppm nonylphenol cocatalyst [167], or for phenolic resin cured with hexamethylene tetramine or unsaturated polyester fumarates cross-linked with styrene [168]. For systems where this relationship does hold, measurement of T_g is equivalent to direct measurement of conversion. It has been suggested [169] that the one-to-one relationship between T_g and extent of reaction occurs when the curing reaction involved the formation of only one type of chemical linkages, or when competing reactions yielding different structures have similar activation energy or occur sequentially. Measurement of T_g is more sensitive than conversion, as measured by the residual heat of reaction, in the later stage of cure [170]. Variation of T_g of the thermosetting polymer with extent of reaction is an important property, which should be established for optimizing the cure process. It is well-established fact that the chain extension and cross-linking increase the T_g of a thermosetting system.

There are several empirical or theoretical equations relating T_g to extent of reaction in the literature. One of the most important equations is the so-called "original" DiBenedetto Equation [171], which could be cast into the form:

$$\frac{T_g - T_{gu}}{T_{gu}} = \frac{(E_x/E_m - F_x/F_m)X}{1-(1-F_x/F_m)X} \qquad (4.21)$$

where X is the crosslink density defined as the fraction of all segments that are crosslinked, T_{gu} denotes the glass transition temperature of the uncrosslinked polymer, E represents the lattice energy, F is the segmental mobility, and subscripts x and m refer to the fully crosslinked and uncrosslinked polymers, respectively. It was suggested [171] that in many cases E_x/E_m should be approximately 1.0 or a little greater, while F_x/F_m should be essentially zero. Because the crosslink density X was difficult to quantitatively measure, some authors [160-165] have regarded X as extent of reaction (p), and T_{gu} as T_{go} (T_g at $p = 0$). Then the relation of $(E_x/E_m)/(F_x/F_m) = T_{g\infty}/T_{go}$. Setting $F_x/F_m = \lambda'$ and rearranging the Equation (4.22), the DiBenedetto Equation is restated as:

$$\frac{T_g - T_{go}}{T_{g\infty} - T_{go}} = \frac{\lambda' p}{1-(1-\lambda')p} \qquad (4.22)$$

From entropic considerations, Couchman [172-173] showed that the compositional variation of the T_g of a solution assumed random mixing may be written as:

$$\sum x_i \int_{T_{gi}}^{T_g} (\Delta C_{pi}/T)\,dT = 0 \qquad (4.23)$$

where T_g is the glass transition temperature of the solution, T_{gi} is the glass transition temperature of pure constituent i, $\Delta C_{pi} = (C_{pi})_l - (C_{pi})_g$ is the change in the isobaric heat capacity of constituent i between liquid and glassy states, and x_i is the amount of constituent i in the solution. Pascault et al. [163] and Venditti et al. [165] utilized the same idea as Couchman to model a thermosetting polymer at conversion p as an equivalent random solution of monomer and a fully cured polymer. The following equation was obtained:

$$p\int_{T_{g\infty}}^{T_g}\left(\frac{\Delta C_{p\infty}}{T}\right)dT + (1-p)\int_{T_{go}}^{T_g}\left(\frac{\Delta C_{po}}{T}\right)dT = 0 \qquad (4.24)$$

where ΔC_{po} and $\Delta C_{p\infty}$ are the differences in heat capacity between the glassy and rubbery (or liquid, prior to gelation) states at T_g for the monomer and fully cured network, respectively. Pascault et al.[171] assumed that $\Delta C_p \propto 1/T$ and showed *that* $\lambda = \Delta C_{p\infty}/\Delta C_{po}$, so the integration of Equation (4.24) leads to:

$$\frac{T_g - T_{go}}{T_{g\infty} - T_{go}} = \frac{\lambda p}{1-(1-\lambda)p} \qquad (4.25)$$

Note that λ (in Equation 4.25) and λ′ (in Equation 4.22) are not the same.

Hale et al. [174] derived the equation to model the dependence of the T_g on the extent of reaction for high crosslinked thermosetting polymers. The model assumes that the increase in T_g was caused by the decrease in free volume from the reduction of chain-end concentration, the reduction of segment mobility from more crosslink, and the departure from Gaussian behavior at high crosslink density. They proposed the following equation:

$$T_g = \frac{\left(\frac{1}{\frac{1}{T_{go}} - kp}\right)}{1 - \frac{K_2 X}{1 - \Psi X^2}} \tag{4.26}$$

where k is the incorporation of the effect of of chain-ends, p is extent of reaction, K_2 is DiMarzio's constant (originally thought to be "universal", but was later shown to vary for different polymers) [175], X is crosslink density (mole of chains per mole of segments), and ψ is an empirical constant that lumps together the effect of nonidealities such as non-Gaussian behavior and steric effects. Lin et al. [176] suggested that K_2 constant in Equation 4.26 is exactly represented by the difference between the ratio of lattice energy (E_x/E_m) and the ratio of segmental mobility (F_x/F_m) in the original DiBenedetto Equation. The correction factor Ψ is related to the deviation of the ratio of lattice energy from the ideal limit of 1.

In our research the modified DiBenedetto Equation (Equation 4.25) has been utilized to calculate T_g of each model epoxy and then compared to the experimental T_g as shown in Figs. 4.72 - 4.74. For AEP-cured diglycidyl ether of bisphenol A and anhydride-cured cycloaliphatic epoxy, the calculated T_g and the experimental T_g agreed well to each other at low extent of reaction; however, at high extent of reaction the calculated T_g was higher than the experimental value. The diffusion-controlled reaction at high extent of reaction could be the reason for the deviation. Oleinik [177] showed that theoretically the maximum extent of reaction that can be expected in an epoxy-amine system is 95-96%. The unreacted epoxy or amino groups are spatially separated from each other and cannot meet and react due to high connectivity of the network. However, the sensitivity of the DSC is not enough to detect the left over part of the sample at the end of the reaction. Therefore, the maximum extent of reaction in case of no vitrification, which was reported in this study, was counted as 100% (fully cured sample). The thermograms of EMI-24-cured diglycidyl ether of bisphenol F at the extent of reaction in the range of 80- 98 % did not reveal the T_g (see Fig.4.76). The T_g possibly fell in the same range as of the reaction peak; therefore there were no experimental data in that range of extent of reaction to compare with the calculated value. In such a system, the predicted T_g by DiBenedetto Equation is imperative. Interestingly, as the reaction progressed in the first period of reaction, the reaction peak occurred at the lower temperature. Eventually the reaction peak shifted to a higher temperature with the increasing of extent of reaction (see Figs.4.75 and 4.77 for EMI-24-cured diglycidyl ether of bisphenol F and anhydride-cured cycloaliphatic epoxy, respectively). This could refer to the difference in activation energy of the sample during the curing. However, in case of AEP-cured diglycidyl ether of bisphenol A (Fig.4.75) the reaction peak only shifted to the higher temperature as the extent of reaction increased. Unlike the other two model epoxies, the thermograms of EMI-24-cured diglycidyl ether of bisphenol F, which partially cured to a certain extent of reaction, exhibited the second reaction peak at higher temperature. This could reveal a difference in reaction mechanism.

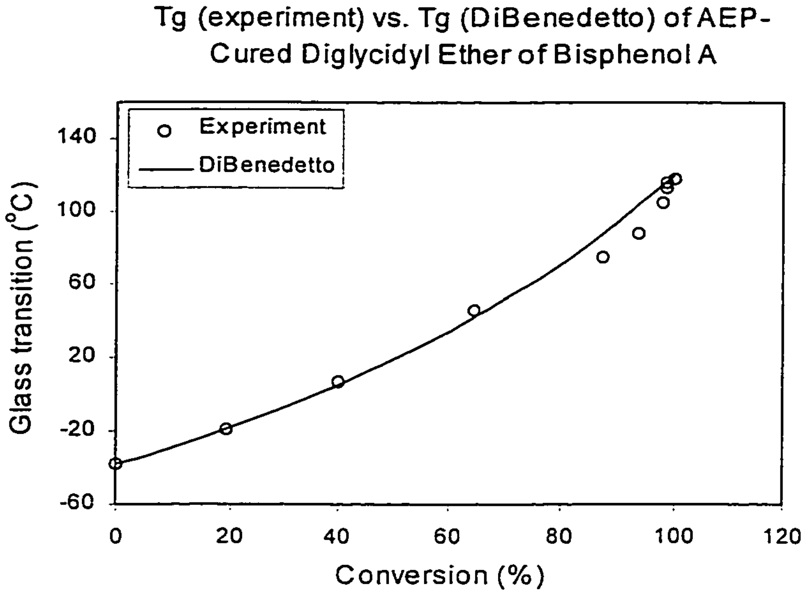

Fig. 4.72: Comparison of the experimental T_g and DiBenedetto Equation calculated T_g of AEP-cured diglycidyl ether of bisphenol A.

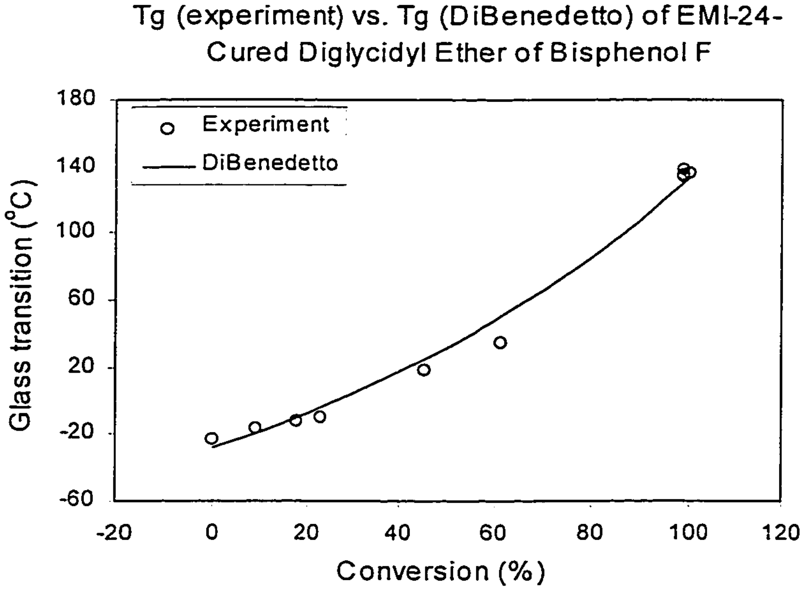

Fig. 4.73: Comparison of the experimental T_g and DiBenedetto Equation calculated T_g of EMI-24-cured diglycidyl ether of bisphenol F.

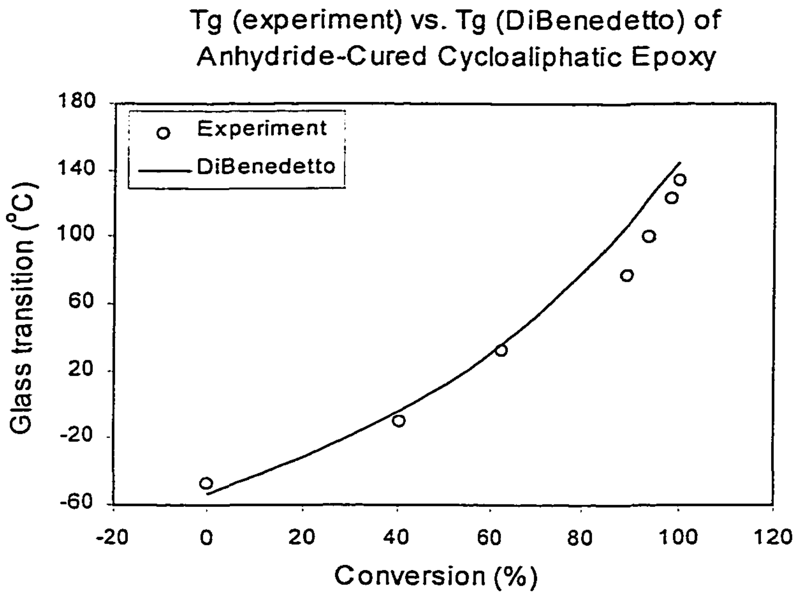

Fig. 4.74: Comparison of the experimental T_g and DiBenedetto Equation calculated T_g of anyghydride-cured cycloaliphatic epoxy.

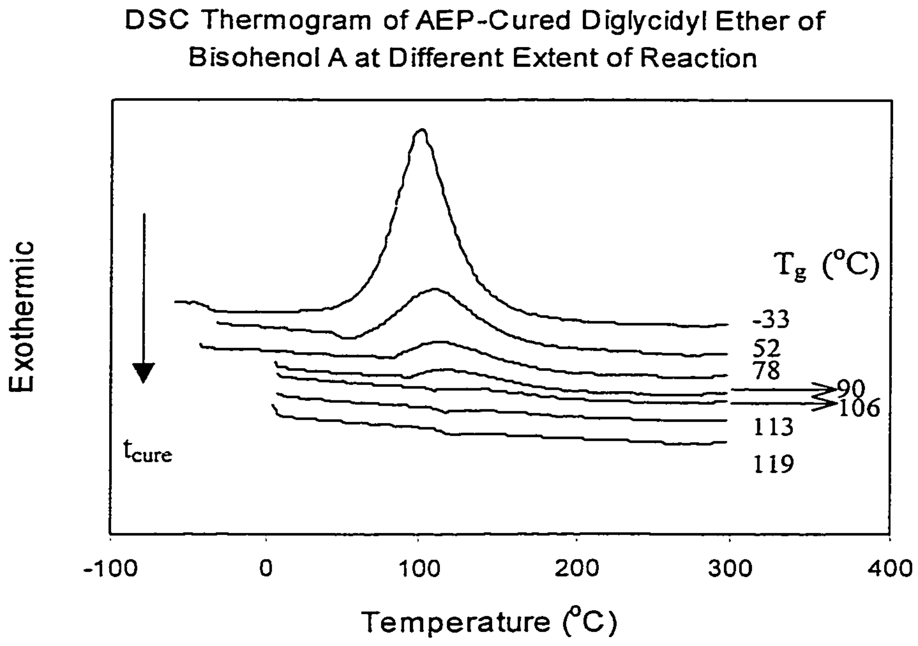

Fig. 4.75: DSC thermograms of AEP-cured diglycidyl ether of bisphenol A show the shifting to higher T_g with the increasing extent of reaction (middle point T_g at T_c = 120 °C).

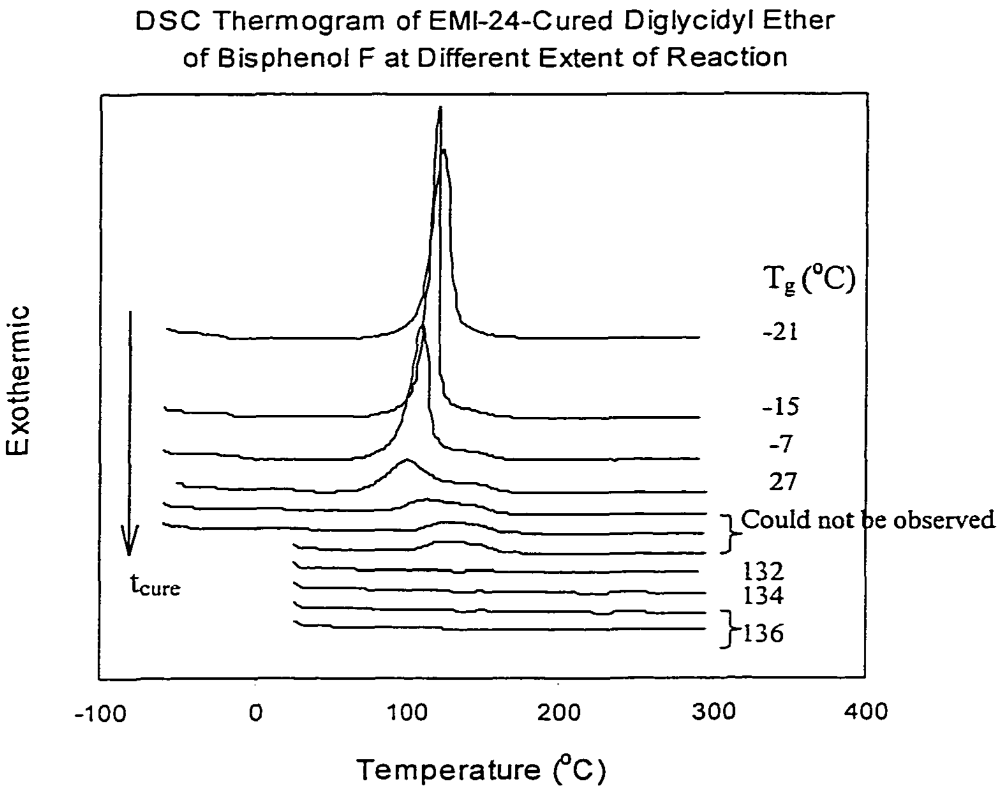

Fig.4.76: DSC thermograms of EMI-24-cured diglycidyl ether of bisphenol F show the shifting to higher T_g with increasing extent of reaction (middle point T_g at T_c = 130 °C).

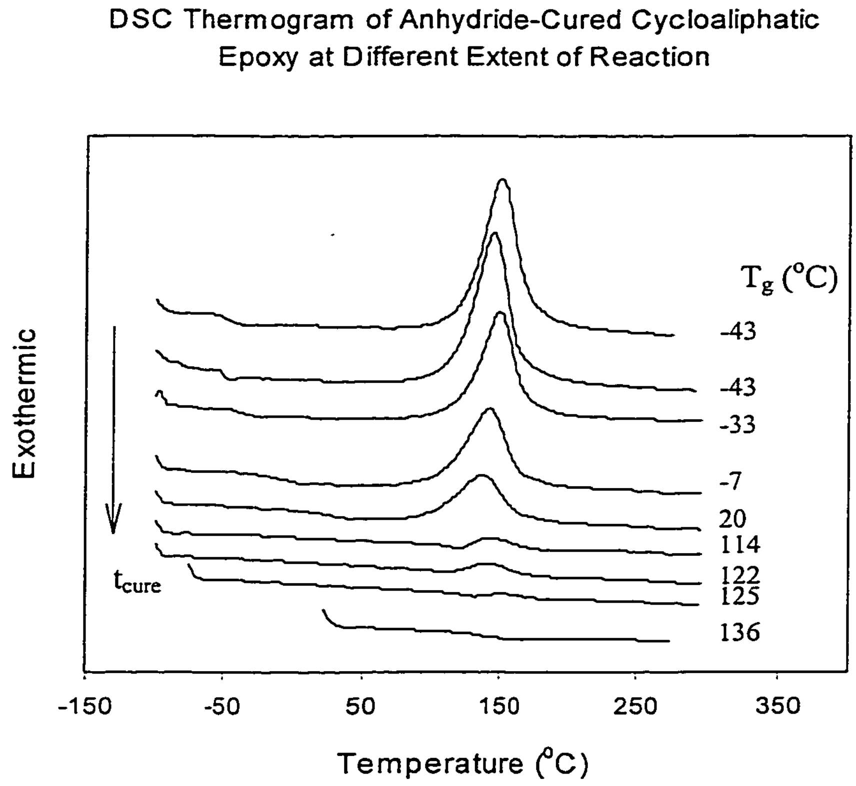

Fig.4.77: DSC thermograms of anhydride-cured cycloaliphatic epoxy show the shifting to higher T_g with increasing extent of reaction (middle point T_g at T_c =150 °C).

4.3.5 The effect of cure temperature on T_g

The samples were cured isothermally until they reached the maximum degree of curing at each temperature and then subjected to the DSC dynamic temperature scan to see the effect of cure temperature on T_g. It is well known that T_g indicates the chain stiffness or the network structure of the sample; therefore, how temperature affects the build-up of network should be disclosed by T_g of the sample. It was found that, for AEP-cured diglycidyl ether of bisphenol A and anhydride-cured cycloaliphatic epoxy, T_g

increased with increasing cure temperature in the studied range (Fig.4.78 and 4.80). This is because a higher cure temperature gives higher extent of reaction and crosslink density, and this causes the higher chain stiffness. However, the effect of cure temperature on T_g of EMI-24-cured diglycidyl ether of bisphenol F system (Fig.4.79) was found to be different; the higher cure temperature, the lower T_g. This system contained an excess of epoxy resin; therefore, there was a high possibility that etherification, due to the formed hydroxyl group, would occur at high cure temperatures (see mechanism scheme in Fig 4.45). The ether linkages separated the chain in the network, and led to the lower T_g due to the increasing of flexibility. Furthermore, the lower value of T_g may be caused from the degradation of some part of chain in the network at high cure temperatures.

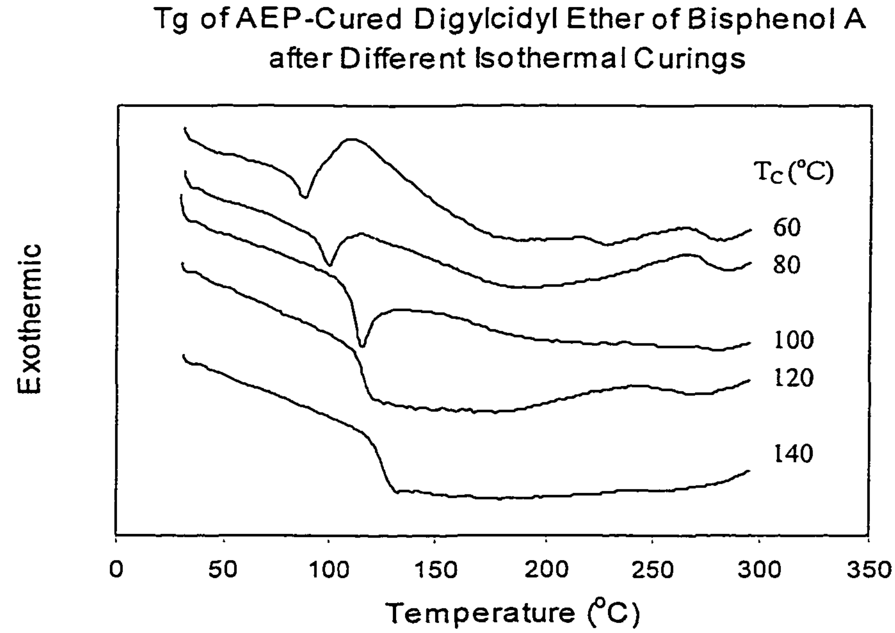

Fig. 4.78: T_g of AEP-cured diglycidyl ether of bisphenol A increased with the increasing of cure temperature.

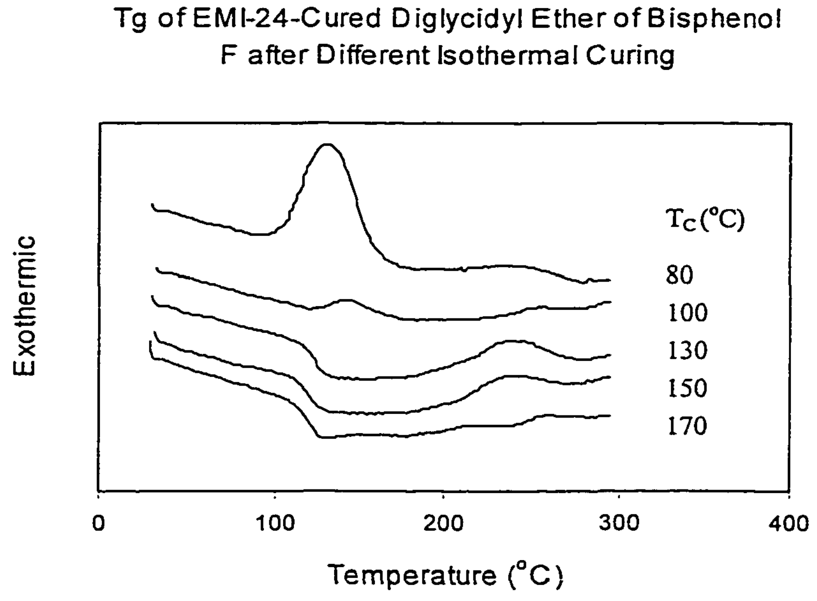

Fig.4.79: T_g of EMI-24-cured diglycidyl ether of bisphenol F decreased with the increasing of cure temperature.

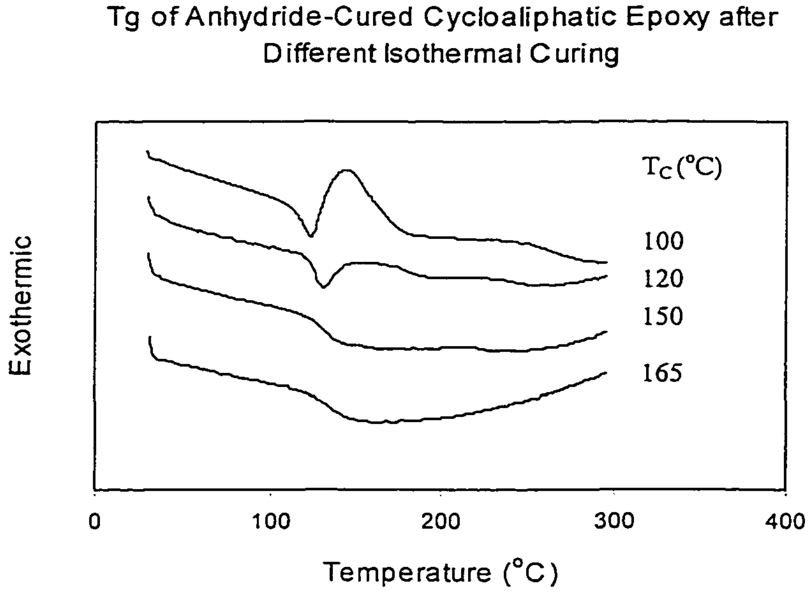

Fig. 4.80: T_g of anhydride-cured cycloaliphatic epoxy increased with the increasing of cure temperature.

4.3.6 Exothermic Heat of Reaction

Crosslinking is an exothermic reaction. Hong et al. [178] studied epoxy/ dicyadiamide (DICY) system and found that the curing heat increased with increasing cure temperature. A higher temperature facilitated the dissolution of DICY, hence, facilitated the reaction between DICY and epoxy and speeded the reaction rate [179-180]. It has been also indicated that in a curing reaction, which was dominated by several different parallel reaction routes, the change in curing temperature resulted in a change in relative rates among curing mechanisms [181]. This caused a difference in reaction exotherms. The heat of reaction from the integration of the reaction thermogram of isothermal DSC of model epoxies is shown in Table 4.8. The heat of reaction increased with the increasing of cure temperature at the lower range of cure temperatures; however, the inverse results were obtained at the higher range of cure temperatures. At the low cure temperatures vitrification occurs as mentioned previously, and the consequence of this occurrence was the decrease of extent of reaction as well as the reaction heat. The explanation for the lower amount of heat of reaction at the high cure temperature is most likely due to neglecting to account for the reaction that occurs during the temperature ramp. The reaction of each system at high cure temperatures is fast, and the DSC could not catch that amount of heat of reaction. Widmann [182] proposed a means to correct the unrecorded heat by rerunning the experiment on the reacted sample under the same condition to obtain an estimate of the "true" baseline, and found that the unrecorded heat of reaction was 5% at 150 °C and 20 % at 170 °C.

Table 4.8: Heat of reaction from isothermal DSC of model epoxies.

Sample/Cure temperature	Heat of reaction (J/g)
AEP-cured diglycidyl ether of bisphenol A	
60 °C	339
80 °C	421
100 °C	372
120 °C	355
140 °C	330
EMI-24-cured diglycidyl ether of bisphenol F	
80 °C	448
100 °C	480
120 °C	488
150 °C	444
170 °C	430
Anhydride-cured cycloaliphatic epoxy	
100 °C	310
120 °C	310
150 °C	297
165 °C	279

The exothermic heat of reaction measurement was also monitored by attaching the PRT to the thin wall of a silicone tube, which contained a sample. The temperature of the sample was detected after the sample was placed in a furnace. By using this method, the heat of reaction could be detected throughout the curing period. Therefore, by assuming the similar heat loss to the environment, the comparison of reaction heat among the different cure temperatures could be done with more reliability than the heat of reaction from DSC. The results are shown in Figs. 4.81 – 4.83 for all three model epoxies. A greater heat of reaction was generated at a higher cure temperature for the AEP-cured diglycidyl ether of bisphenol A system. However, at 100 and 120 °C, the amount of reaction heat were similar. This can be explained by the similar reaction mechanisms and extent of reaction at these two cure temperatures, which was revealed by the extent of reaction data in Fig.4.69. A greater heat of reaction of EMI-24-cured diglycidyl ether of bisphenol F system was found at a higher cure temperature too, but it was not significant. This is because no vitrification was observed in the temperature range studied. For anhydride-cured-cycloaliphatic epoxy, reaction heat was less than the other two model epoxies. The reaction rate of this system was much slower than the other two systems too.

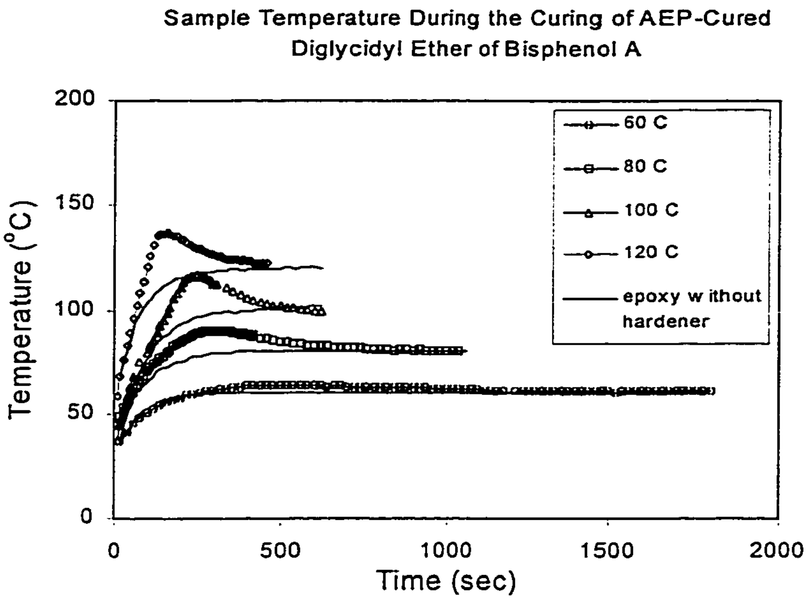

Fig. 4.81: Sample temperature of AEP-cured diglycidyl ether of bisphenol A during the first period of curing increases with the increasing of cure temperature due to the exothermic reaction.

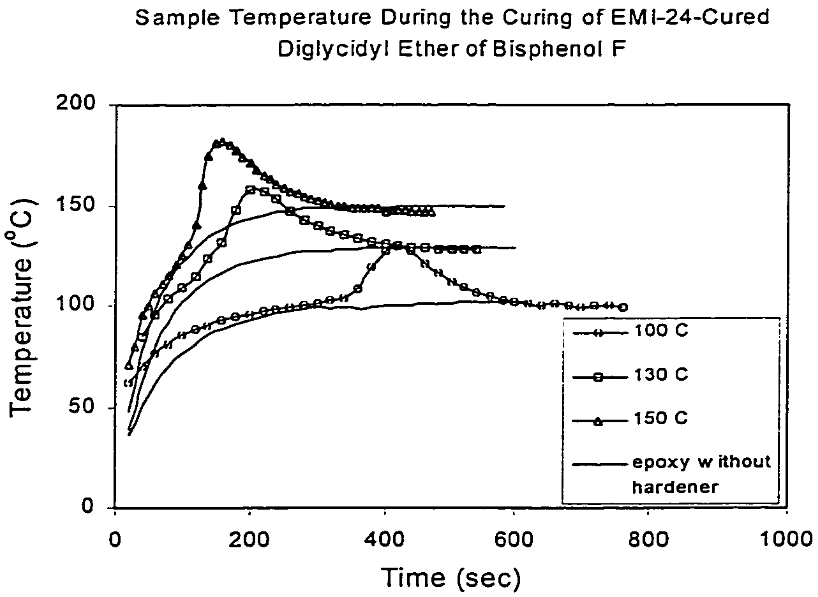

Fig. 4.82: Sample temperatures of EMI-24-cured diglycidyl ether of bisphenol F during the first period of curing were almost similar at different cure temperatures.

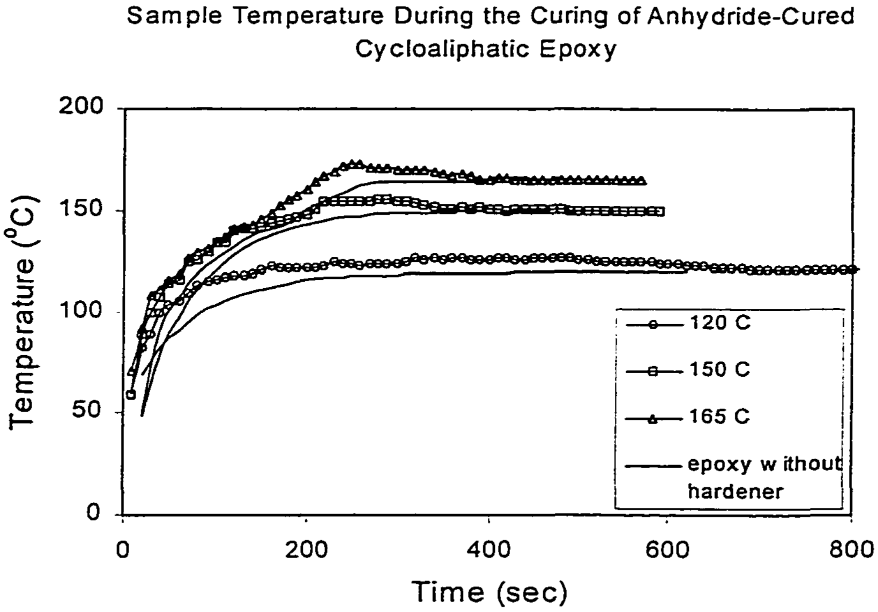

Fig. 4.83: Sample temperature of anhydride-cured cycloaliphatic epoxy. This system generated less reaction heat than the other two model epoxies.

4.3.7 Isothermal Cure Stress

The build-up of a stress within the resin over time is governed by the course of change of volume and stiffness of the resin. A typical curing process involves two steps:

(a) Curing at a constant elevated temperature during which the resin simultaneously shrinks and builds-up stiffness.

(b) On cooling from the cure temperature, the resin shrinks and drastically increases its stiffness.

In this research, only step (a), the isothermal curing, has been studied. Several isothermal curing profiles were examined on model epoxies as shown in Figs. 4.84-4.86 for the three model epoxies. The AEP-cured diglycidyl ether of bisphenol A gave almost similar cure stresses (100-130 kPa) at all cure temperatures studied. The EMI-24-cured diglycidyl ether of bisphenol F gave a higher cure stress than the other two model epoxies. Cure stress was about 300 kPa at 130 and 150 °C isothermal cure temperatures, while at 100 and 80 °C gave about 230 kPa, and about 135 kPa, respectively. Interestingly, no significant cure stress was observed in the anhydride-cured cycloaliphatic epoxy system. In EMI-24 cured diglycidyl ether of bisphenol F system, the reason for the lower cure stress at 80 °C is the vitrification occurrence as shown previously. It has been stated previously that the origins of cure stress are modulus and volume shrinkage of the resin. In the vitrified state, the resin has a higher magnitude of modulus than at the rubbery state. However, if the volume shrinkage is small, the developed cure stress could be small as well. Thus, the effect of volume shrinkage is more significant than the effect of the equilibrium modulus at vitrification in this epoxy system. However, from the MDSC, the occurrance of vitrification was not clear for the 100 °C cure. In this epoxy system, cure stress was developed to a certain peak value, then relaxed for some extent. One of the possibilities that may have caused the relaxation in stress was the exotherm that occurred after the system reached the gelation point. Figs. 4.87-4.89 display the sample temperature and the developed cure stress at the beginning of the reaction. At the high cure temperature EMI-cured diglycidyl ether of bisphenol F gelled before the sample temperature adjusted itself down to the oven temperature. From the rubber elasticity concepts, the retractive stress of an elastomer arises through the reduction of entropy rather than a change of enthalpy [183]. The basic equation relating the retractive stress (σ) of an elastomer is given by:

$$\sigma = nRT\left(\gamma - \frac{1}{\gamma^2}\right) \tag{4.27}$$

where n is the number of active network chain segments per unit volume. From Equation (4.27), if strain is fixed (as in our study), and the temperature increases (due to the heat of reaction), stress will increase. Thus the cure stress in EMI-cured diglycidyl ether of bisphenol F increased. However, after the heat of reaction descended, sample temperature reduced to the oven temperature. During the temperature ramping down, rubbery resin expanded, thus caused the declination of cure stress in this system. The descent of stress was not observed in the other two model epoxies. The gelation of the two epoxies occurred after the sample temperature reduced to the oven temperature, except for the AEP system at 100 °C, when the gelation occurred in the range of the exothermic peak; however, no significant relaxing of stress was observed.

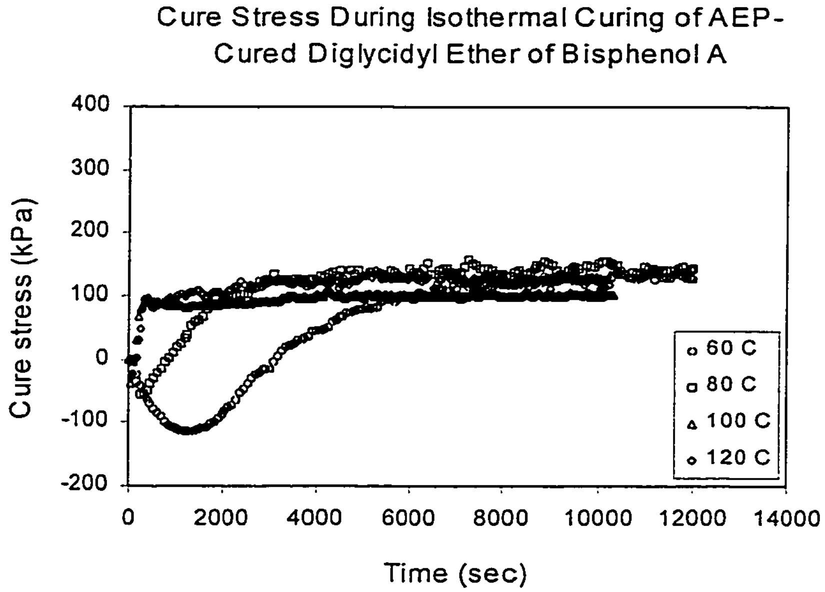

Fig. 4.84: Cure stresses during the isothermal curing of AEP-cured diglycidyl ether of bisphenol A were similar at different cure temperatures.

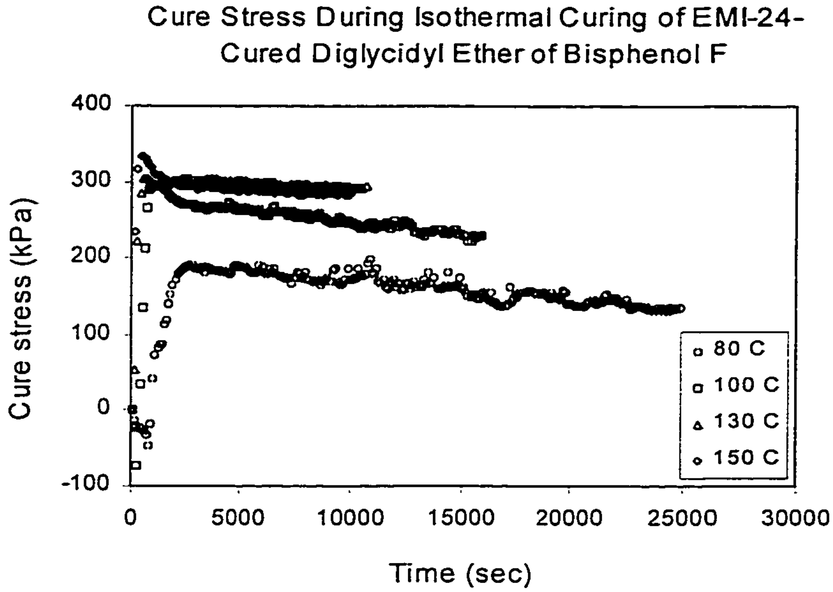

Fig. 4.85: Cure stresses during the isothermal curing of EMI-24-cured diglycidyl ether of bisphenol F were similar at 130 and 150 °C cure temperatures, but greater than that of 100 and 80 °C.

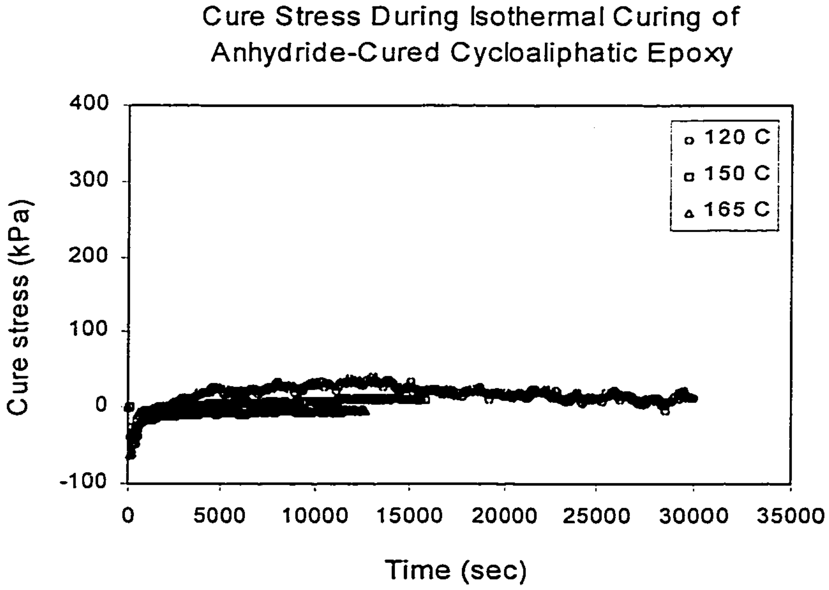

Fig. 4.86: Cure stresses during the isothermal curing of anhydride-cured cycloaliphatic epoxy were small.

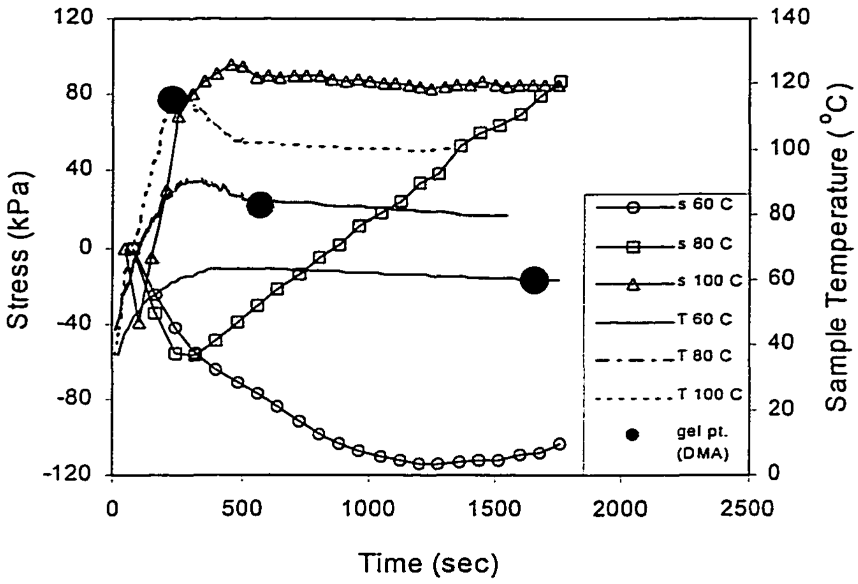

Fig. 4.87: The sample temperatures and developed cure stresses at the beginning period of the reaction of AEP-cured diglycidyl ether of bisphenol A.

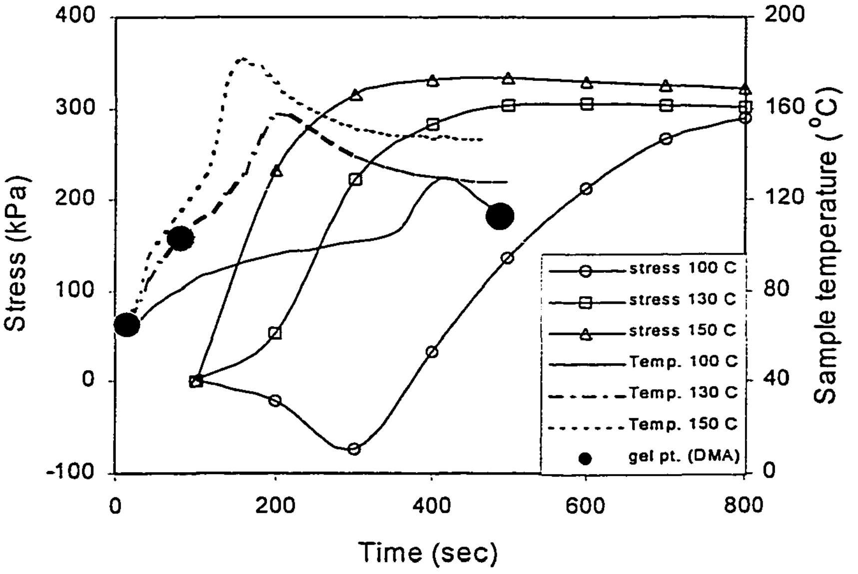

Fig. 4.88: The sample temperatures and developed cure stresses at the beginning period of the reaction of EMI-24-cured diglycidyl ether of bisphenol F.

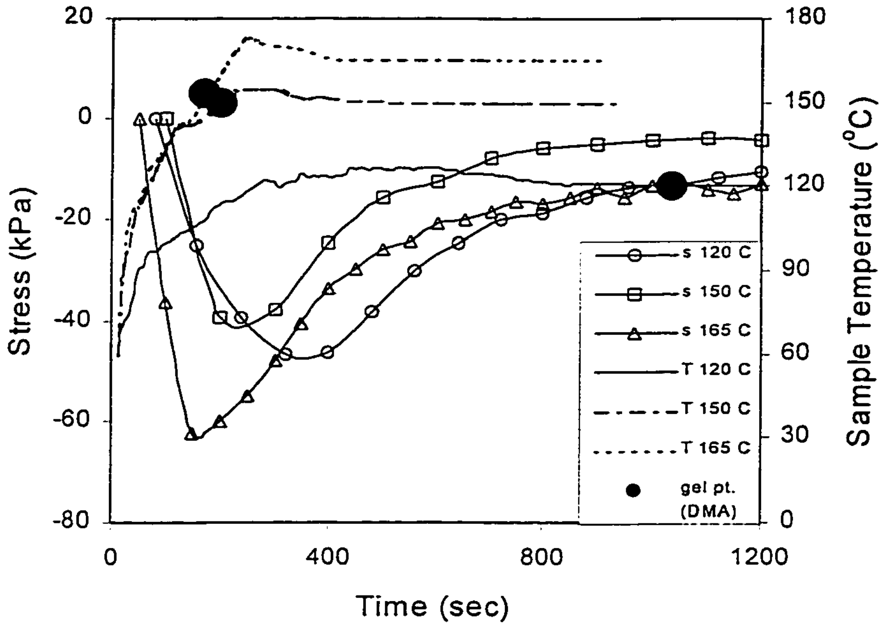

Fig. 4.89: The sample temperatures and developed cure stresses at the beginning period of the reaction of anhydride-cured cycloaliphatic epoxy.

4. 3.8 Stress Model

The prediction of the evolution of stresses for the isothermal cure of model epoxies is one of our missions. In order to complete this objective, the work of Vratsanos [59] and Adolf et al. [63-66] have been studied. The difference between these two works is the former considered the elastic theory during the epoxy curing, while the later group included viscoelasticity in their formalism. The theory of the incremental linear elastic approach is stated in Chapter 2.

The latter group of researchers derived the equation for predicting the cure stress as has been shown in Chapter 2. Equation (2.16) seems complex since it represents a full tensorial nature of stress. It contains both the deviatoric and bulk components. However, it can be simplified by applying some assumptions. The calculation of the evolution of stresses during the cure of crosslinking polymer is complicated by the change in viscoelastic properties with extent of reaction. For example, as the cure progresses the shear modulus and the longest relation time increase as well as the T$_g$. Therefore, all relaxation time increase is due to the increase in monomeric friction. The equation developed by Adolf et al. is addressed again here.

$$\sigma = 2\int_{-\infty}^{t} ds\left[G_d\left(\int_{s}^{t}\frac{du}{\tau(u)}\right) + < G_\infty(t,s) >\right]\left[\frac{d}{dt}\left(\gamma - \left\{\frac{1}{3}tr\gamma\right\}I\right)\right] + \int_{-\infty}^{t} dsK\left(\int_{s}^{t}\frac{du}{\tau(u)}\right)\left[\frac{d}{dt}(tr\gamma)I\right]$$

$$-\Psi(T - T_o)I - \Phi(p - p_{gel})I \qquad (4.28)$$

where, $G(t) = G_d(t) + G_\infty$ is the shear modulus, $K(t)$ is the bulk modulus, γ is the strain tensor, p and T are the extent of reaction and temperature, T_o is the temperature at the gel point; p_{gel}, and I is the identity tensor. ψ is a constant equal to the product of the glassy bulk modulus, K_g, and the glassy volumetric coefficient of thermal expansion, α_g. Φ is a constant equal to the product of the rubbery modulus, K_∞, and the total volumetric strain due to cure, $\Delta_{v_{cure}}$.

The long-time cure strain is linearly dependent on the extent of reaction through $\Delta_{v_{cure}} = (\Delta V / V_o)p = 3\gamma_{vol}p$. Where $\Delta_{v_{cure}}$ is volume metric strain due to cure shrinkage, p is extent of reaction, γ_{vol} is one third of the total volume shrinkage, $\Delta V = V_o - V_f$, V_o and V_f

are the volume of unreacted and fully-cured polymer, respectively. If the sample is fixed in length and is considered in one dimension (tensile strain; $\gamma_{11} = 0$) at the cure temperature (T_c) exceeds the $T_{g\infty}$ and the material is assumed to be incompressible (Poisson's ratio = ν = 0.5), the equilibrium contribution to the stress for the rapid cure limit is:

$$\sigma_{11} = 2G_o(1+\nu)\left(\gamma_{11} - \frac{\Delta_{v_{cure}}}{3}\right) = -3\gamma_{vol}G_{\infty}p \tag{4.29}$$

When the cure is not infinitely fast, the expression for the equilibrium stresses in viscoelastic materials is:

$$\sigma_{11} = -3\gamma_{vol}\int_{-\infty}^{t} ds\left[G_d(t-s) + < G_{\infty}(s) >\right]\frac{dp(s)}{dt} \tag{4.30}$$

The decaying portion of the shear modulus for a wide range of epoxy at all post-gel extents of reaction has been shown to obey the theoretical relationship [184]:

$$G_d(t) = \frac{G_g}{1+(t/\tau)^{2/3}} \tag{4.31}$$

where G_g is the glassy shear modulus, which is independent of extent of reaction, τ is the characteristic relation time, which has the WLF temperature dependence.

$$\log\tau = \frac{-C_1(T-T_g)}{C_2+T-T_g} \tag{4.32}$$

where C_1 and C_2 are the WLF constants. T_g can be can be either measured or one can use a theoretical model to predict.

Adolf et al. [63-66] cited Hale's work (previously mentioned in section 4.3.4), but they have changed the form of the equation to:

$$T_g = \frac{T_{go}}{(1-Ap)\left(1-B\frac{G_\infty}{G_\infty^{final}}\right)} \tag{4.33}$$

where G_{gel}^{final} is the rubbery equilibrium modulus of the full-cured resin, G_∞ is the equilibrium shear modulus at extent of reaction p, and A and B are experimental constants. By comparison Equation 4.26 and 4.33, A is kT_{go} and $B\left(G_\infty / G_\infty^{final}\right)$ is $K_2X / 1-\Psi X^2$. However, the relation between the two equations has not been stated clearly. In this study, DiBenedetto Equation has been used to predict the T_g as a function of extent of reaction as shown previously.

However, at T_c>T_{cure}, all viscoelastic relaxations are fast and the decaying modulus does not contribute to the tensile stress. The equilibrium tensile stress (from Equation 4.29 above) can then be calculated from:

$$\sigma_{11} \cong -3\gamma_{vol} \int_{-\infty}^{t} ds G_\infty(s)\frac{dp(s)}{dt} = -3\gamma_{vol} \int_{p_{gel}}^{p(t)} dp G_\infty(p) \tag{4.34}$$

The equilibrium shear modulus G_∞ becomes nonzero at the gel point, p_{gel}, and then increases with cure. From both the theory [185] and experiment [63] show that G_∞ increases with the extent of reaction as the power law:

$$G_\infty = G_\infty^{final}\left(\frac{b-b_{gel}}{1-b_{gel}}\right)^{8/3} \tag{4.35}$$

where *b* is the "bond probability". For typical condensation reactions where x-functional crosslinker, A_x, reacts with a difunctional extender, B_2 (A reacts only with B), $b = p^2$ when A and B are at stoichiometric ratio.

If the elastic theory is applied to the uniaxial isothermal curing, the stress due to the curing can be calculated by

$$\sigma_{11} = -E\gamma_{11} \tag{4.36}$$

where γ_{11} is the strain due to the cure shrinkage in 1-D. Therefore γ_{11} is 1/3 of the volume shrinkage; $\frac{1}{3}\frac{\Delta V}{V_o}$. Thus, cure stress can be calculated if the equilibrium modulus and the volume shrinkage are known. In this study, shear modulus and volume shrinkage as a function of cure time were measured. Equilibrium tensile modulus (*E*) relates to shear modulus (*G*) by:

$$E = 2(1+\nu)G \tag{4.37}$$

where ν is Poisson's ratio. Therefore Equation (4.36) can be rewritten as:

$$\sigma_{11} = -2(1+\nu)G \times \frac{\Delta V}{3V_o} \tag{4.38}$$

Equation (4.38) will be used to predict the cure stress for each model epoxy in this study. This equation is comparable to Equation (4.34) from Adolf's formalism when viscoelasticity is not included.

The shear moduli for the three model epoxies as a function of cure time (after gelation) are shown in Figs. 4.90 –4.92. The shear moduli increased with the increasing of extent of reaction, and gradually leveled off when it approached to the completion.

However, EMI-24 cured diglycidyl ether of bisphenol F seemed to approach full cure before it was subjected to DMA since the rate of reaction of this system is fast and hard to stop at the gel point. In addition, the partially cured sample could be cured during temperature ramp on DMA. The fully cured samples were subjected to temperature scans on RDA II to measure the glassy and rubbery shear moduli (Figs.4.93-4.95). Rubbery shear modulus of fully cured samples were 6.36 x 10^6, 1.12 x 10^7, and 3.86 x 10^6 Pa for AEP-cured diglycidyl ether of bisphenol A, EMI-24-cured diglycidyl ether of bisphenol F, and anhydride-cured cycloaliphatic epoxy, respectively.

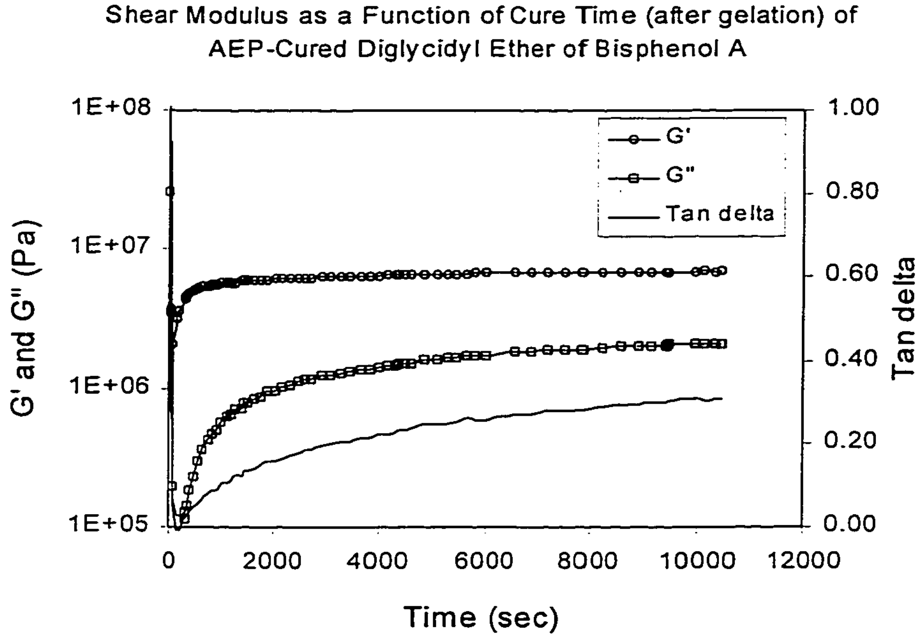

Fig.4.90: Shear modulus as a function of cure time at 140 °C of diglycidyl ether of bisphenol A-cured AEP after the gelation point (at zero time).

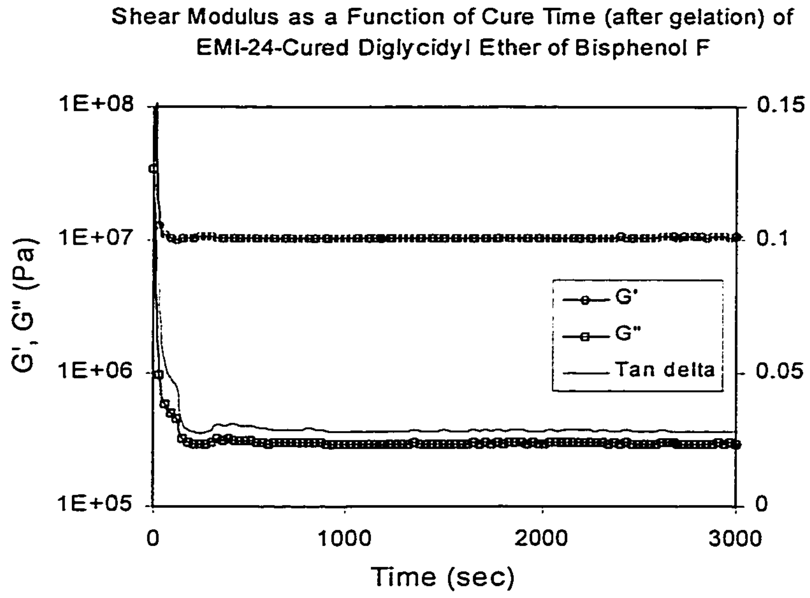

Fig.4.91: Shear modulus as a function of cure time at 150 °C of EMI-24-cured diglycidyl ether of bisphenol F after the gelation point (at zero time).

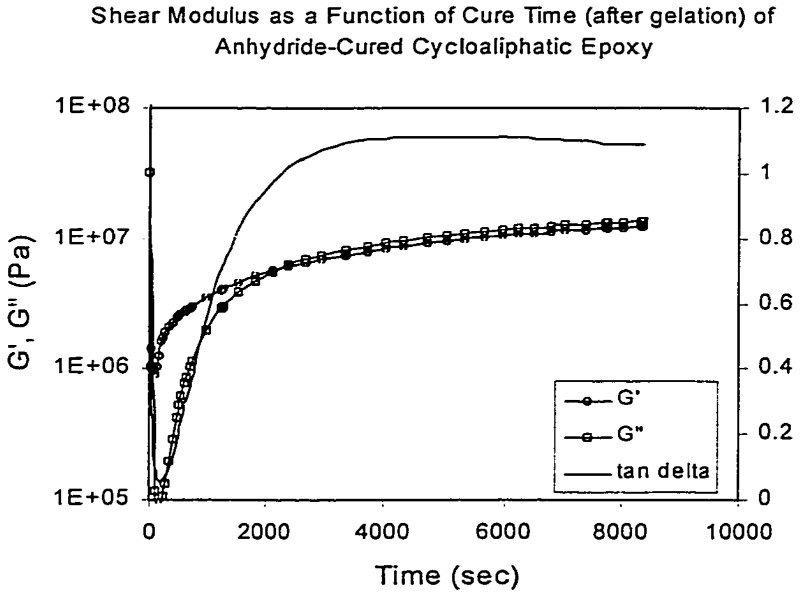

Fig.4.92: Shear modulus as a function of cure time at 150 °C of anhydride-cured cycloaliphatic epoxy after the gelation point (at zero time).

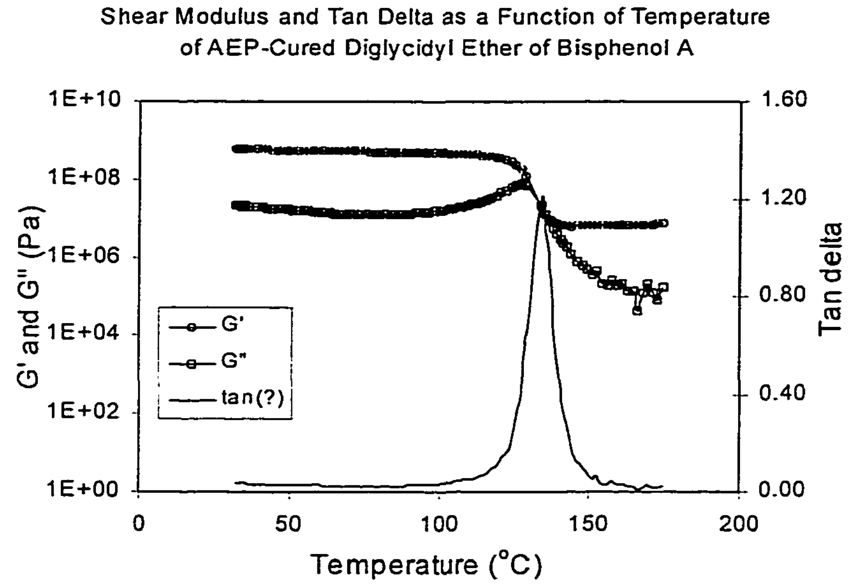

Fig. 4.93: Shear modulus and tan delta as a function of temperature of AEP-cured diglycidyl ether of bisphenol A. G' curve shows T_g of 132 °C.

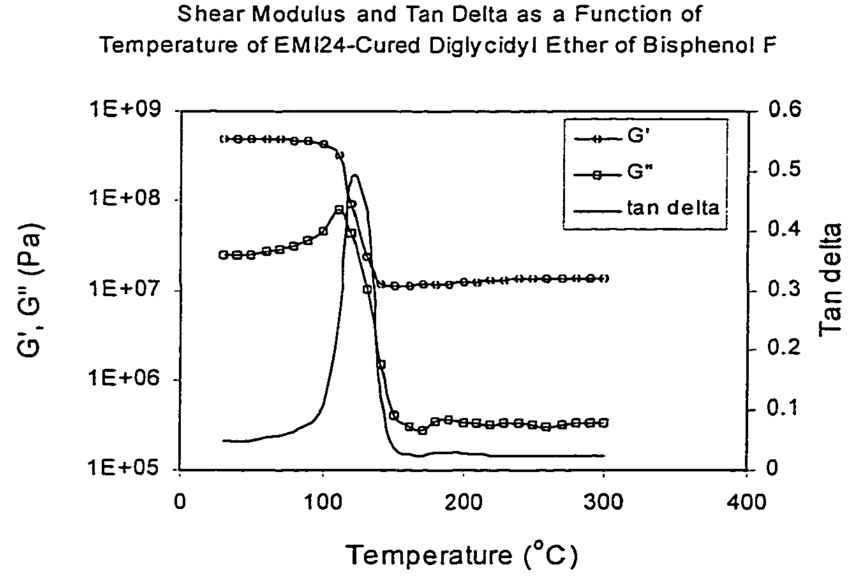

Fig. 4.94: Shear modulus and tan delta as a function of temperature of EMI-24-cured diglycidyl ether of bisphenol F. Tan delta curve shows T_g of 120 °C.

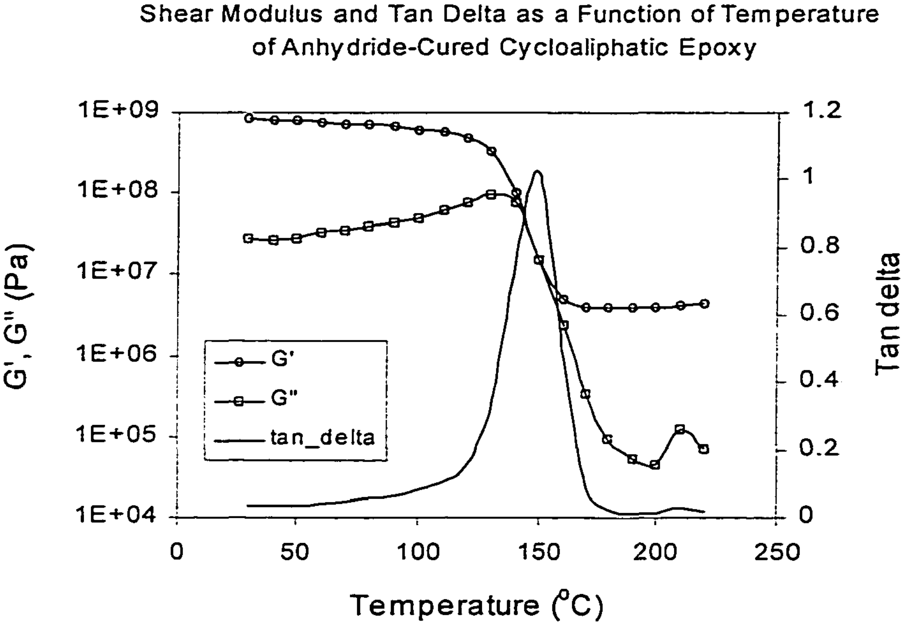

Fig.4.95: Shear modulus and tan delta as a function of temperature of anhydride-cured cycloaliphatic epoxy. Tan delta curve shows T_g of 150 °C.

Volume shrinkage is the other origin of generated cure stress. The post gel volume shrinkage due to the curing was measured by TMA and the results for two model epoxies are shown in Figs. 4.96 - 4.97. By using the Poisson's ratio as 0.49 for rubbery state of polymer, Equation (4.29) was employed to predict the cure stress of each model epoxy. Table 4.9 shows the comparison of calculated cure stresses to the experimental results. The EMI-24-cured diglycidyl ether of bisphenol F generated more cure stress than the anhydride-cured cycloaliphatic epoxy due to the greater equilibrium modulus and the more shrinkage. Calculated cure stresses seem to be larger than the experimental cure stresses, this is possibly due to the viscoelastic effect.

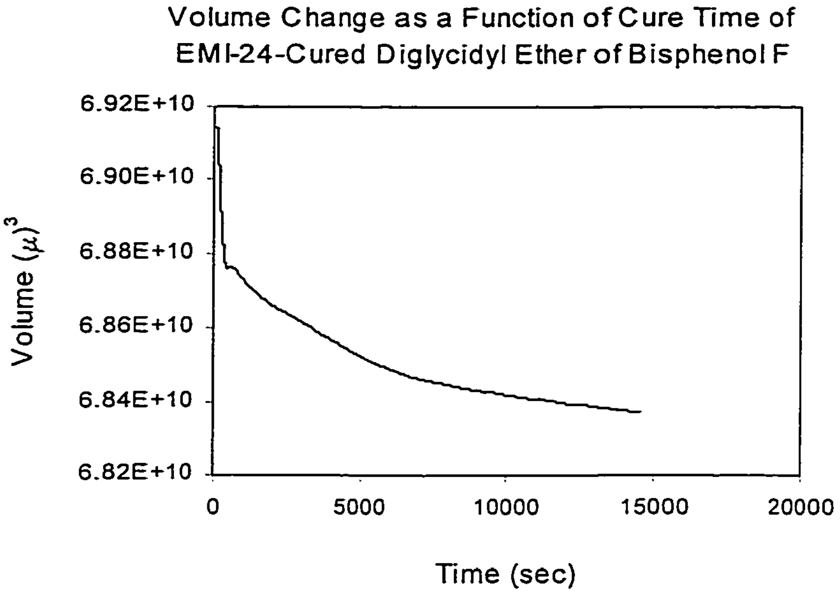

Fig. 4.96: The post gel volume change as a function of cure time at 130 °C of EMI-24-cured diglycidyl ether of bisphenol F shows 1.1 % shrinkage.

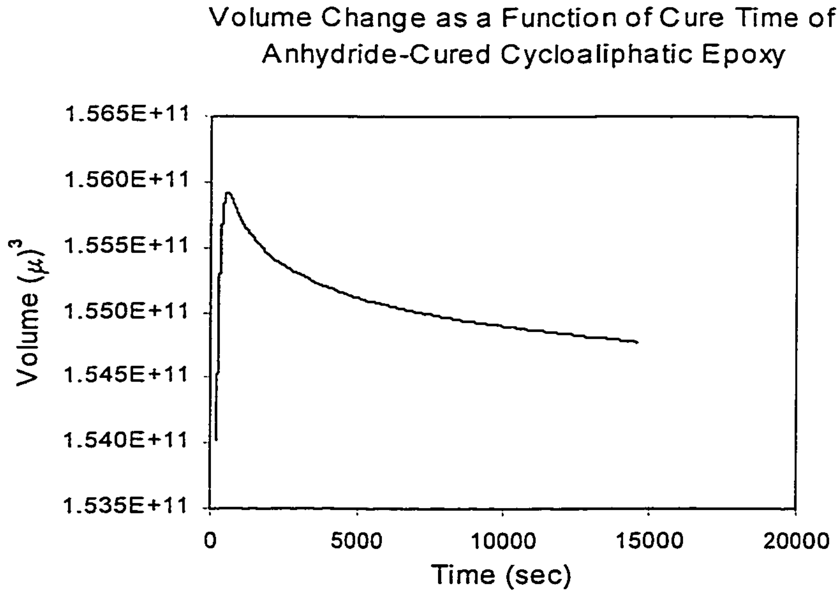

Fig. 4.97: The post gel volume change as a function of cure time at 150 °C of anhydride-cured cycloaliphatic epoxy shows 0.7 % shrinkage.

Table 4.9: The comparison between the experimental and the calculated cure stress.

Model epoxy	Experimental cure stress (kPa)	Calculated cure stress (kPa)
AEP-Bis A	130	N/A
EMI-Bis F	300	370
Anhydride-Cycloaliphatic	10-40	85

To explain the difference in volume shrinkage, the crosslink density should be considered. The crosslink structure (or crosslink density) of cured resin has an effect on the cure stress. In principle, the molecular weight of the chain between crosslinks could be determined using the rubber-elasticity theory [186]:

$$G_{eq} = g\left(\frac{r_e^2}{r_o^2}\right)\nu RT \tag{4.39}$$

where G_{eq} is the equilibrium shear modulus in the rubbery region; ν is the crosslink density; R is the gas constant; T is the absolute temperature; g is a numerical factor approximately equal to 1; r_e^2 is the mean square end-to-end distance of the strands which are crosslinked, and r_o^2 is the mean square end-to-end distance that the same strands would assume if they are not crosslinked. The crosslink density can be calculated by the ratio of density (ρ) to the number-average molecular weight between crosslink ($\overline{M}_C$); $\nu = \rho/\overline{M}_c$. By assuming $g = 1$ and $\frac{r_e^2}{r_o^2} = 1$:

$$\overline{M}_c = \frac{\rho RT}{G_{eq}} \tag{4.40}$$

The molecular weight between crosslinks of the three model epoxies are shown in Table 4.10.

Table 4.10: Molecular weight between crosslinks of model epoxies.

Model epoxy	$\overline{M}_c$	Monomer molecular weight
AEP-cured diglycidyl ether of bisphenol A	676.8	~350
EMI-cured diglycidyl ether of bisphenol F	414.6	~340
Anhydride-cured cycloaliphatic epoxy	1097.1	~275

From Table 4.10, crosslink density of EMI-24 cured diglycidyl ether of bisphenol F is the largest, AEP-cured diglycidyl ether of bisphenol A is in the middle, and anhydride-cured cycloaliphatic epoxy is the least. Shrinkage and internal stress increased with increase in the concentration of network chains and T_g of the cured systems [181]. From the crosslink density result, EMI-24 cured diglycidyl ether of bisphenol F should provide the more shrinkage than anhydride-cured cycloaliphatic epoxy system, which was verified by the post cure volume shrinkage results as shown previously. The cure stress experimental results revealed the same trend as expected from the crosslink density.

CHAPTER 5

Conclusions

This study has searched for an understanding of the fundamental phenomena involved in the processing of commercial underfill resins. The development of processing diagrams for underfill resins is one of the goals for this research. The study also included characterizing of cure behavior of commercial and model epoxy systems. Based on the results from this study, the following conclusions can be made.

5.1 Processing Characteristics of Underfill Resins

Major phenomena that influence the processing of underfill resins were investigated. Flow behavior is one of the most important issues that have to be considered. Therefore, key properties that control the flow such as viscosity, surface tension, contact angle of resin on substrate, and gelation were explored.

The underfill flow can be described by the Washburn model. The two parameters that influence the flow of resin in the gap are viscosity and surface tension of resins. These properties can be controlled by formulation or processing temperature. The higher processing temperature, the lower the viscosity and surface tension; however, the gelation time is shorter. Thus, the optimal filling temperature must balance viscosity and reaction kinetics.

To obtain a reliable adhesive bond, the parameters that impact the adhesive strength have to be addressed. Extent of reaction (which has a significant effect on adhesive strength), cure stress (which can cause delamination), and outgassing and voiding (which can reduce the adhesive strength) were investigated.

A number of researchers have found the extent of reaction to have a great impact on adhesive strength [9, 57]; therefore, this effect was not studied in detail.

There has been some work [9, 120] claimed that higher cure temperatures gave higher cure stresses. Nonetheless, measurements in this study showed similar cure stress at different temperatures if the sample was cured at temperatures higher or in the vicinity of its $T_{g\infty}$. Note that high cure temperatures did accelerate the rate of developed cure stress due to the increasing of rate of reaction, and that higher cure temperatures resulted in higher thermally induced residual stress.

Multistep curing was performed and successfully reduced the cure stress. However, the lower magnitude of the cure stress did not increase the dry adhesive strength. For commercial underfill resins, wetting between the adhesive and substrate may be a more essential factor than cure stress on the adhesive strength of DCB specimen.

Voiding in underfill resin is most likely caused by entrapped air, the dispensing procedure, and the non-uniform flow of an underfill during dispensing. The underfilling temperature was found to influence voiding. The higher processing temperature, the larger content of voids was observed. In this study, void formation was detected in X6-82-5 resin, which has a fast cure reaction and a high heat of reaction. The heat expanded the volume of entrapped air and phase separated out from the resin; however, the short gelation time retarded the diffusion of air from the resin, leaving voids.

5.2 Processing Diagrams for Underfill Resins

Processing diagrams for underfill resin were drawn summarizing relevant resin properties on the time-temperature axes. Such diagrams include the flow characteristics (e.g., viscosity, surface tension, and contact angle), gelation, extent of reaction, reaction onset temperature, $T_{g\infty}$ of cured resin, and solder melting point. However, other factors that should be considered in the underfill resin processing, such as voiding and cure stress, have yet to be mapped on the diagram. This could be the interesting and useful work for the future.

Our preliminary processing diagrams for underfill resins propose the two steps of processing; underfilling and curing. In the underfilling regime, cycle times may be reduced by increasing the filling temperature. However, the tendency for void formation and particle settling can increase with increasing temperature. In the cure regime, cycle times may be shortened also by increasing the cure temperature. However, increasing the temperature will increase the cooling stresses that may promote debonding. These diagrams provide a scientific approach for one to design the proper cure schedule for underfill resin in order to optimize the processing to obtain a satisfied product.

5.3 Cure Characteristics of Model Epoxies

The study on model epoxies has focused on cure kinetics and cure stresses. MDSC was employed to study the occurrence of vitrification at different cure temperatures, and vitrification was found in AEP-cured diglycidyl ether of bisphenol A system at cure temperatures from 60 to 100 °C ($T_{g\infty}$ =120). EMI-24-cured diglycidyl ether of bisphenol F showed vitrification at 80 °C ($T_{g\infty}$= 127 °C). Anhydride-cured cycloaliphatic epoxy displayed vitrification at 100 and 120 °C ($T_{g\infty}$= 124 °C). Thus both the heat of reaction and the steric hindrance influence vitrification manner. An autocatalytic kinetic equation was applied to fit the experimental data to provide the kinetic parameters. Rate constant as a function of temperature of the three systems could be explained by Arrhenius equation. However, the order of reaction parameters changed with temperature suggesting that the nature of the curing reaction also changed.

Generally, T_g increases as the cure temperature increases. The higher T_g represents a more hindered network. AEP-cured diglycidyl ether of bisphenol A and anhydride-cured cycloaliphatic epoxy displayed the higher $T_{g\infty}$ with the higher cure temperature. Interestingly for EMI-cured diglycidyl ether of bisphenol F system, the higher cure temperature exhibited the lower $T_{g\infty}$. This could possibly be explained by the occurrence of etherification at high cure temperatures. Ether linkages separated the chains in the network apart, and provided the more flexibility for the chains.

The evolution of cure stress was monitored during cure. The magnitude of cure stress did not depend on the cure temperature if the cure temperature is higher than the $T_{g\infty}$ of these fully cured samples. However, vitrification lowered the cure stress in EMI-24-cured diglycidyl ether of bisphenol F. Anhydride-cured cycloaliphatic epoxy provided an insignificant cure stress due to the low volume shrinkage and low rubbery modulus. In addition anhydride-cured cycloaliphatic epoxy has a lower crosslink density. EMI-24-cured diglycidyl ether of bisphenol F revealed the largest cure stress. This is probably due to the contraction of rubbery resin when it exposed to the high heat of reaction after the sample had gelled.

5.4 Stress Modeling

An extent of reaction based elastic model was selected to predict the cure stress. Equilibrium shear modulus and volume shrinkage were measured as a function of extent of reaction and used as input for cure stress calculation. The calculated values were higher than the experimental values, but they are comparable in magnitude.

5.5 Suggestions for Future Work

5.5.1 Processing Diagram for Underfill Resin

Although the preliminary processing diagram for underfill resin can be used to be a guide for the processing, there is still room to improve such a diagram. More adhesive strength testing should be investigated to reveal the effect of extent of reaction and cure schedule. The effect of cure stress on debonding could be done on the specimen that can reveal the effect more clearly rather than DCB specimen, which focuses on the propagation of existing flaws. If possible the specimen should be similar in structure to the real product (e.g., between chip and substrate with solder bump), which should provide more obvious effect of cure stress on adhesive strength since stresses take place in both horizontal and vertical directions.

To construct a processing diagram, several different techniques have been applied. Each technique may need different sample size to provide a more sensitivity to get the most reasonable result. However, in epoxy polymerization, which is an exothermic reaction, the heat of reaction depends on the mass of sample. This difference creates an ambiguity when relating results from technique to technique. It is interesting to study the effect of sample size on each technique. Such a study may provide a scaling factor that can be used to normalize the results from different techniques.

Filler settling is also an important issue for underfill resins. 60-70 % of filler is added to reduce the CTE of the resin. Filler settling can take place when the viscosity of the resin is set too low or during the curing process due to a greater density of fillers. The relationship between the cure temperature and the filler settling should be studied by applying a microscopy technique such as SEM.

5.5.2 Kinetic Model

DSC technique is a simple and easy to use technique, but it may not be the best for following the cure kinetics of epoxy polymerization. The thermal system of DSC may shield or distort the result. Therefore, other techniques (e.g., FTIR, HPLC, swelling method) should be applied to compare the result.

The one rate constant autocatalytic model that has been used in this study may not be the most suitable model. It has seen that in some cure conditions, the model does not fit the data well. Therefore, the model should be modified to fit all sets of data. Moreover, one set of order of reaction and rate constant may not be able to fit the data over the whole range of reaction.

5.5.3 Stress Model

The evolution of cure stress has not been mapped between the experimental result and the calculation by the model for the whole range of reaction temperatures due to the limitation of the instrument at the moment. Several factors have to be considered in order to be able to map the two sets of cure stress values, including the sample size and thermal system of the instruments.

The elastic model that was used to predict the cure stress may need some modifications. The effect due to heat of reaction should be addressed when the resin gels before the temperature has dropped to that of the oven.

Appendix I

Cure Stress and Adhesive Strength of Die Attach Adhesive (H35-175MP)

The processing of die attach adhesive was studied intensively by Hsiung [9] and focused on the fundamental phenomena including gelation time, outgassing phenomena, the relation of shear strength and extent of reaction, and cure stress. In his study, he focused on the isothermal curing. However, he applied a multistep cure condition to the die attach adhesive to see the effect of cure cycle on the outgassing. It was found that by selecting the proper multistep cure schedule, the amount of weight loss could be reduced. Therefore, he suggested the application of a multistep curing in cure stress studies.

In this study the evolution of cure stress was measured by utilizing both isothermal and multistep cure schedules, and the effect of cure stress on the adhesive strength was also investigated.

AI.1 Polymeric Die Attach Adhesives

Polymeric die attach adhesive is conductive adhesive and consists of two main components, which are polymer (epoxy or polyimide are the most widely used) and conductive filler (e.g., silver, alumina, and silica). In addition to polymer and filler, hardener, catalyst, solvent, and other additives are added. Polymeric die attach adhesive can be classified into three types due to the difference in the rate of curing:

(a) conventional (an hour cure at 150-180 °C)

(b) fast cure (2-15 minutes cure at 100-200 °C)

(c) snap cure (30-90 seconds cure at 150-225 °C)

In this study conventional silver-filled polymeric die attach adhesive was selected to study.

AI.2 Material

H35-175MP silver-filled epoxy from Epoxy Technology was selected for study. The T_g of this resin is 130 °C (DMA), and the recommended cure schedule is 180 °C for 1 hour.

AI.3 Experimental Approach

AI.3.1 Cure Stress and Cooling down Stress

Cure stress measurements were performed on the Rheovibron DDV II (see the detail in Section 3.2.1.2). Three different isothermal cure temperatures (160, 170 and 180 °C) were used followed by cooling down process to 150 °C. In an attempt to reduce the cure stress, multistep schedules were applied to the sample (see Table AI.1).

Table AI.1: Multistep cure schedule for H35-175MP.

Multistep	Temperature (°C)/time (min)
2 step	155/30→180, 155/45→180, 155/60→180
3 step	120/30→155/30→180
4 step	120/30→155/30→165/30→180

AI.3.2 Adhesion Test

Adhesion of H35-175MP to copper (0.8 mm thick Olin copper plates from Somer Thin Strip/Brass Group) was studied using the width-tapered double cantilever beam (WTDCB). See Fig. AI.1. One wedge was polished to 1μm finish, while the mating was ground to 400 grit finish. Experiments were performed on a mini-servohydraulic materials testing machine (Rheovibron DDV III, which is similar to DDV II, but includes a hydraulic system and has a larger load capacity (5000 gf)). The interfacial fracture energy (G_{IC}) was calculated by the equation, which was proposed by Lui and Gent [187]:

$$G_{IC}=(12P^2/EK^2D^3)[1+(9\alpha/4)]/(1+\alpha)[(1+3\alpha/2)]^2 \qquad \text{(AI.1)}$$

Where, P is an applied force, E is the Young's modulus of a copper plates, D is the thickness of a copper plate, $\alpha = B_o/Kc$, $K = 2\tan\theta/2$, B_o is an end width, and θ is the wedge angle (35°).

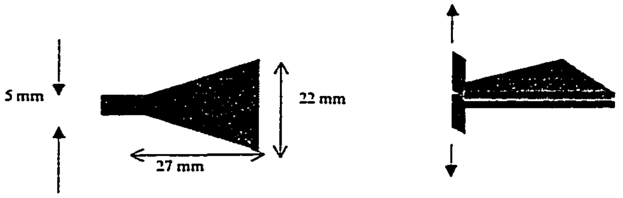

Adhesive thickness
= 250 μm

Fig. AI.1: The copper wedge for WTDCB testing

AI.4 Results and Discussion

AI.4.1 Isothermal and Cooling down Stresses

It was found that at higher cure temperature the stress developed faster than at lower temperature but once they reached a plateau, the magnitudes of cure stresses were similar at about 450 kPa as shown in Fig. AI.2. Upon cooling, cure stress significantly increases due to the thermal contraction of the sample. The stress then decreases presumably due to a viscoelastic effect. Note that the greater the temperature excursion, the higher the residual stress.

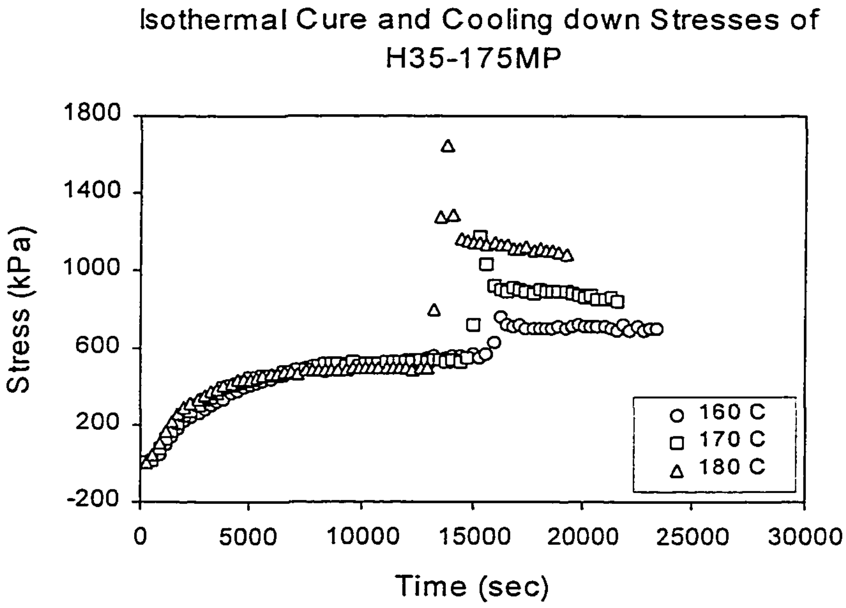

Fig. AI.2: Isothermal cure stresses are similar (~450 kPa) at different cure temperatures, but the cooling down stresses (cooled to 150 °C) depend on the temperature excursion.

Multistep curing can reduce the cure stress as shown in Fig. AI.3. At the plateau, the cure stress is about 300 kPa for 2-step curing, about 275 kPa for 3-step curing, and about 170 kPa for 4-step curing. These are lower than the ~450 kPa for isothermal curing.

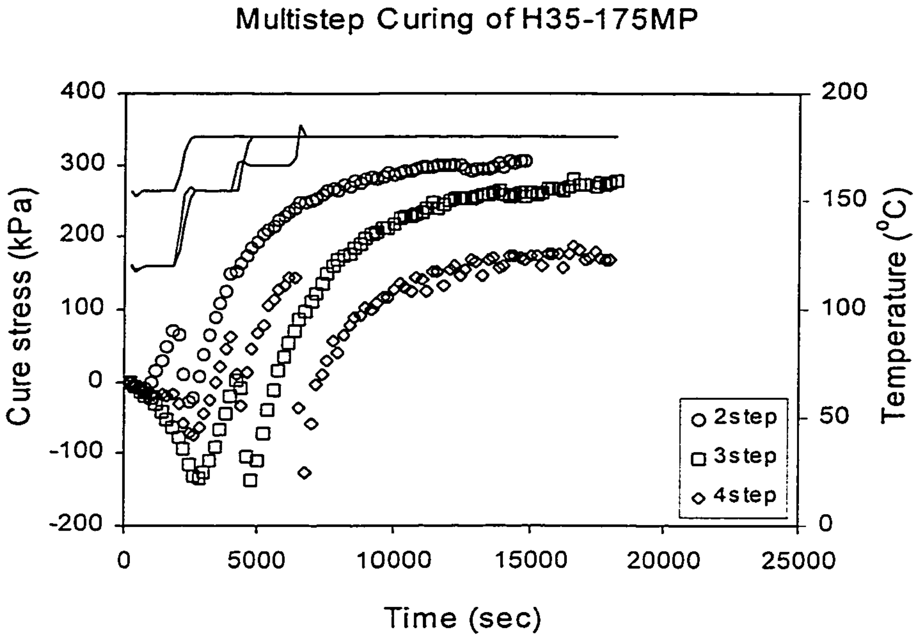

Fig. AI.3: Multistep can reduce the cure stress of H35-175MP.

AI.4.2 Adhesion Test

Table AI.2 shows the adhesive strength and the mode of failure of the specimens. Both adhesive and cohesive failures were observed for the H35-175M/copper interface. For isothermal curing, the higher cure temperature gave the higher fracture energy. This may result from a higher degree of wetting between substrate and resin at higher temperatures, since the adhesive is completely cured in both cases. Interestingly, multistep curing provided lower value of fracture energy, which may also be explained by the difficulty of wetting. Obviously, the cure schedules effect the mode of failure. It is also important to note that the multistep cure schedule gave a higher probability on adhesive failure.

Table AI.2: Interfacial adhesive strength and mode of failure of H35-175MP.

Cure schedule	G_{IC} (J/m^2), cohesive	G_{IC} (J/m^2), adhesive	% adhesive failure
155 °C	573 ± 42	-	0
180 °C	595 ± 87	481 ± 31	30
2 step	452 ± 31	410	15
3 step	554 ± 52	474 ± 22	50
4 step	542	443 ± 67	90

AI.5 Conclusions

i) Cure stress of isothermal curing was independent to the cure temperature (in the studied range), however it affected the thermally induced stress.

ii) Multistep curing can reduce the cure stress.

iii) The reduction in cure stress did not increase the dry adhesive strength. The wettability between the adhesive and substrate seemed to be more significant than the cure stress.

Appendix II

Relationship Between Adhesive Strength and Residual Stress

The adhesive strength data of X6-82-5 in Table 4.3 shows that the interfacial fracture energy (G_{IC}) of the sample to polyimide was ~ 90 J/m^2. One may wonder whether this value is large enough for the sample to be an effective adhesive, and also whether the residual stress is high enough to cause spontaneous delamination.

A number of researchers have studied the G_{IC} of underfill resins. Gurumurthy et al. [188] studied the adhesion between commercial underfill resins and polyimide, and found that G_{IC} ranged from 30 J/m^2 (Hysol FP4511) to 45 J/m^2 (Ablestik-4). Snodgrass et al. [189] investigated the bond between underfill epoxy (Hysol FP4527) and polyimide, and found that without adhesion promoter G_{IC} was ~20 J/m^2 and adhesion promoter increased G_{IC} to ~50 J/m^2. Zimmerman [123] reported a range of G_{IC} values from 20 –80 J/m^2 for various underfill resins bonded to PI. Therefore, the values reported here appear reasonable.

Residual stress depends on the geometry of specimens. In microelectronic assembly (see Fig. AII.1), shear stress is developed with the temperature change due to the CTE mismatch between silicon and substrate. The maximum shear stress (τ_{max}) is a function of the difference in coefficient thermal expansion (α_1-α_2), temperature change, shear modulus of an adhesive, Young's moduli of silicon and substrate, and the thickness of silicon, substrate, and adhesive as shown in Equations AII.1 and AII.2.

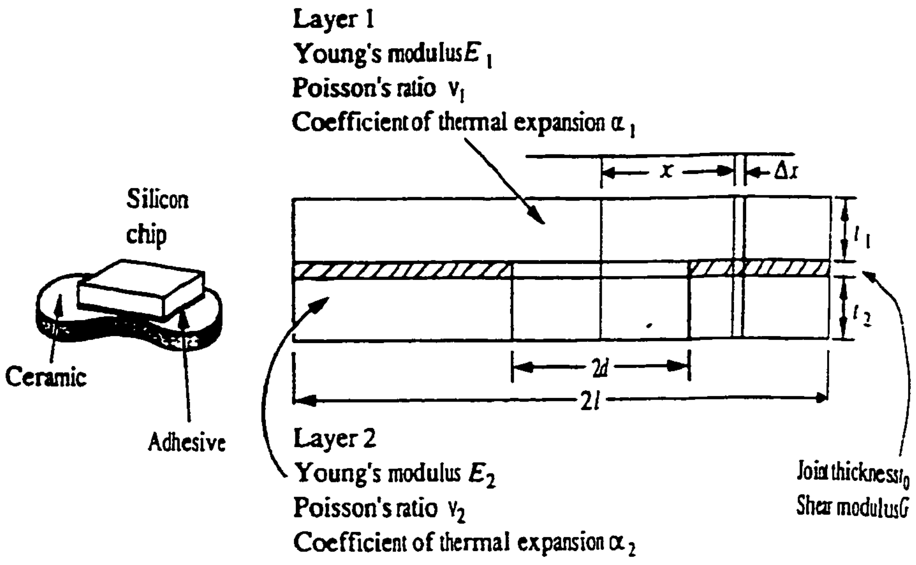

Fig AII.1: Microelectronic assembly diagram.

$$\tau_{\max} = \frac{(\alpha_1 - \alpha_2)\Delta T G}{\beta t_o} \qquad \text{(AII.1)}$$

$$\beta^2 = \frac{G}{t_o}\left[\frac{1}{E_1 t_1} + \frac{1}{E_2 t_2}\right] \qquad \text{(AII.2)}$$

For the flip-chip assembly that consists of a silicon die (0.686 mm thick and 20.32 mm wide) bonded to an organic substrate (1.016 mm thick and 23.0125 wide). The bond thickness is 76.2 μm. The material properties are shown in Table AII.1.

Table AII.1: The material properties of underfill resin/organic substrate system.

Material	Young's modulus (GPa)	Poisson's ratio	CTE (ppm/°C)
Silicon	129.9	0.279	3.3
Substrate	23.5	0.330	15.0
X6-82-5	9.2	0.350	22.9

If this assembly is cooled for 100 degrees, the calculation gives the shear stress of 33.8 MPa.

The residual stress of DCB specimen has a different character from the microelectronic assembly that shown above. The two bars are made from the same material (aluminum, see also Fig. 3.10 for the geometry of DCB), therefore, there is no CTE mismatch. Consequently, no shear stress is developed.

Nairn [188] studied the effect of residual stress on the interfacial fracture energy of adhesive DCB specimen, and found that ignoring residual stress cause a deviation in calculated toughness from the experimental value. He proposed an equation that can be used to indicate whether specimen will fail due to residual stress alone or not (Equation AII.2).

$$P = \frac{\sqrt{G_{IC}} - C_r \Delta T}{C_m (a + 1.15\Delta_w)} \tag{AII.2}$$

where P is an applied force, a is a true crack length, $a+\Delta_w$ is an effective crack length, C_r and C_m are the mechanical and residual coefficients for determining G_{IC}.

$$C_r = -\Delta\alpha(1+\lambda)\sqrt{\frac{3E_1h_1}{(1-R\lambda)\left[3(1-\lambda)^2+(1+R\lambda)\left(\lambda^2+\frac{1}{R\lambda}\right)\right]}} \qquad \text{(AII.3)}$$

$$C_m = \frac{2\lambda}{Bh_1}\sqrt{\frac{3(1+R\lambda)}{E_1h_1\left[3(1-\lambda)^2+(1+R\lambda)\left(\lambda^2+\frac{1}{R\lambda}\right)\right]}} \qquad \text{(AII.4)}$$

$$\Delta_w = h_1\left(\frac{1+(R/\lambda)}{6}\right)^{1/4} \qquad \text{(AII.4)}$$

where $R=\frac{E_1}{E_2}$, and $\lambda=\frac{h_1}{h_2}$, where E_1 and E_2 are the Young's moduli of substrate and adhesive and h_1 and h_2 are the thickness of substrate and adhesive, respectively.

In our study, aluminum (0.5 thickness) with the bond thickness of 250 μm was studied. The material properties are shown in Table AII.2.

Table AII.2: The material properties of X6-82-5/PI on aluminum interface system.

Material	Young's modulus (GPa)	Thickness (m)	CET (ppm/°C)
Aluminum	69	1.27x10-2	23
X6-82-5 resin	3.4 (<Tg), 0.087 (>Tg)	2.50x10-4	22.9 (<Tg), 85.3 (>Tg)

The failure of DCB specimen due to residual stress alone occur when P = 0 and $G_{IC} < C_r^2 \Delta T^2$.

By using the parameter values at lower than T_g, $C_r^2 \Delta T^2$ is 6.08×10^{-8} J/m^2, while it is 5.05×10^{-6} J/m^2 by using the higher than T_g parameter values. Comparing these two numbers to the experimental G_{IC}, spontaneous crack propagation will not occur.

References

1. D. P. Seraphim, R. Lasky, and C.-Y. Li, "Principles of Electronic Packaging", New York, McGraw-Hill, Inc., 1989.
2. S. Rzepka, M. A. Korhonen, E. Meusel, and C. –Y. Li, *J. Electronic Packaging, Trans. ASME*, **120**, 342 (1998).
3. J. Jiao, C.K. Gurumurthy, E. J. Kramer, Y. Sha, C.-Y. Hui, and P. Borgesen, *ASME International Mechanical Engineering Congress and Exhibition, AMD*, **222**/EEE, **20**, 97 (1997).
4. M. Pecht, "Handbook of Electronic Package Design", Marcel Dekker, Inc., New York, 1991.
5. L. T. Manzione, "Plastic Packaging of Microelctronic Devices", Van Nostrand Reinhold, New York, 1990.
6. W. D. Brown, "Advanced Electronic Packaging With Emphasis on Multichip Modules", IEEE Press, New York, 1998.
7. G. Wisanrakkit, J. K. Gillham, and J. B. Enns, J. Appl. Polym. Sci., 41, 1895 (1990).
8. J. W. Sinclair, J. Adhesion, 38, 219 (1992).
9. J.-C. Hsiang, Ph.D. Thesis, Lehigh University, U.S.A., 1998.
10. J. H. Hsiung, and R. A. Pearson, *Proc. Of 47th ECTC Conference*, 536 (1997).
11. G. O. Malley, J. Giesler, and S. Machuga, *Proc. 44th Electron. Comp. Technol. Conf.*, 387 (1994).
12. R. Marrs, *Electron. Proc.*, **36**, 24 (1996).

13. J. Clementi, J. McCreary, T. M. Niu, j. Polomaki, and J. Varcoe, *Proc. 43rd Electron. Comp. Technol. Conf.*, 175 (1993).

14. A. J. Babiarz, *Solid State Tech.* **April**, 77 (1997).

15. C. P. Wong, M. B. Vincent, and s. Shi, *IEEE Tran. on Components, Packaging, and Manufacturing Technology-Part A*, **21** (2), 360 (1998).

16. D. Zoba, and M. E. Edwards, *ISHM'95 Proc.*, **2649**, 354 (1995).

17. C. A. Steidel, R. C. Sundahland, and N. Grayeli, Presented at the Spring 95 MRS Symposium Electronic Packaging Material Science (1995).

18. G. Lehmann, A. Maria, Pin-Chou Lee, and E. J. Cotts, *Proc. Of The Technical Program*, **1**, 340 (1996).

19. E. W. Washburn, *Physical Review*, **17**, 273 (1921).

20. T. E. Driscoll, P. C. Li, G. L. Lehmann, and E. J. Cotts, *Mat. Res. Soc. Symp. Proc.*, **445**, 69 (1997).

21. D Suryanarayana, R. Hsiao, T. P. Gall, J. M. McCreary, *IEEE*, **14**(1), 218 (1991).

22. D Suryanarayana, T. Y. wu, and J. A. Varcoe, *Proc. 43rd Electron.Comp. Technol. Conf.*, 193 (1993).

23. K. Sumita, K. Kumagae, K. Dobashi, T. Shiogara, M. Kuroda, *Mater. Res. Soc. Symp. Proc.*, **445**, 69(1997).

24. D. Hesekamp, H. C. Broecker, and M. H. Pahl, *Chem. Eng. Technol.*, **21**, 149 (1998).

25. J. –P. Eloundou, J. –F. Gerard, D. Harran, and J. P. Pascault, *Macromolecules*, **29**, 6917 (1996).

26. B. Ellis, "Chemistry Technology of Epoxy Resins", Chapman & Hall, 1993.

27. H. H. Winter, MRC Bulletin, **August**, 44 (1991).

28. H. H. Steinour, Ind. *Eng. Chem.*, **36**, 618 (1994).

29. J. Fukushima, K. Yasuda, H. Teratani, and S. Nishizaki, *J. Appl. Polym. Sci.*, **22**, 1700 (1978).

30. L. J. Matienzo, and F. D. Egitto, *Solid State Technology*, **July**, 99 (1995).

31. G. Fourche, *Polym. Eng. & Sci.*, **35**(12), 957 (1995).

32. W. F. Fox, and W. A. Zisman, *J. Colloid Sci.*, **5**, 514 (1950).

33. F. M. Fowkes, *J. Adhesion Sci., Technol.* **1**, 7 (1987).

34. D. Maugis, *J. Mater. Sci.*, **20**, 3041 (1985).

35. F. M. Fokes, D. C. McCarthy, and M. A. Mostafa, *J. Colloid Interface Sci.*, **78**, 200 (1980).

36. R. E. Johnson, Jr., R. H. Dettre, *Surfactant Sci., Ser.*, **49**, (1993).

37. T. B. Lloyd, *Colloids & Surfaces*, **93**, 25 (1994).

38. J. R. Huntsberger, *Advan. Chem. Ser*, **43**, 180 (1964).

39. R. E. Johnson, Jr., R. H. Dettre., *Advan. Chem. Ser*, **43**, 112 (1963).

40. C. P. Wong, and R. McBride, *IEEE Tran. on Components, Packaging, and Manufacturing Technology-Part A*, **17**, 542 (1994).

41. I. Mathieson, and R. H. Bradley, *J. Adhesion &Adhesives*, **16**, 29 (1996).

42. P. Lennon, e. Espuche, H. Sautereau, and D. Sage, *Adhesion & Adhesives*, **19**, 273 (1999).

43. E. D. Wachsman, P. S. Martin, and C. W. Frank, *ACS Symp. Ser.*, 407, *Amer. Chem. Soc.*, 26 (1989).

44. H. K. Yun, K. Cho, J. K. Kim, C. E. Park, S. M. Sim, S. Y. Oh, and J. M. Park, *Polymer*, **38**(4), 827 (1997).

45. A. J. Kinloch, "Adhesion and Adhesives: Science and Technology", Chapman & Hall, London, 1987.

46. B. Zhang, and M. K. Chaudhury, *Langmuir*, **14**, 4865 (1998).

47. J. A. Greenwood, K. L. Johnson, *Philos. Mag.* **43A**(3), 697 (1981)

48. P. G. de Gennes, C. R. *Acad. Sci. Paris*, **307**(II), 1949 (1988).

49. C. –Y. Hui, D. –B. Xu, and E. J. Kramer, J. Appl. Phys, 72(8),3294 (1992).

50. D. –B. Xu, C.-Y. Hui, and E. J. Kramer, *J. Appl. Phys*, **72**(8),3305 (1992).

51. A. N. Gent, and J. Schultz, *J. Adhes*, **3**, 281 (1972).

52. E. H. Andrew, and A. J. Kinloch, *Proc. R. Soc. London*, **A322**, 385 (1973).

53. A. N. Gent, S.-M. Lai, *J. Polym. Sci. (Phys.)*, **32**, 1543 (1994).

54. W. J. Canwell, and J. Morton, *J. Strain Anal. Eng. Design Rev.*, **27**, 29 (1992).

55. K. J. Bowles, and S. Frimpong, *J. Comp. Mater.*, **26**, 1487 (1992).

56. M. R. Wisnom, T. Reynolds, and N. Gwilliam, *Copm. Sci. Technol.*, **56**, 93 (1996).

57. R. K. Shukla, N. P. Mencinger, *Solid State Tech.*, **July**, 67 (1985).

58. D. R. Edwards et al., *Proc Of 37th Conference*, 48 (1987).

59. M. S. Vratsanos, Ph.D Thesis, UMSS, U.S.A., 1987.

60. A. R. Plepys, and R. J. Farris, *Polymer*, **31**, 1932 (1990).

61. A. Plepys, M. S. Vratsanos, and R. J. Farris, *Composite Structure*, **27**, 51 (1994).

62. R. S. Chambers, R. R. Lagasse, T. R. Guess, D. J. Plazek, and C. Bero, *EEP, Proc. of the Joints ASME/ JSME*, **1**, 537 (1992).

63. D. B. Adolf, and J. E. Martin, *Macromolecules*, **23**, 3700 (1990).

64. D. B. Adolf, and R. Chambers, *Polymer*, **38**, 5481 (1997).

65. D. B. Adolf, J. E. Martin, R. S. Chambers, S. N. Burchett, and T. R. Guess, *J. Mater. Res.*, **13**(3), 530 (1998).

66. D. B. Adolf, and J. E. Martin, *J. Comp. Mater.*, **30**(1), 13 (1996).

67. M. Cassettari, G. Salvetti, E. Tombari, S. Veronesi, G. P. Johari, *J. Polym. Sci., Polym. Phys.*, **31**, 199 (1993).

68. H. J. Flammersheim and J. Opfermann, *Thermochemica Acta*, **337**, 141 (1999).

69. L. Nunez, J. Taboada, F. Fraga, and M. R. Nunez, *J. Appl. Polym. Sci.*, **66**, 1377 (1997).

70. I. Alig, W. Jenninger, J. E. K. Schawe, *Thermochimica*, **330**, 167 (1999).

71. S. Montserrat, *J. Appl. Polym. Sci.*, **44**, 545 (1992).

72. S. Montserrat, I. Cima, *Thermochimica Acta*, **330**, 189 (1999).

73. W. H. Park, and J. K. Lee, *J. Appl. Polym. Sci.*, **67**, 1101 (1998).

74. Y. Tanaka and H. Kakiuchi, *J. Appl. Polym. Sci.*, **7**, 1063 (1963).

75. P. Guerrero, k. De la Caba, A. Valea, M. A. Corcuera, and I. Mondragon, *Polymer*, **37**, 2195 (1996).

76. N. Bouillon, J. P. Pascault, and L. Tighzert, *J. Appl. Polym. Sci.*, **38**, 2103 (1989).

77. H. J. Flammersheim, *Thermochimica Acta* **310**, 153 (1998).

78. Q. Wang, T. He, P. Xia, T. Chen, B. Huang, *J. Appl. Polym. Sci.*, **66**, 789 (1997).

79. S.-N. Lee, M.-T. Chiu and H. –S. Lin, *Polym. Eng. & Sci.*, **31**(15), 1037 (1992).

80. K.-C. Cheng, K. C. Lia, W.-Y. Chiu, *J. Appl. Polym. Sci*, **71**, 721 (1999).

81. C. P. Malhotra, and R. L. Mahajan, *EEP*, **vol. 26-1**, *Advances in Electronic Packaging, ASME*, **1**, 589 (1999).

82. K.-C. Cheng, W.-Y. Chiu, *Macromolecules*, **26**, 4658 (1993).

83. K.-C. Cheng, W.-Y. Chiu, *Macromolecules*, **26**, 4665 (1993).

84. K.-C. Cheng, W.-Y. Chiu, *Macromolecules*, **27**, 3406 (1994).

85. C. S. Chern and G. W. Poehlein, *Poly. Eng. Sci.*, **27**, 788 (1987).

86. H. Lee, and K. Neville, "Handbook of Epoxy Resins", McGraw-Hill Inc., New York, 1967.

87. M. DiBeradino, Ph. D. Thesis, Lehigh University, U.S.A. 1999.

88. J. Vogt, *J. Adhesion*, **22**, 139 (1987).

89. EMI-24 Curing Agent for Epoxy Resin Systems, Houdry Process & Chemical Co., A Division of Air Products and Chemicals Inc., 1965.

90. Phillips, "Curable Compositions Comprising a Diepoxide, a Polycarboxylic Anhydride, and a Polyhydric Compound, U. S., 2, 890, 196.

91. E. J. Kramer, Discussion.

92. Manual of RDA II by Rheometrics Inc.

93. T. Hatakeyama and F. X. Quinn, "Thermal Analysis" Fundamentala and applications to Polymer Science, 2nd ed., John Wiley & Sons. Inc., New York, U.S.A. (1999).

94. K. P. Menard, "Dynamic Mechanical Analysis", CRC Press LLC, New York, 1999.

95. C. Y. Tung and P. J. Dynes, *J. Appl. Polym Sci.*, **27**, 56 (1982).

96. H. H. Winter, *Polym Eng. Sci.*, **27**, 1698 (1987).

97. C.-Y. M. Tung, and P. J. Dynes, *J. Appl. Polym. Sci.*, **27**, 569 (1982).

98. Rheovibron. Manual

99. A. F. Yee, and M. T. Takemori, *J. Appl. Polym. Sci.*, **21**, 2597 (1977).

100. S. M. Webler, J. A. Manson, and R. W. Lang, Am. *Chem. Soc.*, **203**, 109 (1983).

101. DSC (TA2920) Manual by TA Instruments.

102. E. A. Turi, "Thermal Characterization of Polymeric Materials", 2nd ed., vol.1, Acadamic Press, New York, 1997.

103. DSC (TA2920) Isothermal Software Manual by TA Instruments.

104. TGA (TA2950) Manual by TA Instruments.

105. F. Daniels, J. H. Mathews, J. W. Williums, P. Bender, and R. A. Alberty, "Experimetal Physical Chemistry", 6th ed., McGraw-Hill Co., Inc., New York, 1962.

106. W. D. Harkins, and H. F. Jordan, *J. Am. Chem. Soc.*, **52**, 1751 (1930).

107. S. Mostovoy and E. J. Ripling, *J. Appl. Polym. Sci.*, **10**, 1351 (1966).

108. ASTM D3433-75, American Society for Testing and Materials, Philadelphia, PA, 1985.

109. S. Mostovoy, P. B. Crosley, and E. Ripling, *J. Materials*, **2**, 661 (1967).

110. W. A. Zisman, "Advance in Chemistry Series 43" (R. F. Gould, ed.,), *Am. Chem. Soc.*, Washington D. C., 1964.

111. S. Wu, *J. Macromol Sci.*, **C10**, 1 (1974).

112. S. Wu in J. Brandrup and E. H. Immergut, "Polymer Handbook", 3rd ed.VI 414, Wiley, New York, 1987.

113. D. Klosterman, L. Li, and J. Morris, *IEEE Transactions on Components, Packaging, and Manufacturing Technology*, Part A, **21 (1)**, March, 23 (1998).

114. S. D. Lubetkin, "Controlled Particle, Droplet and Bubble Formation", edited by D. J. Wedlock, Butterworth-Heinemann Ltd., Oxford, 1994.

115. J. R. Wood, Ph. D Thesis, University of Surry, England, 1992.

116. J. R. Wood, and M. G. Bader, *J. Mat. Sci.*, **29**, 844 (1994).

117. J. R. Wood, and M. G. Bader, *J. Mat. Sci.*, **30**, 916 (1995).

118. S. Wu, *J. Phys. Chem.*, **72**, 3332 (1968).

119. V. N. Korotkov, Y. A. Chekanov, and B. A. Rozenberg, *J. Mat. Sci. Lett.*, **10**, 896 (1991).

120. Y. A. Chekanov, V. N. Korotkov, B. A. Rozenberg, E. A. Dhzavadyan, and L. M. Bogdanova, *Polymer*, **36**, 2013 (1995).

121. Y. A. Chekanov, and V. N. Korotkov, *Polymer*, **15**, 2168 (1996).

122. R. W. Biernath, Ph. D Thesis, University of Berkeley, 1990.

123. W. Zimmerman, Master thesis, Lehigh University, 1998.

124. S. Katsurayama, and M. Wada, *EEP- vol. 26-1, Advance in Electronic Packaging, ASME*, **1**, 391 (1999).

125. M. S. Schwiebert and W. H. Leong, *IEEE Transactions on Components, Packaging, and Manufacturing Technology*, Part C, **19** (2), 133 (1996).

126. J. H. Espenson, "Chemical Kinetics and Reaction Mechanisms", MaGraw-Hill, New York, 1981.

127. D. R. Olsen, H. M. Berg, *IEEE, 27th Electronics Components Conf.*, 193 (1977).

128. G. A. Lang, B. J. Feder, W. D. Williums, *IEEE Tr. Electr. Dev.*, **27**, 787 (1970).

129. D. P. Galloway and M. N. Nguyen, *Mat. Res. Soc. Symp. Proc.* **264**, 271 (1992).

130. I. Y. Chien and M. N. Nguyen, *Electr. Eng.*, **February**, 41 (1995).

131. T. D. Chang, S. H. Carr, and J. O. Brittain, *Polym. Eng. Sci.*, **22**, 1213 (1982).

132. S. Mostovoy and E. J. Ripling, *J. Apply. Polym. Sci.*, **10**, 1351 (1966).

133. J. P. Bell, *J. Apply. Polym. Sci.*, **14**, 1901 (1970).

134. S. L Kim, M. D. Skibo, J. A. Manson, R. W. Hertzberg, and J. Janiszewski, *Polym. Eng. Sci.*, **18**, 1093 (1978).

135. K. Selby, and L. E. Miller, *J. Mater. Sci.*, **10**, 12 (1975).

136. L. Shechter and J. Wynstra, *Ind. Engng. Chem.*, **48**, 86 (1956).

137. I. T. Smith, *Polymer*, **2**, 95 (1961).

138. N. B. Chapman, R. E. Parker, and N. S. Isaacs, *J. Chem. Soc.*, **2**, 1925 (1959).

139. T. Dyakonov, Y. Chen, K. Holland, J. Drbohlav, D. Burns, D. V. Velde, L. Seib, E. J. Soloski, J. Kuhn, P. J. Mann, and W. T. K. Stevenson, *Polymer Degradation and Stability*, **53**, 217 (1996).

140. Y. Tanaka and H. Kakiuchi, *J. Appl. Polym. Sci.*, **7**, 1063 (1963).

141. K. Dusek, *Polym Bull*, **13**, 321 (1985).

142. A. Vazquez, L. Matejka, P. Spacek, and K. Dusek, *J. Polym Si., Polym Chem. Ed.*, **28**, 2305 (1990).

143. A. Farkas and P. F. Strohm, *J. Apply. Polym. Sci.*, **12**, 159 (1968).

144. W. H. Carothers , *Trans. Faraday Soc.*, **32**, 39 (1936).

145. S. H. Pinner, *J. Polym. Sci.*, **21**, 153 (1956).

146. P. J. Flory, "Principle of Polymer Chemistry", Cornell University Press, Ithaca, New York, 1953

147. W. H. Stockmayer, *J. Chem. Phys.*, **11**, 45 (1943).

148. D. Durand. and C-M. Bruneau, *Polymer,* **23**, 69 (1982)

149. D. Durand and C-M. Bruneau, *Makromol. Chem.*, **183**, 1021 (1982)

150. J. W. Stafford, *J. Polym. Sci. Polym. Chem. Ed.*, **19**, 3219 (1981).

151. D. R. Miller,E. M. Valles, and C. W. Macosko, *Polym. Eng. Sci.*, **19**, 272 (1979).

152. L. J. Gough and I. T. Smith, *J. Appl. Polym. Sci.*, **3**, 362 (1960).

153. T. Kakurai and T. Nogoshi, *Chem. High. Polym.*, **20**, 213, 21 (1963).

154. S. Sourour and M. R. Kamal, *Thermochim. Acta*, **14**, 41 (1976).

155. A. Shimazaki, *J. Appl. Polym. Sci.*, **12**, 2013 (1968).

156. J. Mijovic, J. Kim, and J, Slaby, *J. Apply. Sci.*, **29**, 1449 (1984).

157. S.-N. Lee, M.-T. Chiu, and H.-S. Lin, *Polym. Eng. Sci.*, **32**, 1037 (1992).

158. S. Han, W. G. Kim, G. H. Yoon, and T. J. Moon, *J. Polym. Sci.*, **36**, 773 (1998).

159. A. F. Kah, M. E. Koehler, T. H. Grentzer, T. F. Niemann, and T. Provder, *Amer. Chem. Soc.*, 297 (1982).

160. X. Wang and J. K. Gillham, *J. Appl. Polym. Sci.*, **43**, 2267 (1991).

161. S. L. Simon and J. K. Gillham, *J. Appl. Polym. Sci.*, **46**, 1245 (1992).

162. S. L. Simon and J. K. Gillham, *J. Appl. Polym. Sci.*, **53**, 709 (1994).

163. J. P. Pascault and R. J. J. Williams, *J. Polym. Sci., Part B:Polym Phys.*, **28**, 85 (1990).

164. H. Stutz, K. H. Illers, and J. Mertes, *J. Polym. Sci., Part B:Polym Phys.*, **28**, 1483 (1990).

165. R. A. Venditti and J. K. Gillham, *J. Appl. Polym. Sci.*, **64**, 3 (1997).

166. Y. G. Lin, J. Galy, H. Sautereau, and J. P. Pascault, "Crosslinked Epoxies", de Gruyter, Berlin, 1989.

167. O. A. Owusu, G. C. Martin, and J. T. Gotro, *Polym. Eng. Sci.*, **31**, 1604 (1991).

168. H. E. Adabbo and R. J. J. Williams, *J. Appl. Polm. Sci.*, **29**, 1327 (1982).

169. S. L. Simon and J. K. Gillham, *J. Apply. Polym. Sci.*, **47**, 461, 1993.

170. C. Jordan, J. Galy, and J.-P. Pascault, *J. Appl. Polm. Sci.*, **46**, 859 (1992).

171. A. T. DiBenedetto, Unpublished results, as cited by L. E. Nielsen, *Macromol. Sci. Rev. Macromol. Chem.* **C3**, 69 (1969).

172. P. R. Couchman and F. E. Karasz, *Macromolecules*, **11**, 117 (1978).

173. P. R. Couchman, *Macromolecules,* **20**, 1712, (1987).

174. A. Hale and C. W. Macosko, *Macromolecules*, **24**, 2610 (1991).

175. R. H. Lin, "Ph. D. Dissertation, institute of Material Science and Engineering", National Sun Yet-Sen University, Taiwan, 1996.

176. R. H. Lin, A. C. Su, and J. L. Hong, *J. Polym. Sci.*, **38**, 762 (2000).

177. E. F. Oleinik, Pure. *Appl. Chem.*, **53**, 1567 (1981).

178. S. G. Hong and C. S. Wu, *Thermochim. Acta*, **316**, 167 (1998).

179. S. G. Hong and T. C. Wang, *Thermochim. Acta,* **237**, 305 (1994).

180. S. G. Hong and J. J. Lin, J. *Appl. Polym. Sci.*, **59**, 1597 (1996).

181. R. Jenkin and L. Karre, *J. Appl. Polym. Sci.*, **10**, 303 (1966).

182. G. Widmann, *Thermochim. Acta*, **11**, 331 (1975).

183. L. H. Sperling, "Introduction to Physical Polymer Science", 2nd ed., John Wiley & Sons Inc., New York, 1992.

184. J. E. Martin and D. B. Adolf, *Phys. Rev. A.*, **39**, 1325 (1989).

185. D. B. Adolf and J. E. Martin, *Macromolecules*, **24**, 6721 (1991).

186. J. D. Ferry, "Viscoelastic Properties of Polymers", 3rd ed., John Wiley & Sons, New York, 1980.

187. G. Liu and A. N. Gent, *J. Adhesion*, **38**, 79 (1992).

Vita

Jantrawan Taweeplengsangsuke was born on February 16, 1965. She received the B. Sc. (Chemistry) in 1988 from Chiangmai University, Thailand. In 1988, she was granted by Science and Technology Development Board (STDB, Thai-American Technical Cooperation Project) to achieve her M. Sc. on Polymer Science. She graduated with her master in 1990. Her master thesis focused on medical polymers. Then she worked as a junior lecturer in the Department of Industrial Chemistry, Faculty of Science, Chiangmai University. Meanwhile she was awarded a research scholarship from British Council to do the research on polymer composite at Leeds University, England in 1992. She has become a member of "Biomedical Research Unit", Thailand (a branch of MTEC) since 1995. In 1996, she awarded a scholarship from Thai Government and went to Lehigh University to pursue her Ph. D. in Polymer Science and Engineering. She chose to work on the polymer for microelectronics under the supervision of Dr. Raymond A. Pearson.

During her study at Lehigh University, she was awarded the "Ticona Award" for excellence in polymer study and research in 1999.